

DISSERTATION

MEDIATION OF KINETOCHORE-MICROTUBULE INTERACTIONS THROUGH THE
NDC80 COMPLEX COMPONENT HEC1

Submitted by

Geoffry J. Guimaraes

Department of Biochemistry and Molecular Biology

In partial fulfillment of the requirements

For the Degree of Doctor of Philosophy

Colorado State University

Fort Collins, Colorado

Fall 2011

Doctoral Committee:

Advisor: Jennifer DeLuca

James Bamberg

Olive Peersen

A.S.N. Reddy

ABSTRACT

MEDIATION OF KINETOCHORE-MICROTUBULE INTERACTIONS THROUGH THE NDC80 COMPLEX COMPONENT HEC1

The vertebrate kinetochore is a large proteinaceous complex comprised of over 100 different proteins, of which the Ndc80 complex (consisting of Hec1, Nuf2, Spc24, and Spc25) is a member. In numerous systems, the Ndc80 complex has been shown to be essential for microtubule (MT) binding at the kinetochore. Of particular interest to the Ndc80-kinetochore-MT interface is Hec1, which is positioned at the outer-kinetochore poised for interaction with MTs of the bi-polar spindle. Both the Hec1 80 amino acid tail domain and calponin homology (CH) domain have been implicated in the establishment, and regulation of, tension generating kinetochore-MT attachments.

During mitosis, bi-orientation occurs when sister-kinetochore pairs attach to MTs of sister poles, and regulation of this process is essential for chromosome congression and eventual metaphase plate formation. The integrity of dynamic kinetochore-MT interactions observed during bi-orientation helps to ensure that equal segregation of chromosomes is achieved into two new daughter cells, thereby preventing aneuploidy. The integrity of these bi-oriented kinetochore-MT attachments requires that the binding between kinetochore proteins and MTs is functionally flexible enough to maintain an association during states of MT polymerization and depolymerization. The KMN network, comprised of Knl-1, the Mis12 complex, and Ndc80 complex, has been shown to be essential for the formation of stable kinetochore-MT attachments. For example, in

multiple cell types depletion of Hec1, one of the four protein components found to comprise the Ndc80 complex, results in a kinetochore “null” phenotype, in which stable kinetochore-MT formation is prevented. It has been suggested that an electrostatic interaction exists between the basic tails of Hec1 and the acidic tails of tubulin. Manipulation to this electrostatic interaction through phosphorylation of the Hec1 tail domain could serve to regulate kinetochore-MT interactions. Additionally, the length of the Hec1 80 amino acid tail domain may be essential to Ndc80 complex oligomerization or direct binding of Hec1 to the MT lattice. *In vitro*, point mutations within the Hec1 CH domain have demonstrated this region as being essential for MT binding. Still, the exact role that these regions play in mediation of kinetochore-MT attachments remains unknown.

The work presented in this dissertation addresses how regions of Hec1 contribute to the formation of kinetochore-MT interactions. Specifically, a silence and rescue strategy was employed whereby Hec1 was targeted for knockdown using siRNA and cells were subsequently rescued with various Hec1-GFP constructs. Initially, silence and rescue experiments were used to address if specific domains of Hec1 protein were essential for protein function. Cells depleted of endogenous Hec1 and rescued with Hec1 Δ^{1-80} , which encodes for a tail-less Hec1 protein, failed to form stable kinetochore-microtubule attachments. Further probing the role of the Hec1 80 amino acid tail domain, nine Aurora B Kinase (ABK) phosphorylation sites, shown to be phosphorylated *in vitro*, were mutated to mimic constitutive phosphorylation (Hec1^{9D}-GFP). It has been hypothesized that upon phosphorylation, the charge of the Hec1 tail domain is reduced to prevent binding to the negatively-charged tail domains of tubulin. Cells rescued with Hec1^{9D}-GFP are also impaired in kinetochore-MT attachments, indicating that phosphorylation of the Hec1 tail domain may regulate kinetochore-MT association. These

results clearly demonstrate that the Hec1 80 amino acid tail is essential for the generation of stable kinetochore-MT attachments in cells.

Of the nine ABK phosphorylation sites mapped *in vitro* by mass spectroscopy, four have been identified as bona fide phosphorylation target sites in cells. To determine the role of phosphorylation of these specific sites *in vivo*, a sequential series of phospho-mimetic mutants to these sites were made. Interestingly, upon stepwise introduction of phospho-mimetic mutations, a decrease in kinetochore-MT attachment stability was observed, suggesting that phosphorylation of the Hec1 tail may play a role in fine-tuning the binding strength between kinetochores and microtubules.

The highly basic Hec1 tail is an intrinsically disordered domain. It has been demonstrated that for some intrinsically disordered proteins the composition alone, and not necessarily primary sequence, can mediate MT binding function. To this end, a Hec1 mutant was developed whereby the amino acids of the Hec1 80 amino acid tail domain were randomized, yielding a loss of primary sequence while retaining native tail composition. Cells rescued with this construct were capable of forming stable kinetochore-MT attachments, but were also impaired in their ability to properly align chromosomes and faithfully progress through mitosis. Scrambling of the Hec1 80 amino acid tail domain likely disrupts the native ABK phosphorylation sites needed for dynamic kinetochore-MT interactions, and may explain the phenotype for cells rescued with scrambled 80 Hec1-GFP. Indeed, this phenotype is very similar to the Hec1^{9A} rescue, where the 9 phosphorylation sites along the Hec1 80 amino acid tail domain have been mutated to alanines, thus precluding their phosphorylation. In the Hec1^{9A}-GFP rescue, the loss of dynamic phosphorylation of the Hec1 tail domain results in hyper-stable kinetochore-MT attachments that lack the flexibility needed for proper chromosome alignment. Together, these works suggest that composition, and not primary sequence of

the Hec1 80 amino acid tail domain can mediate stable kinetochore-MT attachments. However, more dynamic kinetochore-MT attachments needed for chromosome alignment and a faithful mitotic progression likely require Hec1 tail domain phosphorylation.

The length of the Hec1 80 amino acid tail domain has been proposed to contribute towards Ndc80-complex binding along the MT lattice through two different models; 1) by directly binding the MT lattice 2) by oligomerizing Ndc80 complexes bound to the MT lattice. Regardless of which of these two models is correct, Hec1 mutants with truncated tail domains were used to assess if the entire Hec1 tail sequence is required for kinetochore-MT binding. Interestingly, cells rescued with Hec1 containing a short, positively charged tail domain (Hec1^{57-61Δ80}) were capable of stable kinetochore-MT attachments. However, these cells lacked dynamic kinetochore-MT attachments, and exhibited an impaired ability to form metaphase plates while still proceeding through mitosis. This phenotype is strikingly similar to the Hec1^{9A}-GFP rescue, where phosphorylation of the 80 amino acid tail domain is impaired, resulting in stable, non-dynamic, kinetochore-MT attachments, which ultimately yielding chromosome alignment defects and segregation errors. It is likely that phosphorylation of the tail domain of Hec1^{57-61Δ80}-GFP construct is impaired, as no ABK phosphorylation sites remain in the tail of this mutant. The loss of phosphorylation of the truncated Hec1 tail domain may explain the presence of stable kinetochore-MT attachments in cells where mitotic progression is impaired. From these experiments it has been demonstrated that the entire length of the Hec1 80 amino acid tail domain is not essential for kinetochore-MT attachments, however a more complete segment of the tail domain may be needed for dynamic regulation of the kinetochore-MT interaction.

In addition to the Hec1 80 amino acid tail domain, a calponin homology (CH) domain exists within the N-terminus of Hec1. *In vitro* MT co-pelleting assays have

indicated residue K166 within the Hec1 CH domain is essential for Ndc80-MT binding, and have suggested that the positive charge to this residue contributes to MT binding. Additionally, crystal structures of the Ndc80^{Bonsai} complex and the tubulin dimer were docked onto cryo-EM images of MT-bound Ndc80 complexes in an effort to reconstruct the Ndc80 complex/MT lattice interface, and suggests residue K166 directly contacts the MT lattice. Using a point mutation analysis to the Hec1 CH domain, cells rescued with Hec1^{K166D}-GFP yielded a kinetochore-null phenotype, as no kinetochore-MT attachments formed. These data strongly suggest that the Hec1 CH domain is essential for the generation of stable kinetochore-MTs.

The work discussed here suggests that two regions within the Hec1 N-terminus mediate kinetochore-MT binding. Neither the 80 amino acid tail domain nor the CH domain of Hec1 are dispensable in kinetochore-MT binding, as removal or inhibition to one of these domains can not be rescued by the other. We suggest a bi-partite mechanism of Ndc80 complex-MT binding; the Hec1 CH domain stabilizes an interaction along the MT lattice through a direct point of contact while regulation to the 80 amino acid tail domain mediates a flexible association with the MT lattice, allowing for a dynamic Ndc80 complex-MT interaction.

ACKNOWLEDGEMENTS

I would like to acknowledge my advisor Jennifer DeLuca for her role in shaping my graduate career. Through her support I have developed an understanding of the scientific process. Additionally, her insight has lead to a number of successful experiments and eventual publications, and for this I am thankful. I would also like to thank my lab members, not only for their support scientifically, but also for serving as great friends. I am also grateful to my thesis committee members for offering their time and scientific insight throughout the course of my graduate career. Lastly, I would like to thank my friends and family for their support and encouragement over the past five years.

Table of Contents

Abstract of Dissertation	ii
Acknowledgements	vii
Table of Contents	viii
List of Tables and Figures	xi
Chapter 1. Introduction	1
1.1 Mitosis: An overview.....	1
1.2 Chromosome congression in mitosis	1
1.3 The Ndc80 complex/kinetochore: structure and key components	3
1.4 Chromosome movements and kinetochore-MT dynamics	11
1.5 Ndc80 as a participant in the spindle assembly checkpoint (SAC).....	14
Chapter 2. Materials and Methods	17
2.1 Cell culture, plasmids, siRNA and transfection protocols	17
2.1.1 General PtK1 cell culture.....	17
2.1.2 Hec1 siRNA.....	18
2.1.3 Hec1 plasmids.....	18
2.1.4 Oligofectamine transfection protocol	18
2.1.5 Nucleofector transfection protocol	19
2.2 Immunofluorescence, microscopy, fixed and live cell measurements	20
2.2.1 Immunofluorescence solutions and buffers	20
2.2.2 Immunofluorescence fixation procedure	21
2.2.3 Delta-Vision microscope.....	23
2.2.4 Fixed Cell microscopy measurements	23
2.25 Live cell microscopy measurements	25

Chapter 3. Kinetochores-microtubule attachment relies on the disordered N-terminal tail domain of Hec1	30
3.1 Introduction	30
3.2 Results	32
3.2.1 Hec1 depletion from PtK1 cells results in mitotic defects	32
3.2.2 The N-terminus of Hec1 is required for kinetochores-microtubule attachment.....	45
3.2.3 Kinetochores ultrastructure in Hec1-depleted and Δ 1-80 Hec1-GFP rescued PtK1 cells.....	54
3.3 Discussion.....	64
Chapter 4. The CH domain of Hec1 is essential for mediating kinetochores-MT attachments	67
4.1 Introduction	67
4.2 Results	68
4.2.1 K166D point mutation to the Hec1 CH domain results in a kinetochores-null phenotype.....	68
4.2.2 A hyper-attaching Hec1 tail domain is not sufficient to rescue defects induced by the K166D point mutation	69
4.3 Discussion.....	75
Chapter 5. Phosphorylation, length, and charge composition of the Hec1 80 amino acid tail domain contribute to kinetochores-MT interactions	78
5.1 Introduction	78
5.2.1 Results	84
5.2.1 Hec1 tail phospho-mimetic mutation to conserved aurora B kinase phosphorylation sites impairs kinetochores-microtubule attachments.....	84
5.2.2 Hec1 tail phospho-mimetic mutation to conserved aurora B kinase phosphorylation sites disrupts normal mitotic progression	94
5.2.3 Disrupting kinetochores-MT attachments through phospho-mimetic mutations yields aberrant kinetochores movements	99

5.2.4 A truncated Hec1 tail domain mutant can mediate kinetochore-microtubule interaction.....	106
5.2.5 Cells expressing a truncated Hec1 tail domain mutant display defects in mitotic progression.....	116
5.2.6 Cells expressing a truncated Hec1 tail domain mutant display dampened kinetochore oscillation.....	121
5.2.7 Primary sequence of the Hec1 80 amino acid tail domain mutant is not required for establishing kinetochore-MT interactions	127
5.2.8 Cells rescued with a scrambled 80 amino acid Hec1 tail domain mutant display defects in mitotic progression	128
5.2.9 Cells rescued with a scrambled 80 amino acid Hec1 tail domain mutant display dampened kinetochore oscillations	139
5.3.1 Discussion.....	145
Chapter 6. Discussion and future directions	149
6.1 Discussion.....	149
6.2 Future directions	154
References.....	156

List of Tables and Figures

Chapter 1

1.1 Major components of the mitotic spindle in vertebrate cells	2
1.2 Organization of the vertebrate kinetochore	5
1.3 Components of the essential KMN network and model for binding along the MT lattice.....	7
1.4 Organization of the Ndc80 complex.....	8
1.5 Model for multiple Ndc80 complexes binding to a MT.....	9
1.6 Crystal structure of an engineered Ndc80 complex (Ndc80 ^{Bonsai}).....	10
1.7 Surface views representing the electrostatic potential for the Hec1 and Nuf2 CH domains	12
1.8 Model for regulation an electrostatic interaction between the 80 amino acid tail domain of Hec1 and the C-terminal tails of tubulin	15

Chapter 3

3.1A PtK1 Hec1 sequence analysis	33
3.1B Hec1 intrinsic disorder plots	34
3.2A-G Hec1 depletion from PtK1 cells results in mitotic defects.....	36-42
3.3 Timing through mitosis: mock-transfected & Hec1-siRNA transfected PtK1 cells in the absence and presence of nocodazole.....	43
3-4 Mad2 is prematurely depleted from unattached kinetochores in Hec1-depleted PtK1 cells	44
3-5A&B Summary of inter-kinetochore distance data for N-Terminal GFP fusion proteins.....	46&47
3-6A-E The N-terminus of Hec1 is required for kinetochore-microtubule attachment.....	48-50,52&53
3-7A-E Kinetochore ultrastructure in Hec1-depleted and Δ 1-80 Hec1-GFP- rescued PtK1 cells	55-59
3-8A-C Charge modification of the Hec1 80 amino acid tail domain inhibits kinetochore-microtubule attachment	61-63

Chapter 4

4-1 Point mutation to the Hec1 calponin homology domain results in mitotic defects	70
4-2 Point mutation to the Hec1 calponin homology domain impairs tension generating kinetochore-MT attachments	71
4-3 Point mutation to the Hec1 calponin homology domain impairs stable kinetochore-MT attachments	72
4-4 Point mutation to the Hec1 calponin homology domain impairs chromosome alignment.....	74

Tables

4-1 Inter-kinetochore distance values for cells rescued with Hec1 calponin homology domain mutants	73
4-2 Percent end-associated kinetochore-MT values for cells rescued with Hec1 calponin homology domain mutants	73
4-3 Percent chromosome alignment values for cells rescued with Hec1 calponin homology domain mutants	74

Chapter 5

5.2.1 Phosphorylation of conserved sites regulates kinetochore-MT interactions.....	85
5.2.2 Incrementally introducing phospho-mimetic mutations to phosphorylation sites impairs tension generating kinetochore-MT attachments....	87
5.2.3 Incrementally introducing phospho-mimetic mutations to phosphorylation sites impairs stable kinetochore-MT attachments	89
5.2.4 Phospho-mimetic mutation to conserved residues impairs chromosome alignment	92
5.2.5 Impairing kinetochore-MT attachments through phospho-mimetic mutations results in a mitotic arrest	95
5.2.6 Phospho-mimetic mutations impair metaphase plate formation	96
5.2.7 Phospho-mimetic mutations disrupt kinetochore-MT attachments and result in a mitotic arrest	97
5.2.8 Disruption of kinetochore-MT attachments through phospho-mimetic mutation results in increased kinetochore velocities	100

5.2.9 Phospho-mimetic mutation to all 9 Hec1 phosphorylation sites results in erratic kinetochore movements	101
5.2.10 Precluding phosphorylation of the Hec1 tail domain results in stagnant kinetochore movements	102
5.2.11 Phospho-mimetic mutation to the 4 conserved Hec1 phosphorylation sites results in erratic kinetochore movements	103
5.2.12 Precluding phosphorylation of the Hec1 tail domain yields stagnant kinetochore movements	104
5.2.13 Hec1 tail charge and length contribute towards kinetochore-MT attachments.....	108
5.2.14 Short positively charged Hec1 tail domains are capable of establishing moderate inter-kinetochore tension	110
5.2.15 Short positively charged Hec1 tail domains are capable of establishing stable kinetochore-MT attachments.....	111
5.2.16 Truncating the Hec1 tail domain impairs metaphase plate formation	113
5.2.17 Cells expressing Hec1 with a short tail domain progress through mitosis in a timely fashion.....	118
5.2.18 Cells expressing a short Hec1 tail are impaired in metaphase plate formation	119
5.2.19 Cells expressing a short Hec1 tail mutant can satisfy the SAC and enter anaphase in under two hours	120
5.2.20 Truncating the Hec1 80 amino acid tail domain decreases chromosome oscillation velocities	122
5.2.21 Precluding phosphorylation of the Hec1 tail domain results in stagnant chromosome movements.....	123
5.2.22 Truncation to the Hec1 tail domain results in stagnant chromosome movements.....	124
5.2.23 Precluding phosphorylation of the Hec1 tail domain yields stagnant chromosome movements	125
5.2.24 Truncating the Hec1 tail domain yields stagnant chromosome movements	126

5.2.25 Primary sequence of the Hec1 80 amino acid tail domain is essential for metaphase plate formation	129
5.2.26 Cells expressing a scrambled Hec1 80 amino acid tail domain mutant are capable of establishing kinetochore-MT attachments	130
5.2.27 Cells expressing a scrambled 80 amino acid tail domain establish stable kinetochore-MT attachments.....	131
5.2.28 Cells expressing a scrambled 80 amino acid tail domain mutant exhibit impaired metaphase plate formation	136
5.2.29 Percent chromosome alignment values for cells rescued with a scrambled 80 Hec1 tail.....	137
5.2.30 Scrambling of the Hec1 80 amino acid tail domain impairs metaphase plate formation.....	138
5.2.32 Scrambling of the 80 amino acid tail domain decreases chromosome oscillation velocities	140
5.2.33 Precluding phosphorylation of the Hec1 tail domain results in stagnant chromosome movements	141
5.2.34 Scrambling to the Hec1 80 amino acid tail domain results in stagnant chromosome movements	142
5.2.35 Oscillation kymographs- FL-Hec1 and scrambled 9A-Hec1.....	143
5.2.36 Oscillation kymographs- FL-Hec1 and scrambled 80-Hec1	144
<u>Tables</u>	
5.2.1 Constructs for phospho-mimetic Hec1 mutants	86
5.2.2 Inter-kinetochore distance values for cells rescued with phospho-mimetic Hec1 mutants	88
5.2.3 Percent end-associated kinetochore-MT values for cells rescued with phospho-mimetic Hec1 mutants	90
5.2.4 Percent chromosome alignment values for cells rescued with phospho-mimetic Hec1 mutants	90
5.2.5 Time lapse movies- percent of cells rescued with phospho-mimetic Hec1 mutants that achieve metaphase alignment	96

5.2.6 Time lapse movies- percent of cells rescued with phospho-mimetic Hec1 mutants that entering anaphase in under two hours	97
5.2.7 Kinetochores velocity values for cells rescued with phospho-mimetic Hec1 mutants	100
5.2.8 Hec1 truncation mutant constructs	109
5.2.9 Hec1 truncation mutant charge per amino acid	109
5.2.10 Inter-kinetochore distance for cells rescued with Hec1 truncation mutants	112
5.2.11 Percent end-on kinetochore-MT attachments for cells rescued with Hec1 truncation mutants.....	112
5.2.12 Percent chromosome alignment values for cells rescued with Hec1 truncation mutants.....	113
5.2.13 Time lapse movies- percent of cells rescued with a Hec1 truncation mutant achieving metaphase alignment.....	119
5.2.14 Time lapse movies- percent of cells rescued with a Hec1 truncation mutant entering anaphase in under two hours	120
5.2.15 Oscillation velocity values for cells rescued with a Hec1 truncation mutant	122
5.2.16 Electrostatic potential existing between the Hec1 and tubulin tail domains	132
5.2.17 Amino acid sequence for the scrambled 80 Hec1 tail domain mutants	132
5.2.18 Inter-kinetochore distances for cells rescued with a scrambled 80 Hec1 tail mutant	133
5.2.19 Percent end-on kinetochore-MT attachments for cells rescued with a scrambled 80 Hec1 tail mutant	133
5.2.20 Cells rescued with a scrambled Hec1 80 amino acid tail domain mutant progress through mitosis in a timely fashion	134
5.2.21 Time lapse movies- percent of cells achieving metaphase alignment for cells rescued with a scrambled 80 Hec1 tail mutant.....	137
5.2.22 Time lapse movies- percent of cells entering anaphase in under two hours when rescued with a scrambled 80 Hec1 tail mutant	138

5.2.23 Oscillation velocity values for cells rescued with a scrambled 80 Hec1 tail mutant	140
---	-----

Chapter 6

6.1.A Model for Ndc80 complex binding to the MT lattice	151
---	-----

6.1.B Model for Ndc80 complex binding to the MT lattice	152
---	-----

6.1.C Model for Ndc80 complex binding to the MT lattice	153
---	-----

Chapter 1

Introduction

1.1 Mitosis: An Overview

During the process of mitosis, cells equally segregate their replicated chromosomes into two daughter cells. As early as 1953, accounts of chromosomes interacting with spindle fibers were documented [1]. Since this time the kinetochore has been identified as a network of proteins found to assemble on centromeric DNA and bind microtubules (MTs). Proper chromosome orientation along the spindle equator and eventual segregation in anaphase occurs on the mitotic spindle, and the dynamic interactions that take place between kinetochores and spindle-MTs are essential to these processes (Figure 1.1). Specifically, the pushing and pulling of chromosomes resulting from dynamic MTs attached to kinetochores are responsible for generation of their bi-orientation, alignment, and eventual segregation. A proper attachment necessary for achieving these events is dependent upon not only end-on attachments of MT plus ends into a kinetochore, but also flexible kinetochore-MT binding interactions capable of mediating attachments with both polymerizing and depolymerizing MTs. The mechanism by which kinetochore proteins are manipulated to promote varying MT binding states necessary for tethering to constantly polymerizing/depolymerizing MTs has long been debated in the field [2-6].

1.2 Chromosome Congression in Mitosis

At the onset of nuclear envelope breakdown chromosomes are released into the cytoplasm of the cell and duplicated spindle poles, or centrosomes, separate. Emanating out from the spindle poles are dynamic MTs, whose plus ends serve as the site of tubulin subunit addition and loss. Using a “search and capture” mechanism [7, 8] the dynamic MT plus ends probe the cell for chromosomes recently liberated from nuclear envelope encapsulation. In search and capture, high rates of MT turnover produced from stochastic

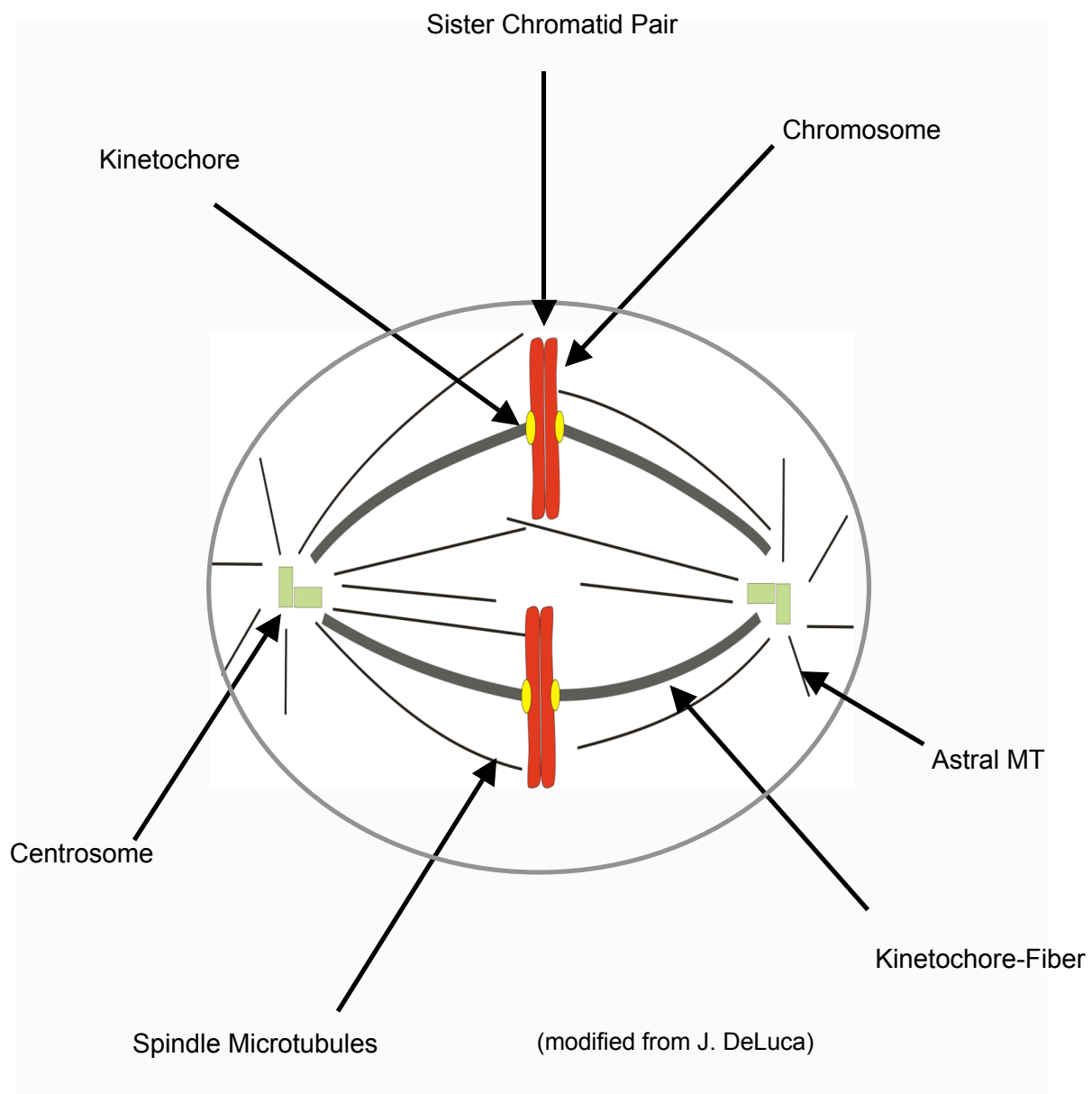


Figure 1.1: Major Components of the Mitotic Spindle in Vertebrate Cells

Chromosome- organized structure of DNA and protein.

Sister Chromatid Pair- Two exact copies of a chromosome.

Kinetochore- protein structure that links chromosomes to MTs.

Centrosome- organelle serving as the microtubule organizing center.

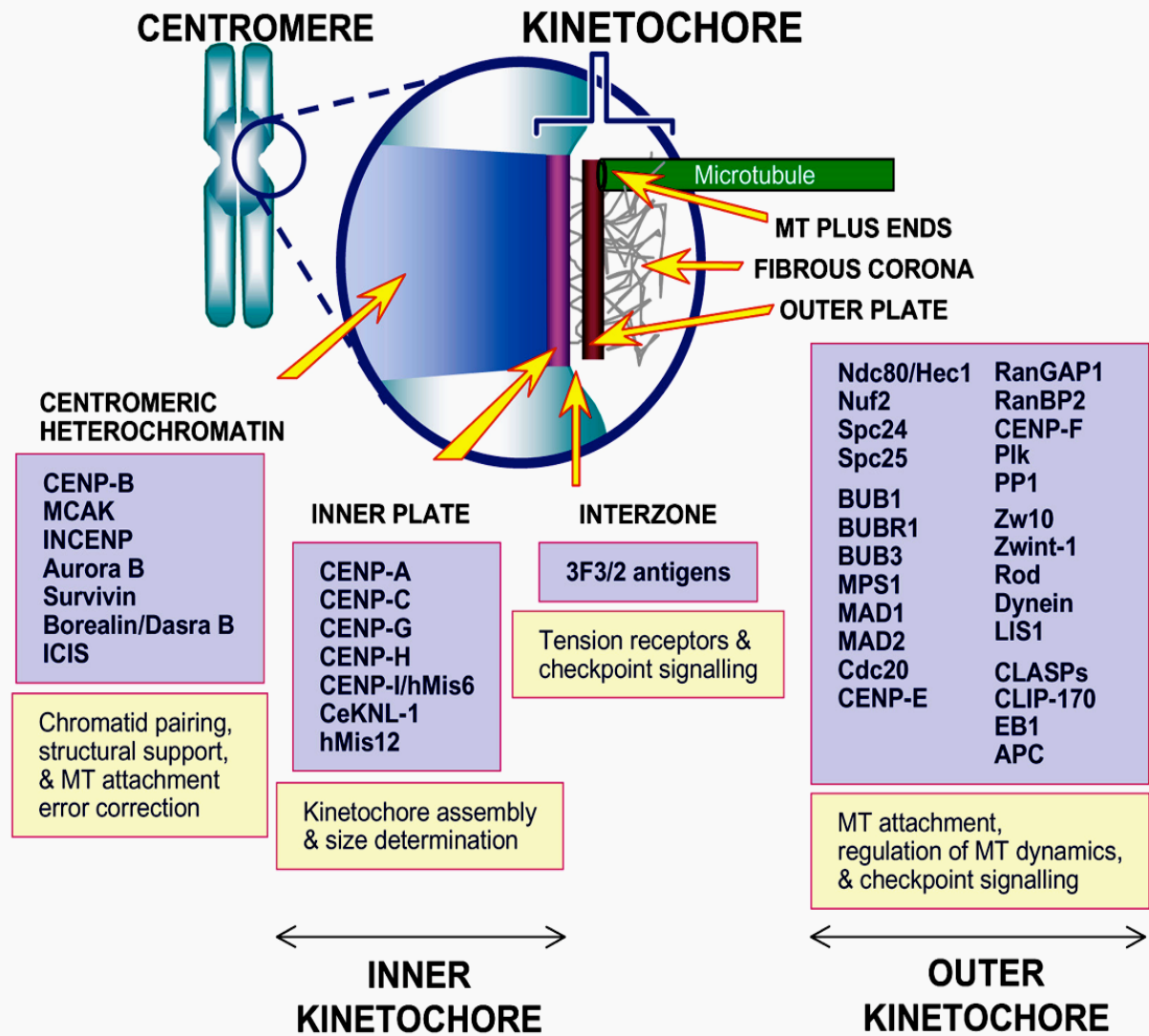
Astral/Spindle Microtubules- MTs growing out from the centrosome with unbound plus end tips, that contribute to spindle structure.

Kinetochore-Fiber-A bundle of MTs extending from the centrosome bound to a kinetochore.

rounds of MT polymerization/depolymerization allow the plus ends of MTs originating from the spindle poles to continuously probe the cell, as they attempt to contact chromosomes. Chromosomes initially become attached to MTs of the mitotic spindle in a lateral manner along the length of a MT, after which the minus-end directed MT motor dynein, known to be concentrated at unattached kinetochores, rapidly transports chromosomes ($25\text{-}55\ \mu\text{m min}^{-1}$) towards the spindle pole from which the MT originated [9-13]. As the kinetochore draws in closer proximity to a spindle pole, it experiences a densely populated region of dynamic MT plus ends. The lateral chromosome-MT interaction is converted into an end-on attachment and many MT plus-ends become anchored into the kinetochore forming a kinetochore-MT bundle or “k-fiber” [14]. The conversion from lateral to end-on kinetochore-MT attachments significantly stabilizes kinetochore-MTs, as they are resistant to depolymerizing conditions, and tubulin subunit turnover is reduced as compared to astral and spindle microtubules [15]. With a kinetochore-MT bundle attached to one of the sister kinetochores, polar ejection forces and the MT motor CENP-E reposition the chromosome back in towards the center of the cell such that interactions with MTs from the opposing centrosome can be made [16-20]. As attachments to both sister kinetochores are established, a pliable interplay between the kinetochore and dynamic MTs is required to produce the forces necessary for chromosome movements. The forces harnessed in a flexible kinetochore-MT interaction are used to oscillate chromosomes between the two poles of the bi-polar spindle until proper bi-orientation occurs and all of the chromosomes in the cell become aligned along the metaphase plate. Once the spindle assembly checkpoint (SAC) has been satisfied (discussed later), sister chromosomes are separated in anaphase and equally distributed into two new daughter cells.

1.3 The Ndc80 Complex/Kinetochore: Structure and Key Components

The vertebrate kinetochore (Figure 1.2) is a protein complex that functions to generate regulatable interactions with spindle MTs [21], as well as to regulate cell cycle progression through interactions with the SAC proteins [22]. Electron microscopy performed on cells prepared using conventional fixation protocols identified the vertebrate kinetochore as having electron dense inner and outer domains [23]. More recently, EM analysis of cells prepared using improved fixation methods has indicated the unbound kinetochore outer domain exists as a fibrous network, interspersed with channels and gaps to which the MT fibers binds into [24]. In *Saccharomyces cerevisiae* the inner-kinetochore is found to assemble on a 150 base pair long centromeric region containing the specialized histone H3 variant, centromere protein A (CENP-A), while the primary constriction site for kinetochore formation in higher eukaryotes extends over millions of base pairs [25]. While CENP-A has a sequence that is largely conserved as compared to H3 histone, deuterium exchange studies have revealed CENP-A to be in a more compact state with slight structural changes believed to be important for centromere targeting [26]. CENP-A is the earliest protein known to bind during kinetochore assembly and serves as the inner-kinetochore “foundation”. Upon CENP-A localization to centromeric chromatin the constitutive centromere-associated network (CCAN), comprised of numerous down-stream CENP proteins, are recruited to assemble the additional framework of the kinetochore [2, 27-30]. Ultimately, with the inner-kinetochore framework established, the outer domain of the kinetochore can assemble. The outer domain of the kinetochore, which resides exterior to the inner-kinetochore, functions to bind 15-30 dynamic MTs, regulate MT assembly/disassembly properties, and engage in force production used for chromosome movement [31, 32]. Consistent with the outer-kinetochore serving a functional role exclusive to mitosis, the outer kinetochore is found to assemble around, or just prior to, the time of nuclear envelope breakdown [33]. The KMN network, comprised of KNL-1, the Mis12 complex, and the Ndc80 complex, is essential for kinetochore function and has been termed the core MT binding component at the outer



Maiato et al., 2004

Figure 1.2: Organization of the vertebrate kinetochore

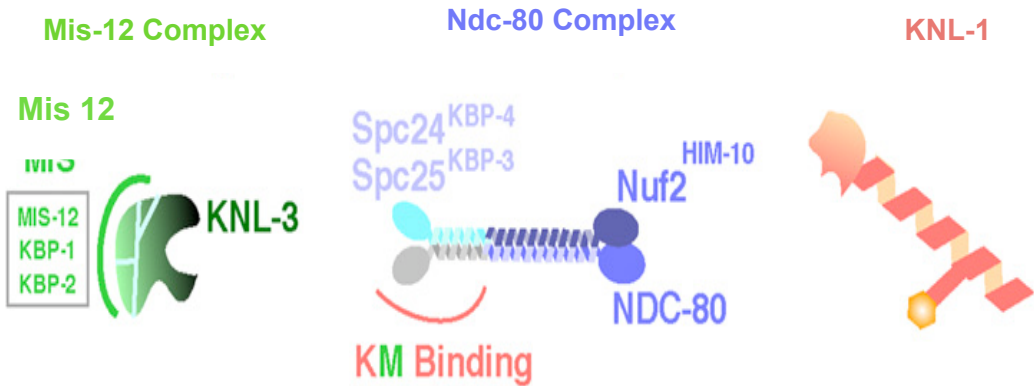
An incomplete list of the proteins found at discrete regions of the kinetochore is shown. The vertebrate kinetochore assembles on the primary construction of chromosomes and is composed of two distinct regions; an inner and outer domain. Four proteins (Ndc80/Hec1, Nuf2, Spc24, and Spc25) comprising the Ndc80 complex are found at the outer domain of the kinetochore and are known to be major contributors to kinetochore-MT interactions. Although not shown in this list, KNL-1 of the KMN network is also found at the outer-kinetochore.

kinetochore [34]; Figure 1.3). Of particular interest is the Ndc80 complex, consisting of Hec1, Nuf2, Spc24, and Spc25. In many systems, the Ndc80 complex has been shown to be essential for establishing stable kinetochore-MT attachments [35-43]. Structurally, the Ndc80 complex is a 57nm dumbbell-shaped hetero-tetramer; the N-terminal portion of the Hec1/Nuf2 dimer and C-terminal portion of the Spc24/Spc25 dimer each form globular “head” domains that reside on the exterior of the “dumbbell”, and are linked through coiled-coil regions [44, 45]. The globular domains of the Ndc80 complex serve distinct functional roles; Hec1/Nuf2 binds MTs, and is positioned away from the chromosomes in a region poised for interactions with MTs [34, 46] whereas Spc24/Spc25 resides proximal to centromeric chromatin and is required for Ndc80 complex localization at the kinetochore [47].

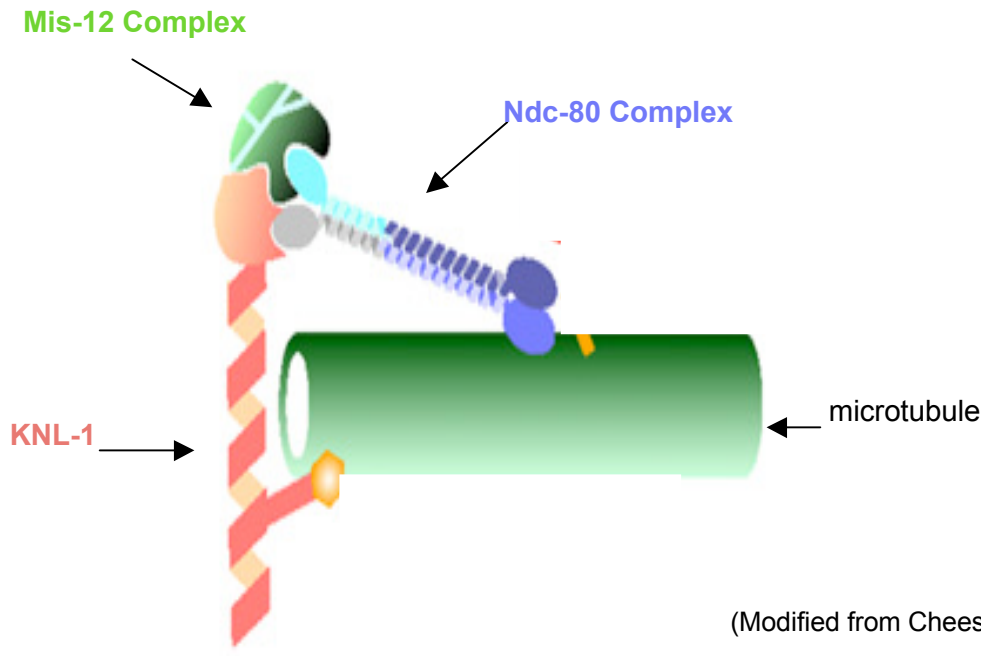
A combination of immunofluorescent, crystallographic, and electron microscopy (EM) based assays have revealed the spatial organization of kinetochore core components with nanometer resolution [2, 46, 48]. Insights from these studies have positioned the Ndc80 complex near the site of MT plus end termination [49]. Early RNAi mediated disruption of the Ndc80 complex was shown to impair kinetochore-MT attachments [36, 38]. More recent work demonstrated that the Ndc80 complex directly contacts MTs [45], with ~22-27 Ndc80's bound per MT (E.D. Salmon, unpublished data; Figure 1.5). Extrapolating from the 25-30 MT fibers that bind a vertebrate kinetochore, this places approximately 750 Ndc80 complexes per kinetochore.

Of particular interest at the Ndc80-kinetochore-MT interface is the N-terminal region of Hec1, which is positioned away from the chromosome poised for interaction with incoming MTs of the bi-polar spindle [46, 48]. Crystallographic studies have revealed calponin homology (CH) domains, a known MT-binding motif, to exist within the globular N-terminus of both Hec1 and Nuf2 [45, 50] (Figure 1.6). The Hec1 and Nuf2 CH domains are found to pack against each other, yielding a structural organization proposed to mediate MT

Components of the KMN Network



Model of KMN Network organization and binding to a MT

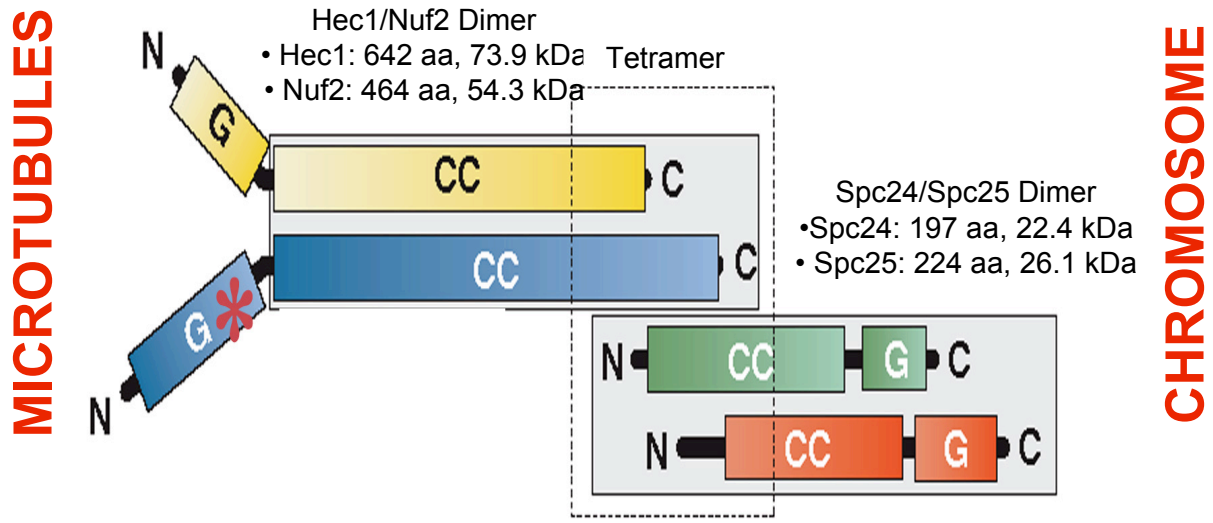


(Modified from Cheeseman et al., 2006)

Figure 1.3: Components of the essential KMN network and model for binding along the MT lattice

The KMN network (*C. elegans* homologs shown) constitutes the core MT binding site of the kinetochore, with all three proteins being essential to this function. Ndc80 and KNL-1 can directly bind MTs, while the MIS-12 complex serves a role in recruitment and structural organization of the complex.

- Full Ndc80 Complex: 57nm long, 170-190 kDa



(Modified from DeLuca et al., 2006)

Figure 1.4: Organization of the Ndc80 complex

The Ndc80 complex is a tetramer, with the C-terminal portion of the Hec1/Nuf2 dimer tetramerizing with the N-terminal region of the Spc24/Spc25 dimer. The Spc24/Spc25 dimer resides proximal to the chromosomes and is essential for the localization of the Ndc80 complex to kinetochores, while the Hec1/Nuf2 dimer resides exterior to the chromosomes and is poised for interactions with MTs.

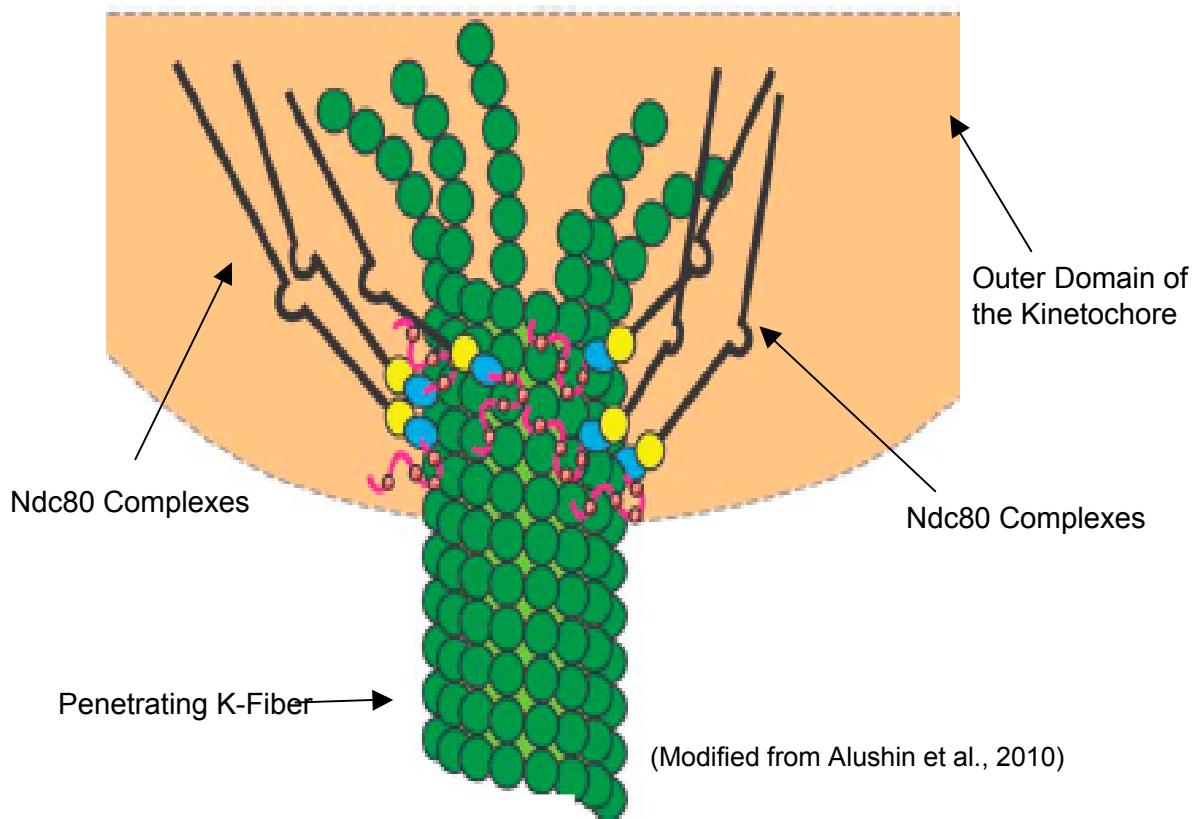
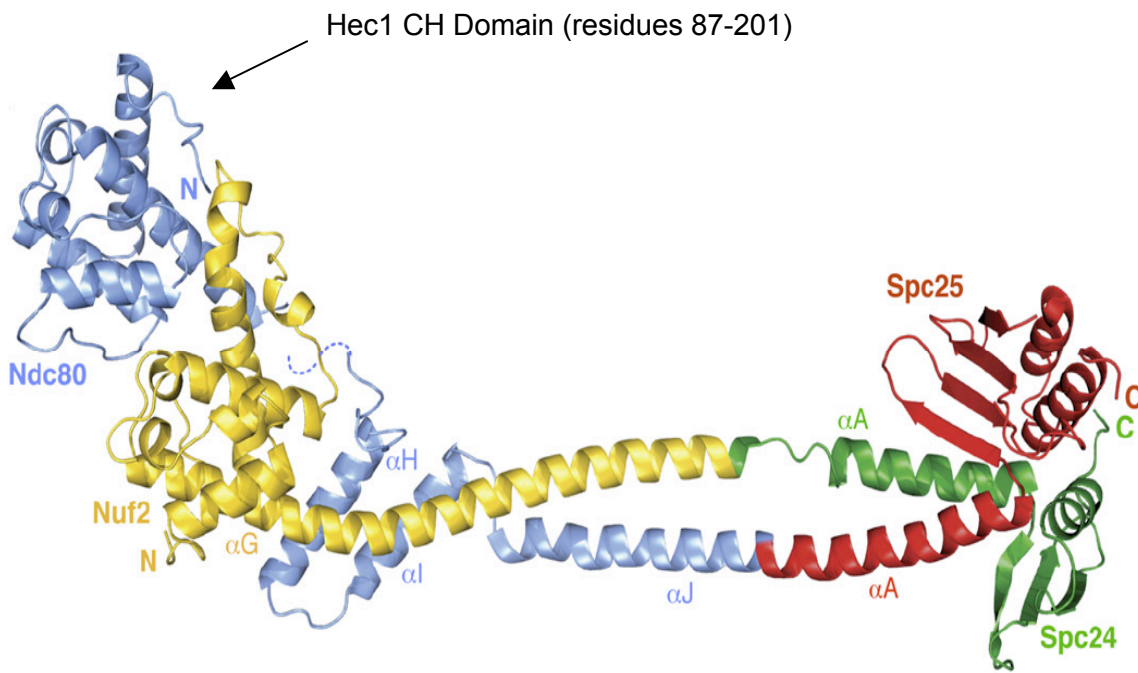


Figure 1.5: Model for multiple Ndc80 complexes binding to a MT

Approximately 25 Ndc80 complexes bind to a single MT penetrating into the outer kinetochore, here only 6 Ndc80 complexes are shown for representation. This work agrees with the originally proposed “Hill Model” (Hill, 1985), stating that multiple low affinity binding sites would comprise the MT binding pocket, and allow for biased diffusion of these MT-coupling proteins.



(Ciferri et al., 2008)

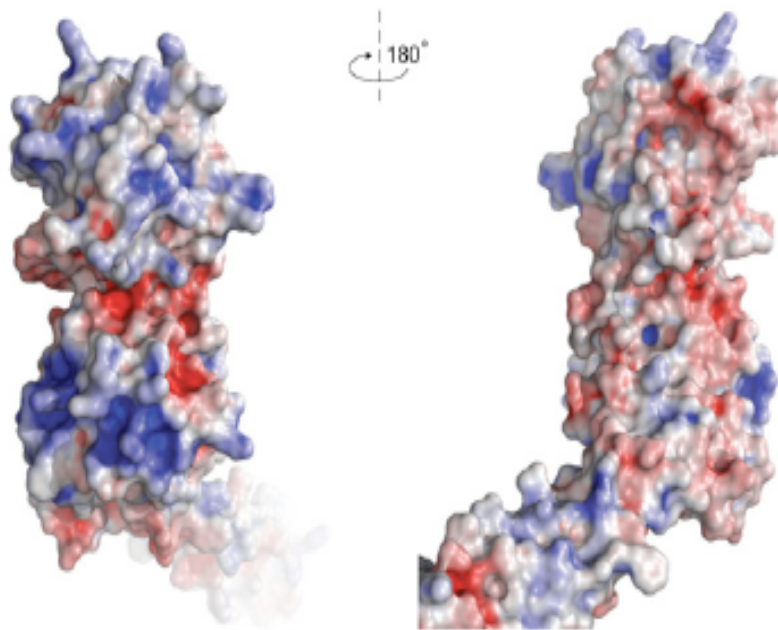
Figure 1.6: Crystal structure of an engineered Ndc80 complex (Ndc80^{Bonsai})

Crystal structure of the Ndc80^{Bonsai} complex, which is lacking much of the coiled-coil domain linking the Hec1/Nuf2 dimer to the Spc24/Spc25. The coiled-coiled domain was removed to induce stability in the complex (Ciferri et al., 2008). The Hec1 CH domain, existing within the N-terminal globular region of of Hec1, is indicated. The 80 amino acid tail domain of Hec1, which extends off the Hec1 CH domain, is not shown, as the intrinsic disorder inherent to this region precludes it's crystallization.

binding for other CH domain containing proteins [51]. The crystal structure of the Hec1 CH domain (residues 87-201) revealed patches of positively charged residues that were shown to be important for MT binding [45] (Figure 1.7). However, the CH domain alone has been shown to bind poorly to MTs, and suggests that an additional region of the Ndc80 complex is required for MT binding [50]. Preceding the CH domain of Hec1 is an unstructured N-terminal 80 amino acid tail domain [45]. This tail domain is critical for MT binding *in vitro* [50], and *in vivo* has been found to be essential for both establishment and regulation of tension generating kinetochore-MT attachments [52, 53]. Cooperativity of Ndc80 complex binding along the MT lattice has been observed *in vitro*, and is suggested to be essential for MT binding [34, 54]. Interestingly, the 80 amino acid Hec1 tail domain has been implicated in Ndc80 complex oligomerization as removal or phospho-manipulation of the tail domain impairs Ndc80 complex clustering along the MT lattice *in vitro* [55].

1.4 Chromosome Movements and Kinetochore-MT Dynamics

During chromosome congression, the dynamic association between kinetochore-MT bundles and the kinetochore is essential for metaphase plate formation and a subsequent faithful progression through mitosis. Despite maintaining attachments to microtubules throughout mitosis, the kinetochore also allows for tubulin subunit addition and subtraction to dynamically unstable MT polymers as they switch between phases of growth and shrinkage [56]. Initial experiments done in the absence of ATP, thus eliminating the possibility of motor driven movements, were used to demonstrate that coupling the energy of MT depolymerization/polymerization to the kinetochore could sufficiently produce the force needed in chromosome movements [57]. Specifically kinetochore-MT interactions are capable of generating as much as 700pN, forces which ultimately aid in kinetochore oscillations needed for bi-orientation and metaphase plate formation [58]. As the name implies, “directional instability of kinetochores”, describes the coordinated pushing and



(Modified Ciferri et al., 2008)

Figure 1.7: Surface views representing the electrostatic potential for the Hec1 and Nuf2 CH domains

Surface representation of the charge distribution along the Hec1/Nuf2 CH domains. Blue = positive charge, Red= negative charge. The charged faces displayed on the Hec1/Nuf2 CH domains have been shown to be important for Ndc80-MT binding (Ciferri et al., 2008). Specifically, charge reversal mutation to residue K166 of the Hec1 CH domain has been shown to be most detrimental.

pulling of kinetochores along the equatorial axis of the cell, ultimately yielding kinetochore oscillatory movements [59]. Kinetochore oscillations are made possible by the unique ability of the kinetochore to bind dynamic k-fibers during polymerization and depolymerization events. Evidence supports a model whereby the kinetochore is capable of switching a majority of the MT fibers in a kinetochore-MT bundle between states of MT polymerization or depolymerization in response to tension; high tension on one side of the sister-kinetochore pair promotes polymerization, while the low tension experienced by the opposing sister kinetochore pair would convert MT dynamics to a state of depolymerization [59]. Synchronizing the pushing and pulling on either side of the kinetochore is thought to coordinate chromosome movements essential to the alignment process [59]. Still, how the kinetochore can remain tethered to growing and shortening microtubules remains a long-standing question in the field.

The “Hill model” originally proposed that coupling the kinetochore to dynamic kinetochore-MT bundles was made possible on the basis of biased diffusion [4]. In such a model, the kinetochore is composed of multiple weak affinity binding sites that form a “sleeve” to which the plus end MT tip can insert into, and allow for addition or subtraction of tubulin subunits to the MT polymer [60-62]. The biased diffusion model suggests that the energy released from MT bundles during depolymerization is used to “slide” the kinetochore down the shortening MT lattice, while the kinetochore can “track” along the MT lattice during periods of MT polymerization; importantly, in either a growing or shortening MT state, the kinetochore can track along the lattice, provided the rates of MT growth/shrinkage are not too fast relative to the sleeve’s tracking ability. In support of this model, the Ndc80 complex has been demonstrated to generate load-bearing attachments capable of diffusion along the MT lattice *in vitro* [54]. In cells, the multiple copies of the Ndc80 complex at the kinetochore may serve as the multiple low affinity MT binding couplers first described in the Hill Model.

While certain aspects of the Hill model are likely to hold true [54], a “modified Hill model” may better describe the regulation of kinetochore-MT interactions. Specifically, the ability to modulate binding affinities at the kinetochore-MT interface could serve as an important switch needed for tethering kinetochore-MT interactions during stochastic changes in MT polymerization/depolymerization. The Ndc80 complex is particularly attractive as a link between the kinetochore and MTs in a “modified Hill model”, in that Ndc80-MT affinity can be manipulated through phosphorylation events induced by the mitotic kinase, Aurora B [63]. Work in the field supports an electrostatic-based model of interaction between the basic tails of Hec1 and the acidic tails of tubulin [45] (Figure 1.8). Regulation of this electrostatic interaction has been shown to be dependent upon phosphorylation status of the Hec1 tail domain, both *in vivo* and *in vitro* [64]. While traditionally thought to correct improper kinetochore-MT attachments Aurora B kinase-mediated phosphorylation of the Ndc80 complex may also serve a role in coordinating the kinetochore-MT attachment status on both sides of the sister-kinetochore pair in a “modified Hill model”. Ultimately, phosphorylation of the Hec1-MT binding interface could be used to modify the kinetochore-MT interaction, and in turn, regulate the forces produced from kinetochore oscillations and chromosome alignment.

1.5 Ndc80 as a Participant in the Spindle Assembly Checkpoint (SAC)

In addition to its contributions in generating attachments at the kinetochore-MT interface, the Ndc80 complex has also been implicated in monitoring these attachments via interactions with the highly conserved spindle assembly checkpoint (SAC) [22]. The SAC serves as a safety device that prevents aneuploidy in cells with chromosomes lacking proper MT attachments, by inhibiting these cells from progressing into anaphase [22]. Functionally, an active SAC inhibits Cdc20, a cofactor necessary for signaling to the anaphase promoting complex/cyclosome (APC/C), and in doing so inhibits anaphase onset

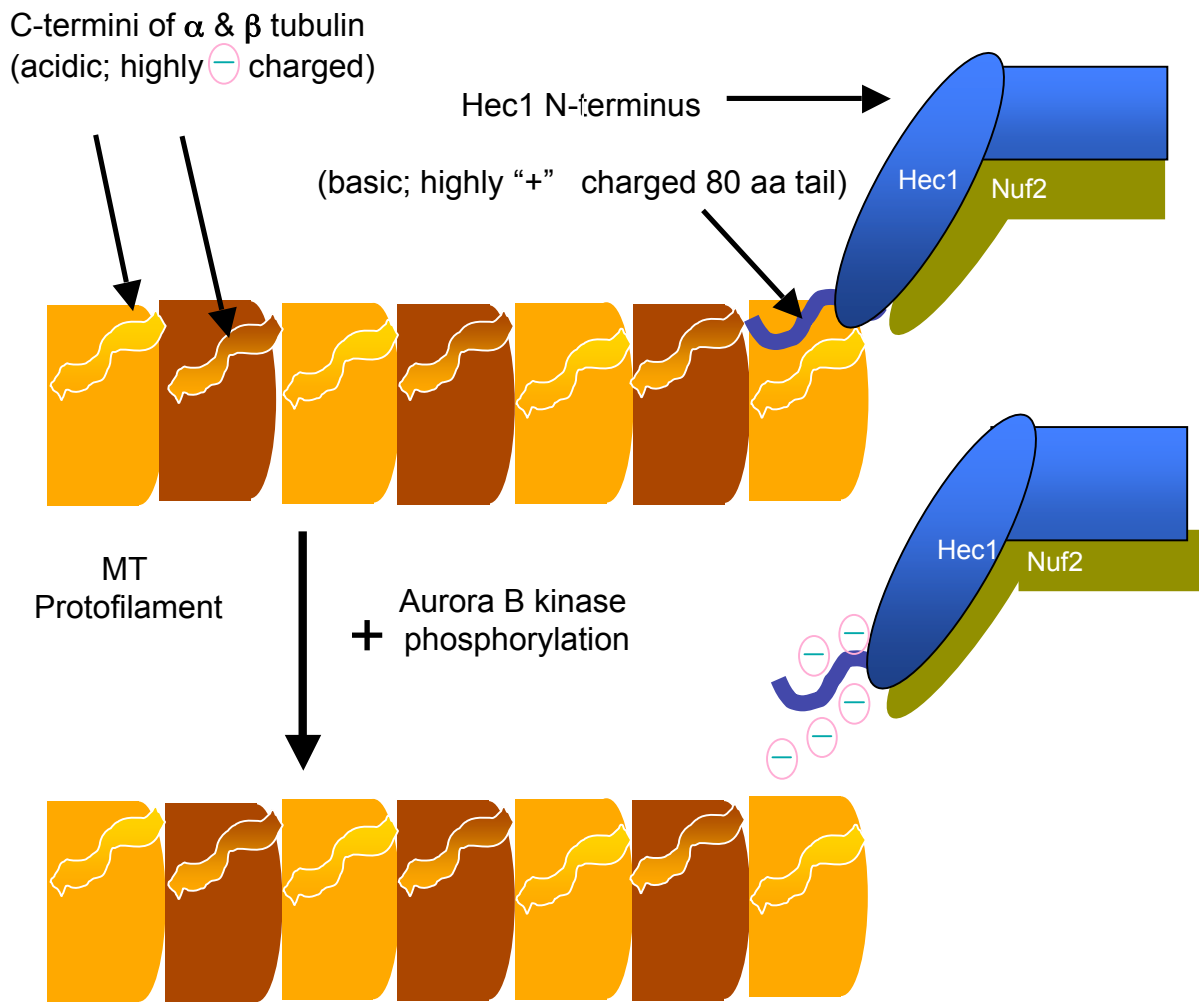
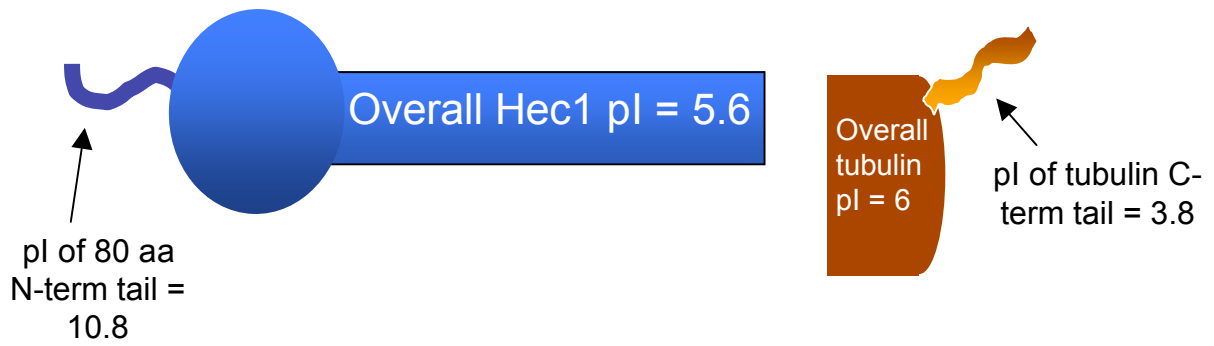


Figure 1.8: Model for binding and regulation of an electrostatic interaction between the 80 amino acid tail domain of Hec1 and the C-terminal tails of tubulin

Under conditions when the Hec1 tail domain is in an unphosphorylated state, an electrostatic binding potential with the C-terminal tails of tubulin exists. However, upon Aurora B kinase phosphorylation of the Hec1 80 amino acid tail domain, the charge on the Hec1 tail drops resulting in a dampened interaction with the C-terminal tails of tubulin.

[65]. However, when the cell has satisfied the SAC's requirements, SAC activity is dampened and Cdc20 activates the APC/C. An active APC/C functions as an E3 ubiquitin ligase that targets mitotic-arresting proteins for degradation once kinetochore-MT attachments are stabilized. Two such proteins targeted by the APC/C are securin and cyclin B, both of which function to arrest a cell in a metaphase state prior to anaphase onset. With degradation of securin and cyclin B, a cell is capable of proceeding through metaphase and entering into anaphase [22].

In instances where cells lack proper kinetochore-MT attachments, a paramount responsibility of a cell is to efficiently activate and amplify its SAC. Two important SAC proteins are Mad2 and BubR1, which are recruited to chromosomes with improper MT attachments and inhibit Cdc20, thus stalling the APC/C. Via a yeast two hybrid assay, previous work has demonstrated an interaction between Hec1 and Mad1, a known recruitment factor for Mad2 [38]. However, how Hec1 functions in Mad2 recruitment to kinetochores is still unknown.

Chapter 2

Materials and Methods

2.1 Cell Culture, Plasmids, siRNA and Transfection Protocols

2.1.1 General PtK1 Cell Culture

PtK1 is a rat kangaroo kidney epithelial mammalian cell line chosen for our experiments as they remain flat during mitosis and have a low number of large chromosomes, both features making this cell line optically favorable for imaging techniques. PtK1 cells were incubated at 5% CO₂ concentration and a temperature of 37°C. For fixed cell analysis, cells were cultured on sterile #1.5 22 mm x 22 mm coverslips. Alternatively, #1.5 glass-bottom 35mm culture dishes were used for live cell analysis. For growth in a T75 flask, 300,000 cells were seeded and cultured in Ham's F-12 Medium (Invitrogen, cat#11765) supplemented with 10% FBS and 1% antibiotic-antimycotic, which was replenished daily. Cells were grown to no higher than 90% confluency before splitting again. After no more than 35 passages a new stock of PtK1 cells was thawed to reduce the chance that mutations accumulated over time contributed to the phenotypes described in the results.

For nocodazole (Sigma) experiments, cells were treated with 20 µM of the drug for 1 h at 37°C and then either fixed for immunostaining or time-lapse imaged (both described below). For cold induced microtubule depolymerization assays, cells were lysed for 5 min at 20°C with 0.5% Triton X-100 in PHEM buffer (60 mM PIPES, 25 mM HEPES, 10 mM EGTA, 4 mM MgSO₄, pH6.9) plus 10 mM ATP. Cells were subsequently incubated at 4°C in a calcium-containing buffer (60 mM PIPES, 25 mM HEPES, 4 mM MgCl₂, and 10 mM CaCl₂, pH 7.0) for 60 min. Cells were then processed for immunofluorescence (described below).

2.1.2 Hec1 siRNA

The sequence for PtK1 *Hec1* was determined using degenerate primers and reverse transcriptase PCR (RT-PCR) as previously described [66]. Briefly, Hec1 nucleotide sequences from *Xenopus laevis*, *Gallus gallus*, *Homo sapiens*, and *Mus musculus* were aligned using the Clustal W program (<http://www.ebi.ac.uk/Tools/clustalw2/index.html>). Both 5' and 3' degenerate primers were designed to flank a region of approximately 1000 base pairs of Hec1 nucleotide sequence. RNA was isolated from PtK1 cells (Mo Bio RNA isolation kit) and RT-PCR was carried out using the 5' and 3' degenerate primers and PtK1 RNA as a template. The amplified PCR fragment was sequenced and aligned with the human Hec1 sequence. A PtK1-specific small, interfering RNA (siRNA) that differed in nucleotide sequence from the human Hec1 sequence was designed so that the siRNA was specific to PtK1 cells, while human Hec1 constructs would be resistant. This feature was essential to the silence and rescue strategy (described below). The Hec1 siRNA (UGAGCCGAAUCGUCUAAUUAU) was ordered from Qiagen.

2.1.3 Hec1 Plasmids

All of the Hec1 constructs were cloned into the pE-GFP N1 vector. In the pE-GFP N1 vector, proteins were C-terminally labeled with a GFP fusion protein. Labeling to the C-terminus of Hec1 was preferred over N-terminal labeling of Hec1, as previous work had indicated that the N-terminal region of Hec1 was required for kinetochore-MT attachment.

2.1.4 Oligofectamine Transfection Protocol

Knockdown: Oligofectamine (Invitrogen, cat#12252-011) is a lipid-based solution used for cellular transfections. Knockdown (“silence”) experiments were performed when Hec1 was to be depleted from cells. Cells were transfected with Hec1 siRNAs using

Oligofectamine (Invitrogen) or mock transfected with Oligofectamine alone. For one coverslip, 4 μ L of Oligofectamine were incubated at room temperature with 46 μ L of OptiMem (Invitrogen) for 5 min with periodic flicking of the tube to mix. After incubation, 8 μ L of 20 μ M siRNA and 142 μ L of OptiMem were added to the tube and incubated for 20-30 min at room temperature with periodic flicking to mix. Following incubation, the solution was added to 800 μ L of Optimem + 10% FBS and added to cells grown on a coverslip in a 6-well dish or 35 mm glass bottom Petri dish. Cells were supplemented with 1 mL of OptiMem + 10% FBS 24 h post-transfection, and assayed at 48 h post-transfection.

Silence/rescue: Co-transfection experiments were used when endogenous Hec1 was to be targeted for knockdown in PtK1 cells and subsequently rescued with siRNA resistant human Hec1-GFP fusion constructs. For coverslips, 7 μ L Oligofectamine were incubated at room temperature with 143 μ L of OptiMem (Invitrogen) for 5 min with periodic flicking. After incubation, 8 μ L of 20 μ M siRNA, 1 μ L of plasmid DNA (1 mg/mL), and 142 μ L of OptiMem were added to the tube and allowed to incubate with periodic flicking for 20-30 min at room temperature. Following incubation, the solution was added to 2 mL of Optimem + 10% FBS and added to a coverslip in a 6-well dish or 35 mm glass bottom Petri dish. Cells were supplemented with 1 mL of OptiMem + 10% FBS 24 h post-transfection and assayed at 48 h post-transfection.

2.1.5 Nucleofector Transfection Protocol

The Nucleofector (Lonza, Germany) is an electroporation based transfection apparatus. Well into my studies we discovered that the Nucleofector resulted in a better transfection efficiency and also appeared to be a milder treatment on the cells. In a T75 flask PtK1 cells were grown to 90% confluency, trypsinized and resuspended in 7 ml of Opti-MEM to yield approximately 2 million cells. A hemocytometer was used to count

cells. A half million cells were sufficient to make up one Nucleofector reaction, and they were transferred with Pasteur pipette into a 15 ml conical tube. The cells were pelleted by centrifugation for 4 min at 120 g and 25°C. Once the pellet was formed, excess Opti-MEM medium was aspirated leaving just the cellular pellet. The cellular pellet was then resuspended gently in the Nucleofector reaction mixture: 100 µL of Nucleofector cocktail mixture, 4 µg of DNA, and 8 µl of a 20 µM stock siRNA solution. The mixture of cells, Nucleofector cocktail mixture, DNA and RNA was then transferred to an electroporation cuvette (Lonza) and subjected to the Nucleofector electroporation using program number T-020 corresponding to the PtK1 cell line (the program number is cell line specific). Cells were immediately plated on acid washed glass coverslips (VWR, cat#16004-302) or into glass bottomed dishes (MatTek, cat#P35G-1.5-20-C) containing 2 ml of Optimem+10% FBS at 37°C. 24 h post-transfection, the medium was completely aspirated from the dish and a fresh 2 ml of Optimem+10% FBS was added to the cells. 48 h post-transfection cells were prepared for fixation or live cell imaging (described below).

2.2 Immunofluorescence, Microscopy, Fixed and Live Cell Measurements

2.2.1 Immunofluorescence Solutions/Buffers

PHEM: 60 mM PIPES, 25 mM HEPES, 10 mM EGTA, 4 µM MgSO₄, pH 7.0.

2X PHEM: 120 mM PIPES, 50 mM HEPES, 20mM EGTA, 8 µM MgSO₄, pH 7.0.

0.1% PHEM-T: PHEM + 0.1% Triton X-100 sonicated for 10 min in sonicator bath. Made fresh prior to use.

0.5% PHEM-T: PHEM + 0.5% Triton X-100 sonicated for 10 min in sonicator bath. Made fresh prior to use.

Permeabilization Buffer: PHEM + 0.5% Triton X-100 sonicated for 5 min in sonicator bath. Made fresh prior to use.

Fixative: 16% stock paraformaldehyde solution (Ted Pella, cat#18505) was diluted to 4% in PHEM buffer.

10% Boiled Donkey Serum (BDS): 10 ml of lyophilized normal donkey serum (Jackson ImmunoResearch, cat#017-000-121) was mixed with 25 ml double-distilled water and boiled for 10 min. 2X PHEM buffer was added to bring to the final total volume of solution to 50 mL and sodium azide to a final concentration of 0.05%. Solution was centrifuged using a JA-20 rotor (Beckman) for 1 h at 40,000xg. The solution was filtered through a 0.22 µM filter and store at 4°C.

4',6-diamidino-2-phenylindole (DAPI): (Invitrogen, cat#D3571) Diluted to 10,000 fold to 10 ng/ml from a 100 µg/ml stock solution in water.

Mounting Medium/Antifade Solution: 0.5% *N*-propyl gallate (AlfaAesar, cat#A10877) was dissolved in a solution of 90% glycerol diluted in PHEM buffer.

Primary Antibodies: The primary antibodies used were: anti- α -tubulin antibody DM1- α , 1:300 (Sigma, cat#T9026); anti-Hec1 antibody 9G3, 1:2000 (Abcam, cat#3613); anti-centromere antibodies, 1:300 (Antibodies, Inc., cat#15-134). All primary antibodies were diluted in 5% boiled donkey serum in 1xPHEM buffer.

Secondary Antibodies: The secondary antibodies used were: donkey anti-human IgG, Cy-5 conjugated (Jackson Immuno Research, cat#709-175-149); donkey anti-mouse IgG, rhodamine Red-X conjugated (Jackson Immuno Research, cat#715-486-150). All secondary antibodies were diluted 1:300 in 5% boiled donkey serum in 1xPHEM buffer.

Microscope Slides: (VWR, cat#16004-368)

2.2.2 Immunofluorescence Fixation Procedure

1xPHEM, 0.5% PHEM-T and 4% paraformaldehyde were heated to 37°C in a water bath. Because these solutions were used to treat the cells before a final fixation step, the sensitivity that MT polymers have to temperature requires that these solutions were

heated to 37°C to ensure that thick bundles of MT polymers are maintained. To prepare a fixation chamber, the bottom of a large glass dish was covered with moist filter paper, followed by laying a strip of parafilm atop the moist filter paper, and layering moist KimWipes along the sides of the glass dish. The dish was kept hydrated with the moist filter paper/KimWipes, as this prevents evaporation of small volumes of solutions during incubation periods. During the fixation/staining process transitioning from one solution to the next solution requires complete aspiration of the initial solution followed by the addition of approximately 200 µl of the next solution. All steps were carried out at room temperature unless otherwise noted.

Once the fixation chamber and solutions reached 37°C, coverslips were removed from the Petri dishes in which they were grown and rapidly placed atop the parafilm in the fixation dish at room temperature. The first wash was performed with 1xPHEM (37°C) for 10 s. An initial quick fixation was then performed for 10 s with 4% paraformaldehyde (37°C). This initial fixation was done to assist in cell adherence to the coverslip, which becomes important during subsequent cell permeabilization steps. Following the quick fixation, 0.5% PHEM-T (37°C) was added to permeabilize the cells. The fixation dish was then returned to the 37°C incubator for 5 min to minimize depolymerization of MTs that might occur if the cells cooled. After permeabilization, the coverslips were again treated 4% paraformaldehyde fixative, and incubated at 37°C for 20 min. During this step the internal structures of the cells were preserved in a fixed state. A 10 s wash with 1xPHEM was performed to remove residual 4% paraformaldehyde. Next, 3x5 min 0.1% PHEM-T washes were performed, and were followed with a quick wash in 1xPHEM. Coverslips were then blocked for 1 h in 10% boiled donkey serum (BDS) to reduce non-specific binding of primary antibodies. The primary antibody mixture was next applied to the cells and allowed to incubate overnight

at 4°C in the hydrated fixation chamber sealed with saran wrap to prevent solution evaporation. The next day, coverslips were rinsed 3x5 min with 0.1% PHEM-T, followed by a 1xPHEM quick rinse. Cells were then treated with fluorescently-conjugated secondary antibodies and allowed to incubate for 45 min at room temperature protected from the light. Non-specific secondary antibody staining was then rinsed off with 3x5 min 0.1% PHEM-T washes, followed by a quick rinse in 1xPHEM. The chromosomes were then fluorescently stained by incubating for 1 min at room temperature in 4',6-diamidino-2-phenylindole (DAPI). Following 2x5 min washes in 0.1% PHEM-T coverslips were drained, blotted, gently at the edge of KimWipe to remove buffer, and mounted in 10 µl of mounting medium on ethanol cleaned microscope slides. Gently, a KimWipe was placed on top of the coverslips to wick away extra fluid. To seal, nail polish was applied along the side of the coverslip. Coverslips were stored in the dark at 4°C.

2.2.3 Delta-Vision Microscope

Fixed and live cell image acquisition was carried out on a DeltaVision Personal DV Imaging System (Applied Precision, Issaquah, WA) equipped with a Photometrics CoolSnap HQ2 camera (Roper Scientific, Sarasota, FL) and either a 60X/1.42NA Planapochromat DIC oil immersion lens (Olympus) or a 100x/1.30NA Phase Planapochromat oil immersion lens (Olympus). For all live-cell imaging, stage temperature was maintained at 37°C with an environmental chamber. A 20X/0.5NA Phase Planapochromat objective (Olympus) was used for low magnification time-lapse imaging. For these experiments, transmitted light and fluorescence images were collected every 3-5 min for 10 h.

2.2.4 Fixed Cell Microscopy Measurements

Fluorescence Intensity: The relative intensity of a test protein was measured as

previously described [67], by determining the ratio of its fluorescent intensity as compared to the corresponding fluorescent intensity of the stable kinetochore marker, anti-centromere antibody (ACA). When determining the knockdown efficiency via fluorescence intensity, the ratio of test protein to ACA and the ratio of test protein to ACA in the presence of siRNA were first measured. Subsequently, the percentage of fluorescence observed in the knockdown as compared to the control was determined.

Inter-Kinetochore Distance:

Data Acquisition: The DeltaVision microscope was used to acquire Z-stack images of mitotic cells, using 200 nm step sizes and a total thickness of approximately 10 μm (cell dependent).

Measurement Procedure: The SoftWorx analysis program was used to measure the distance from kinetochore marker centroid to kinetochore marker centroid of sister kinetochore pairs. To ensure that distances between kinetochore centroids were accurately taken, only sister-kinetochores with maximal fluorescent intensity in same z-plane of focus were measured. “Rest length” measurements were obtained from control prophase cells which lack kinetochore-MT attachments, and were thus under no tension. Conversely, the distance correlating with a full establishment of tension was measured from control metaphase cells, where sister-kinetochores have accumulated a full complement of MT attachments. Depending on the phenotype arising from cell treatments (drug induced, or silence/rescue induced), the inter-kinetochore distance values indicated whether attachments were destabilized, unaffected, or hyper-stabilized. Statistical analysis was performed using a student’s t-test.

Percent End-Associated Kinetochore-MT Attachments:

Data Acquisition: The DeltaVision microscope was used to acquire Z-stack images of mitotic cells, using 200 nm step sizes and a total thickness of approximately 10 μm (cell dependent).

Measurement Procedure: Using the SoftWorx analysis program, the images corresponding to the MTs and kinetochores were overlaid at each plane in the z-position. These overlays were then built into a z-stack of the entire cell. Scrolling up and down through the z-stack of the cell, one could determine if a MT is bound at a kinetochore based on 1) overlap of the two channels as well as 2) termination of the overlapping MT within the kinetochore (indicative of a MT that has penetrated into a kinetochore). Depending on the phenotype arising from experimental treatment to cells (drug induced, or silence/rescue induced), the percent of kinetochores with MT bundles penetrating into them indicated whether attachments were destabilized, unaffected, or hyper-stabilized. Statistical analysis was performed using a student's t-test.

2.2.5 Live Cell Microscopy Measurements

Oscillation Movie Measurements

Data Acquisition: Cells expressing a Hec1-GFP fusion protein (Nucleofector silence/rescue) were cultured on #1.5 glass-bottom 35mm culture dishes for live cell analysis. The day of filming (48 h post-Nucleofection) cultured medium was removed and replenished with 2 ml of filming media (37°C) over-layered with 1 ml of mineral oil (37°C). The lid was returned to the top of the culture dish, which was placed in the DeltaVision environmental chamber where it was allowed to incubate at 37°C for approximately 10 min. It was essential that the culture dish reach 37°C, as slight temperature changes could result in thermal chromosome movements that disrupt

tracking of kinetochore oscillations. Hec1-GFP expressing mitotic cells in a metaphase-like state with a partially aligned plate were identified, and the presence of Cy-5 Hec1 siRNA was confirmed. For filming purposes, it was important that cells with a true metaphase plate were not chosen, as in the 10 min of filming, these would often approach or enter anaphase, where dynamics of chromosome oscillation dampen dramatically. By choosing cells in a partially aligned state, the dynamics of oscillations remained high, and alignment continued within the 10 min of filming while avoiding anaphase onset. The central plane of focus was selected by choosing cells with multiple kinetochore pairs located in the center/interior of the bi-polar spindle where kinetochore-MT dynamics were most robust. For time-lapse experiments, Z-stacks containing 3 images 500 nm apart were taken, with the central plane of focus serving as the middle of the Z-stack. By collecting a Z-stack that could later be maximally projected into a single image, it was possible to track kinetochore pairs that drifted slightly above or below the original central plane of focus. Z-stacks were collected every 3 s for 10 min. To prevent photobleaching of other cells on the dish, GFP exposure was set to 100% transmittance for 0.175 s and the fluorescence diaphragm was closed down. Once the image collection was complete, maximal projections of individual Z-stacks were made and represent an individual frame in the 10 min oscillation movie. Each frame in the time-lapse was then converted into a TIFF and was imported into MetaMorph for analysis described below.

Measurement Procedure: Kinetochore movements were first tracked in MetaMorph, and then parameters of velocity, percent pause, and deviation from average position (DAP) were measured from the same data set. In MetaMorph, the TIFF images produced from the maximal projections of the oscillation movies were built into a movie by using the commands “File→Open Special→Build Stack→Quick” or by

simply hitting “Control+Q” and selecting the first TIFF in the movie. With the movie built in MetaMorph, a calibration of the images (“Measure→Calibrate Distances”) was required to ensure that pixel-to-pixel distances correlate with the original objective used for data acquisition (if using the 60X/1.42NA Planapochromat DIC oil immersion lens, then calibration is; $X=0.067$, $Y=0.067$). With the quick stack distances properly calibrated, “Apps→Track Points” was selected and the Track Points window appeared. Finishing calibrations to the quick stack, the time interval (if following the protocol from above, 3 s) between each frame in the movie was set by selecting the “Set Interval” tab in the “Track Points” window. Next, by selecting the tab “Configure Log” in the “Track Points” window, the parameters to be measured and eventually exported in an excel sheet were selected. The important parameters selected for export are: Image Name, Track #, X, Y, Distance, Time Interval, Velocity, and Distance To Origin. The data collected in MetaMorph was transferred to Excel by establishing a log file. To do this, “Track Points→Open Log→Dynamic Data Exchange (DDE) →OK” was selected, after which an “Export Log Data” window appeared, and the following parameters were selected for “Application: Microsoft Excel, Sheet Name: Sheet 1, Starting Row: 2, Starting Column: 1”. Lastly, an origin from which all kinetochores were measured against was set in the quick stack. “Set Origin” was selected from the “Track Points Window” after which a point in the quick stack was selected, and the origin was set. With calibrations completed, parameters to be exported selected, an origin set, and the excel log file setup, the kinetochore tracking now took place. When selecting a kinetochore pair for tracking, it was important to first scroll through the movie and select a kinetochore pair in which both sister kinetochores stayed in focus for the duration of the movie and resided within the interior of the bi-polar spindle where the most robust oscillation dynamics were

observed. With a kinetochore pair chosen, the “Add Track” tab in the “Track Points” window was selected, and the center of the kinetochore pair closest to the point of origin that was originally marked was clicked on (It was important to keep this method of tracking consistent, as downstream calculations depended on the order in which kinetochore pairs were selected). Upon clicking on the kinetochore pair, the position of this pair was recorded in MetaMorph, and the next frame in the stack was automatically brought up. The center of the kinetochore pair was continually clicked on, until completion of the movie. After clicking through every frame in the movie, “Done” was selected to store the data. The opposite sister-kinetochore pair was then tracked by selecting “Add Track” in the Track points window. This process of tracking kinetochores was done for all measurable sister kinetochore pairs, after which “F9 Log Data” was selected to export the data to an excel file. With all of the data collected, velocity measurements could now be calculated.

Average Velocity- With the excel sheet produced from the MetaMorph oscillation analysis, the column labeled “Velocity” represents the kinetochore velocity observed as a kinetochore shifted from a position in one frame, to a different position 3 s later in the next frame. Thus, to obtain the average velocity for an individual kinetochore, the data from this column was averaged. Statistical analysis was performed using a student’s t-test.

Timing Through Mitosis (Live Cell DIC):

Data Acquisition: Cells expressing a Hec1-GFP fusion protein (Nucleofector silence/rescue) were cultured on #1.5 glass-bottom 35mm dishes for live cell analysis. The day of filming (48 h post-Nucleofection) live cell dishes were first aspirated of their cultured medium is removed, and replenished with 2 ml of filming

medium (37^o) layered with 1 ml of mineral oil (37^oC). The lid to the dish was left off because its presence reduces the quality of the DIC images. The dish was moved into the environmental incubation chamber of the DeltaVision microscope where it was allowed to incubate at 37^oC for approximately 10 min. Hec1-GFP expressing prophase cells were identified, and the presence of Cy-5 Hec1 siRNA was confirmed. The center of the cell was identified via DIC, where a clear image of the chromosomes was chosen. For time-lapse experimentation, a DIC image was taken at the center of the cell every 3 min for 3 h. Of note, if the focus on the center of the cell was lost, or the cell moved, the image could be adjusted in-between the 3 min time intervals. Time-lapse imaging was stopped for cells that entered anaphase before 3 h.

Measurement Procedure:

Calculation of the timing through mitosis was performed using the SoftWorx analysis program. Nuclear envelope breakdown marked time point 0 and occurred when the condensed mass of chromosomes was liberated from the nuclear envelope and spilled out into the cytoplasm of the cell. Anaphase onset was defined by the initial separation of sister chromatids into two daughter cells. Statistical analysis was performed using a student's t-test.

Chapter 3

Kinetochores-microtubule attachment relies on the disordered N-terminal tail domain of Hec1

3.1 Introduction

Accurate chromosome segregation is dependent upon stable attachment of kinetochores to spindle microtubules during mitosis. At the onset of nuclear envelope breakdown in mitosis, microtubules (MTs) emanating from duplicated centrosomes of the mitotic spindle probe the cell in a “search and capture” mechanism looking to make contact with chromosomes [7]. Upon an initial lateral-based interaction between a chromosome and MT, a rapid dynein directed poleward movement transports chromosomes along the MT lattice towards the centrosome from which the MT originated [68]. Once positioned proximal to the centrosome, the chromosome experiences an environment densely populated with MTs nucleating from the centrosome [7]. Eventually, a stable interaction between the kinetochore and a MT is established when a MT directly penetrates into a kinetochore. A number of similar end-associated kinetochore-MT attachments form and establish a stable kinetochore-MT bundle. The association between the kinetochore and MTs has a stabilizing effect on MTs [69]. Together the kinetochore-MT bundle and polar ejection forces, produced from non-kinetochore bound MTs pushing on chromosome arms, aid in chromosome positioning towards the equator of the cell. Once repositioned at the cell's equator, kinetochore-MT attachments are established on the opposite sister kinetochore. When both sister-kinetochores have established a full complement of MT attachments from opposite spindle poles, the chromosome is bioriented. Coupling the kinetochore to growing and disassembling MTs then coordinates chromosome positioning and eventual metaphase plate formation. A long-standing question is how kinetochores maintain stable attachment to the plus ends of dynamic microtubules that are continually

growing and shortening.

The vertebrate kinetochore assembles on the primary constriction site of chromosomes, and is comprised of over 100 different proteins [2]. The vertebrate kinetochore is essential for mitotic progression and the partitioning of sister chromatids into two daughter cells via regulation of load bearing interactions with spindle MTs [70]. Of particular interest to the field is the highly evolutionarily conserved Ndc80 complex, comprised of four proteins; Hec1, Nuf2, Spc24, and Spc25. Structurally the Ndc80 complex is comprised of two dimers, whereby the C-terminal coiled-coil region of Hec1/Nuf2 associates with the N-terminal coiled-coil region of Spc24/Spc25. Rotary shadow EM and atomic force microscopy have revealed the Ndc80 complex to be a 55 nm long rod-shaped structure, flanked on either end by regions of globular protein [44, 71]. Recent work has demonstrated that the Ndc80 complex is essential for persistent end-on kinetochore-microtubule attachment in cells [34, 47, 50] but how the Ndc80 complex forms functional microtubule-binding sites remains unknown.

Hec1, a component of the Ndc80 complex, is located exterior to the centromere and has been shown to be essential for establishing stable kinetochore-MT attachments [36, 37, 46]. Hec1 is positioned with the N-terminus facing outwards away from the chromosome, poised for an interaction with MTs. Indeed, binding studies have revealed that the Hec1/Nuf2 dimer is capable of directly binding MTs [45]. Structural studies have revealed an unstructured N-terminal 80 amino acid tail (Figure 3.1-B) that extends off of a calponin homology (CH) domain in Hec1 [45]. Cryo-electron microscopy, crystallographic studies and computer reconstitution image analysis have provided insight into the interaction of the Hec1/Nuf2 dimer with microtubules, and these studies implicate both the 80 amino acid tail and CH domains of Hec1 as directly contacting the MT lattice [72]. *In vitro*, a significant reduction in MT binding affinity is observed for “tailless” Ndc80 or charge reversal mutations to the CH domain of Hec1, and further support a role for these domains in MT binding [45,

50].

We show that the 80 amino acid N-terminal unstructured “tail” of Hec1 is required for generating stable kinetochore microtubule attachments. PtK1 cells depleted of endogenous Hec1 and rescued with Hec1-GFP fusion proteins deleted of the entire N terminus or the disordered N-terminal 80 amino acid tail domain fail to generate stable kinetochore-microtubule attachments. Mutation of nine amino acids within the Hec1 tail to reduce its positive charge also abolishes stable attachment. Furthermore, the mitotic checkpoint remains functional after deletion of the N-terminal 80 amino acid tail, but not after deletion of the N-terminal 207 amino acid region containing both the tail domain and a calponin homology (CH) domain. These results demonstrate that kinetochore-microtubule binding is dependent on electrostatic interactions mediated through the disordered N-terminal 80 amino acid tail domain and mitotic checkpoint function is dependent on the CH domain of Hec1.

3.2 Results

3.2.1 Hec1 Depletion from PtK1 Cells Results in Mitotic Defects

We set out to determine the molecular requirements for kinetochore-microtubule attachment *in vivo* by utilizing a silence and rescue system for Hec1 in PtK1 cells. The PtK1 genome is not yet sequenced; thus, to deplete Hec1 with RNA interference (RNAi), we cloned PtK1 HEC1 by using techniques described previously [66]. Consistent with its highly conserved role in chromosome segregation, PtK1 Hec1 is 71% identical to human Hec1 at the amino acid level (Figure 3.1A). Treatment of PtK1 cells with small interfering RNA (siRNA) targeted to Hec1 for 48 h resulted in a reduction of Hec1 in the cell population to approximately 50% of control as determined by western blotting (data not shown). This is probably reflective of poor transfection efficiency, given that cells positively transfected with fluorescently labeled Hec1 siRNA were depleted of kinetochore-bound Hec1 to an average

A

Human	MRKSSVSSGGAGRLSMQELRSQDVNKQGLYTPQTKEKPTFGKLSIN-----KPTSERKVS	
PtK1	MKCSSVSSGAHGRQSMQSLRSQDFNKQGLYTPQTKERPAFWKLSTSRTPGTSTSERKIS	60
Human	LFGKRTSGHGSRNSQLGIFSSSEKIKDPRPLNDKAFIQQCIRQLCEFLTENGYAHNVSMK	
PtK1	LFGKASGPGSRNSLLGVFVGNEKIKDPRPLNDKAFIQQYIRQLYEFLAENGYACGISMK	120
Human	SLQAPSVKDFLKI FTFLYGFCLPSYELPDTKFEEVPRIFKDLGYPFALS KSSMYTVGAP	
PtK1	SLQSPSVKDFLKI FTFFIFAF LSPSYELPDSKFEEIIPRILKDLGYPFTLPKSSMYTVGAP	180
Human	HTWPHIVAALVWLIDCIKIHTAMKESPLFDDGQFWGEEEDGIMHNKFLDYTIKCYES	
PtK1	HTWPHVLASLNWLIDCFKLI FVGKQSSPSFDDGQFWGGESEDGIMHNKFLDYTVKCYEN	240
Human	FMSGADSFDEMNAELQSKLKDLEFNVD AFKLESLEAKNRALNEQIARLEQEREKEPNRLES	
PtK1	FMTGADSFEDLDTELYSKLKDLEFNVDSSKLES LASENKRLTEEIARVEREKENEPNRLIS	300
Human	LRK LKASLQGDVQKYQAYMSNLESHSAILDQKLNGLNEE IARVELECETIKQENTRLQNI	
PtK1	LRKVKASLKADVQKYQAYMNNLESHSSILDQKLSGFNEEVPAVELELEAVKQENARLQSI	360
Human	IDNQKYSVADIERINHERNELQQTINKLTKDLEAEQQKLWNEELKYARGKEA IETQLAEY	
PtK1	MDNQKYSIADIERIHHERNEIQQTIVKKLTTELATEQKQLWNEELKYARSKEAIEAQL E EY	420
Human	HKLARKLKLIPKGAENSKGYDFEIKFNPEAGANCLVKYRAQVYVPLKELLNETEE EINKA	
PtK1	HKLARKLKLIPKSAENSKGYDFEVKFNPEVGTNCLVKYRTQVYIPLKELLNQYEERISSV	480
Human	LNKKMGLED TLEQLNAMITESKR SVRTLKEEVQKLD DLYQQKIKEAEEDEKCASELES L	
PtK1	QHKKMGSEETLEQVNTMVREVKRSTKMLNNEVQKLD FIEQKIKEAEEKDRKCTAEVESL	540
Human	EKHKHLLESTVNQGLSEAMNELDAVQREYQLVVQTTTEERRKVGNNLQR LLEMVATHVGS	
PtK1	DNHKHLES GVN EGPSEAI SELDAIQQQYQLVLQMTTEERRKASSYLQKTLEMVATHIGS	600
Human	VEKHLEEQIAKVDREYEECMS EDLS ENIKEIRD KYEKKATLIK SSEE	
PtK1	VEKYLEDQIGRVDRECEESIT ED FLENIREMGDKY-----	635

Figure 3.1A: PtK1 Hec1 sequence analysis.

(A) Amino acid alignment of PtK1 and human Hec1. Aurora B phosphorylation target sites are denoted with an asterisk (DeLuca et al., 2006; Ciferri et al., 2008). We were unable to obtain sequence for the extreme 3' end of PtK1 Hec1 (approximately 36 nucleotides). The red bar represents the region of the PtK1 sequence targeted by the siRNA.

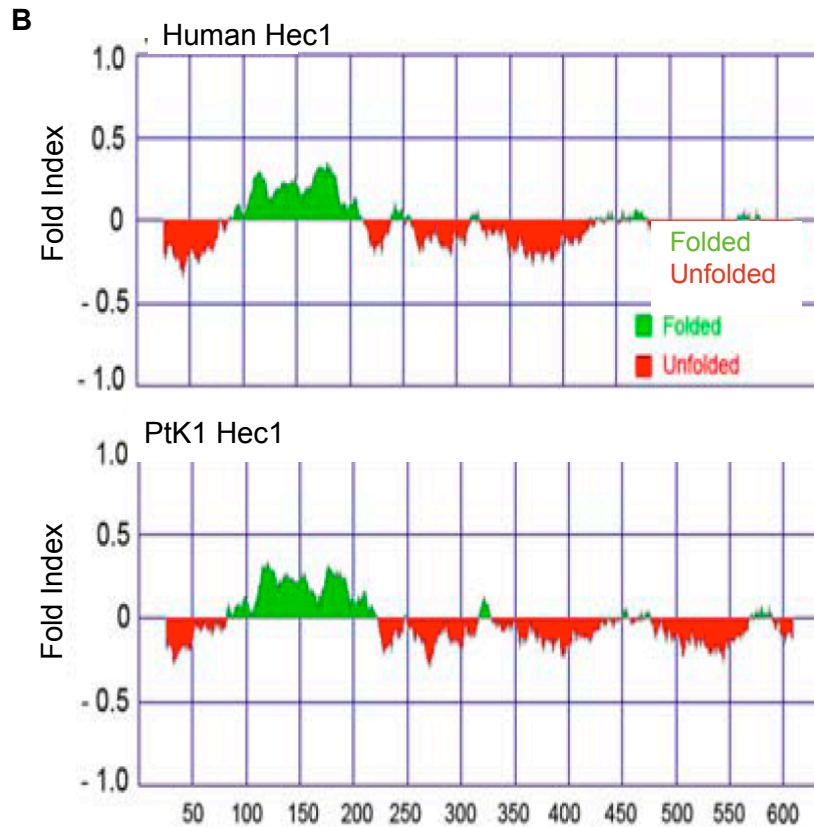


Figure 3.1B: Hec1 intrinsic disorder plots.

(B) Intrinsic disorder plots for Human Hec1 (top) and PtK1 Hec1 (bottom) based on the “Fold Index” algorithm (Prilusky et al., 2005). Red regions are predicted to be intrinsically disordered and green regions are predicted to maintain a stably folded conformation based on parameters including sequence charge and average residue hydrophobicity (Prilusky et al., 2005). The 80 amino acid N-terminal regions of both human and PtK1 Hec1 are largely intrinsically disordered.

of 8%, with many kinetochores from individual cells binding undetectable levels of Hec1, as determined by fluorescence-intensity measurements (Figure 3.2A). Hec1-depleted PtK1 cells were able to form bipolar spindles, but they failed to align their chromosomes at the spindle equator (Figure 3.2B), consistent with findings in other cell types [2, 73]. We determined whether kinetochores were associated with the ends of spindle microtubules by analyzing deconvolved images of PtK1 cells fixed and immunostained for microtubules and kinetochores. On average, only 5% of kinetochores in Hec1-depleted cells contained end-on microtubule attachments, compared to 60% and 84% of kinetochores in early-to-mid-prometaphase and late-prometaphase control cells, respectively (Figure 3.2C). We measured the interkinetochore distance between sister kinetochores to determine whether they were under tension, and we found that, in contrast to mock-transfected cells, Hec1-depleted cells failed to establish tension across sister kinetochores during progression through mitosis (Figure 3.2D). Additionally, Hec1-depleted cells retained few microtubules after a cold-induced microtubule depolymerization assay (Figure 3.2E). Together, these results demonstrate that Hec1 is required for stable kinetochore-microtubule attachment in PtK1 cells. Time-lapse imaging demonstrated that Hec1-siRNA-transfected cells failed to align their chromosomes, but they did not arrest in mitosis and entered anaphase after a 40 min delay when compared to mock-transfected cells (Figures 3.2F and 3.2G, Movies 1 and 2, and Figure 3.3). Hec1-depleted PtK1 cells failed to retain high levels of the spindle-checkpoint protein Mad2 at unattached kinetochores (Figure 3.4), consistent with findings in other cell types [38-40, 74, 75]. The decrease in kinetochore-bound Mad2 was not due to a defect in Mad2 recruitment, given that kinetochores in Hec1-depleted, nocodazole-treated PtK1 cells bound high levels of Mad2 and subsequently arrested in mitosis for approximately 5 h, similar to mock-transfected cells treated with nocodazole (Figures 3.3 and 3.4 and Movies 3 and 4).

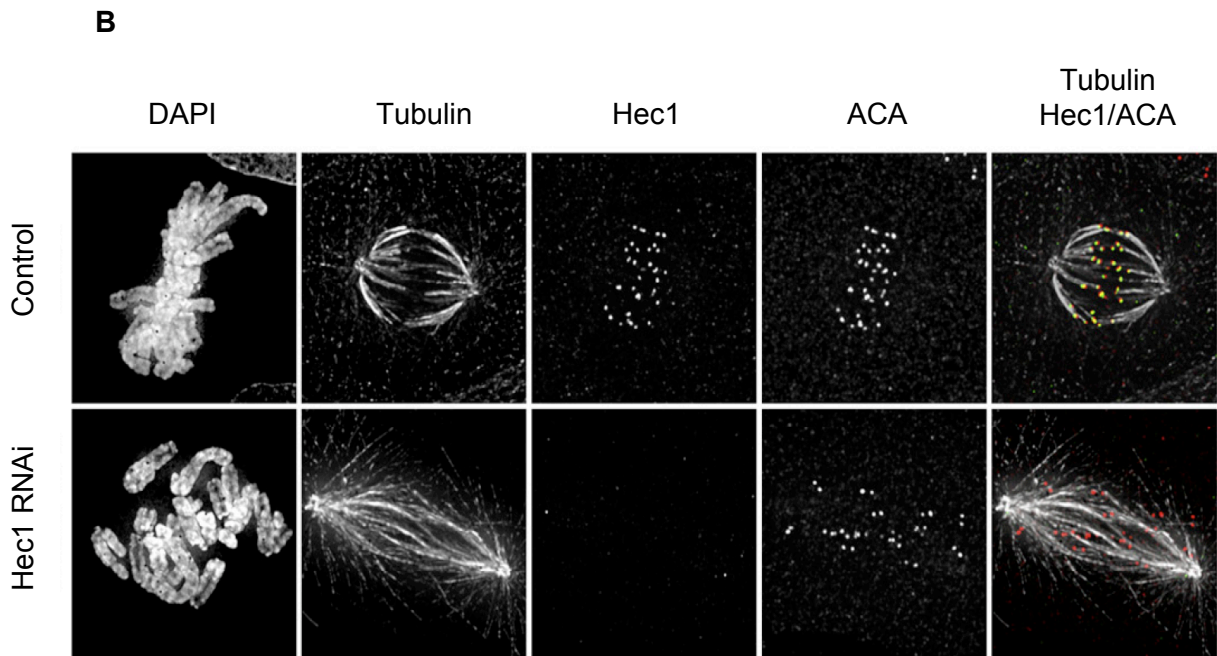


Figure 3.2B: Hec1 depletion from PtK1 cells results in mitotic defects

(B) Images of mock-transfected and Hec1-siRNA transfected cells. Cells were fixed 48 hr after transfection, immunostained with the indicated antibodies, imaged, and deconvolved. Projections of image stacks are shown. The overlay shows tubulin (white), anti-centromere antibodies (ACA; red), and Hec1 (green).

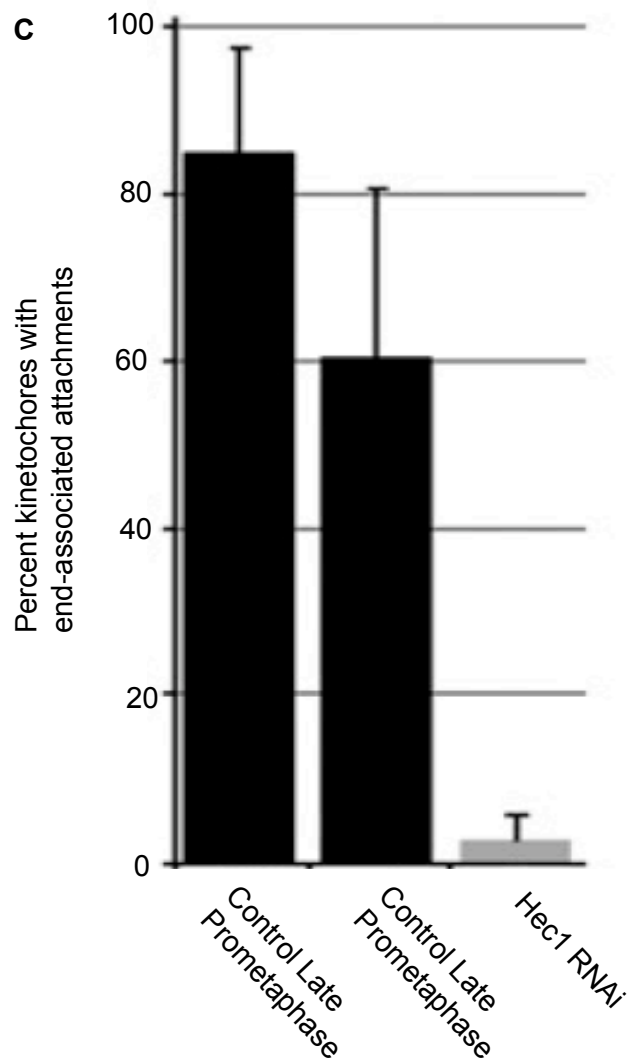


Figure 3.2C: Hec1 depletion from PtK1 cells results in mitotic defects
 (C) Quantification of end-on microtubule association with kinetochores (mock-transfected, late prometaphase: n = 10 cells, 212 kinetochores; mock-transfected, early-mid prometaphase: n = 10 cells, 208 kinetochores; Hec1-siRNA-transfected: n = 10 cells, 229 kinetochores).

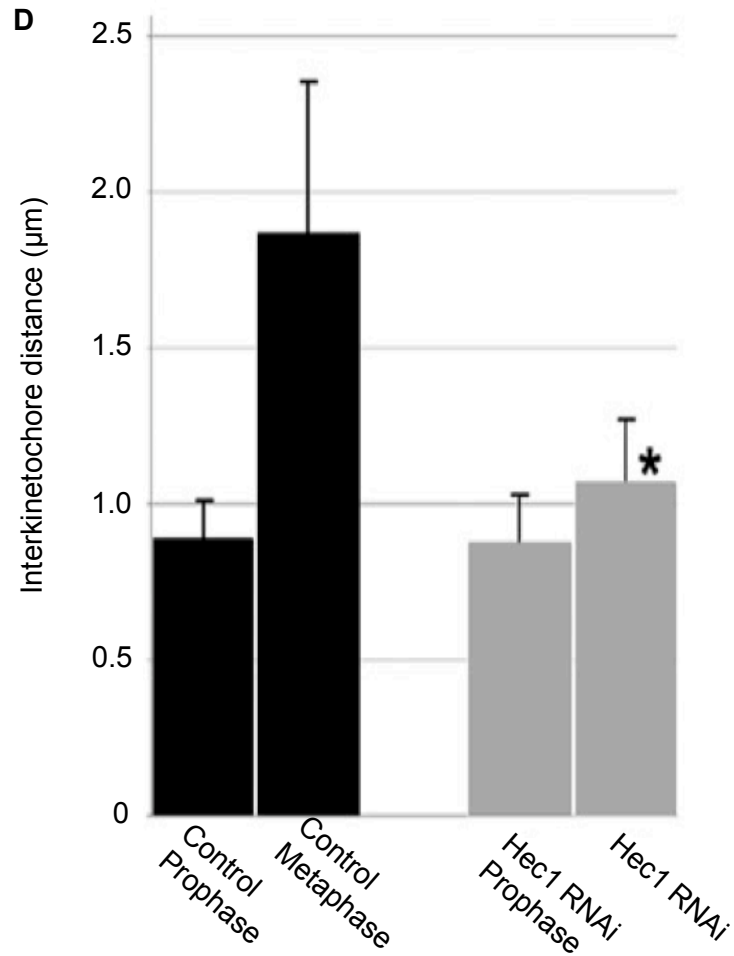


Figure 3.2D: Hec1 depletion from PtK1 cells results in mitotic defects
 (D) Quantification of interkinetochore distances, which were measured from ACA centroid to ACA centroid (mock-transfected, prophase: n = 5 cells, 25 kinetochore pairs; mock-transfected, metaphase: n = 14 cells, 61 kinetochore pairs; Hec1-siRNA-transfected, prophase: n = 10 cells, 77 kinetochore pairs; Hec1-siRNA-transfected: n = 32 cells, 307 kinetochore pairs). The asterisk indicates a p value of <0.0005 (Hec1-siRNA-transfected versus mock-transfected, metaphase).

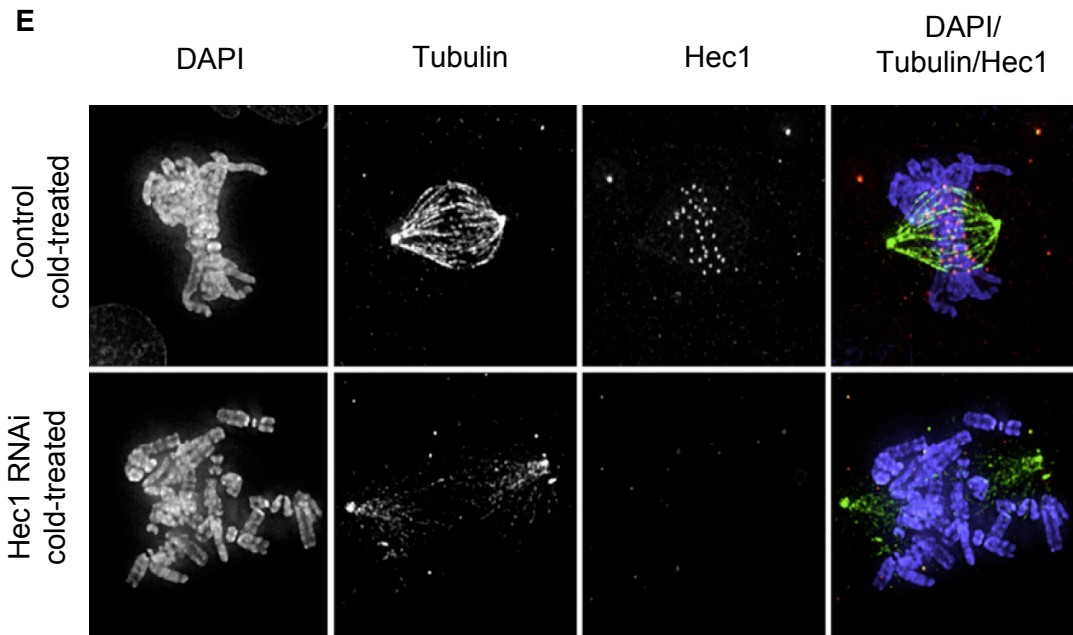


Figure 3.2E.: Hec1 depletion from PtK1 cells results in mitotic defects

(E) Mock-transfected and Hec1-siRNA-transfected cells were subjected to a cold-induced microtubule-depolymerization assay, processed for immunofluorescence, immunostained with the indicated antibodies, imaged, and deconvolved. Projections of image stacks are shown.

F

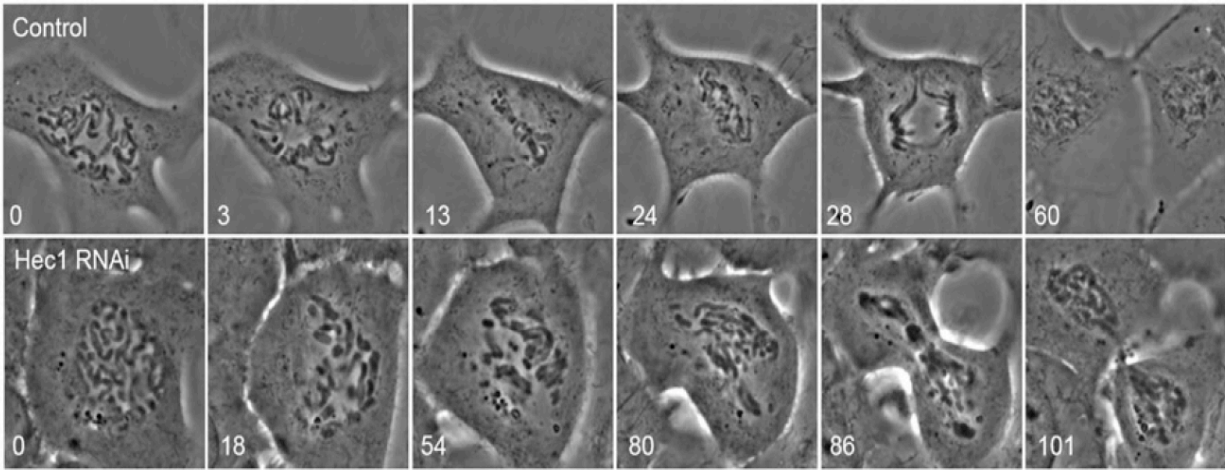


Figure 3.2F: Hec1 depletion from PtK1 cells results in mitotic defects

(F) Time-lapse image stills of mock-transfected and Hec1-siRNA-transfected cells. Elapsed time is indicated in min.

G

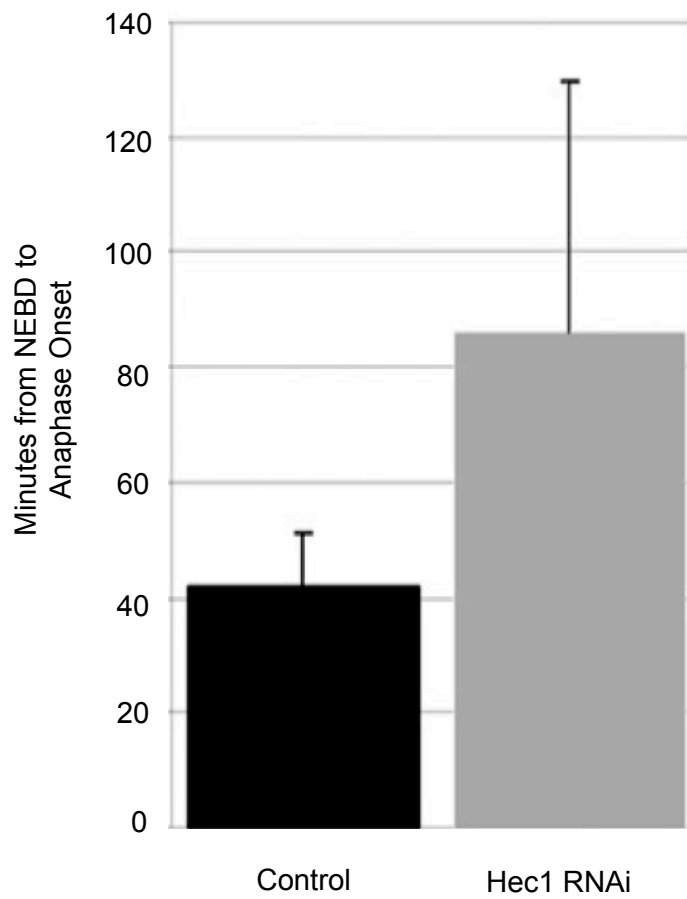


Figure 3.2G: Hec1 depletion from PtK1 cells results in mitotic defects

(G) Average time for progression through mitosis for mock-transfected (n = 28 cells) and Hec1-siRNA-transfected (n = 86 cells) PtK1 cells. Time was scored from nuclear-envelope breakdown (NEBD) to anaphase onset. The vertical line in all bar graphs indicates the standard deviation.

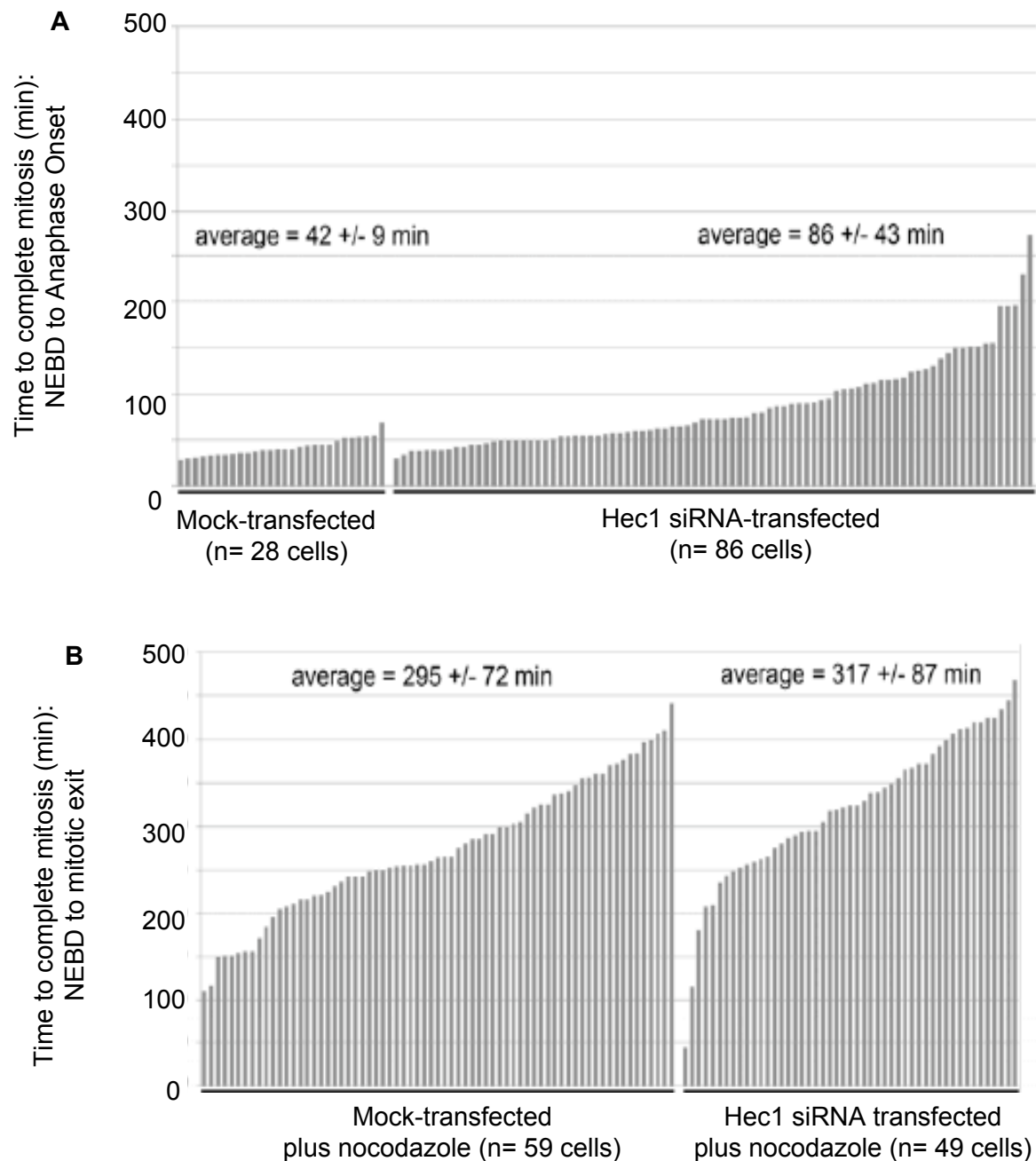


Figure 3.3: Timing through mitosis: mock-transfected & Hec1-siRNA transfected PtK1 cells in the absence and presence of nocodazole.

Cells were mock-transfected or transfected with Cy5-labeled Hec1 siRNA. Forty-eight h post-transfection or mock-transfection, cells were incubated with filming media or filming media plus 20 μ M nocodazole and time-lapse imaged. Phase-contrast and Cy5 fluorescence images were captured every 5 min for 10 h. Time-lapse movies were used to determine timing through mitosis. Each bar represents an individual cell, and the cells are displayed in ascending order of timing through mitosis. (A) No drug treatment: timing through mitosis was scored from nuclear envelope breakdown (NEBD) to anaphase onset, as determined by sister chromatid separation. (B) Nocodazole treatment: timing through mitosis was scored from NEBD to mitotic exit, as determined by chromosome decondensation and cell re-spreading. Mitotic exit was scored here as opposed to anaphase onset due to difficulty discerning anaphase onset in nocodazole treated cells.

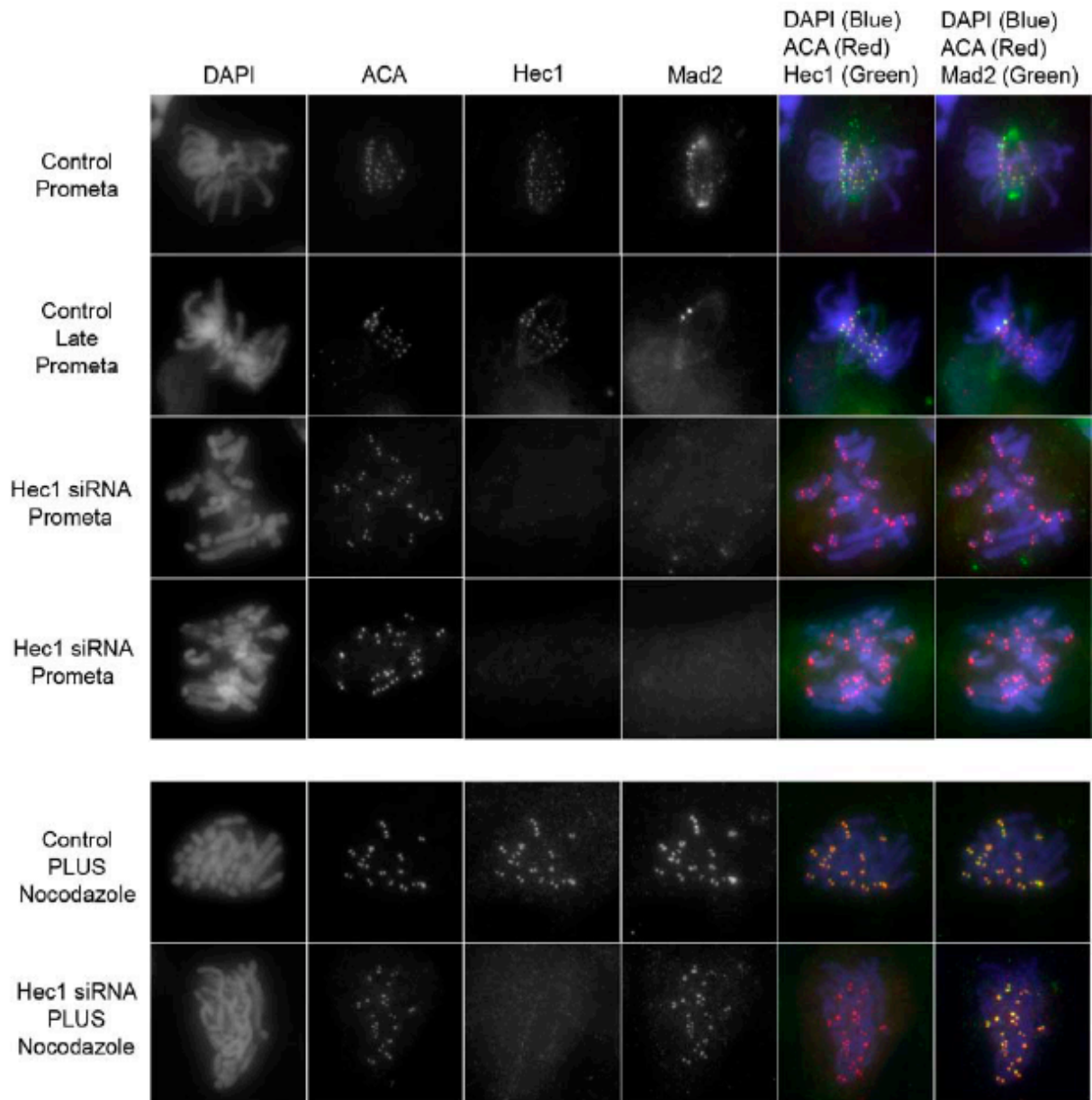


Figure 3.4: Mad2 is prematurely depleted from unattached kinetochores in Hec1-depleted PtK1 cells.

Mock-transfected or Hec1 siRNA-transfected PtK1 cells were fixed and immunostained with the indicated antibodies. For nocodazole experiments, the drug was added at 20 μ M for 1 h prior to fixation. (Top) Kinetochores in mock-transfected cells bind high levels of Mad2 at early mitosis, and levels decrease as chromosomes align. Kinetochores in Hec1 siRNA-transfected cells do not bind high levels of Mad2 in the presence of unaligned chromosomes. (Bottom) Kinetochores in both mock-transfected and Hec1 siRNA-transfected cells bind high levels of Mad2 in the absence of microtubules.

3.2.2 *The N-Terminus of Hec1 is Required for Kinetochores-Microtubule Attachment*

A portion of the N terminus of Hec1 folds into a calponin homology (CH) domain, which is a motif found in both actin and microtubule-binding proteins [51, 76, 77]. N-terminal to the CH domain is a highly basic 80 amino acid tail domain. Its structure is unknown because it was deleted for facilitating production of crystals for X-ray crystallographic studies [45, 50]. This is not surprising, given that it is predicted to be intrinsically disordered and has a low probability of maintaining a stably folded conformation [78]. The remainder of Hec1 is also predicted to be largely intrinsically disordered, but its dimerization with Nuf2 results in a stably maintained coiled-coil domain [73, 78]. To determine the role of the N terminus of Hec1 in mitosis, we depleted PtK1 cells of endogenous Hec1 and carried out rescue experiments by expressing C-terminal GFP fusions of human Hec1 (full-length) and Hec1 deleted of both its CH domain and 80 amino acid tail ($\Delta 1-207$ Hec1-GFP). N-terminal GFP fusions were also generated for Hec1 full-length and deletion constructs, and their expression produced results similar to those of the corresponding C-terminal fusion proteins (Figures 3.5-A&B). Rescue experiments in which either full length Hec1-GFP or $\Delta 1-207$ Hec1-GFP were expressed in PtK1 cells depleted of endogenous Hec1 demonstrate that $\Delta 1-207$ Hec1-GFP was able to localize to kinetochores identically to full-length Hec1-GFP (Figure 3.6A). However, cells rescued with $\Delta 1-207$ Hec1-GFP failed to align their chromosomes at the spindle equator, in contrast to cells rescued with full-length Hec1-GFP (Figure 3.6A). The $\Delta 1-207$ Hec1-GFP rescue resulted in a reduction of end-on kinetochores-microtubule attachments, given that only ~20% of kinetochores were associated with microtubule plus ends in these cells (Figure 3.6B). This is significantly lower than that in cells rescued with full-length Hec1-GFP, whose end-on attachments increased from ~60% in early-to-mid prometaphase to ~80% in late prometaphase (Figure 3.6B). In addition, we measured interkinetochore distances between sister kinetochores in $\Delta 1-207$ Hec1-GFP rescued cells and found that these kinetochores exhibited reduced tension (Figure 3.6C).

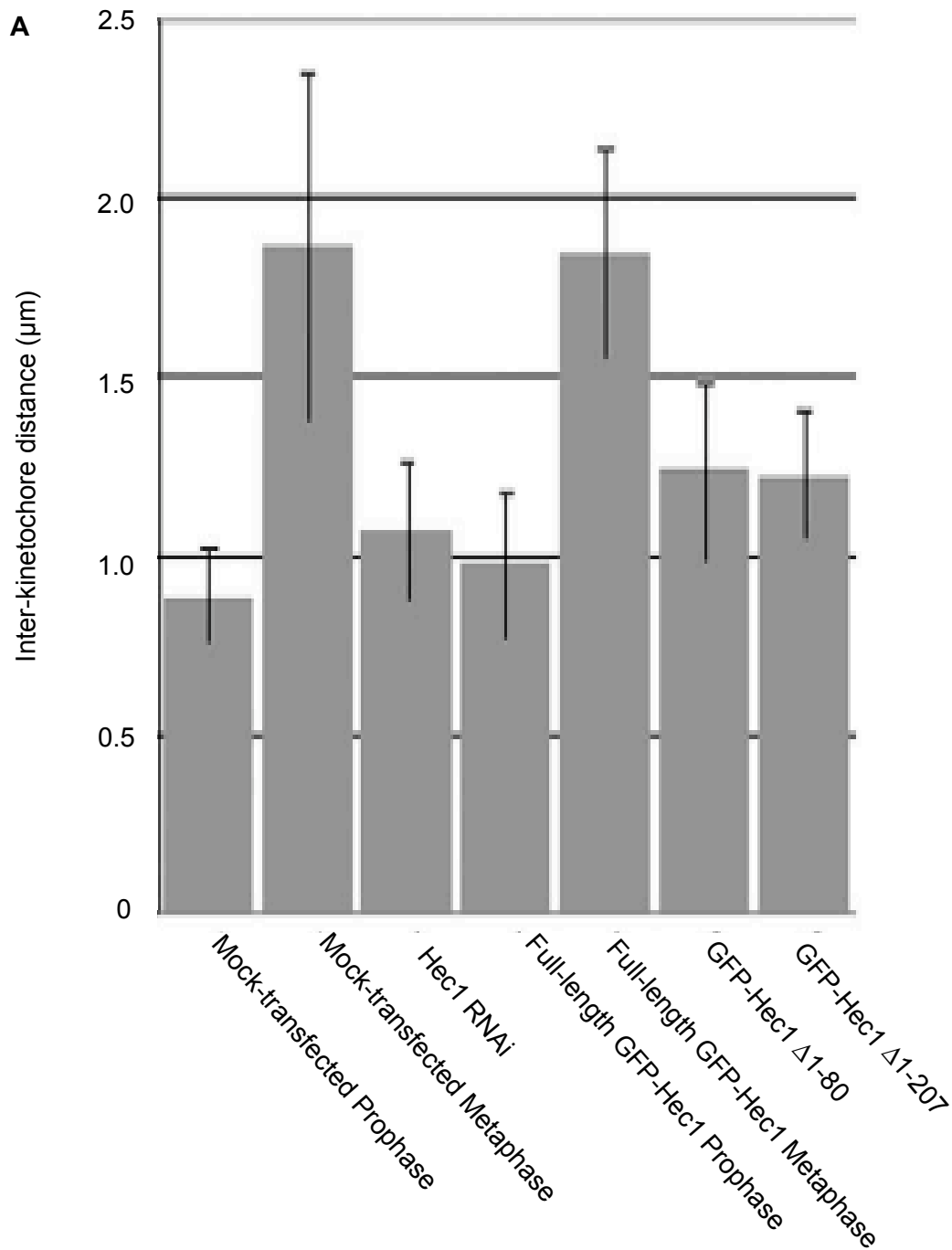


Figure 3.5A: Summary of inter-kinetochore distance data for N-terminal GFP fusion proteins.

(A) In addition to the N-terminal fusion protein data, data for mock-transfected and Hec1 siRNA-transfected cells (without expression of exogenous GFP fusion proteins) are included. For mock-transfected and Hec1 siRNA-transfected, distances were measured from ACA centroid to ACA centroid. For silence and rescue experiments, distances were measured from GFP centroid to GFP centroid. Vertical line in the bar graphs indicates standard deviation.

B

	distance (μm)	standard deviation	Kinetocho re n value	cell n value
Mock- transfected Prophase	0.88	0.13	20	5
Mock- transfected Metaphase	1.87	0.49	61	14
Hec1 RNAi	1.07	0.20	307	42
Full-length GFP-Hec1 Prophase	0.97	0.20	8	1
Full-length GFP-Hec1 Metaphase	1.84	0.30	69	10
GFP-Hec1 Δ 1- 80	1.23	0.25	64	17
GFP-Hec1 Δ 1- 207	1.22	0.19	88	21

Figure 3.5B: Summary of inter-kinetochore distance data for N-terminal GFP fusion proteins.

(B) In addition to the N-terminal fusion protein data, data for mock-transfected and Hec1 siRNA-transfected cells (without expression of exogenous GFP fusion proteins) are included. For mock-transfected and Hec1 siRNA-transfected, distances were measured from ACA centroid to ACA centroid. For silence and rescue experiments, distances were measured from GFP centroid to GFP centroid. Vertical line in the bar graphs indicates standard deviation.

A

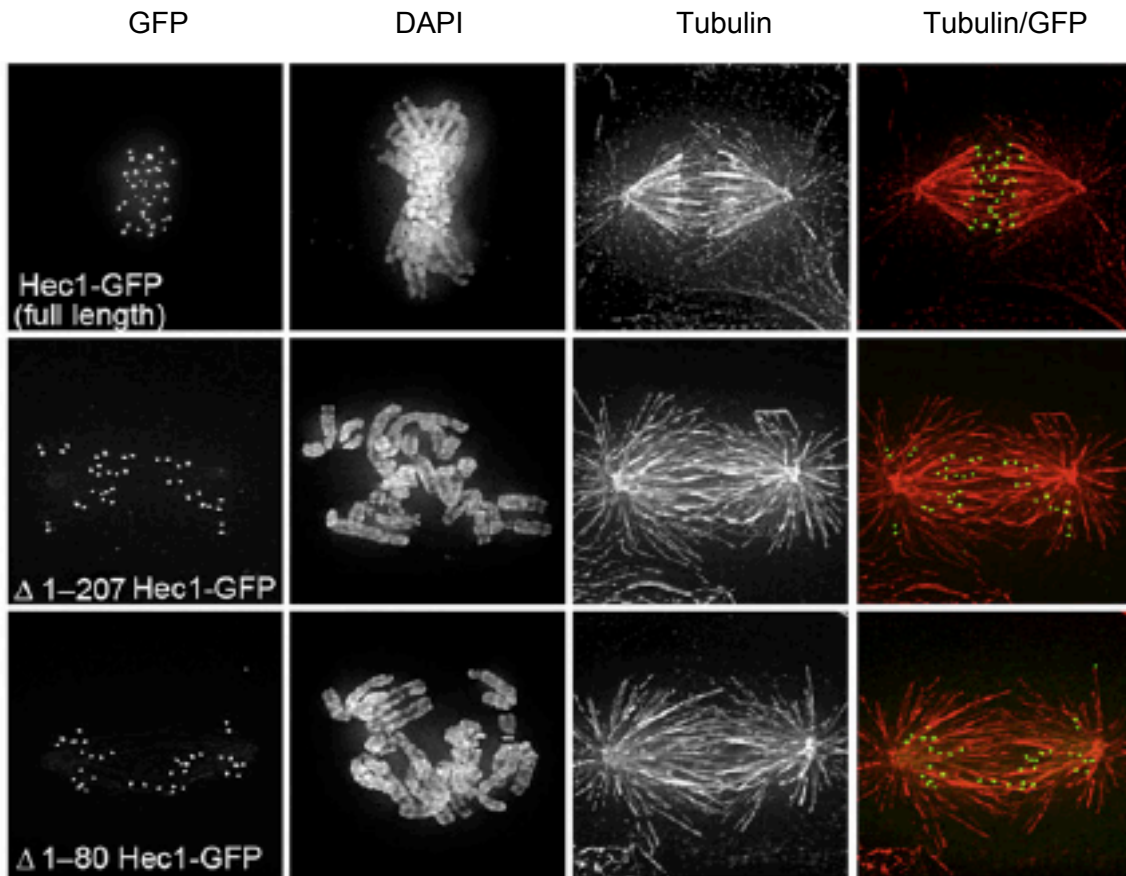


Figure 3.6A: The N-terminus of Hec1 is required for kinetochore-microtubule attachment

(A) Projections of deconvolved immunofluorescence images of PtK1 cells depleted of endogenous Hec1 and rescued with the indicated GFP fusion proteins.

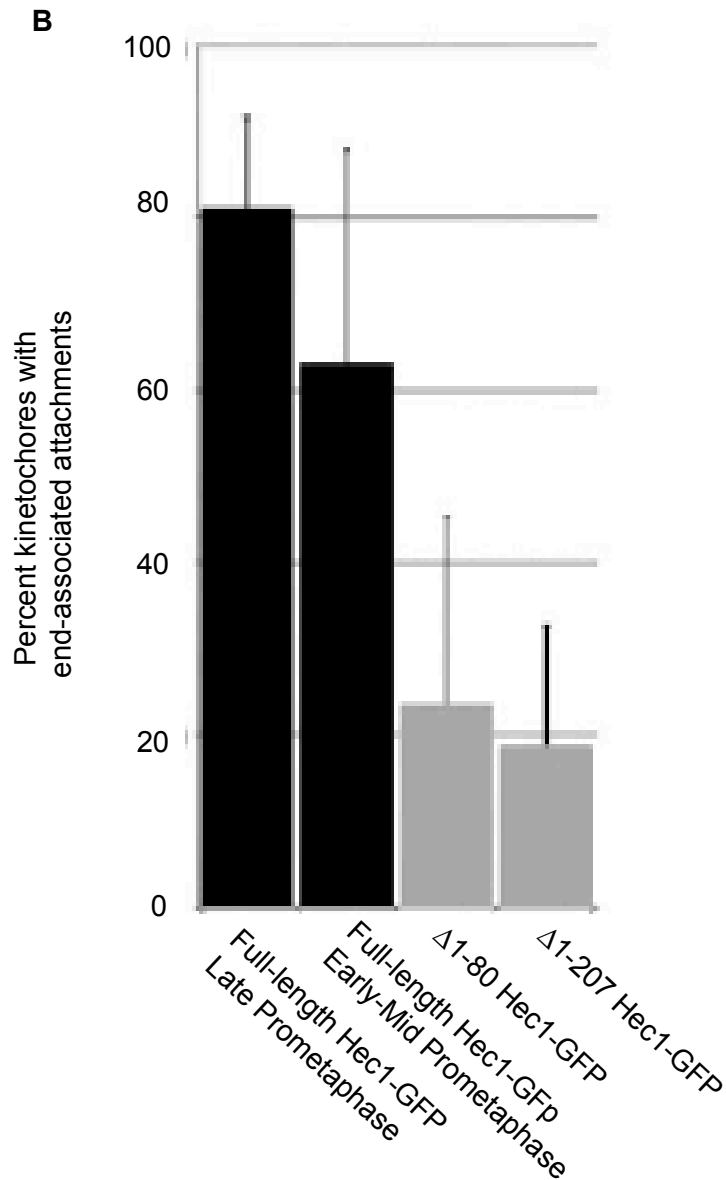


Figure 3.6B: The N-terminus of Hec1 Is required for kinetochore-microtubule attachment

(B) Quantification of end-on microtubule association with kinetochores (full-length Hec1-GFP, late prometaphase: n = 10 cells, 256 kinetochores; full-length Hec1-GFP, early-mid prometaphase: n = 10 cells, 251 kinetochores; Δ1-207 Hec1-GFP: n = 10 cells, 214 kinetochores; Δ1-80 Hec1-GFP: n = 10 cells, 217 kinetochores).

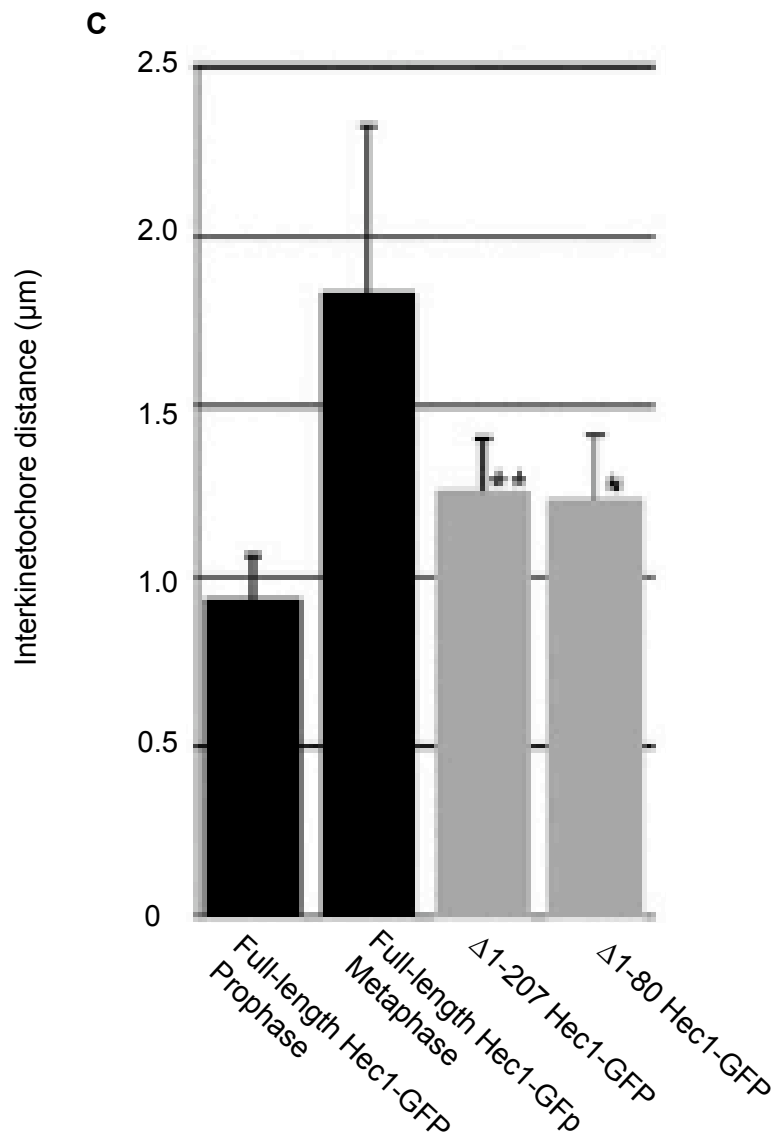


Figure 3.6C: The N-terminus of Hec1 is required for kinetochore-microtubule attachment

(C) Quantification of interkinetochore distances, which were measured from Hec1-GFP centroid to Hec1-GFP centroid (full-length Hec1-GFP, prophase: n = 11 cells, 46 kinetochore pairs; full-length Hec1-GFP, metaphase: n = 12 cells, 75 kinetochore pairs; Δ1–207 Hec1-GFP: n = 21 cells, 88 kinetochore pairs; Δ1–80 Hec1-GFP: n = 21 cells, 90 kinetochore pairs). The p values (indicated by the asterisk and double asterisk) are <0.0005, (single asterisk: Δ1–80 Hec1-GFP versus full-length Hec1-GFP, metaphase; double asterisk: Δ1–207 Hec1-GFP versus full-length Hec1-GFP, metaphase).

These results demonstrate that the N-terminal 207 amino acids of Hec1 are required for efficient formation of kinetochore microtubules in PtK1 cells. We next tested the role of the disordered 80 amino acid tail of Hec1 in kinetochore-microtubule attachment by generating a $\Delta 1-80$ Hec1-GFP mutant. Previous *in vitro* studies have shown that removal of the 80 amino acid tail domain from Hec1 does not disrupt the structure of the CH domain [45, 50]. When expressed in PtK1 cells, $\Delta 1-80$ Hec1-GFP localized to kinetochores but was incapable of compensating for endogenous Hec1-depletion defects. Similar to cells rescued with $\Delta 1-207$ Hec1-GFP, cells rescued with $\Delta 1-80$ Hec1-GFP failed to align their chromosomes, exhibited a reduction in end-on kinetochore-microtubule attachments, and exhibited reduced tension across sister kinetochore pairs (Figures 3.6-A,B,&C). Thus, deletion of the 80 amino acid disordered tail domain of Hec1 results in kinetochores that are unable to generate a sufficient number of stable microtubule attachments required for chromosome biorientation in cells. To determine the effect of expression of the Hec1 N-terminal deletion mutants on mitotic progression, we imaged cells transfected with Cy5-labeled Hec1 siRNA and GFP-labeled Hec1 fusion proteins via time-lapse microscopy. As shown in Figure 3.6D, cells rescued with $\Delta 1-207$ Hec1-GFP or $\Delta 1-80$ Hec1-GFP were unable to align their chromosomes at the spindle equator (Movies 5 and 6), confirming our fixed-cell immunofluorescence data. In contrast, most of the cells rescued with full-length Hec1-GFP managed to align their chromosomes into a metaphase plate (13 of 15 cells) and enter anaphase with an average time of 44 ± 15 min from nuclear-envelope breakdown (NEBD) to anaphase onset (Figures 3.6D and 3.6E and Movie 7). Similar to cells transfected with Hec1 siRNA alone, most $\Delta 1-207$ Hec1-GFP-rescued cells were not able to sustain a mitotic arrest in the presence of unaligned chromosomes, and they entered anaphase after a ~ 45 min delay (NEBD to anaphase onset: 86 ± 36 min, $n = 23$ cells; Figure 3.6E). However, most of the cells rescued with $\Delta 1-80$ Hec1-GFP maintained a mitotic arrest for at least 3 h (33 of 38 cells). These results suggest that the CH domain of Hec1, but not the 80 amino

D

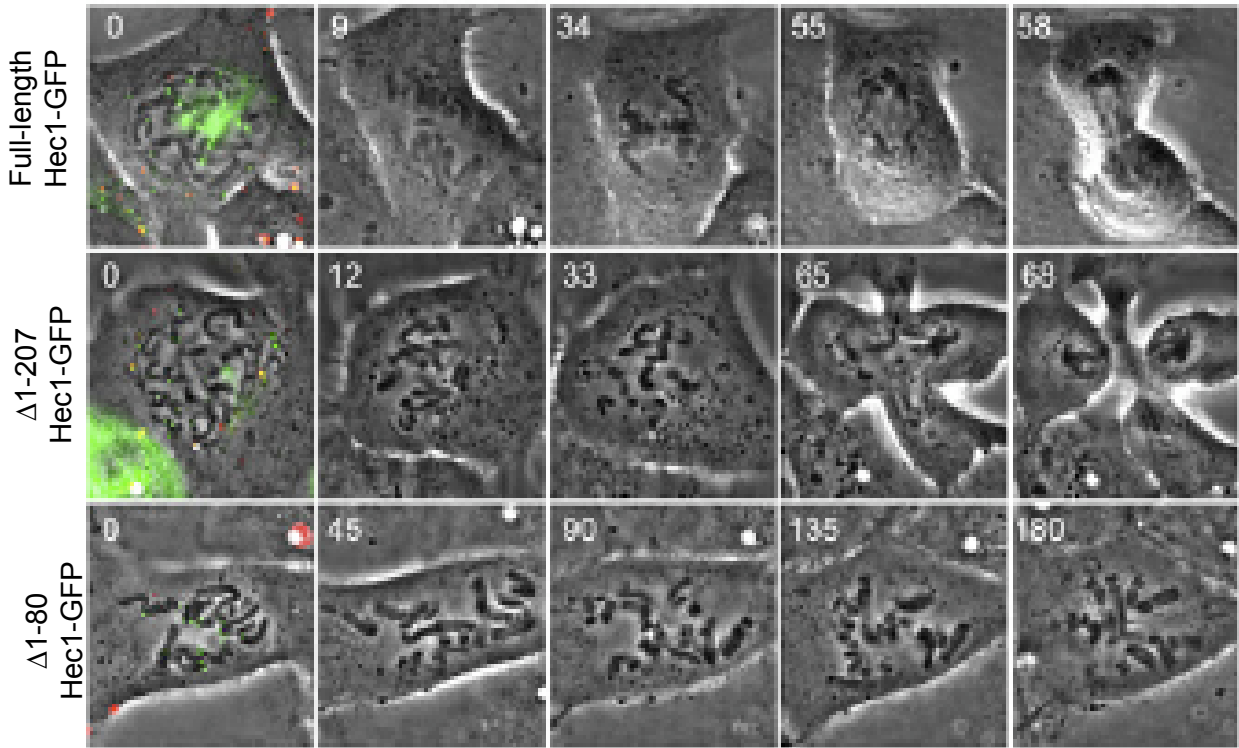


Figure 3.6D: The N-terminus of Hec1 Is required for kinetochore-microtubule attachment

(D) Image stills from time-lapse image acquisitions. Cells positive for both Cy5-labeled Hec1 siRNA and the GFP fusion protein indicated (first panel of each series) were identified and imaged with a 1003 phase-contrast objective. Time is indicated in min.

E

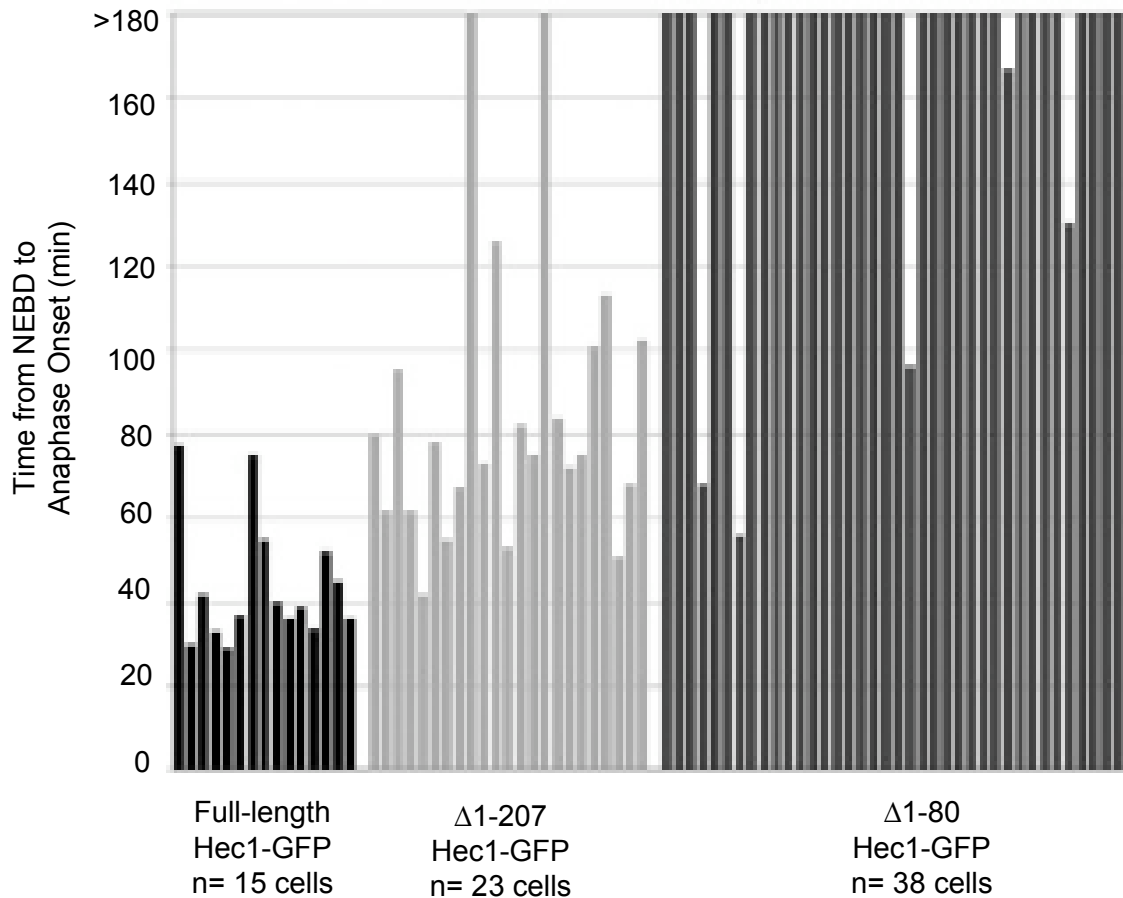


Figure 3.6E: The N-terminus of Hec1 Is required for kinetochore-microtubule attachment

(E) Quantification of mitotic timing (full-length Hec1-GFP: n = 15 cells; Δ 1–207 Hec1-GFP: n = 23 cells; Δ 1–80 Hec1-GFP: n = 38 cells). Time was scored from NEBD to anaphase onset. Cells were imaged for 3 hr, and those cells still in mitosis at the end of imaging were scored as >180 min. The vertical line in all bar graphs indicates the standard deviation.

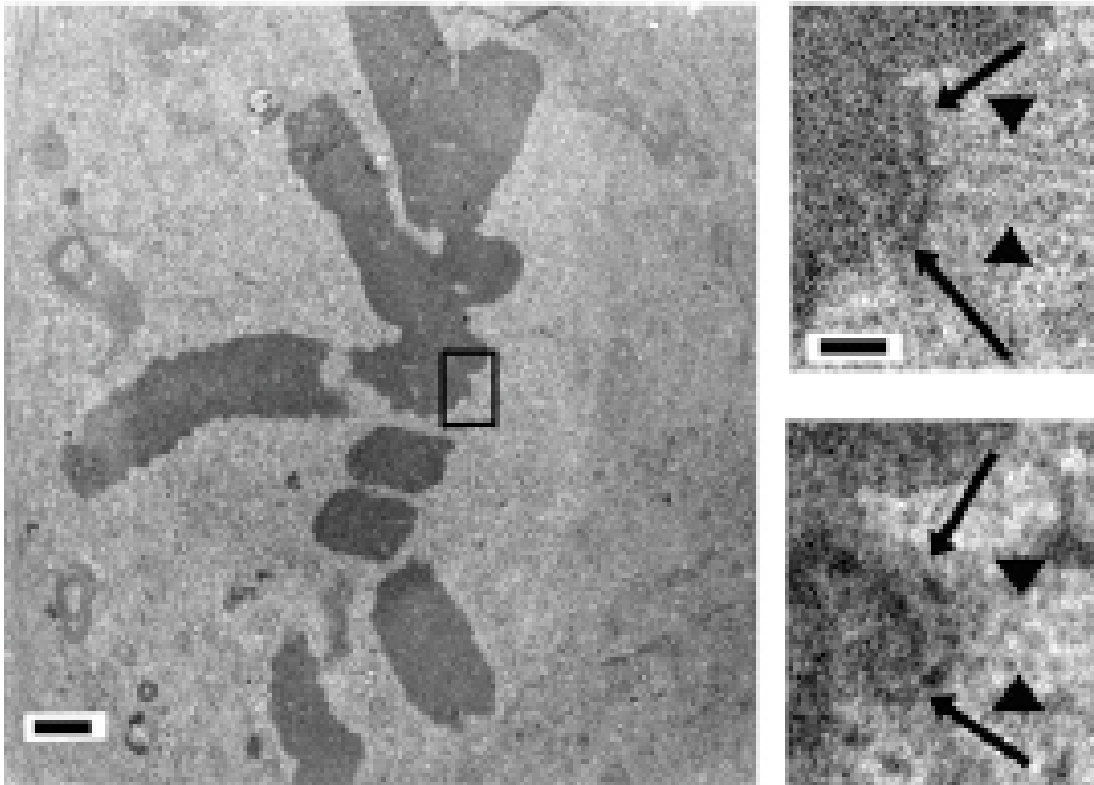
acid tail, is required to maintain a functional spindle-assembly checkpoint in the presence of unattached kinetochores in PtK1 cells.

3.2.3 Kinetochores Ultrastructure in Hec1-Depleted and $\Delta 1-80$ Hec1-GFP-Rescued PtK1 Cells

Given the striking effect on kinetochores-microtubule attachment in cells rescued with $\Delta 1-80$ Hec1-GFP, we investigated the ultrastructure of these kinetochores by electron microscopy. As shown in Figure 3.7A, serial section images of kinetochores in mock-transfected cells often displayed a distinct outer plate with multiple microtubules bound. Depletion of Hec1 resulted in distinct outer plates with few microtubules bound (Figure 3.7B). Rescue with full-length Hec1-GFP restored microtubule binding (Figure 3.7C), whereas rescue with $\Delta 1-80$ Hec1-GFP did not (Figure 3.7D), confirming our light-microscopy data. Kinetochores in Hec1-depleted cells with no rescue or rescued with $\Delta 1-80$ Hec1-GFP rarely bound more than four microtubules (Figure 3.7E). The detection of corona material also indicated that these kinetochores were in a largely unbound state [79, 80] (Figures 3.7B&D). In contrast, all kinetochores in mock-transfected cells and full-length Hec1-GFP-rescued cells had many bound microtubules, with an average of more than 20 microtubules per kinetochores (Figure 3.7E). Detection of an outer plate in Hec1-depleted PtK1 cells is somewhat surprising because Nuf2 depletion from HeLa cells, which causes a concomitant reduction in Hec1, results in loss of the outer-plate structure [81]. Currently, it is not clear whether this is due to a difference in cell type or other factors. Furthermore, it is not possible from two-dimensional images of conventionally prepared specimens to know for certain that the outer plates in the unbound kinetochores of Hec1-depleted and $\Delta 1-80$ Hec1-GFP-rescued cells are structurally the same as in unbound kinetochores of control cells. This issue will have to be resolved by more extensive structural studies.

The positively charged tail domain of Hec1 is a substrate for Aurora B kinase

A

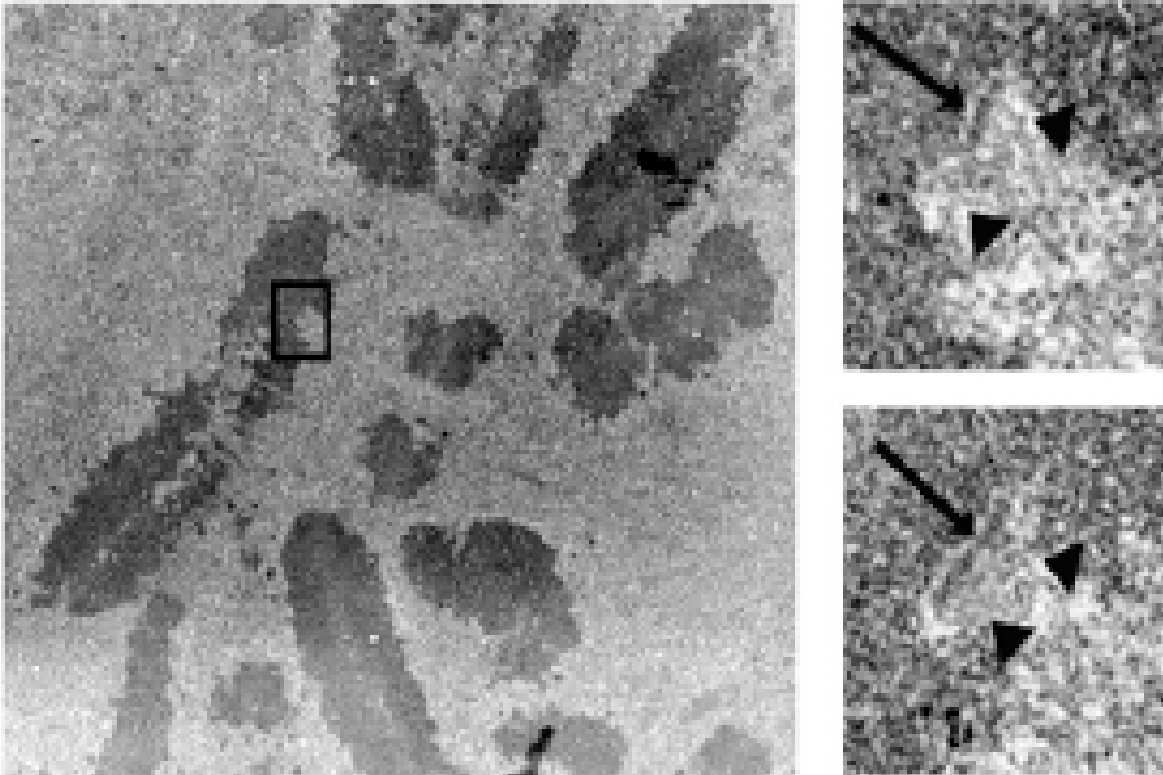


Control

Figure 3.7A: Kinetochore ultrastructure in Hec1-depleted and $\Delta 1-80$ Hec1-GFP-rescued PtK1 cells

(A) Mock-transfected cell. On the left is a low magnification image showing the metaphase alignment of the chromosomes. On the right are higher-magnification images of two serial sections through the kinetochore indicated by the box in the low-magnification view. Images show a distinct outer plate (indicated by arrows) and robust kinetochore fibers (indicated by arrowheads). The scale bar for low-magnification images represents 1.0 μm . Electron microscopy work performed by Yimin Dong and Bruce McEwen at the Wadsworth Center, New York.

B

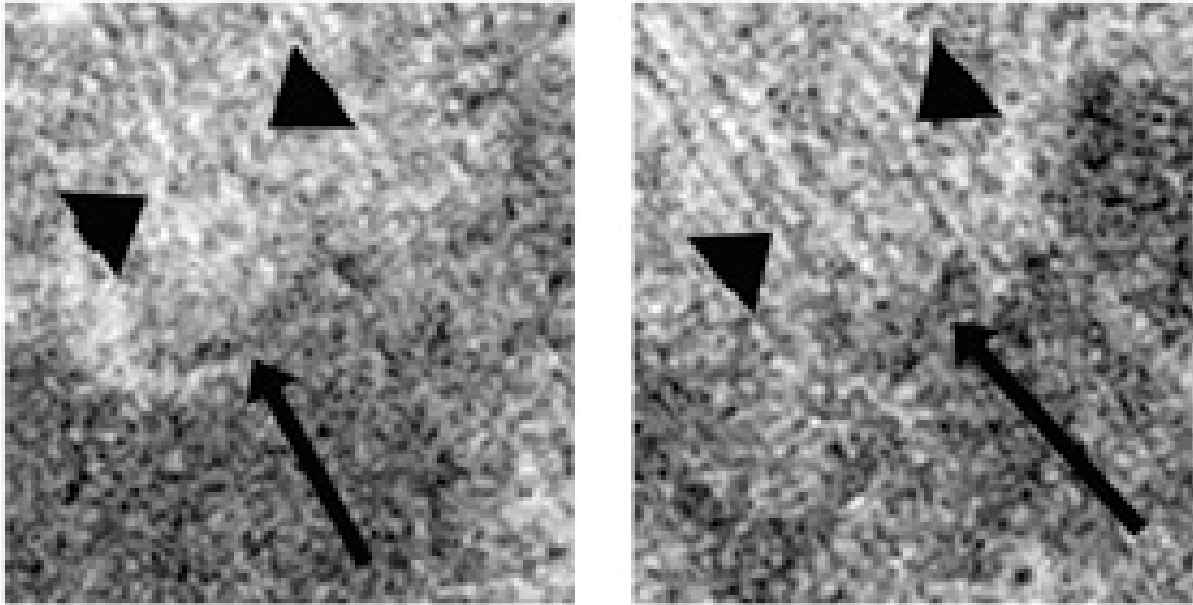


Hec1 RNAi

Figure 3.7B: Kinetochore ultrastructure in Hec1-depleted and $\Delta 1-80$ Hec1-GFP-rescued PtK1 cells

(B) Hec1-siRNA-transfected cell. On the left is a low-magnification image showing that Hec1 cells are unable to achieve metaphase alignment or form robust kinetochore fibers. On the right are higher-magnification images of two serial sections through the kinetochore indicated by the box in the low magnification image. Although a distinct outer plate is frequently observed (indicated by arrows), few bound microtubules were detected. In addition, a fibrous corona characteristic of unbound kinetochores is evident (indicated by arrowheads). The scale bar for low-magnification images represents 1.0 μm . Work performed by Yimin Dong and Bruce McEwen, the Wadsworth Center, NY.

C

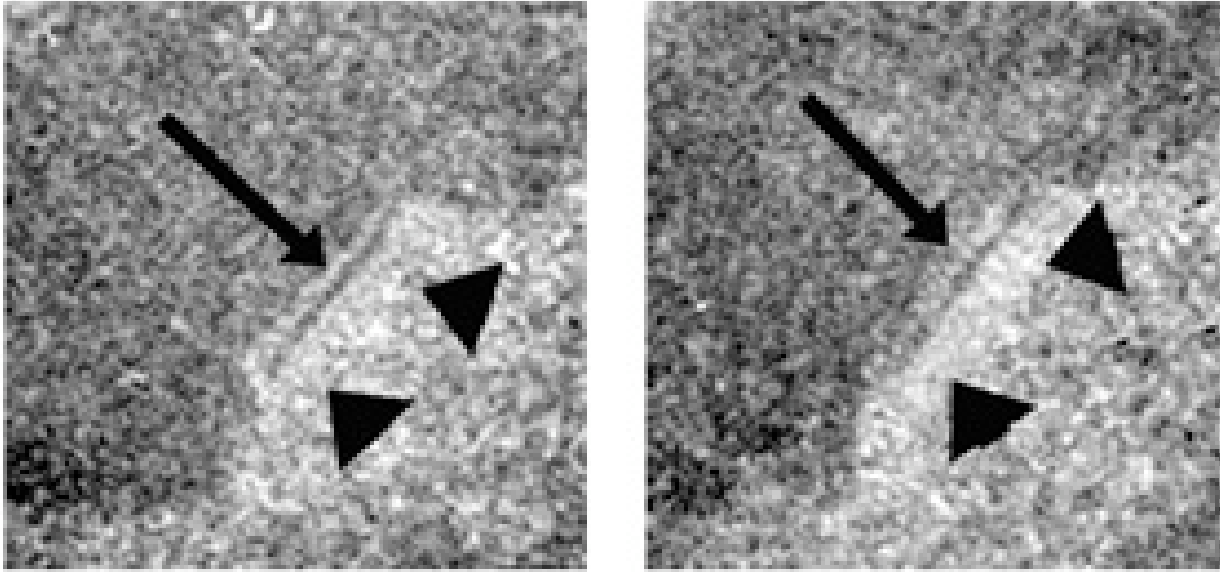


Hec1-GFP (full-length)

Figure 3.7C: Kinetochore ultrastructure in Hec1-depleted and $\Delta 1-80$ Hec1-GFP-rescued PtK1 cells

(C) Hec1-depleted cells rescued with full-length Hec1-GFP. High-magnification views showing a distinct outer plate (indicated by arrows) with numerous bound microtubules (indicated by arrowheads), similar to that seen in (3.7A).

D



Δ 1-80 Hec1-GFP

Figure 3.7D: Kinetochore ultrastructure in Hec1-depleted and Δ 1–80 Hec1-GFP-rescued PtK1 cells

(D) Hec1-depleted cells rescued with Δ 1–80 Hec1-GFP. High-magnification views show unbound kinetochores with distinct outer plate (indicated by arrows) and corona (indicated by arrowheads), similar to that seen in (3.7B).

E

	# kt	# cell	Avg.	Std. Dev.	Range
Control	54	3	20.3	4.3	11-32
Hec1 RNAi	38	3	2.5	2.2	0-10
Hec1-GFP (full-length)	49	3	19.5	4.1	8-28
Δ 1-80 Hec1-GFP	51	3	1.8	1.3	0-5

Figure 3.7E: Kinetochores ultrastructure in Hec1-depleted and Δ 1–80 Hec1-GFP-rescued PtK1 cells

(E) Quantification of kinetochores-microtubule attachment. The number of kinetochores scored (# kt), number of cells analyzed (# cell), average number of attached microtubules per kinetochore (avg), standard deviation (std), and range of attached microtubules per kinetochore (range) are listed for each experimental condition.

phosphorylation *in vitro*, and nine target sites within this domain of human Hec1 of have been identified by mass spectrometry [45, 47]. Two recent *in vitro* studies have shown that inclusion of purified Aurora B kinase in microtubule-pelleting assays decreased the binding affinity of purified Ndc80 complexes for microtubules [34, 45]. In addition, overexpression of a Hec1 mutant in which six Aurora B target serine/threonine residues within the tail domain were mutated to alanine to prevent phosphorylation resulted in robust kinetochore-microtubule attachment, but defects in chromosome alignment and kinetochore-microtubule attachment-error correction were observed [47]. These studies have led to the hypothesis that phosphorylation of Hec1 by Aurora B kinase may prevent tight binding of microtubules to kinetochores to promote microtubule release in cells. This is consistent with findings that Aurora B promotes microtubule turnover and attachment error correction in budding yeast and mammalian cells [82, 83]. We tested this hypothesis by expressing a mutant in which the nine identified target Aurora B phosphorylation serine (S) or threonine (T) residues within the Hec1 N terminus were mutated to aspartic acid (D) to mimic constitutive phosphorylation and reduce the overall positive charge of the tail domain (Figure 3.1A). Hec1-depleted cells rescued with 9D-Hec1-GFP were unable to align their chromosomes, exhibited a decrease in kinetochore-microtubule end-on attachments, and failed to generate wild-type tension across sister kinetochores (Figures 3.8-A,B,&C). This is in contrast to cells rescued with either full-length Hec1-GFP or a mutant in which the nine phosphorylation target sites were mutated to alanine (9A-Hec1-GFP), in which robust kinetochore-microtubule attachments were observed (Figure 3.8A). Although cells rescued with 9A-Hec1-GFP were able to generate kinetochore-microtubule attachments, they often exhibited defects in chromosome alignment, consistent with a previous overexpression study using a Hec1 alanine (A) mutant [47]. These experiments suggest that the charge composition of the 80 amino acid tail domain of Hec1 is a critical determinant of kinetochore-microtubule attachment.

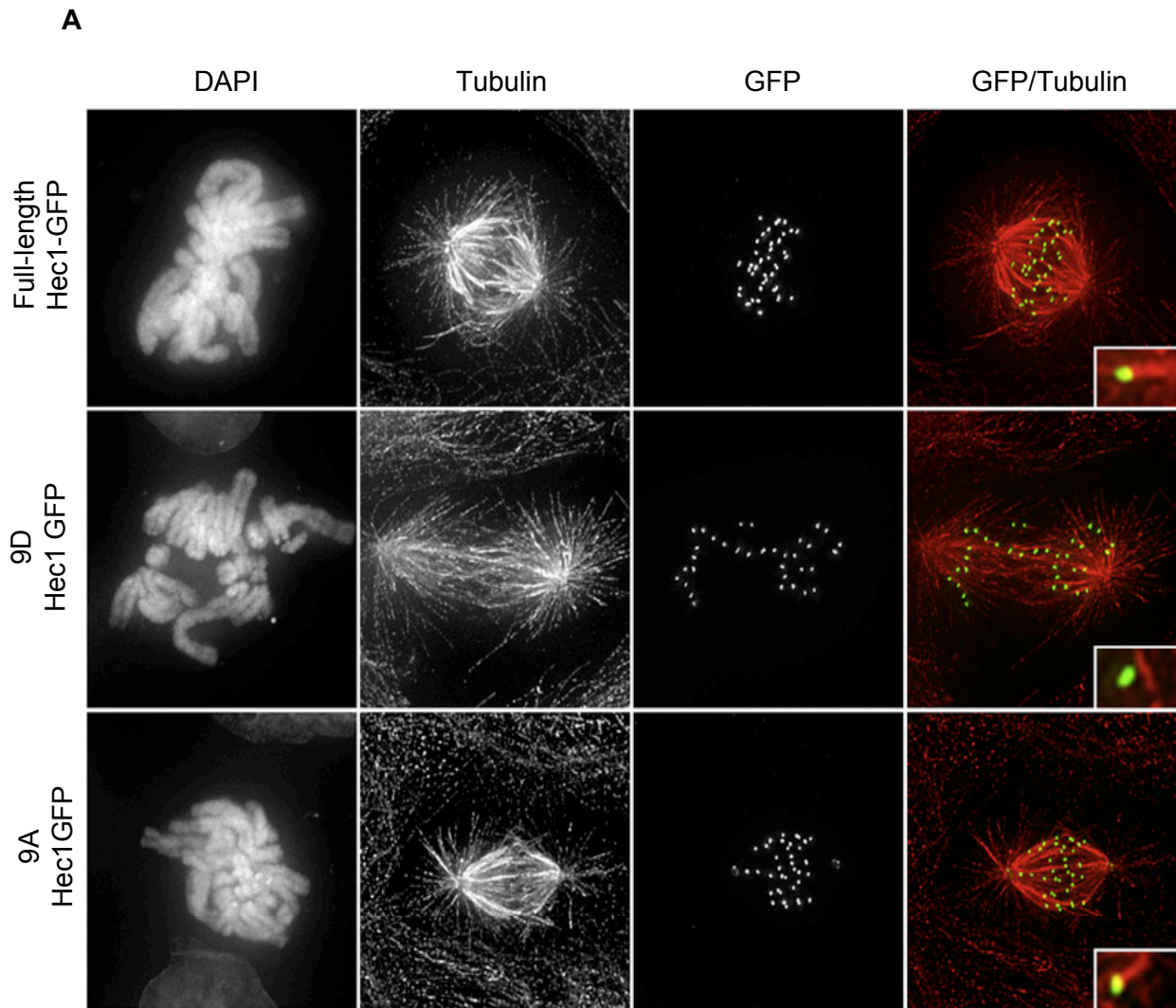


Figure 3.8A: Charge modification of the Hec1 80 amino acid tail domain inhibits kinetochore-microtubule attachment

(A) Deconvolved immunofluorescence images of Hec1-depleted PtK1 cells expressing the indicated GFP fusion proteins. The insets show higher-magnification images of individual kinetochores.

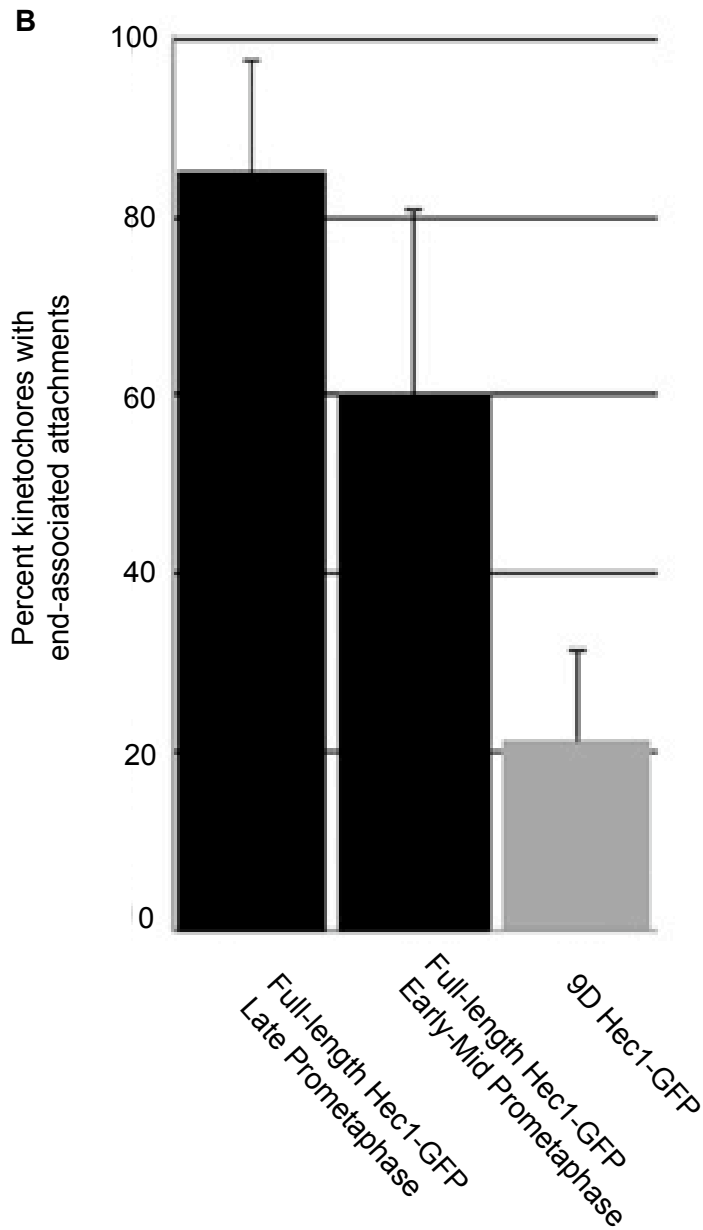


Figure 3.8B: Charge modification of the Hec1 80 amino acid tail domain inhibits kinetochore-microtubule attachment

(B) Quantification of end-on microtubule association with kinetochores. Full-length Hec1-GFP data from Figure 2 are compared to data from 9D-Hec1-GFP-expressing cells: n = 10 cells, 295 kinetochores.

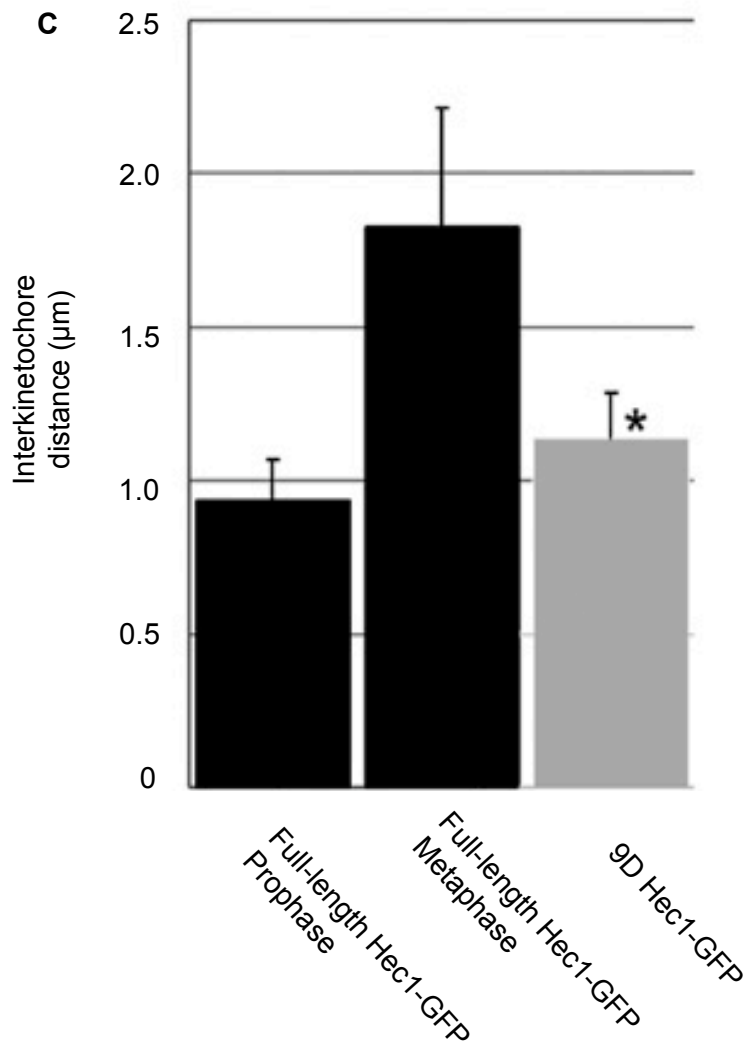


Figure 3.8C: Charge modification of the Hec1 80 amino acid tail domain inhibits kinetochore-microtubule attachment

(C) Quantification of interkinetochore distances, measured from Hec1-GFP centroid to Hec1-GFP centroid (full-length Hec1-GFP, metaphase data from Figure 2 are compared to data from 9D-Hec1-GFP: n = 10 cells, 82 kinetochore pairs). The p value (indicated by asterisk) is <0.0005 (9D-Hec1-GFP versus full-length Hec1-GFP, metaphase). The vertical line in all bar graphs indicates the standard deviation.

3.3 Discussion

We show here that the 80 amino acid unstructured tail domain of Hec1 is required for the efficient formation of stable kinetochore-microtubule attachments in cells, and the CH domains of Hec1 and Nuf2 are not sufficient to carry out this task alone. Our findings are corroborated by recent *in vitro* data that demonstrate a decrease in binding affinity of the Ndc80 complex for microtubules upon deletion of the 80 amino acid Hec1 tail domain [45, 50]. It is surprising, however, that in the context of a living cell, defects due to deletion of this domain are not rescued by either redundant microtubule-binding factors at kinetochores or by the CH domains in Hec1 and Nuf2 themselves [34, 45].

What is the role of the 80 amino acid tail domain at the kinetochore-microtubule interface? Our results suggest that the tail domain mediates kinetochore-microtubule binding through electrostatic interactions. Nine amino acid substitutions within the Hec1 tail domain were made to mimic the charge brought on by phosphorylation. When these nine target residues within the tail domain were mutated to aspartic acid (D), the isoelectric point of this domain decreased from 10.8 to 8.0, and we observed a kinetochore-null phenotype in which chromosomes failed to align and very few stable end-on kinetochore-microtubule attachments were generated. Loss of kinetochore-microtubule attachments due to a change in the charge composition of the Hec1 tail domain has important implications for how the cell generates and regulates kinetochore-microtubule attachments. Microtubules extend from their surface highly acidic C-terminal tail domains of alpha and beta tubulin. These tail domains can be cleaved by subtilisin, which reduces the affinity of a truncated, engineered Ndc80 complex (Ndc80 bonsai) for microtubules *in vitro* [45]. A model for kinetochore-microtubule attachment can be envisioned in which the N-terminal tail domain of Hec1 binds directly to the C-terminal acidic domain of tubulin and charge modification of Hec1 tails through phosphorylation regulates attachment status.

In support of this model, the tail domain of Hec1 is a substrate for Aurora B kinase *in*

vitro [34, 45, 47]. Mutation of multiple residues in the tail domain to prevent phosphorylation *in vivo* results in robust kinetochore-microtubule attachment, whereas mutation of these residues to mimic constitutive phosphorylation *in vivo* results in loss of kinetochore-microtubule attachment (Figure 1.8). It is likely that phosphorylation of multiple sites is required for an effect on kinetochore microtubule attachment, and a single site may not modify the charge to a level that will induce detachment. Aurora B kinase phosphorylates *C. elegans* Ndc80 *in vitro*, and mutation of four consensus Aurora B kinase phosphorylation sites to alanine (corresponding to residues 5, 15, 44, and 55 in human Hec1) prevents phosphorylation [45, 73], suggesting that one or more of these four residues is a key phosphorylation target. Future work is needed to test the minimum number of Hec1 point mutations that are required to elicit a detachment phenotype in vertebrate cells and to determine which specific residues or combinations of residues are the effectors of the phenotype. Our data support a model in which the tail domain of Hec1 acts as a regulator of kinetochore-microtubule attachment in cells. When kinase activity is elevated, the tail domain is phosphorylated, and microtubule turnover at the kinetochore microtubule interface is high. As chromosomes align at the spindle equator, kinase activity decreases at the outer kinetochore, the tail domain of Hec1 becomes dephosphorylated, and kinetochore-microtubule attachments are stabilized. Future studies that correlate Hec1 phosphorylation *in vivo* with chromosome biorientation status will be key in testing this model.

Our findings do not rule out recently proposed alternative models in which the N-terminal tail domain of Hec1 mediates kinetochore-microtubule binding by tethering Ndc80 complexes together at the kinetochore-microtubule interface [73]. Here, it is proposed that direct binding of the Ndc80 complexes to microtubules is largely mediated by electrostatic interactions between positive residues within the CH domains of Nuf2 and Hec1 and the C-terminal tubulin tails. In support of this model, the affinity of the Ndc80^{bonsai} complex for microtubules was significantly reduced when point mutations were made in the CH domain

of either Nuf2 or Hec1 that reduced the positive charge of these domains [73].

Although the 80 amino acid N-terminal tail domain is required for kinetochore-microtubule attachment, it is not needed to maintain the mitotic checkpoint. The CH domain, however, is required. A previous study has demonstrated an interaction between Hec1 and the Mad2-binding partner Mad1 in a yeast two-hybrid assay [38]. It will be important to establish whether the CH domain of Hec1 directly mediates this binding to Mad1 or to other mitotic-checkpoint factors. It will also be important to determine whether loss of the Hec1 CH domain affects the ability of Nuf2 to participate in checkpoint protein binding.

Chapter 4

The CH Domain of Hec1 is Essential for Mediating Kinetochores-MT Attachments

4.1 Introduction

The Ndc80 complex is localized at the outer kinetochore, with the N-terminal region of Hec1 and Nuf2 oriented distal to the chromosome and positioned for an interaction with incoming microtubules [47]. Recent structural studies from an engineered Ndc80 complex (Ndc80^{Bonsai}) indicate that the N-terminal domains of Hec1 and Nuf2 are folded into calponin homology (CH) domains, which are found to pack against each other [45, 51]. While CH domains were initially identified as actin binding domains, instances of coupled CH domains being essential for MT binding and MT plus end tip tracking do exist [84]. Negative stain EM of Ndc80 complexes bound to microtubules reveals a decoration of Ndc80 complexes along the MT lattice [34]. Interestingly, the binding of Ndc80 complexes along the MT lattice was shown to occur with consistent orientation and angular projection away from the MT lattice [72, 73]. Further implicating the Hec1/Nuf2 CH domains as the MT binding components in the Ndc80 complex, *in vitro* binding assays have demonstrated that the Hec1/Nuf2 heterodimer did bind to MTs, while the Spc24/Spc25 heterodimer was dispensable for MT binding [34, 50]. A combination of cryo-EM microscopy and crystallization docking studies have been used to visualize the Hec1/Nuf2-MT interaction, and while the points of contact were minimal, discrete regions within the CH domain of Hec1 and the MT lattice were identified [55, 72]. Additionally, crystallographic studies have revealed positively charged ridges on the surface of the Hec1 CH domain that are proposed to mediate an interaction with MTs. Of particular interest was residue Hec1 K166, as charge reversal mutation to this residue decreased the Ndc80 complex-MT binding affinity by approximately 54 fold [45]. Interestingly, the previous biophysical mapping studies have positioned residue Hec1 K166 at one of the few direct points of contact in the Ndc80-MT interaction [55, 72]. These studies

strongly implicate the Hec1 CH domain as a binding factor for MTs, but *in vivo* its role has not been tested.

Extending N-terminally off of the Hec1 CH domain is an unstructured 80 amino acid tail domain. While the 80 amino acid tail domain structure evades structural insights due to the inherent flexibility within the tail, *in vivo* and *in vitro* work has indicated the tail domain to be essential in MT binding and faithful mitotic progression [45, 50, 52, 53]. Additionally, the 80 amino acid tail domain has been implicated as a regulator of kinetochore-MT attachment through 9 Aurora B Kinase (ABK) phosphorylation sites. While the exact mechanism of ABK regulation remains unknown, it has been demonstrated that ABK phosphorylation of the 80 amino acid tail domain occurs during mitosis, and upon doing so, significantly alters MT binding affinity both *in vivo* and *in vitro* [34, 47, 52, 64].

Together, it has been demonstrated that two regions within the N-terminal portion of Hec1 have MT binding potential. Previous work has demonstrated that upon removal of the 80 amino acid tail domain, the CH domain was not sufficient for establishing kinetochore-MT attachments *in vivo* [52, 53]. But is the converse true? When the Hec1 CH domain is impaired in MT binding function, can the 80 amino acid tail domain of Hec1 rescue kinetochore-MT attachments?

4.2 Results

4.2.1 K166D Point Mutation to the Hec1 CH Domain Results in a Kinetochore-Null Phenotype

Hec1's CH domain contains numerous surface exposed lysine residues, which form positively charged ridges shown to be important for MT binding *in vitro* [45]. Specifically, mutation of lysine 166 was shown to have the most dramatic affect on MT binding, yielding nearly a 54 fold decrease in MT binding. To assess the significance of this residue *in vivo*, a charge-reversal mutant was generated in which lysine 166 was mutated to aspartic acid

(Hec1^{K166D}-GFP). Cells expressing the Hec1^{K166D}-GFP exhibited a kinetochore-null phenotype, as they were incapable of aligning chromosomes in a metaphase plate (Figures 4.1&4; Table 4.3). Sister kinetochore pairs had both rest length inter-kinetochore measurements (Figure 4.2; Table 4.2) and a decreased percentage of end-associated kinetochore-MT attachments (Figure 4.3; Table 4.3). These results demonstrate that the CH domain of Hec1 is essential for kinetochore-MT attachments and the 80 amino acid tail domain can not sufficiently overcome a defective CH domain to establish a functional kinetochore.

4.2.2 A Hyper-Attaching Hec1 Tail Domain is not Sufficient to Rescue Defects Induced by the K166D Point Mutation

The 80 amino acid tail domain of Hec1 has been shown to be essential for Ndc80-MT binding as well as a faithful progression through mitosis [45, 52]. It has been proposed that an electrostatic interaction exists between the basic tail of Hec1 and the acidic tails that extend off of tubulin. The 80 amino acid tail domain of Hec1 contains 9 ABK phosphorylation sites, shown to be important for regulation of kinetochore-MT attachment [45, 47, 52, 85]. A current model suggests that ABK mediated phosphorylation of the 80 amino acid tail domain of Hec1 results in an electrostatic repulsion between the Hec1 tail and the tails of tubulin (Figure 1.8). Supporting this model is recent *in vitro* work, demonstrating that inclusion of activated ABK significantly decreased MT binding affinity for the Ndc80 complex [45]. Furthermore, when mutation to the 9 putative phosphorylation sites precludes phosphorylation (Hec1^{9A}) or conversely mimics phosphorylation (Hec1^{9D}), contrasting phenotypes of kinetochore-MT hyper-attachment and kinetochore-MT detachment are observed, respectively [47, 52, 85]. Given the hyper-attachment phenotype observed in cells expressing a non-phosphorylatable Hec1 tail domain (Hec1^{9A}), this mutant was used as a tool to assess the relative contributions that the CH domain and 80 amino acid tail domain

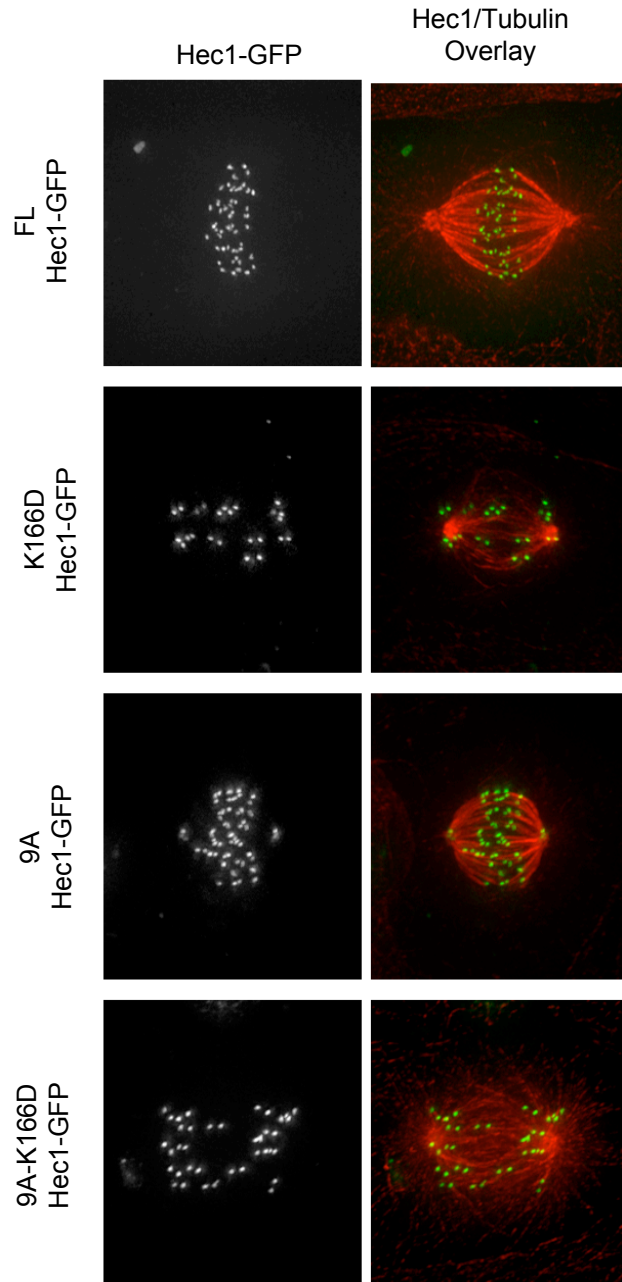


Figure 4.1: Point mutation to the Hec1 calponin homology domain results in mitotic defects

Projections of deconvolved immunofluorescent images of PtK1 cells depleted of endogenous Hec1 and rescued with the indicated GFP-fusion protein.

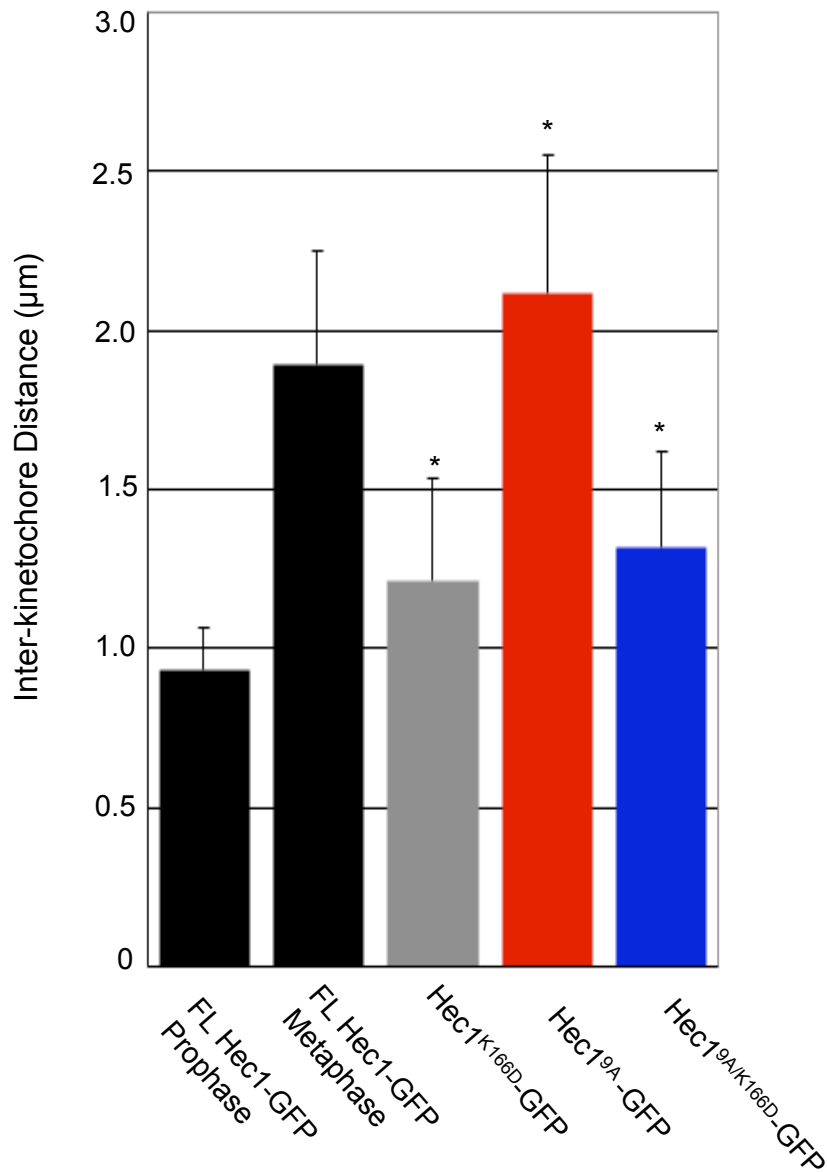


Figure 4.2: Point mutation to the Hec1 calponin homology domain impairs tension generating kinetochore-MT attachments

Quantification of inter-kinetochore distances, which were measured from Hec1-GFP centroid to Hec1-GFP centroid (Prophase FL Hec1-GFP: IKD=0.93±0.13, n=11 cells, 46 kinetochores; Biooriented FL Hec1-GFP: IKD=1.89±0.36, n=33 cells, 426 kinetochores; Prometa K166D Hec1-GFP: IKD=1.21±0.33, n=69 cells, 740 kinetochores; Biooriented Hec1-GFP^{K166D}: IKD=1.4±0.27, n=19 cells, 259 kinetochores; Biooriented Hec1^{9A}-GFP: IKD=2.11±0.44 n=19 cells, 224 kinetochores; Prometa Hec1^{9A/K166D} Hec1-GFP: IKD=1.22±0.28 n=34 cells, 85 kinetochores). Measurements were made from the terminal phenotype achieved in cells expressing a given construct. Black asterisk indicates a statistically significant difference with respect to FL Hec1 Metaphase (p<.001).

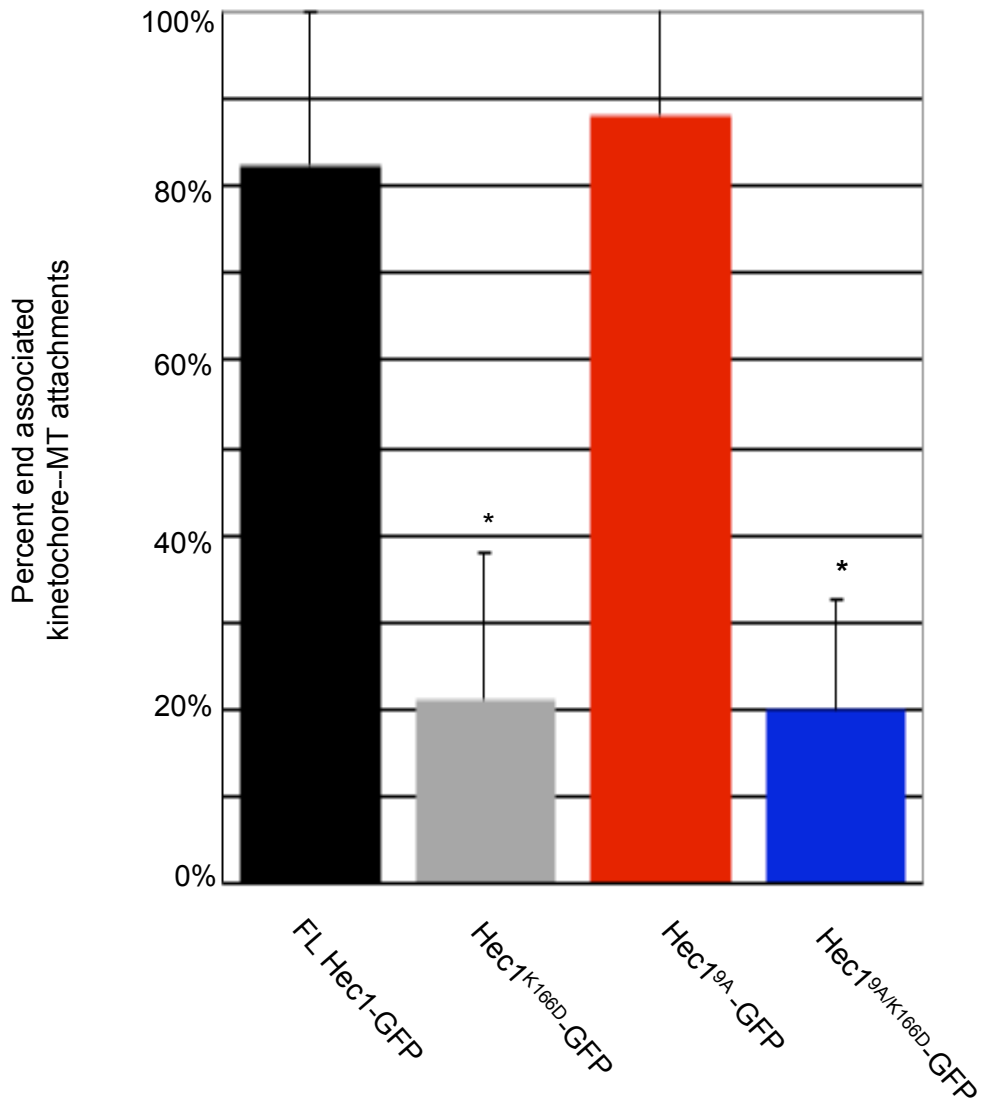


Figure 4.3: Point mutation to the Hec1 calponin homology domain impairs stable kinetochore-MT attachments

(FL Hec1-GFP: Attachment=82.5±17.4%, n=63 cells, 2155 kinetochores; Hec1^{K166D}-GFP: Attachment=21.0±16.8%, n=52 cells, 1812 kinetochores; Hec1^{9A}-GFP: Attachment=88.1±21.0%, n=28 cells, 829 kinetochores; Hec1^{9A/K166D}-GFP: Attachment=20.0±12.7%, n=17 cells, 536 kinetochores). Measurements were made by averaging values of cells rescued with a given construct from all phases of mitosis. Black asterisk indicates a statistically significant difference with respect to FL Hec1 (p<.001).

Table 4.1: Inter-kinetochore distance values for cells rescued with Hec1 calponin homology mutants

Hec1 Construct	IKD Average	Std. Dev.	# of Ks	# of Cells
FL Prophase	0.93	0.13	46	11
FL Partial	1.89	0.36	243	18
FL Metaphase	1.89	0.36	183	15
FL Bioriented	1.89	0.36	426	33
K166D Prometa	1.21	0.33	740	69
9A Bioriented	2.11	0.44	224	19
9A/K166D Prometa	1.32	0.30	187	34

Table 4.2: Percent end associated kinetochore-MTs for cells rescued with Hec1 calponin homology mutants

Hec1 Construct	# of Attach. Ks	# of Unattach.Ks	Total # of Ks	% of Attach. Ks	Std. Dev.	# of Cells
FL	1778	377	2155	82.5	17.4	63
K166D	380	1432	1812	21.0	16.8	52
9A	730	99	829	88.1	21.0	28
9A/K166D	107	429	536	20.0	12.7	17

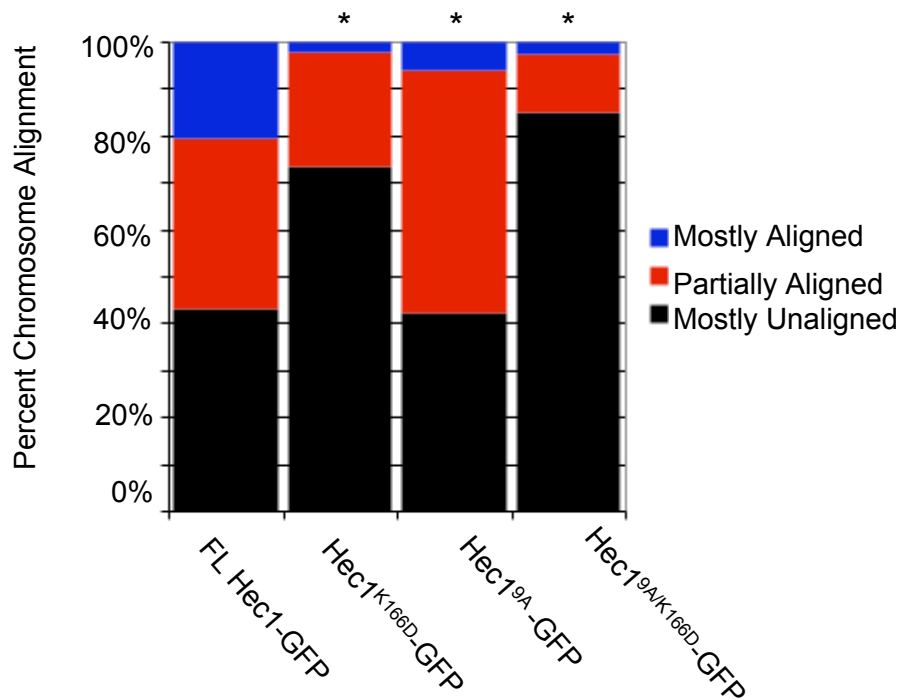


Figure 4.4: Point mutation to the Hec1 calponin homology domain impairs chromosome alignment

Quantification of chromosome alignment phenotypes in cells depleted of Hec1 and rescued with Hec1-GFP mutant constructs. Cells with Mostly Aligned (MA) chromosomes (blue) had no chromosomes off the metaphase plate, cells with Partially Aligned (PA) chromosomes (red) had 1-4 chromosomes off of a metaphase plates, and cells with Mostly Unaligned (MU) chromosomes (black) had either no chromosome alignment or more than 4 chromosomes off of the metaphase plate. Black asterisk indicates a statistically significant difference with respect to the percent of cells rescued with FL Hec1-GFP achieving metaphase plates.

Table 4.3: Percent chromosome alignment values for cells rescued with Hec1 calponin homology mutants

Phenotype	FL	K166D	9A	9A/K166D
% Mostly Unaligned	44	73.4	42.4	85
% Partially Aligned	30	24.5	51.5	12.5
% Mostly Aligned	26	2.1	6.1	2.5
Total # of Cells	58	94	33	40

make in establishing kinetochore-MT attachments. To delineate if a non-phosphorylatable 80 amino acid tail domain of Hec1 could compensate for a defective CH domain, a hybrid mutant construct was developed by combining the Hec1^{K166D} CH domain mutation with the Hec1^{9A} 80 amino acid tail mutation (Hec1^{9A/K166D}).

First, kinetochore-MT attachment phenotypes were analyzed in cells expressing Hec1^{9A}-GFP to determine if hyper-attachment was observed (Figure 4.1). Indeed, inter-kinetochore distances and percent end-associated kinetochore-MT values were all elevated in the FL Hec1-GFP rescue (Figures 4.2&3; Tables 4.2&3). Additionally, a partial alignment phenotype was observed for Hec1^{9A}-GFP rescued cells, and likely resulted from kinetochore-MT attachments that lacked the dynamic phospho-regulation needed for proper chromosome alignment (Figure 4.4; Table 4.4). Phenotypically, cells expressing the Hec1^{9A/K166D}-GFP were indistinguishable from Hec1^{K166D}-GFP cells, as a lack of chromosome orientation and non-robust bi-polar spindles were observed (Figure 4.1). Scoring of cells expressing Hec1^{9A/K166D}-GFP indicated a lack of chromosome orientation at the spindle equator (Figure 4.4; Table 4.4) decreased inter-kinetochore distances (Figure 4.2; Table 4.2), and a decreased percentage of end-associated kinetochore-MT attachments (Figure 4.3; Table 4.3). From these experiments it is clear that a hyper-attaching 9A Hec1 tail domain cannot compensate for defects resulting from the K166D Hec1 mutation.

4.3 Discussion

Together, the results presented here suggest that a positively charged ridge within the CH domain of Hec1 is essential for kinetochore-MT attachments. Our work compliments previous *in vitro* work which demonstrated that a charge reversal at residue K166 resulted in a significant reduction in MT binding affinity [45]. Additionally, two recent cryo-EM/crystal docking studies have positioned the CH domain of Hec1 at the Ndc80-MT interface [55, 72]. A closer evaluation of these models reveals that residue K166 of the Hec1 CH domain is a

point of contact between Hec1 and the MT lattice, further supporting the significance of this residue as an essential factor at the Hec1/MT interface[55].

Previous work has demonstrated the 80 amino acid tail domain of Hec1 to be essential for mediating stable kinetochore-MT attachments. When the Hec1 80 amino acid tail domain was removed, kinetochore-MT interactions were significantly impaired, suggesting that the Hec1 CH domain alone cannot sufficiently establish kinetochore-MT attachments [52, 53]. However, other work has implicated the CH domain of Hec1 as an additional essential MT binding factor in the N-terminal portion of Hec1 [45]. To delineate *in vivo* if these binding regions were mutually exclusive, the Hec1^{9A/K166D} was used. These studies revealed that a hyper-attaching tail domain could not compensate for defects in the Hec1 CH domain, and imply that these two regions make distinct binding contributions that are both required for an interaction with MTs.

What is the mechanism of Hec1-MT binding? Given that the 80 amino acid tail and CH domains of Hec1 reside within N-terminus of the same protein, with both conferring MT binding, it is plausible that these regions work in tandem to coordinate binding. But the question remains, by what means? The recent cryo-EM studies referred to earlier have fit the crystal structures for Ndc80^{Bonai} and tubulin into the electron density of Ndc80 complex bound along that of MT lattice, and revealed that discrete points of contact existed [55]. Specifically, residue K166 of the Hec1 CH domain was found to reside within a small domain that interfaced along the MT lattice. Because the Ndc80 crystal structures used in these docking studies lack the 80 amino acid tail domain (removed for the crystallization process due to its inherent flexibility), the exact position of the tail domain could not be precisely defined. However, the authors made predictions based on the length of the 80 amino acid tail domain and suggest it could serve an essential role in kinetochore-MT attachment either as 1) an oligomerizing linker between Ndc80 complexes with the Hec1 CH still serving as a direct point of contact between Ndc80 and MTs, or 2) an extension from the

Ndc80 complex used to bind and ratchet adjacent MT dimers during translation of the kinetochore along the MT lattice, all the while maintaining points of contact between the Hec1 CH domain and MTs [55].

The models and work discussed here implicate a joint role in binding for the 80 amino and tail and CH domain of Hec1, whereby each domain is essential for a strong kinetochore-MT attachment. In the future, it will be important to define the exact mechanism of how these regions work together to coordinate a binding interaction as the Ndc80 complex translates along the MT lattice. In previous structural experiments, the intrinsically disordered Hec1 80 amino acid tail domain was removed to facilitate Ndc80 complex crystallization. The lack of structural data for the Hec1 80 amino acid tail domain has made it difficult to understand Ndc80 binding to the MT lattice. In future studies, crystallization of either the Ndc80 complex, or just the 80 amino acid tail domain of Hec1, directly bound to a short MT fragment such as the C-terminal tubulin tail domain, whereby the 80 amino acid tail domain could confer structural stability upon binding, will be helpful for understanding how Ndc80 binds to and translocates along the MT lattice.

Chapter 5

Phosphorylation, Length, and Charge Composition of the Hec1 80 Amino Acid Tail Domain Contribute to Kinetochores-MT Interactions.

5.1 Introduction

During mitosis, the versatile linkage between the kinetochore and MTs undergoing dynamic instability produces forces used for proper orientation of chromosomes along the metaphase plate and a faithful progression through mitosis [59]. Linking the kinetochore to stochastically disassembling/assembling MT ends requires a flexible interaction between the kinetochore and MT. Specifically, the attachments must be strong enough to generate forces for chromosome movement yet loose enough to track continually polymerizing and depolymerizing MT plus-ends. Key to the flexible interaction at the kinetochore-MT interface is Hec1, a component of the Ndc80 complex. Deciphering what properties of Hec1 allow for flexible kinetochore-MT interactions will provide insight not only into the mechanism of how kinetochore-MT linkages are maintained, but also how *dynamic* kinetochore-MT interactions are promoted in mitosis.

Previous *in vivo* work has identified the 80 amino acid tail domain of Hec1 as being essential for establishment of kinetochore-MT attachments, metaphase plate formation, and a faithful progression through mitosis [52, 53]. Similarly, removal of the 80 amino acid tail domain significantly decreases MT binding affinity *in vitro* [45]. An electrostatic binding interaction is proposed to exist between the highly basic, positively charged tail domain of Hec1 and the highly acidic, negatively charged tail domains of tubulin [45]. The ability to modulate this electrostatic binding interaction through ABK-mediated phosphorylation of the Hec1 80 amino acid tail domain has been demonstrated, and may explain the mechanism by which kinetochore-MT interactions are regulated [64]. Features of the Hec1 80 amino acid tail proposed to contribute to a faithful kinetochore-MT interaction include its 1) Aurora B kinase-mediated phosphorylation 2) length, and 3) charge. However, a thorough *in vivo*

investigation of the contribution that these features make to kinetochore-MT binding has not been done.

Aurora B Kinase Regulation of the Hec1-MT Interaction:

Accurate chromosome segregation requires a flexible linkage between the kinetochore and MTs, capable of generating tension from dynamic spindle microtubules to promote chromosome biorientation. Imperative to faithful kinetochore-MT interactions is the targeting of the conserved chromosomal passenger complex (CCPC) to the kinetochore [86]. Aurora B kinase (ABK), the enzymatic component of the CCPC, has been previously shown to destabilize incorrect kinetochore-MT attachments upon localization to and phosphorylation of substrates at the outer-kinetochore [82, 87, 88]. While a previous role for ABK phosphorylation in detachment of kinetochore-MT attachments has been demonstrated, an additional role for ABK phosphorylation as a regulatory switch of dynamic kinetochore-MT interactions has been suggested [85].

If the hypothesis that ABK regulates kinetochore-MT interactions in mitosis is true, ABK must target an outer-kinetochore protein required in kinetochore-MT binding. Indeed, ABK phosphorylates multiple components of the KMN (Knl-1, Mis12 and Ndc80) network including Ndc80, a complex capable of directly binding MTs. The fact that ABK targets Ndc80, an essential MT binding factor, makes the Ndc80 complex an ideal candidate protein for regulation of dynamic kinetochore-MT interactions. Essential to Ndc80 complex function as a kinetochore-MT binding component is the N-terminal 80 amino acid tail domain of Hec1 [52, 53]. Within this 80 amino acid tail exist 9 ABK phosphorylation sites, as identified by mass spectroscopy following *in vitro* phosphorylation [45, 47]. While the primary sequence of the Hec1 tail domain is divergent, the general clustering of ABK phosphorylation sites in fission yeast, human and *C. elegans* suggests a conserved functional role for these sites potentially in the regulation of kinetochore-MT attachments [34]. *In vitro*, the 80 amino acid

tail domain of Hec1 has been shown to be a substrate for active ABK phosphorylation [34]. Additionally, ABK mediation of Ndc80-MT interaction has been demonstrated in an *in vitro* MT binding assay, as inclusion of active ABK significantly decreased the Ndc80-MT binding affinity [34]. *In vivo*, cells expressing a phospho-mimetic version of Hec1, where all nine phosphorylation sites were mutated to aspartic acid to mimic the maximally constitutively phosphorylated state of Hec1 (Hec1^{9D}-GFP), a kinetochore-null phenotype was observed [52]. Conversely, when these phosphorylation sites have been mutated to alanine (Hec1^{9A}-GFP), thus precluding phosphorylation of the Hec1 80 amino acid tail domain, a hyper-attachment phenotype was observed [47, 52]. The expression of a non-phosphorylatable 80 amino acid Hec1 tail domain (Hec1^{9A}-GFP), resulting in inter-kinetochore distances that exceeded control metaphase values, supports the notion that dynamic control of Hec1 tail phosphorylation is required to engage a flexible kinetochore-MT association. Together, these results strongly support a model whereby addition of phosphate groups to the 80 amino acid tail domain impairs MT binding affinity, possibly by reducing the electrostatic binding potential existing between an unmodified Hec1 tail and MTs. This is a particularly attractive model, as manipulation of Hec1-MT binding through phosphorylation of the Hec1 80 amino acid tail could explain the mechanism by which kinetochore-MT attachments are modulated.

Indeed, Hec1 phosphorylation of a subset of sites may be favored in instances where a weakened, but not completely abolished, MT binding interaction is desired. Particular interest resides with serine residues 8, 15, 44, and 55, which are conserved phosphorylation sites from *C. elegans* to humans [34]. *In vivo* our lab has demonstrated that phosphorylation of these conserved sites is indeed dependent upon Aurora B kinase, with high levels of phosphorylation observed early in mitosis, followed by a significant decrease to lower levels of phosphorylation which persist as a cell enters anaphase [64]. Further supporting the potential importance of these residues, EM analysis has been performed where phospho-

mimetic mutation to the four conserved residues significantly changed the kinetochores ability to bind MTs, and structurally the kinetochore existed in a more compact state, indicating a lack of tension-generating forces [89]. While previous work has successfully demonstrated that aspartic acid mutation to all 9 phosphorylation sites can ablate kinetochore-MT interactions [52], understanding the individual contributions that the 4 conserved phosphorylation sites make towards fine tuning the kinetochore-MT binding affinity is important.

Hec1 Tail Domain Length as a Necessary Component of the Hec1-MT Interaction:

It has been suggested that the length of the 80 amino acid tail domain is required to maintain a functional interaction at the kinetochore-MT interface through 1) oligomerization of Ndc80 complexes [55, 72], or 2) directly binding the MT lattice [53]. Evidence for Ndc80 complex oligomerization has been observed in numerous *in vitro* assays. EM analysis of purified Ndc80 complexes bound to MTs demonstrated that Ndc80 complexes did not bind uniformly along the MT lattice but instead in patches, suggesting a cooperative binding interaction that has been further confirmed through MT co-sedimentation assays [34, 55]. Crystal structures of the Ndc80^{Bonsai} complex [45] and the tubulin dimer were docked onto cryo-EM images of MT-bound Ndc80 complexes in an effort to reconstruct the Ndc80 complex/MT lattice interface [55]. These studies additionally supported cooperative binding as the calculated difference between the electron densities of the cryo-EM reconstructions and the x-ray crystallography structures depicted significant electron density between adjacent Ndc80 complexes bound along the MT lattice [55, 90]. However, the electron density existing between adjacent Ndc80 molecules could not be accounted for from the Ndc80^{Bonsai} crystal structure. The authors hypothesized that the 80 amino acid Hec1 tail domain, which was missing from the Ndc80^{Bonsai} crystal structure, was responsible for this unaccounted electron density [55]. Additionally the authors demonstrated that phospho-

mimetic mutations to the Hec1 80 amino acid tail domain reduced Ndc80 complex clustering along the MT lattice, suggesting that modulation of Hec1 tail charge influenced Ndc80 complex oligomerizing and ultimately mediated Ndc80-MT binding [55].

The 80 amino acid tail domain of Hec1 has also been suggested to mediate kinetochore-MT binding through a direct interaction with the MT lattice. *In vivo*, silence and rescue experiments have demonstrated that removal of, or charge manipulation to, the Hec1 80 amino acid tail disrupts normal kinetochore-MT interactions [47, 52, 53, 90]. Additionally, *in vitro* binding studies have revealed the Hec1 80 amino acid tail domain alone bound MTs with an affinity comparable to the full Ndc80 complex [53]. Lastly, support is growing for an electrostatic model of interaction facilitating direct binding between the acidic, C-terminal tails of tubulin, and the basic, N-terminal 80 amino acid tails of Hec1 [45].

Regardless of which model proves to be true for the Hec1 80 amino acid tail domain (direct MT binder vs. Ndc80 complex oligomerizing factor), it remains unknown what length of the tail is essential to the formation of a dynamic kinetochore-MT interaction. Additionally, in either model charge associated with the Hec1 tail domain contributes towards kinetochore-MT binding, and this raises the question; can a Hec1 construct, expressing a short tail domain with high charge, mediate faithful kinetochore-MT attachments, or is a longer segment of the native tail domain required?

Composition vs. Primary Sequence for the Hec1 80 Amino Acid Tail Domain:

The 80 amino acid tail domain of Hec1 is predicted to be an unstructured region of the protein, required for establishment of kinetochore-MT interactions [45, 52, 53]. For crystallization, the Ndc80^{Bonsai} complex was engineered lacking the inherently flexible 80 amino acid tail domain to facilitate the crystallization process, and thus structural data for the 80 amino acid tail is lacking [45]. Using the Ndc80^{Bonsai} and tubulin dimer crystal structures fit into cryo-EM maps of Ndc80 complexes bound along the MT lattice, two roles for the 80

amino acid tail domain have been proposed. One model suggests that the 80 amino acid tail domain of Hec1 is positioned in the vicinity of the C-terminal tubulin tail domains (“E-hooks”) extending from the MT. The close proximity of the Hec1 and tubulin tail domains may enable a direct contact, however the precise Hec1 tail/MT contacts remain unknown [55].

Interestingly, the 80 amino acid tail domain of Hec1 has been suggested to bind MTs through E-hooks [34, 55]. When the E-hooks were cleaved through protease digestion, the Ndc80-MT interaction was lost *in vitro*, and strongly implicates Ndc80 and the tubulin-tail as significant binding partners [34]. The high basicity associated with the 80 amino acid tail (# of acids= 5, # of bases= 16, sum of charge=11; 11/80 amino acids=+0.14 charge per amino acid; Table 5.2.16) is a property which has been suggested to mediate an electrostatic interaction with the acidic tails of tubulin (C-terminal tubulin tail isotype 1: acids= 11, # of bases= 0, sum of charge=-11; -11/18 amino acids= -0.61 charge per amino acid; Table 5.2.16) [45]. Supporting the hypothesis of a charge based interaction between Hec1 and MTs, a recent study demonstrated that when a subset of basic residues within the 80 amino acid tail domain were mutated to neutral alanines, the reduced charge on the Hec1 tail impaired kinetochore-MT attachments both *in vivo* and *in vitro* [90].

If the basis of interaction between Hec1 and MTs is dependent upon an electrostatic charge-charge interaction, then does the primary sequence of the unstructured 80 amino acid tail domain matter? Traditional biochemical principles state that protein function is dependent upon primary sequence and the well-ordered structure of a protein. However, recent work on intrinsically disordered proteins has shifted the way some think of the traditional sequence-structure-function protein relationships. Specifically, in 2004 Ross et al. showed that upon scrambling the primary sequence of intrinsically disordered amyloid-forming protein, the proteins ability to produce amyloid fibrils was maintained [91]. Indeed, a demonstration of dependence on amino acid composition, rather than primary sequence, for intrinsically disordered protein function has been observed in other systems. In the context

of a flexible kinetochore-MT interaction, is composition of the intrinsically disordered Hec1 80 amino acid tail domain sufficient to establish a faithful attachment, or is primary sequence required to mediate the native function of the 80 amino acid tail domain?

Described above are three features intrinsic to the Hec1 80 amino acid tail domain (ABK-mediated phosphorylation, length, and charge), proposed to contribute in the establishment and regulation of faithful kinetochore-MT interactions. Through manipulation designed to individually address each of the three Hec1 80 amino acid tail domain features, we aimed to extract the individual contribution that these features make to the establishment and regulation of flexible kinetochore-MT interactions. Ultimately, a better understanding of how the Hec1 80 amino acid tail domain contributes to MT binding will provide a clearer understanding of how faithful kinetochore-MT interactions are achieved.

Chapter 5.2 Results

5.2.1 Hec1 Tail Phospho-mimetic Mutation to Conserved Aurora B Kinase Phosphorylation Sites Impairs Kinetochore-Microtubule Attachments

Previous *in vitro* work has identified 9 ABK phosphorylation sites on the Hec1 80 amino acid tail domain [45, 47]. When mutated to aspartic acid to mimic constitutive phosphorylation, kinetochore-MT attachments were significantly impaired [52]. More recent work has demonstrated that 4 of these sites (serine 8,15,44,55) are conserved from *C. elegans*, and have been shown to be phosphorylated *in vivo* [64]. With emphasis on these conserved residues, we wanted address how discrete phosphorylation events at these 4 residues affected kinetochore-MT interactions. The silence and rescue strategy previously described [52] was used to demonstrate that cells expressing the Hec1-GFP SD^{8,15,44,55} mutant (Figure 5.2.1; Table 5.2.1) exhibited significantly decreased levels for both inter-kinetochore tension and the percent of stable kinetochore-MT attachments, as compared to cells expressing FL Hec1-GFP (Figure 5.2-2&3, Table 5.2-2&3). Consistent with this

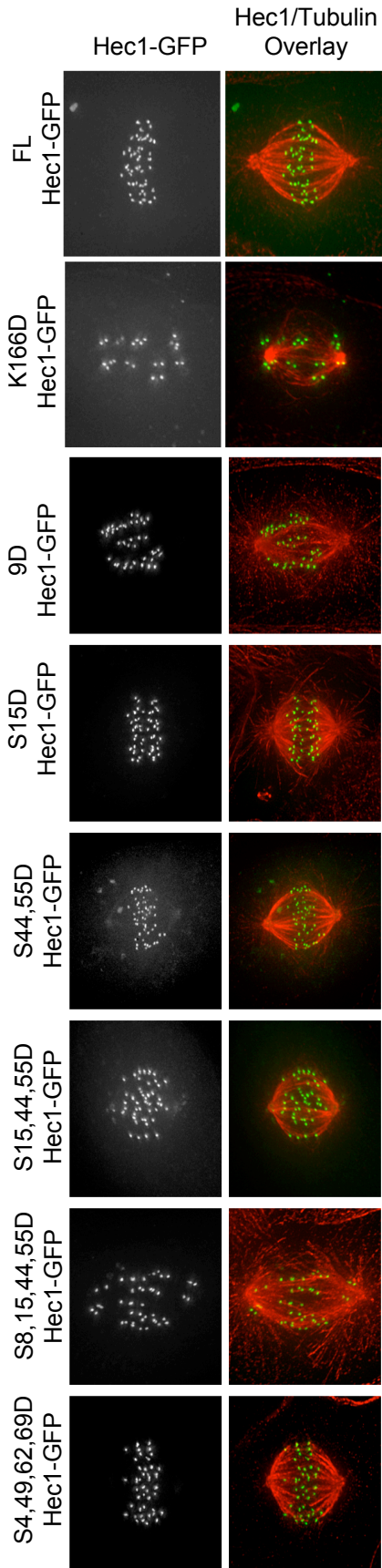


Figure 5.2.1: Phosphorylation of conserved ABK sites regulates kinetochore-MT interactions

Projections of deconvolved immunofluorescent images of PtK1 cells depleted of endogenous Hec1 and rescued with the indicated GFP-fusion protein.

Table 5.2.1: Constructs for phospho-mimetic Hec1 mutants

Hec1 Mutant Construct	Amino Acid Sequence: Only the 80 amino acid tail domain sequence is shown
S15D Hec1-GFP Red=Aspartic Acid Mutation	MKRSSVSSGGAGRLDMQELRSQDVNKQGLYTPQT KEKPTFGKLSINKPTSERKVSLFGKRTSGHGSRNSQ LGIFSSSEKI
S44,55D Hec1-GFP Red=Aspartic Acid Mutation	MKRSSVSSGGAGRLSMQELRSQDVNKQGLYTPQT KEKPTFGKLDINKPTSERKVDLFGKRTSGHGSRNS QLGIFSSSEKI
S8,44,55D Hec1-GFP Red=Aspartic Acid Mutation	MKRSSVSDGGAGRLSMQELRSQDVNKQGLYTPQT KEKPTFGKLDINKPTSERKVDLFGKRTSGHGSRNS QLGIFSSSEKI
S8,15,44,55D Hec1-GFP Red=Aspartic Acid Mutation	MKRSSVSDGGAGRLDMQELRSQDVNKQGLYTPQT KEKPTFGKLDINKPTSERKVDLFGKRTSGHGSRNS QLGIFSSSEKI
S4,49,62,69D Hec1-GFP Red=Aspartic Acid Mutation	MKRDSVSSGGAGRLSMQELRSQDVNKQGLYTPQT KEKPTFGKLSINKPDSERKVSLFGKRTDGHGSRND QLGIFSSSEKI
9D Hec1-GFP Red=Aspartic Acid Mutation	MKRDDVSDGGAGRLDMQELRSQDVNKQGLYTPQ TKEKPTFGKLDINKPDSERKVDLFGKRTDGHGSRN DQLGIFSSSEKI
9A Hec1-GFP Blue=Alanine Mutation	MKRAAVSAGGAGRLAMQELRSQDVNKQGLYTPQ TKEKPTFGKLAINKPTAERKVALFGKRTAGHGSRN AQLGIFSSSEKI
S8D A Background Hec1-GFP Red=Aspartic Acid Mutation Blue=Alanine Mutation	MKRAAVSDGGAGRLAMQELRSQDVNKQGLYTPQ TKEKPTFGKLAINKPTAERKVALFGKRTAGHGSRN AQLGIFSSSEKI
S44,55D A Background Hec1-GFP Red=Aspartic Acid Mutation Blue=Alanine Mutation	MKRAAVSAGGAGRLAMQELRSQDVNKQGLYTPQ TKEKPTFGKLDINKPTAERKVDLFGKRTAGHGSRN AQLGIFSSSEKI
S8,44,55D A Background Hec1-GFP Red=Aspartic Acid Mutation Blue=Alanine Mutation	MKRAAVSDGGAGRLAMQELRSQDVNKQGLYTPQ TKEKPTFGKLDINKPTAERKVDLFGKRTAGHGSRN AQLGIFSSSEKI
S8,15,44,55D A Background Hec1-GFP Red=Aspartic Acid Mutation Blue=Alanine Mutation	MKRAAVSDGGAGRLDMQELRSQDVNKQGLYTPQ TKEKPTFGKLDINKPTAERKVDLFGKRTAGHGSRN AQLGIFSSSEKI

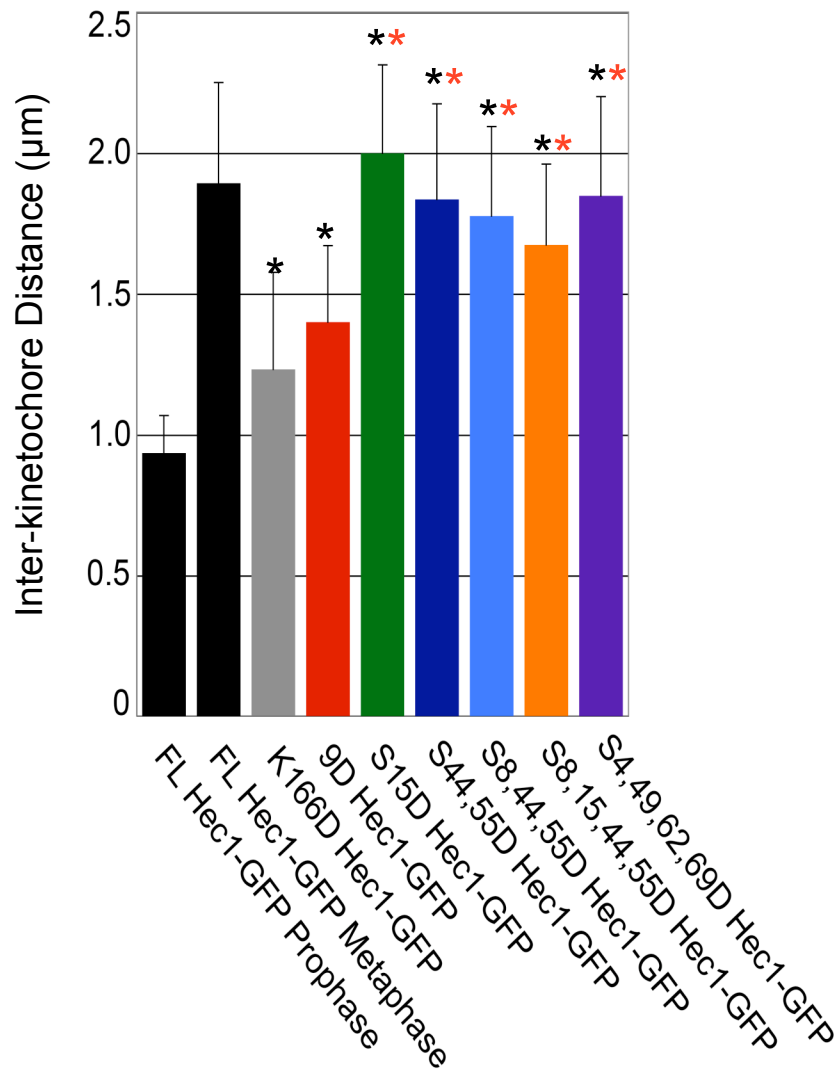


Figure 5.2.2: Incrementally introducing phospho-mimetic mutation to phosphorylation sites impairs tension generating kinetochore-MT attachments

Quantification of inter-kinetochore distances, which were measured from Hec1-GFP centroid to Hec1-GFP centroid (Prophase FL Hec1-GFP: IKD=0.93±/0.13, n=11 cells, 46 kinetochores; Bioriented FL Hec1-GFP: IKD=1.89±/0.36, n=33 cells, 426 kinetochores; Prometa K166D Hec1-GFP: IKD=1.21±/0.33, n=69 cells, 740 kinetochores; Bioriented 9D Hec1-GFP: IKD=1.4±/0.27, n=19 cells, 259 kinetochores; Bioriented S15D Hec1-GFP: IKD=2.07±/0.34 n=22 cells, 268 kinetochore pairs; Bioriented S44,55D Hec1-GFP: IKD=1.85±/0.35, n=24 of cells, 283 kinetochore pairs; Partially Aligned S8,44,55D Hec1-GFP: IKD=1.79±/0.31, n=27 cells, 235 kinetochore pairs; Partially Aligned S8,15,44,55D Hec1-GFP: IKD=1.62±/0.30, n=18 cells, 225 kinetochore pairs; Bioriented S4,49,62,69D Hec1-GFP: IKD=2.0±/0.39, n=10 cells, 95 kinetochore pairs).

Measurements were made from the terminal phenotype achieved in cells expressing a given construct. Black asterisk indicates a statistically significant difference with respect to FL Hec1 Metaphase, while a red asterisk indicates a statistically significant difference with respect to K166D Hec1 (p<0.001).

Table 5.2.2: Inter-kinetochore distance values for cells rescued with phospho-mimetic Hec1 mutants

Hec1 Construct	IKD Average	Std. Dev.	# of Ks	# of Cells
FL Prophase	0.93	0.13	46	11
FL Partial	1.89	0.36	243	18
FL Metaphase	1.89	0.36	183	15
FL Bioriented	1.89	0.36	426	33
K166D Prometa	1.21	0.33	740	69
9D Prometa	1.33	0.28	524	45
S15 D Bioriented	2.07	0.33	268	22
S44,55D Bioriented	1.85	0.35	283	24
S8,44,55D Bioriented	1.79	0.31	235	27
S8,15,44,55D Partial	1.62	0.30	225	18
S4,49,62,69D Bioriented	1.85	0.35	298	22

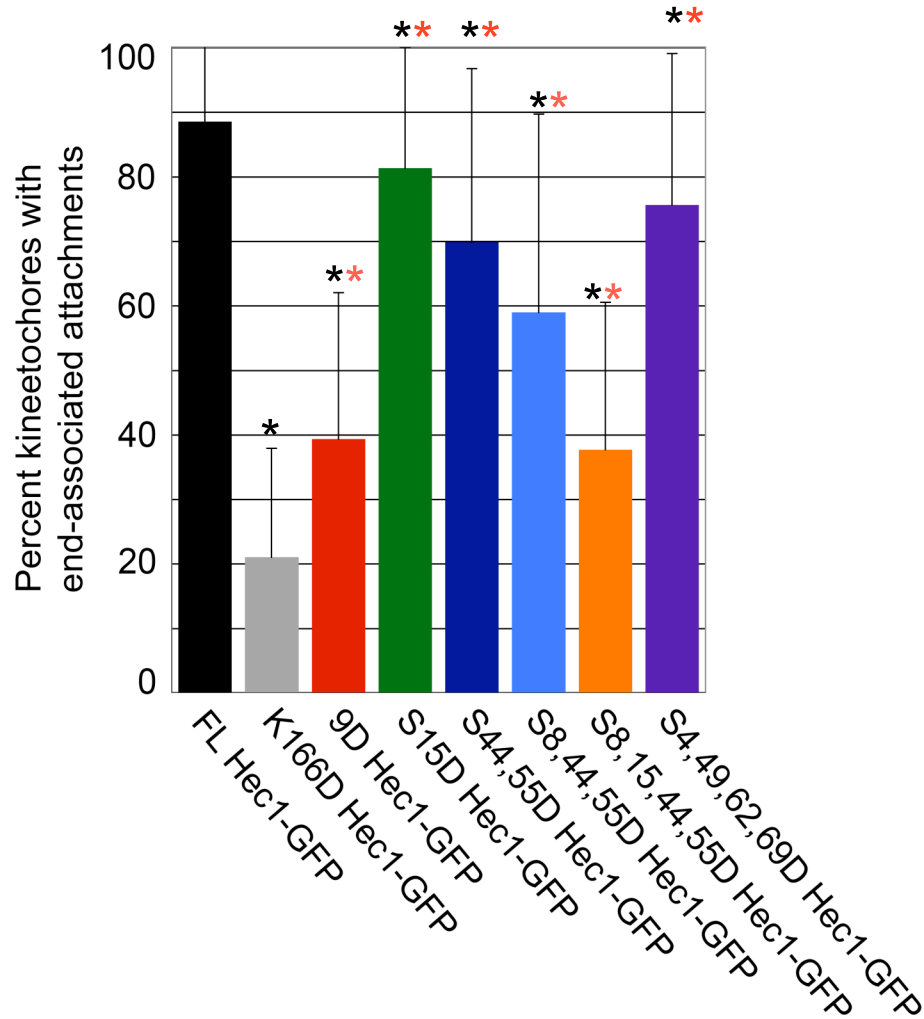


Figure 5.2.3: Incrementally introducing phospho-mimetic mutation to phosphorylation sites impairs stable kinetochore-MT attachments

(FL Hec1-GFP: Attachment=82.5±/17.4%, n=63 cells, 1778 kinetochores; K166D Hec1-GFP: Attachment=21.0±/16.8%, n=52 cells, 1812 kinetochores; 9D Hec1-GFP: Attachment=39.2±/22.6%, n=58 cells, 1841 kinetochores; S15D Hec1-GFP: Attachment=76.9±/20.8%, n=15 cells, 506 kinetochores; S44,55D Hec1-GFP: Attachment=69.8±/26.8%, n=28 cells, 995 kinetochores; S8,44,55D Hec1-GFP: Attachment=58.9±/30.7%, n=32 cells, 1154 kinetochores; S8,15,44,55D Hec1-GFP: Attachment=38.9±/22.6%, n=25 cells, 818 kinetochores; S4,49,62,69D Hec1-GFP: Attachment=75.6±/23.5%, n=23 cells, 626 kinetochores). Measurements were made by averaging values of cells rescued with a given construct from all phases of mitosis. Black asterisk indicates a statistically significant difference with respect to FL Hec1, while a red asterisk indicates a statistically significant difference with respect to K166D Hec1 ($p < 0.001$).

Table 5.2.3: Percent end-associated kinetochore-MT values for cells rescued with phospho-mimetic Hec1 mutants

Hec1 Construct	# of Attach. Ks	# of Unattach h.Ks	Total # of Ks	% of Attach. Ks	Std. Dev.	# of Cells
FL	1778	377	2155	82.5	17.4	63
K166D	380	1432	1812	21.0	16.8	52
9D	723	1118	1841	39.3	22.7	58
S15D	741	171	912	81.3	18.7	26
S44,55D	694	301	995	69.7	26.9	28
S8,44,55D	680	474	1154	58.9	30.7	32
S8,15,44,55 D	448	744	1192	37.6	22.9	36
S4,49,62,69 D	473	153	626	75.6	23.5	23

Table 5.2.4: Percent chromosome alignment values for cells rescued with phospho-mimetic Hec1 mutants

Phenotype	FL	K166D	9D	S15D	S to D 44,55	S to D 8,44,55	S to D 8,15, 44,55	S to D 4,49, 62,69
% Mostly Unaligned	43.2	73.4	70.3	48.1	46.7	60.4	57.5	46.3
% Partially Aligned	36.4	24.5	21.9	37.0	28.9	40.0	37.5	29.3
% Mostly Aligned	20.4	2.1	7.8	14.8	24.4	5.6	5.0	24.4
Total # of Cells	88	94	63	36	45	53	40	41

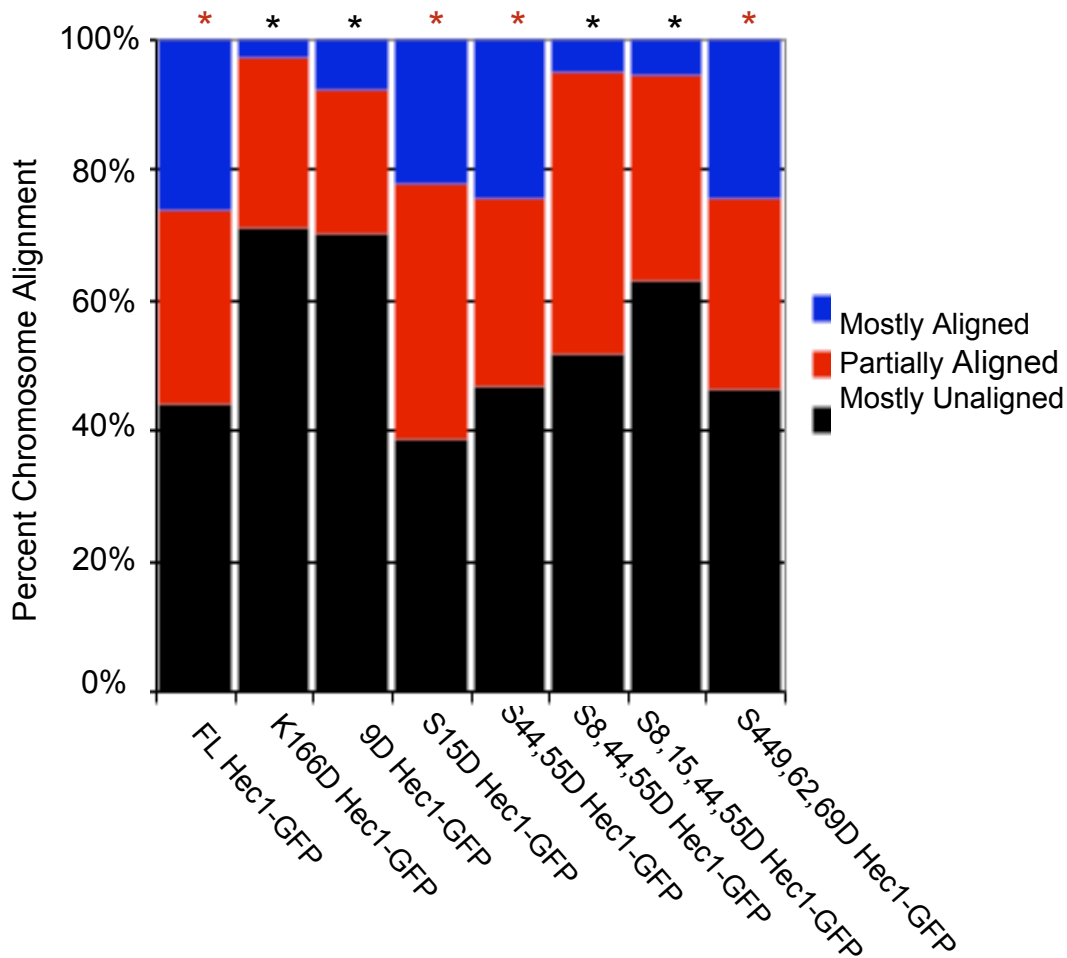


Figure 5.2.4: Phospho-mimetic mutation to conserved residues impairs chromosome alignment

Quantification of chromosome alignment phenotypes in cells depleted of Hec1 and rescued with Hec1-GFP D mutant constructs. Cells with Mostly Aligned (MA) chromosomes (blue) had no chromosomes off the metaphase plate, cells with Partially Aligned (PA) chromosomes (red) had 1-4 chromosomes off of a metaphase plates, and cells with Mostly Unaligned (MU) chromosomes (black) had either no chromosome alignment or more than 4 chromosomes off of the metaphase plate. FL Hec1-GFP: MU=43.2% n=38, PA=36.4% n=32, MA=20.4% n=18; K166D Hec1-GFP: MU=73.4% n=69, PA=24.5% n=23, MA=2.1% n=2; 9D Hec1-GFP: MU=70.0% n=45, PA=22.0% n=14, MA=8.0% n=5; S15D Hec1-GFP: MU=38.9% n=14, PA=38.9% n=14, MA=22.2% n=8; S44,55D Hec1-GFP: MU=46.7% n=21, PA=28.9% n=13 MA=24.4% n=11; S8,44,55D Hec1-GFP: MU=51.6% n=32, PA=43.6% n=27, MA=4.8% n=3; S8,15,44,55D Hec1-GFP: MU=63.1% n=36, PA=31.6% n=18, MA=5.3% n=3; S4,49,62,69D Hec1-GFP: MU=47.0% n=19, PA=29.0% n=12, MA=24.0% n=10, a black asterisk indicates statistically significant difference with respect to the percent of FL Hec1-GFP rescued cells achieving metaphase, while a red asterisk indicates statistically significant difference with respect to the percent K166D Hec1-GFP rescued cells achieving metaphase (p<0.001).

phenotype, cells expressing Hec1-GFP SD^{8,15,44,55} were found to be largely incapable of metaphase plate formation (scored as having complete chromosome alignment) and predominately existed in the prometaphase (scored as having more than 4 chromosome pairs off the central mass of chromosomes that congress to the spindle equator) and partially aligned states (scored as having between 4 and 1 chromosome pairs off the central mass of chromosomes that congress to the spindle equator) (Figure 5.2.4; Table 5.2.4), a phenotype which is very similar to the Hec1^{9D} rescue. The ability of Hec1-GFP SD^{8,15,44,55} expressing cells to exist in a partially aligned state (similar to the Hec1^{9D} rescue), in the absence of inter-kinetochore tension or end-associated attachments is striking, and suggests a different component of Hec1 regulates initial chromosome positioning towards the center of the cell.

Intriguingly, cells expressing one S to D mutation (Hec1-GFP SD¹⁵; Table 5.2.1) were modestly impeded in the formation of stable kinetochore-MT attachments, indicating a single phosphorylation event to 1 of the 4 conserved residues affected the kinetochore-MT interaction. Cells expressing Hec1 mutants with increasing numbers of phospho-mimetic mutations (Hec1-GFP SD^{44,55} and Hec1-GFP SD^{8,44,55}; Table 5.2.1) displayed a stepwise amplification of defects in kinetochore-MT attachments (Figures 5.2-2,3&4; Table 5.2-2,3&4). This suggests that the effect of individual phosphorylation events to conserved residues on the Hec1 80 amino acid tail are summed together when contributing to the kinetochore-MT interaction (as is seen in cells expressing Hec1 SD^{8,15,44,55}). The impairment of metaphase plates in cells expressing the Hec1 D mutants containing either three or four conserved phospho-mimetic mutations (Hec1-GFP SD^{8,44,55}, SD^{8,15,44,55}; Figure 5.2.4) is not statistically different when compared to cells rescued with Hec1^{9D}-GFP and suggests that the defective kinetochore-MT attachments induced through the sum of these phospho-mimetic events can not be rescued by other components of the kinetochore. This raises the question; in what instance would the cell exist in a partially phosphorylated Hec1 state, and

why would this be beneficial? Recent work has demonstrated that upon nuclear envelope breakdown, high levels of Hec1 phosphorylation at kinetochores existed and are proposed to facilitate high turnover of kinetochore-MT turnover early in mitosis when incorrect kinetochore-MT attachments are abundant [64]. Cells were allowed to progress through mitosis, such that faithful kinetochore-MT attachments could be established, and Hec1 phosphorylation was found to decrease but did persist as a cell aligned its chromosomes at the spindle equator [64]. This is consistent with a model where an incomplete phosphorylation of the four conserved Aurora B kinase phosphorylation residues (Hec1 SD^{44,55}, for example) would still allow for flexible kinetochore-MT interactions, bi-orientation and metaphase plate formation. Indeed, it may be beneficial for Hec1 to exist in a partially phosphorylated state (such as Hec1 SD^{44,55}), balancing MT attachment/detachment status, thus sensitizing the tail to further phosphorylation/de-phosphorylation events. Taken together, the stepwise impairment of kinetochore-MT attachments observed in cells expressing Hec1 mutants with an increasing number of phospho-mimetic mutations implies that contributions are made from individual phosphorylation events, and the summation of these contributions progressively affects kinetochore-MT attachments.

From the Hec1^{S8,15,44,55D} data, it was unclear whether region specific phosphorylation was required to perturb kinetochore-MT attachment, or if four negative charges dispersed throughout the Hec1 tail domain could achieve the same phenotype. To this end four Aurora B kinase phosphorylation sites (S4,62,69 T49) [45], non-conserved from *C. elegans* to humans, were targeted for phospho-mimetic mutagenesis (Table 5.2.1). In cells rescued with Hec1-GFP SD^{4,49,62,69} inter-kinetochore tension, percent of kinetochores with end-associated MTs, and percent chromosome alignment phenotype were all restored to levels similar to cells rescued with Hec1-GFP SD¹⁵ (Figures 5.2-1,2,3,&4; Table 5.2-2,3,&4). In cells expressing Hec1-GFP SD^{4,49,62,69} the ability to achieve a rescue was significantly elevated above Hec1-GFP SD^{8,15,44,55} for every parameter measured. This demonstrates

that localization of charge to regions containing conserved residues (Hec1 SD^{8,15,44,55}) is required for phosphorylation-induced kinetochore-MT release, and a simple drop in charge to the Hec1 tail domain (Hec1 SD^{4,49,62,69}) is not sufficient to trigger this effect. Together, the ability of Hec1 GFP SD^{4,49,62,69} expressing cells to establish kinetochore-MT attachments and form metaphase plates strengthens support for a model that dynamic regulation of conserved serine residues 8, 15, 44 and 55 is needed in bi-orientation. While not investigated here, it is also possible that if the spacing of phosphorylation along the Hec1 tail domain were exactly the same as the Hec1 SD^{8,15,44,55} mutant, this too could regulate kinetochore-MT attachments and metaphase plate formation.

5.2.2 Hec1 Tail Phospho-mimetic Mutation to Conserved Aurora B Kinase Phosphorylation Sites Disrupts Normal Mitotic Progression

As cells progress through mitosis with correct kinetochore-MT attachments, chromosomes are aligned at the spindle equator before division into two daughter cells during anaphase/cytokinesis. If a faithful mitotic progression is observed, cells will exit mitosis in a repeatable window of time. As determined by time-lapse microscopy, 84.6% of FL Hec1-GFP rescued cells were capable of forming metaphase plates, and 100% went through mitosis in under 2 h (Figure 5.2-5,6&7; Table 5.2-5&6). To confirm that phosphorylation of the Hec1 80 amino acid tail domain induces defects in kinetochore-MT attachments, cells expressing various D mutants were observed via time-lapse microscopy. In Hec1^{9D}-GFP rescued cells where kinetochore-MT attachments have been disrupted by phospho-mimetic mutation to all 9 ABK sites, only 11.8% of cells were capable of metaphase plate formation, and only 48.6% entered anaphase in under 2 h, values statistically significant from the FL Hec1-GFP rescue (Figure 5.2-5,6&7; Table 5.2-5&6). The impaired ability of 9D Hec1-GFP rescued cells to form metaphase plates indicates a loss of stable kinetochore-MT attachments. In addition to the impairment of metaphase plate

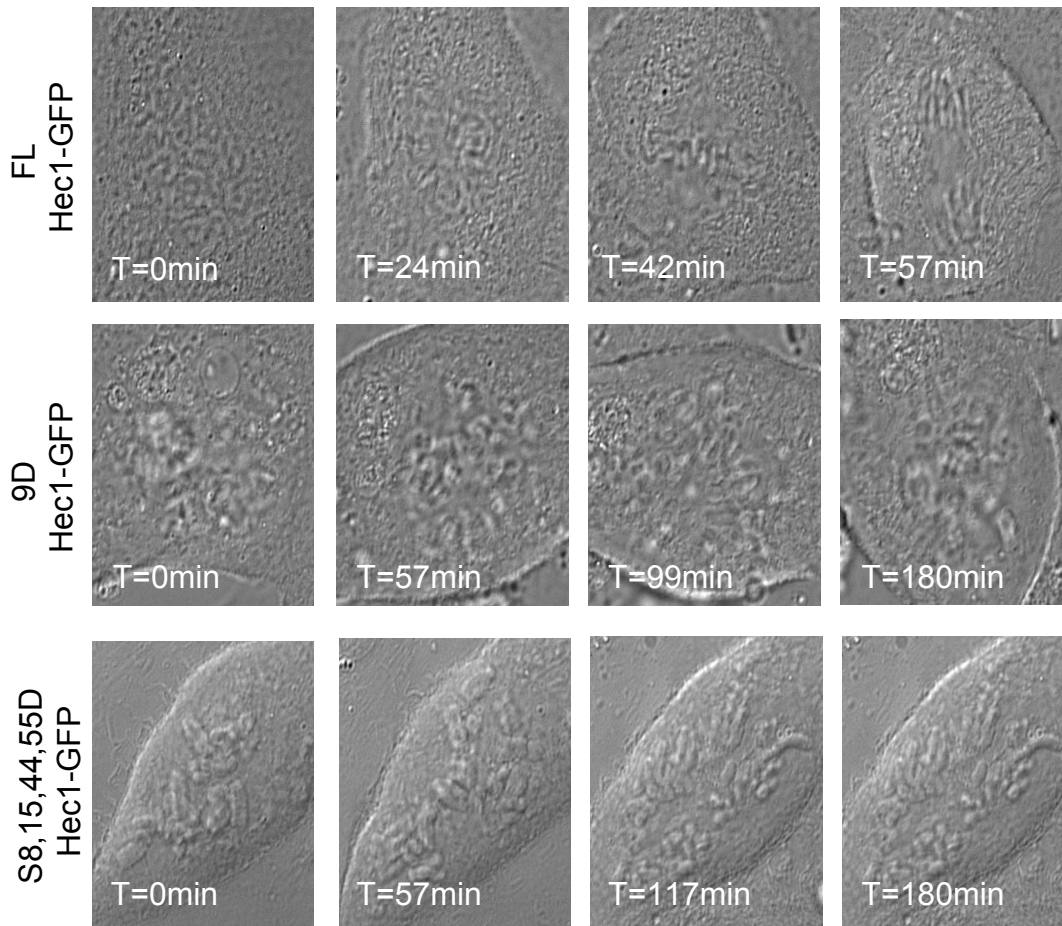


Figure 5.2.5: Impairing kinetochore-MT attachments through phosphomimetic mutations results in prolonged mitosis

Using time-lapse DIC microscopy, timing through mitosis was recorded for cells rescued with various Hec1 mutants. Cells were initially identified as being GFP positive for a particular Hec1 construct, and then confirmed to have a Cy5 labeled Hec1 siRNA. Individual images shown for each panel are still images from time lapse-movies, with time stamps indicating the elapsed time in min.

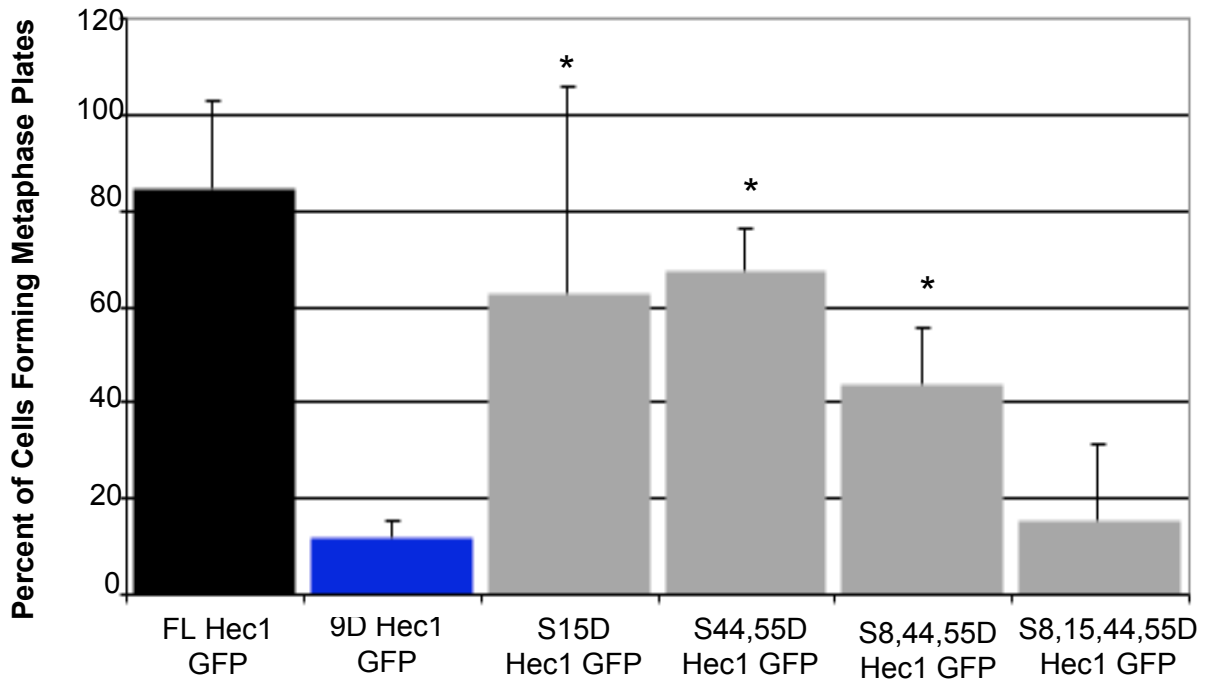
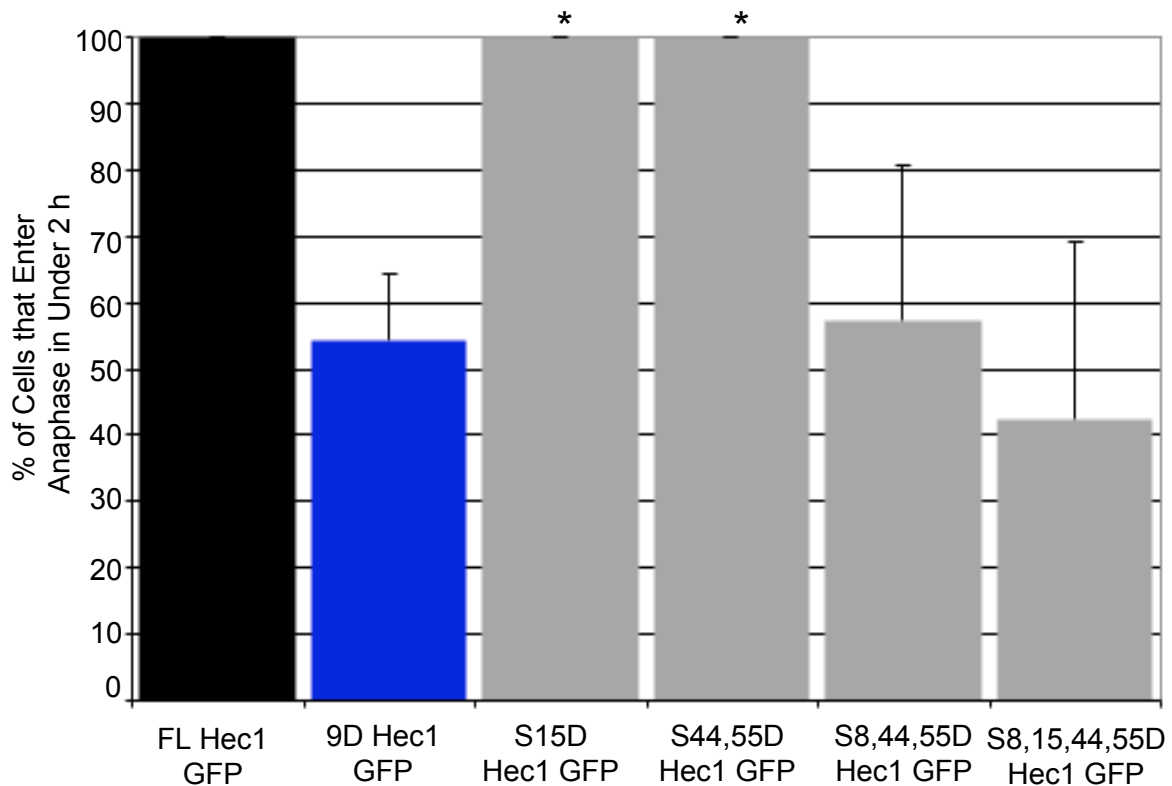


Figure 5.2.6: Phospho-mimetic mutations impair metaphase plate formation
 Quantification of metaphase plates formed during live cell imaging. Bar graph represents the percent of cells that form metaphase plates during the time-lapse imaging. FL-Hec1= 84.6%, 9D-Hec1 = 11.8%, S15D-Hec1= 62.5%, S44,55D-Hec1= 67.5%, S8,44,55D-Hec1= 43.6%, S8,15,44,55D-Hec1= 15.1%. A black asterisk indicates a statistically significant difference as compared to 9D Hec1-GFP.

Table 5.2.5: Time lapse movies- percent of cells rescued with phospho-mimetic Hec1 mutants that achieve metaphase alignment

Hec1 Mutant	% of Cells that form Metaphase Plates	Standard Dev.	Total # of Cells
FL	84.6	18.2	39
9D	11.8	3.6	35
S15D	62.5	43.3	24
S44,55D	67.5	9.0	16
S8,44,55D	43.6	12.1	39
S8,15,44,55D	15.1	16.3	53



5.2.7: Phospho-mimetic mutations disrupt kinetochore-MT attachments and result in a mitotic arrest

Quantification of cells that enter anaphase during live cell imaging. Bar graph represents the percent of cells which entered anaphase within 2 h of time-lapse imaging. FL-Hec1=100%, 9D-Hec1=54.2%, S15D-Hec1= 100%, S44,55D-Hec1= 100%, S8,44,55D-Hec1= 57.1%, S8,15,44,55D-Hec1= 42.3%. A black asterisk indicates a statistically significant difference with respect to 9D Hec1-GFP ($p < 0.001$).

Table 5.2.6: Time lapse movies- percent of cells rescued with phospho-mimetic Hec1 mutants that entering anaphase in under two hours

Hec1 Construct	% of cells entering anaphase under 2 h	Std. Dev.	Total # of cells
FL	100	0.0	22
9D	48.6	10.0	35
S15D	100	0.0	8
S44,55D	100	0.0	8
S8,44,55D	57.1	23.6	16
S8,15,44,55D	42.3	26.9	26

formation, the time spent in mitosis was prolonged. The function of the spindle assembly checkpoint (SAC) is to ensure that cells will only enter anaphase after a full complement of kinetochore-MT attachments has been established, after which the SAC can be satisfied and a cell is allowed to enter anaphase. However, the lack of kinetochore-MT attachments observed for cells expressing Hec1^{9D}-GFP resulted in a prolonged activation of the SAC, and subsequent arrest in mitosis was observed. While Hec1^{9D}-GFP expressing cells entered anaphase at a statistically significant value from the FL Hec1-GFP rescue, it is somewhat surprising that 48.6% of the Hec1^{9D}-GFP expressing cells were capable of entering anaphase. It is possible that constitutive phosphorylation of the Hec1 tail domain is prohibiting the SAC from performing its normal function, thus allowing for anaphase onset in some cells lacking kinetochore-MT attachments. With an understanding of how complete phospho-mimetic mutation of the Hec1 tail domain affects a cells progression through mitosis, we next observed how a subset of Hec1 tail phospho-mimetic mutations affected mitotic progression.

In cells rescued with either Hec1-GFP SD¹⁵ or Hec1-GFP SD^{44,55} metaphase alignment and anaphase onset were achieved at levels comparable to the FL Hec1-GFP rescue (Figure 5.2-6&7; Table 5.2-5&6). However, cells rescued with Hec1-GFP SD^{8,44,55} exhibited an impaired phenotype as compared to the FL Hec1-GFP rescue, as only 43.6% of cells formed metaphase plates, and 57.1% of cells entered anaphase in under 2 h, values which were statistically similar to the Hec1^{9D}-GFP rescue (Figures 5.2-6&7; Table 4.2-5&6). Finally, in cells rescued with Hec1-GFP SD^{8,15,44,55}, only 15.1% were found to form metaphase plates, and 42.3% entered mitosis in under 2 h, and these values were also statistically similar to the Hec1^{9D}-GFP rescue (Figure 5.2-5,6&7; Table 5.2-5&6). The live cell defects observed for Hec1-GFP SD^{8,15,44,55} rescued cells indicate that mimicking constitutive phosphorylation at the 4 conserved phosphorylation sites is sufficient to achieve a kinetochore defective phenotype similar to the Hec1^{9D}-GFP rescue. The live cell data

shown here correlate nicely with the fixed cell data, where the most dramatic kinetochore-MT null binding phenotypes were observed in Hec1-GFP SD^{8,44,55} GFP and Hec1-GFP SD^{8,15,44,55}, while Hec1-GFP SD¹⁵ GFP or Hec1-GFP SD^{8,44,55} phenotypes were less severe.

5.2.3 Disrupting Kinetochore-MT Attachments through Phospho-mimetic Mutations Yields Aberrant Kinetochore Movements

As chromosomes congress toward the equator of the cell, oscillations brought on by dynamic interactions between the kinetochore and attached MTs allow for chromosome positioning at the metaphase plate [2]. Still, in cells, how the kinetochore can remain tethered to growing and shortening microtubules remains an unanswered question.

Interestingly, the Ndc80 complex has been shown to be capable of generating load-bearing, diffusive attachments *in vitro* [54]. Recent work here, and in other published studies, suggest that phosphorylation of the Hec1 80 amino acid tail domain can modulate Ndc80-MT binding affinity, and is required for dynamic regulation of kinetochore-MT interactions [45, 47].

To observe how dynamic kinetochore-MT behaviors are affected in cells rescued with Hec1 expressing tail phospho-mimetic mutants, kinetochore oscillations were tracked. Briefly, for Hec1-GFP rescued cells in a metaphase-aligned state, 3 planes 500 nm apart were imaged every 3 s for 10 min. After compressing the z-stacks and building the movies, oscillation parameters were measured. The average oscillation velocity in cells expressing FL Hec1-GFP was $2.13 \pm 0.37 \mu\text{m}/\text{min}$ (Figure 5.1.8; Table 5.1.7). The movements observed for the FL Hec1-GFP rescue are characteristic of cells that have dynamic regulation of kinetochore-MT attachments at either side of the sister kinetochore pair, allowing chromosomes to track with MTs during multiple rounds of polymerization-depolymerization. Graphically, kinetochores from FL Hec1-GFP oscillation movies displayed long, uninterrupted excursions away and towards a pole, producing an oscillatory movement (Figure 5.1-9&12). To address how constitutive ABK phosphorylation at all 9 sites on the

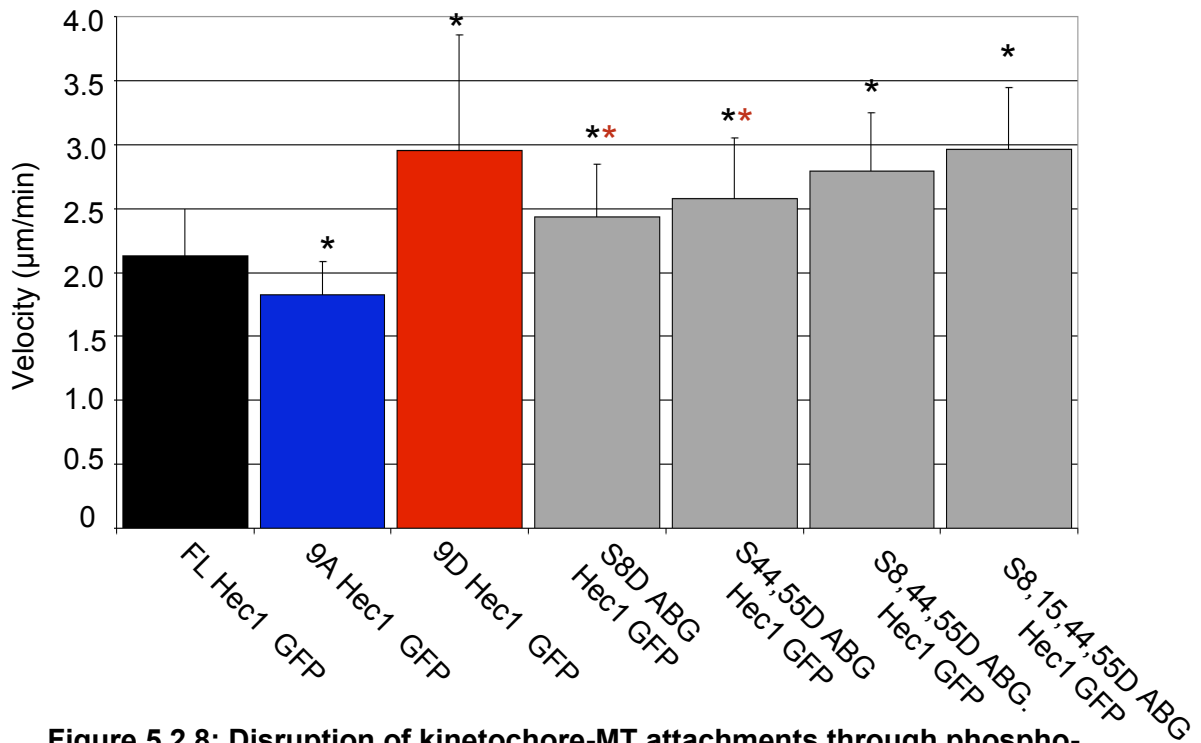


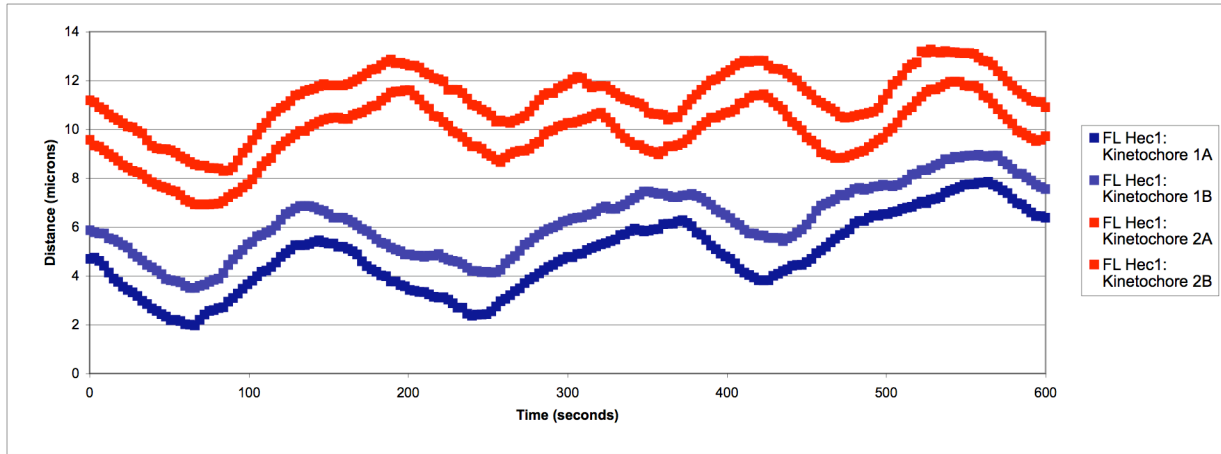
Figure 5.2.8: Disruption of kinetochore-MT attachments through phospho-mimetic mutation results in increased kinetochore velocities

Kinetochores were filmed by imaging the GFP channel in 3x500 nm thick Z-stacks, every 3 s for 10 min. Z-stacks were compressed at each time point, and movies were built. Individual kinetochore pairs found to exist at the metaphase plate were tracked using Metamorph software. FL-Hec1 GFP= 2.13±0.37 µm/min; 9A-Hec1= 1.83±0.25 µm/min; 9D-Hec1 GFP= 2.96±0.90 µm/min; S8D ABG-Hec1= 2.43±0.41 µm/min; S44,55D ABG-Hec1= 2.58±0.47 µm/min; S8,44,55D ABG-Hec1= 2.79±0.46 µm/min; S8,15,44,55D ABG-Hec1= 2.96±0.48 µm/min. A black asterisk indicates a statistical difference with respect to FL Hec1-GFP, while a red asterisk indicates a statistical difference with respect to 9D Hec1-GFP (p<0.001).

Table 5.2.7: Kinetochore velocity values for cells rescued with phospho-mimetic Hec1 mutants

Hec1 Construct	Avg. Vel. (µm/min)	Std. Dev.	# of Cells
Full Length	2.13	0.36	14
9A	1.83	0.25	16
9D	2.96	0.90	10
S8D ABG	2.43	0.41	16
S44,55D ABG	2.58	0.47	18
S8,44,55D ABG	2.79	0.46	12
S8,15,44,55D ABG	2.96	0.48	10

FL Hec1-GFP



Hec1^{9D}-GFP

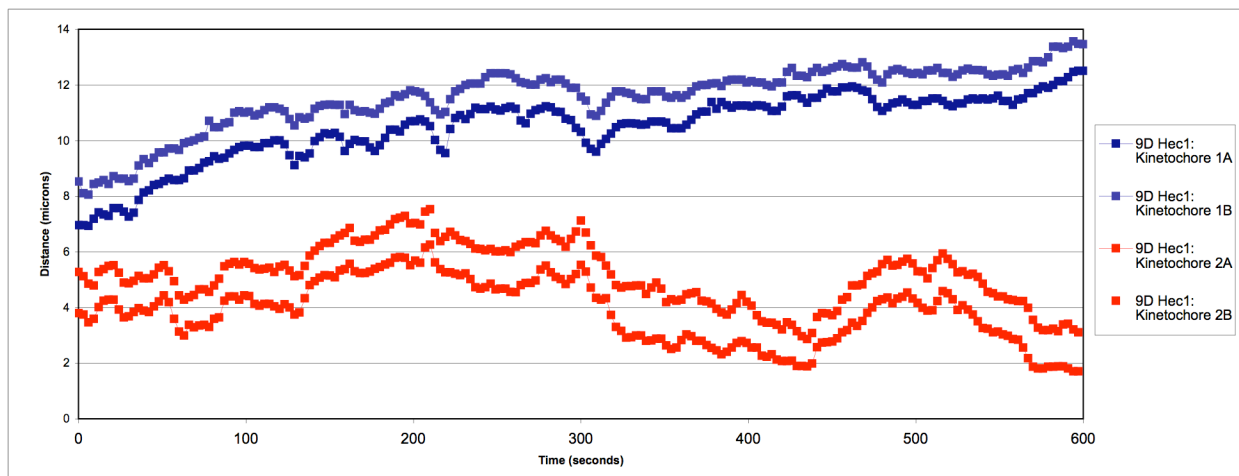
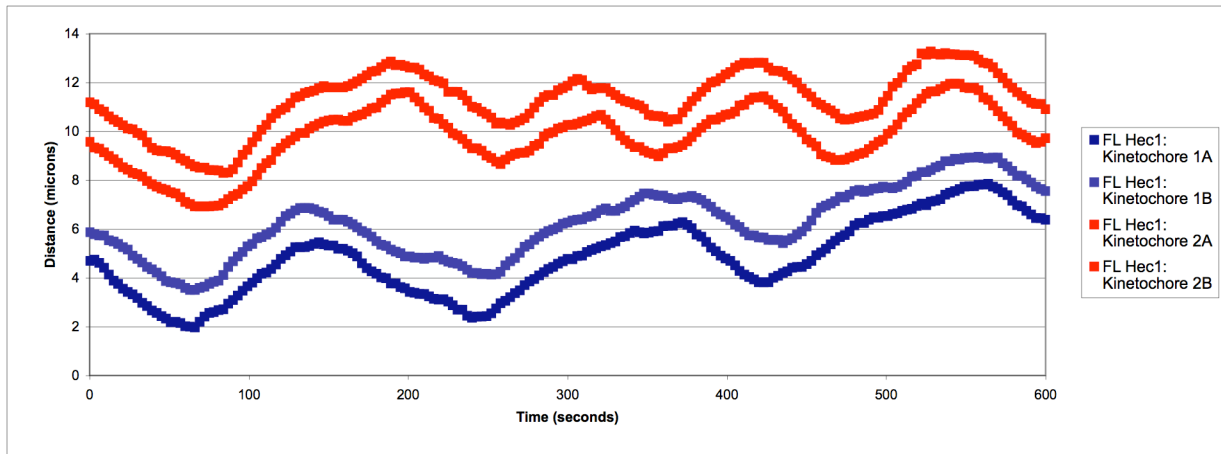


Figure 5.2.9: Phospho-mimetic mutation to all 9 Hec1 phosphorylation sites results in erratic kinetochore movements

Representative graphs for kinetochore-tracking movies where cells were rescued with either FL (top) or Hec1^{9D}-GFP (bottom). The points in the graph represent the track of a given kinetochore as it moves through a cell (distance in μm) over time (movie length = 600 s).

FL Hec1-GFP



Hec1^{9A}-GFP

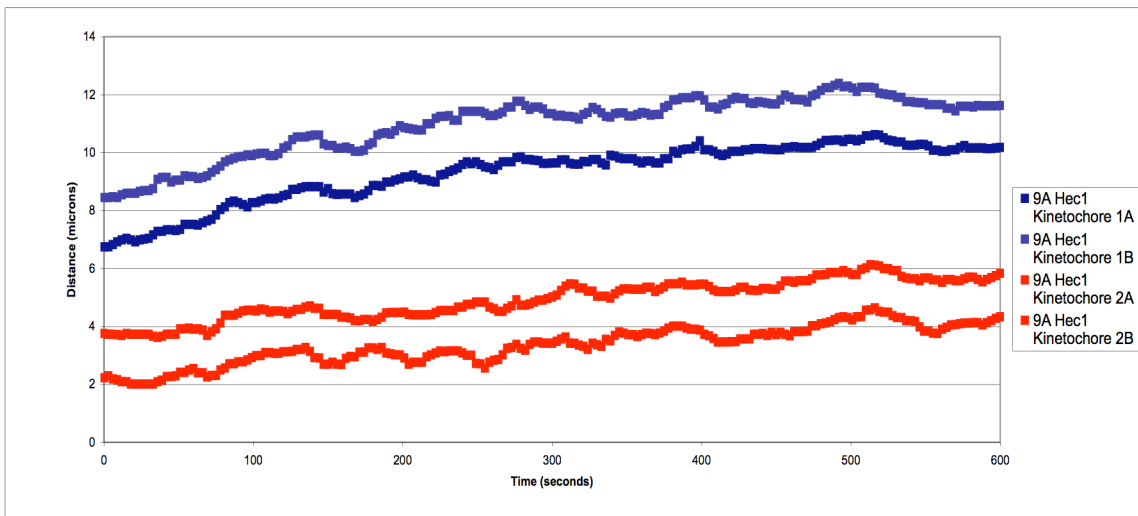
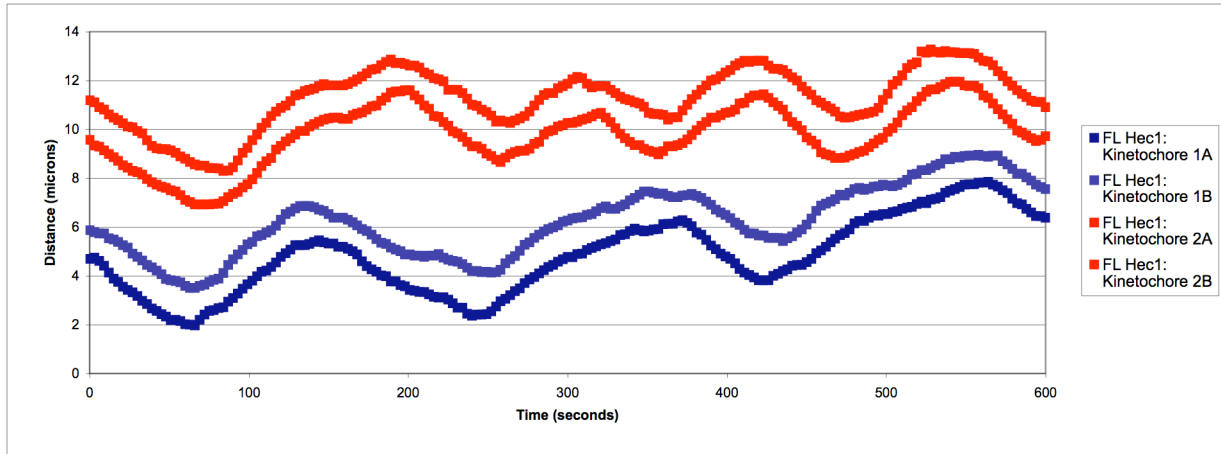


Figure 5.2.10: Precluding phosphorylation to the Hec1 tail domain results in stagnant kinetochore movements

Representative graphs for oscillation movies where cells were rescued with either FL (top) and Hec1^{9A}-GFP (bottom). The points in the graph represent the track of a given kinetochore as it oscillates through a cell (distance in μm) over time (movie length = 600 s).

FL Hec1-GFP



Hec1^{S8,15,44,55D}-GFP

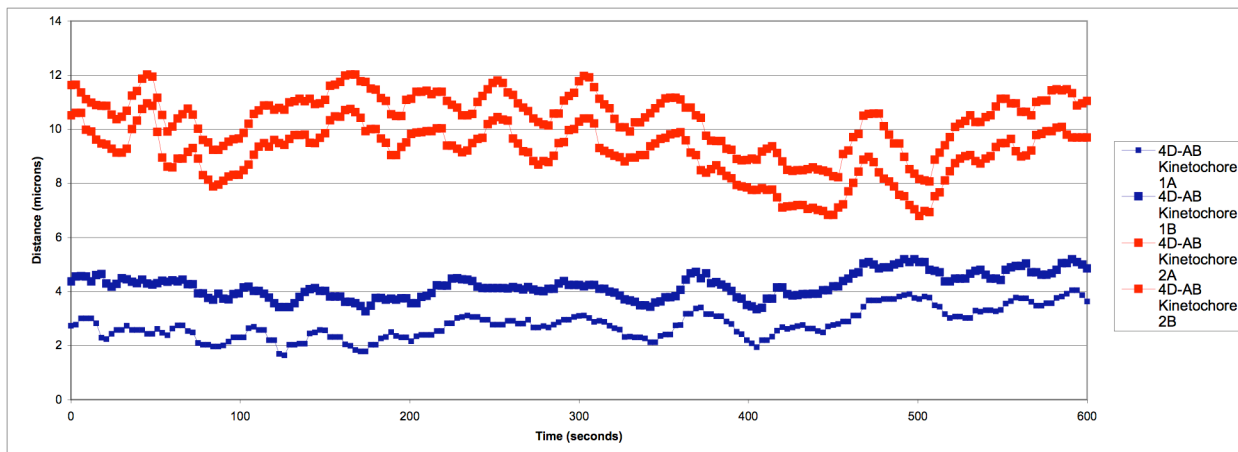
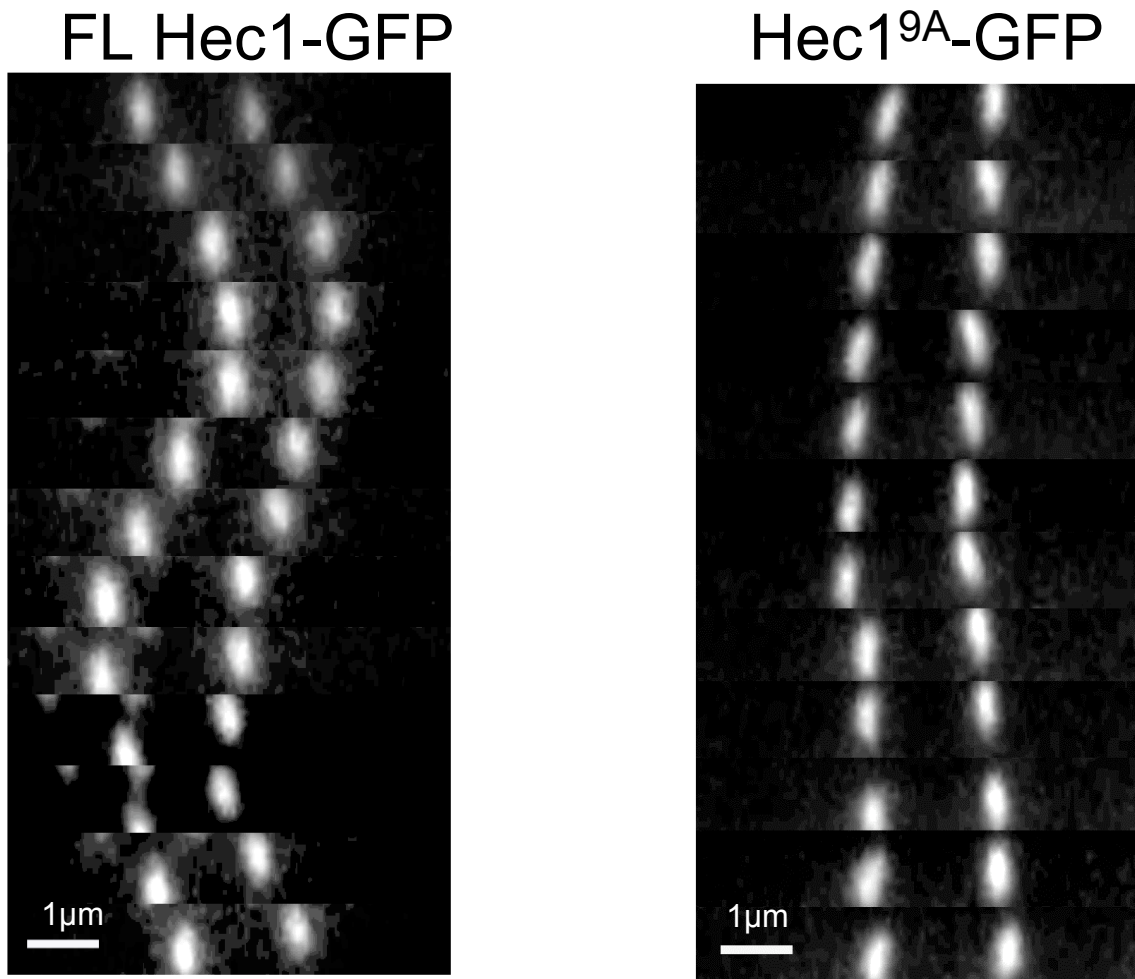


Figure 5.2.11: Phospho-mimetic mutation to the 4 conserved Hec1 phosphorylation sites results in erratic kinetochore movements

Representative graphs for oscillation movies where cells were rescued with either FL (top) and Hec1^{S8,15,44,55D} ABG Hec1-GFP (bottom). The points in the graph represent the track of a given kinetochore as it moves through a cell (distance in μm) over time (movie length = 600 s).



5.2.12: Precluding phosphorylation to the Hec1 tail domain yields stagnant kinetochore movements

Kinetochore oscillation kymographs for the FL and 9A Hec1-GFP rescued cells. Frames in the kymograph were taken every 9 s.

Hec1 tail affects kinetochore dynamics, live cell kinetochore movements for Hec1^{9D}-GFP rescued cells were imaged. In contrast to the coordinated kinetochore oscillations observed in FL Hec1-GFP expressing cells, spurious, stochastic kinetochore movements were observed in cells expressing Hec1^{9D}-GFP (Figure 5.1.9; unable to produce an oscillation kymograph due to erratic kinetochore movements). Because cells expressing Hec1^{9D}-GFP lacked stable kinetochore-MT attachments, and thus were impaired in chromosome bi-orientation, the kinetochore motions observed could not be termed kinetochore *oscillations* but rather kinetochore *movements*. Ultimately, an increased velocity resulted from the spurious movements observed in cells rescued with for Hec1^{9D}-GFP ($2.96 \pm 0.89 \mu\text{m}/\text{min}$; Figure 5.1.8; Table 5.1.7; 5.1.8). Conversely, in cells expressing Hec1^{9A}-GFP, where dynamic phosphorylation of the Hec1 tail domain is precluded resulting in hyper-stable attachments, dampened oscillation movements were observed (Figure 5.1-10&12) yielding a subsequent decrease in velocity ($1.83 \pm 0.25 \mu\text{m}/\text{min}$; Figure 5.1.8; Table 5.1.7). With a baseline for wild-type, hyper-attaching, and kinetochore-null MT binding phenotypes, Hec1 constructs expressing a subset of phospho-mimetic tail mutants could next be assessed.

To address how an incremental series of phosphorylation events affected dynamic kinetochore movements, kinetochores in live cells were imaged. To do so, the four conserved phosphorylation sites along the Hec1 80 amino acid tail domain were incrementally mutated to aspartic acid. Additionally, the remaining phosphorylation sites, which had not been mutated to aspartic acid, were mutated to alanine, thus preventing their phosphorylation. By mimicking a defined phosphorylation state at specific sites (D mutations) while precluding native ABK phosphorylation of the remaining phosphorylation sites (A mutations), the “D Mutant A-Background” (D ABG) constructs ensured that the effects observed for cells expressing these constructs could be attributed to a definitive phospho-mimetic Hec1-tail state (Table 5A-1). Starting with the Hec1^{S8D ABG} mutant, a slight but significant increase in kinetochore oscillation velocity was observed ($2.43 \pm 0.41 \mu\text{m}/\text{min}$;

Figure 5.1.8; Table 5.1.7), velocity values that exceeded the FL Hec1 rescue but did not approach the values observed for cells expressing Hec1^{9D}-GFP. With incremental introduction of phospho-mimetic mutations along the 80 amino acid tail domain, a stepwise increase in kinetochore velocity was observed (Hec1^{S44,55D ABG}-GFP= 2.58±0.47µm/min; Hec1^{S8,44,55D ABG}-GFP= 2.79±0.46µm/min; Hec1^{S8,15,44,55D ABG}-GFP= 2.96±0.48µm/min; Figure 5.1.8; Table 5.1.7). The phenotype for cells expressing Hec1^{S8,15,44,55D ABG}-GFP was very similar to that of Hec1^{9D}-GFP, as the kinetochore movements were sudden and erratic as compared to the FL Hec1-rescue (Figure 5.1.11). Of note, the velocity of movement in cells expressing Hec1^{S8,15,44,55D ABG} GFP was statistically similar to Hec1^{9D} GFP, indicating that phosphorylation of the four conserved residues was sufficient in disrupting kinetochore-MT dynamics. The incremental increase in velocity associated with the stepwise gain of Hec1 tail phospho-mimetic mutations supports the hypothesis that individual Hec1 tail phosphorylation events at conserved sites make distinct contributions towards modulation of kinetochore-MT interactions, as was observed for the fixed cell analysis. Additionally, the effect of phosphorylation of the four conserved residues is cumulative. This suggests that the kinetochore-MT interaction can be discretely modulated by the summation of Hec1 tail phosphorylation events, a mechanism potentially useful during chromosome oscillations and alignment into a metaphase plate.

5.2.4 A Truncated Hec1 Tail Domain Can Mediate Kinetochore-Microtubule Interactions

With a better understanding of the contributions that individual Hec1 tail phosphorylation events make towards kinetochore-MT interactions, we next assessed how Hec1 tail length contributed towards generating and regulating kinetochore-MT interactions. *In vivo* and *in vitro* assays have demonstrated that the 80 amino acid tail domain is essential for MT binding [45, 52], but it is still unknown if a smaller segment of the Hec1 tail domain could mediate its function. Much work in the field has led to two models that describe the 80

amino acid tail domain function in relation to Ndc80-MT binding. The first model suggests that the 80 amino acid tail domain serves to oligomerize adjacent Ndc80 complexes bound to the MT lattice, while the second model suggests that the 80 amino acid tail domain of Hec1 directly binds “E-hooks” extending off the MT lattice (discussed in detail in section 5.1). In either instance, oligomerizer vs. direct binder, having a flexible extension from Hec1 in the form of an 80 amino acid tail domain appears to contribute Ndc80-MT binding. But is the entire length of the Hec1 80 amino acid tail domain essential to faithful kinetochore-MT binding? Additionally, the work discussed by others and here in sections 5.2.1 through 5.2.3 strongly supports a model whereby charge on the Hec1 tail domain contributes significantly to the electrostatic based kinetochore-MT interaction. If the Hec1 tail charges make a significant contribution to kinetochore-MT interactions, the entire length of the Hec1 tail domain may not be essential to forming kinetochore-MT attachments. In such an instance, it may be possible to render kinetochores either proficient or deficient in MT binding when expressing Hec1 constructs with truncated tail domains of appropriately high or low charge, respectively.

Cells rescued with Hec1^{Δ1-55}-GFP (Figure 5.2.13, Table 5.2.8), in which 70% of the tail was removed, were first evaluated. Hec1^{Δ1-55}-GFP rescued cells established intermediate kinetochore-MT tension and percent of end-associated kinetochore-MT attachments, levels that were statistically different from both the FL and Hec1^{K166D}-GFP rescued cells (Figures 5.2-14&15, Tables 5.2-10&11). While cells rescued with Hec1^{Δ1-55}-GFP were able to establish kinetochore-MT attachments better than cells rescued with Hec1^{K166D}-GFP, these attachments did not permit metaphase plate formation (Figure 5.2.16; Table 5.2.12).

Previously, phosphorylation status of the Hec1 80 amino acid tail domain has been shown to dictate kinetochore-MT attachment status [47, 52]. From such studies, it has been proposed that manipulation of the electrostatic binding potential existing between Hec1 and

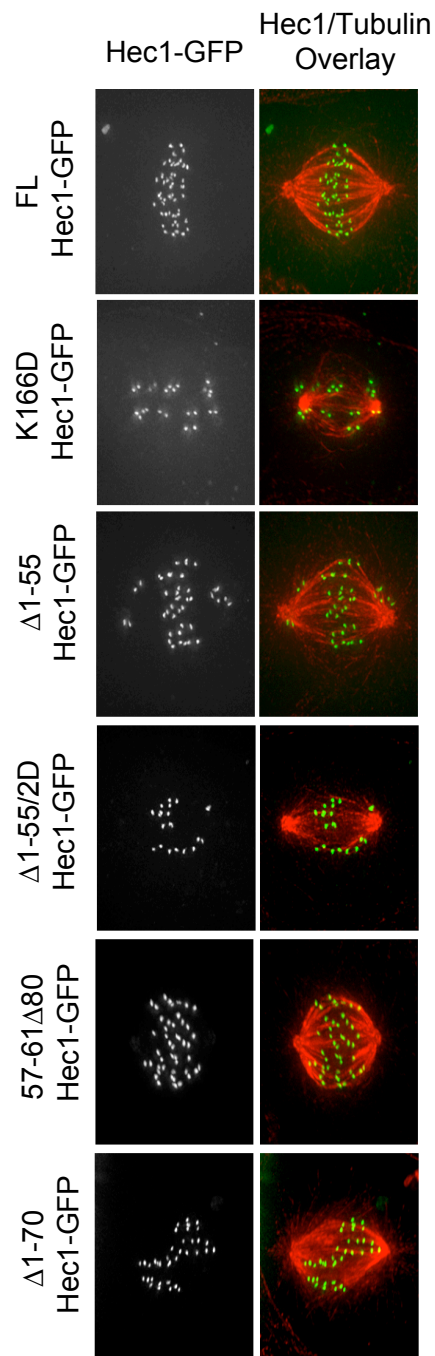


Figure 5.2.13: Hec1 tail charge and length contribute to kinetochore-MT attachments
 Projections of deconvolved immunofluorescent images of PtK1 cells depleted of endogenous Hec1 and rescued with the indicated GFP-fusion protein.

Table 5.2.8: Hec1 truncation mutant constructs

pE-GFP N1 Vector Human Hec1 Mutant Name	Amino Acid Sequence Only the 80 amino acid tail is shown
FL Hec1-GFP	MKRSSVSSGGAGRLSMQELRSQDV NKQGLYTPQTKEKPTFGKLSINKPTS ERKVSLFGKRTSGHGSRNSQLGIFS SSEKI
Δ 1-55 Hec1-GFP	LFGKRTSGHGSRNSQLGIFSSSEKI
Δ 1-55/2D Hec1-GFP Red= Aspartic Acid Mutation	LFGKRTDGHGSRNDQLGIFSSSEKI
57-61 Δ 80 Hec1-GFP Black= Native sequence residues Red=Additional residues engineered for cloning purposes	MFGKRKEL
Δ 1-70 Hec1-GFP	QLGIFSSSEKI

Table 5.2.9: Hec1 truncation mutant charge per amino acid

Hec1 Construct	Net Charge(Sum of charge for acids & bases at pH 7.0)	Charge Per Amino Acid
WT Hec1	11	0.14
Δ 1-55	4	0.16
Δ 1-55/2D	2	0.08
57-61 Δ 80	2	0.22
Δ 1-70	0	0.00

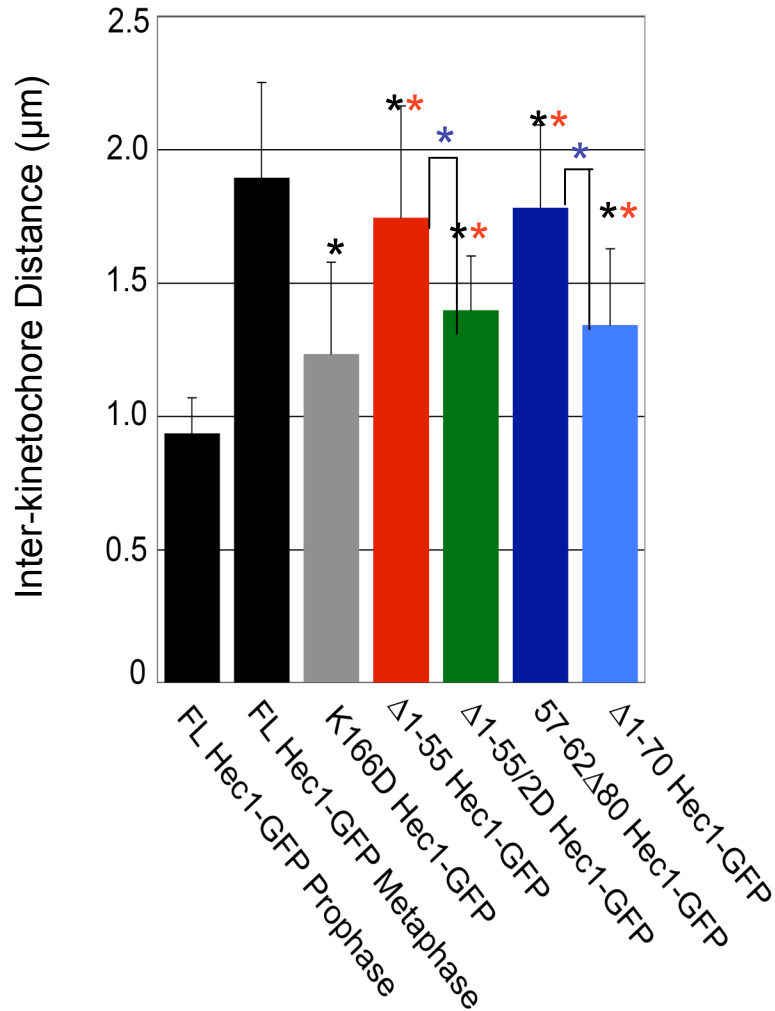


Figure 5.2.14: Hec1 expressing a short positively charged tail domain is capable of establishing inter-kinetochore tension

Quantification of inter-kinetochore distances, which were measured from Hec1-GFP centroid to Hec1-GFP centroid (Prophase FL Hec1-GFP: IKD= 0.93 ± 0.13 , $n=11$ cells, 46 kinetochores; Bioriented FL Hec1-GFP: IKD= 1.89 ± 0.36 , $n=33$ cells, 426 kinetochores; Prometa K166D Hec1-GFP: IKD= 1.21 ± 0.33 , $n=69$ cells, 740 kinetochores; Bioriented 1-55 Hec1-GFP: IKD= 1.74 ± 0.42 , $n=33$ cells, 487 kinetochores; Partially Aligned $\Delta 1-55/2D$ Hec1-GFP: IKD= 1.4 ± 0.20 , $n=93$ cells, 127 kinetochores; Bioriented 57-61 $\Delta 80$ Hec1-GFP: IKD= 1.78 ± 0.31 , $n=15$ cells, 187 kinetochores; Partially Aligned $\Delta 1-70$ Hec1-GFP: $n=9$ cells, 105 kinetochores). Measurements were made from the terminal phenotype achieved in cells expressing a given construct. Black asterisk indicates a statistically significant difference with respect to the FL Hec1-GFP rescue, while a red asterisk indicates a statistically significant difference with respect to Hec1^{K166D}-GFP rescue, and a blue asterisk indicates a statistically significant difference between two compared groups ($p < 0.001$).

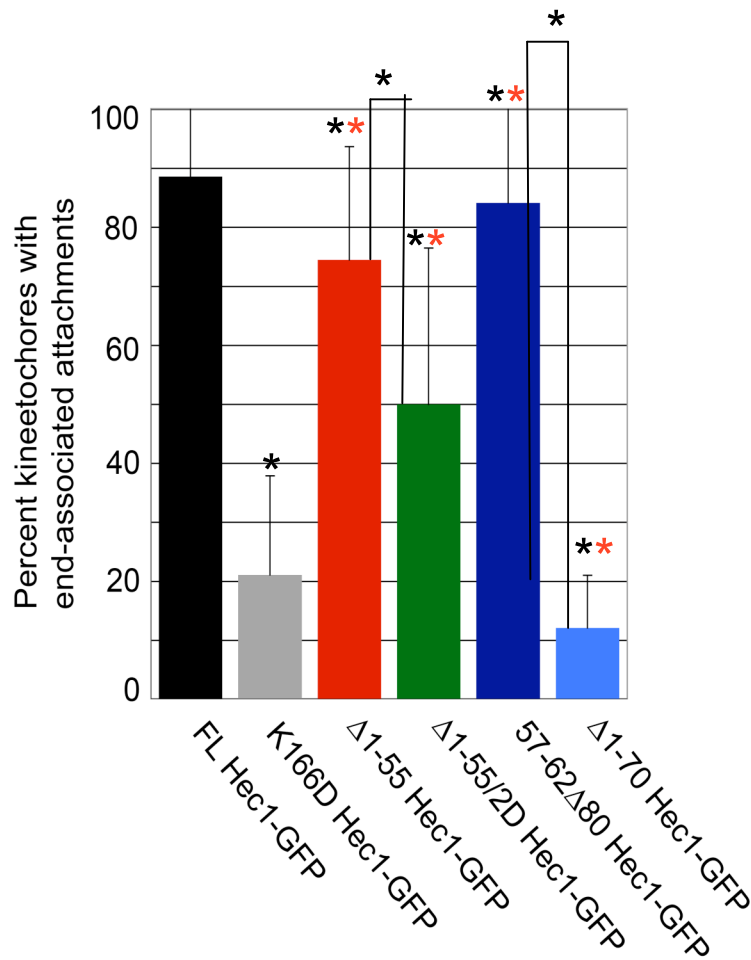


Figure 5.2.15: Short positively charged Hec1 tail domains are capable of establishing stable kinetochore-MT attachments

Quantification of end-on microtubule association with kinetochores (FL Hec1-GFP: Attachment=82.5±17.4%, n=63 cells, 2155 kinetochores; Hec1^{K166D}-GFP: Attachment=21.0±16.8%, n=52 cells, 1812 kinetochores; Δ1-55 Hec1-GFP: Attachment=74.4±19.2%, n=68 cells, 2294 kinetochores; Δ1-55/2D Hec1-GFP: Attachment=50±26.5%, n=28 cells, 774 kinetochores; 57-61Δ80 Hec1-GFP: Attachment=84.1±20.4%, n=32 cells, 1229 kinetochores; Δ1-70 Hec1-GFP: Attachment=12±9.0%, n=24 cells, 542 kinetochores). Measurements were made by averaging values of cells rescued with a given construct from all phases of mitosis. Black asterisk indicates a statistically significant difference with respect to FL Hec1, while a red asterisk indicates a statistically significant difference with respect to K166D Hec1, and a blue asterisk indicates a statistically significant difference between two compared groups (p<0.001).

Table 5.2.10: Inter kinetochore distance for cells rescued with Hec1 truncation mutants

Hec1 Construct and Mitotic Phase	IKD Average	Std. Dev.	# of Ks	# of Cells
FL Prophase	0.93	0.13	46	11
FL Partial	1.89	0.36	243	18
FL Metaphase	1.89	0.36	183	15
FL Bioriented	1.89	0.36	426	33
K166D	1.21	0.33	740	69
Δ 1-55 Bioriented	1.74	0.42	487	33
Δ 1-55/2D Prometa	1.21	0.22	254	19
57to61 Δ 180 Bioriented	1.78	0.31	181	15
Δ 70 Partial	1.34	0.29	105	9

Table 5.2.11: Percent end on kinetochore-MT attachments for cells rescued with Hec1 truncation mutants

Hec1 Construct	# of Attach. Ks	# of Unattach. Ks	Total # of Ks	% of Attach. Ks	Std. Dev.	# of Cells
FL	1778	377	2155	82.5	17.4	63
K166D	380	1432	1812	21.0	16.8	52
Del 55	1707	587	2294	74.4	19.2	68
Del 55/2D	386	388	774	49.9	26.5	28
57to61 Δ 80	1033	196	1229	84.1	20.4	32
Del 70	65	477	542	12.0	8.9	24

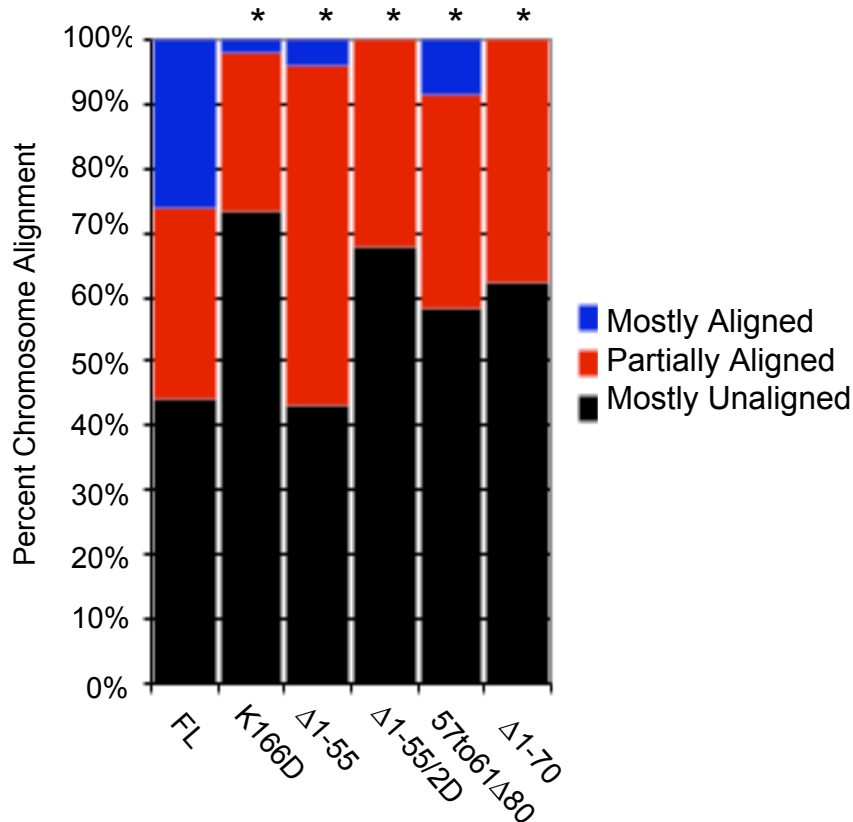


Figure 5.2.16: Truncating the Hec1 tail domain impairs metaphase plate formation

Quantification of chromosome alignment phenotypes for cells depleted of Hec1 and rescued with Hec1-GFP truncation mutant constructs. Cells with Mostly Aligned (MA) chromosomes (blue) had no chromosomes off the metaphase plate, cells with Partially Aligned (PA) chromosomes (red) had 1-4 chromosomes off of a metaphase plates, and cells with Mostly Unaligned (MU) chromosomes (black) had either no chromosome alignment or more than 4 chromosomes off of the metaphase plate. Black asterisk indicates a statistically significant difference as compared to the percent of metaphase cells for the FL Hec1-GFP rescue ($p < 0.001$).

Table 5.2.12: Percent chromosome alignment values for cells rescued with Hec1 truncation mutants

% Alignment	FL	K166D	Del 55	Del 55/2D	57-61Δ80	Δ1-70
% Mostly Unaligned	43.2	73.4	43.0	67.9	58.3	62.5
% Partially Aligned	36.4	24.4	53.0	32.1	33.3	37.5
% Mostly Aligned	20.4	2.1	4.0	0.0	8.3	0.0
Total # of Cells	88	94	68	28	31	34

MTs is responsible for disrupting the Hec1-MT interaction. Additionally, the ability of a constitutively phosphorylated Hec1 tail to trigger kinetochore-MT detachment has been further supported here in sections 5.2.1 through 5.2.3. Being conscious of the role that Hec1 tail charge plays in kinetochore-MT attachments, we next wanted to address how a Hec1 mutant expressing a short tail with low charge would affect kinetochore-MT binding. Within the 25 amino acids remaining on the tail of the Hec1^{Δ1-55}-GFP construct, there exist two, non-conserved, ABK phosphorylation sites (serine 62 and 69). Phosphorylation to serine 62 has been confirmed *in vitro*, while its *in vivo* phosphorylation has not been confirmed. In the Hec1^{Δ1-55/2D}-GFP construct (Table 5.2.8), serine 62 and 69 were mutated to aspartic acid, thus mimicking the phosphorylated state, which provided a useful tool in assessing how charge manipulation of a truncated Hec1 tail domain would affect kinetochore-MT attachments. With introduction of two aspartic acids, the charge per amino acid drops from 0.16 in Hec1^{Δ1-55}-GFP (Table 5.2.9) to 0.08 in Hec1^{Δ1-55/2D}-GFP (Table 5.2.9). Cells expressing Hec1^{Δ1-55/2D}-GFP (Figure 5.2.13) exhibited impaired kinetochore-MT binding when compared to cells rescued with Hec1^{Δ1-55}-GFP. Levels of tension across sister kinetochore pairs and the percent of end-associated kinetochore-MT attachments were significantly reduced below levels measured in cells expressing Hec1^{Δ1-55}-GFP (Figures 5.2-14&15; Tables 5.2-10&11), resulting in significantly impaired metaphase plate formation (Figure 5.2.16; Table 5.2.12). From these data it appears that when a highly positively charged Hec1 tail of 25 amino acids is present, the entire 80 amino acid tail domain of Hec1 is not required for building a kinetochore competent in MT binding. However, a more complete section of the tail may be required for regulation of the kinetochore-MT attachments needed in metaphase plate formation. Interestingly, when Hec1 expressed a 25 amino acid tail of low charge, kinetochore-MT attachments were significantly impaired. This further strengthens the argument that electrostatics play an important role in the Hec1/kinetochore-MT interaction (as was observed in 5.2.1 through 5.2.3).

The Hec1^{Δ1-70}-GFP construct was next assayed, in which 87.5% of the tail domain was truncated (Table 5.2.8), and the remaining 10 amino acids exhibited a charge per amino acid ratio of zero (Table 5.2.9). The trends for cells rescued with Hec1^{Δ1-70}-GFP were very similar to those of cells rescued with Hec1^{Δ1-55/2D}. Specifically, a kinetochore null phenotype was observed, where levels of inter-kinetochore tension and end-associated kinetochore MT attachments were most comparable with cells expressing Hec1^{K166D}-GFP (Figures 5.2-13,14&15; Tables 5.2-10&11), yielding cells incapable of metaphase plate formation (Figure 5.2.16; Table 5.2.12). The low charge per amino acid ratio associated with the Hec1^{Δ1-70}-GFP made it difficult to discern whether defects in kinetochore-MT attachments resulted from truncation to the tail domain or a low charge per amino acid present on the truncated tail (similar to cells rescued with Hec1^{9D}-GFP). To this end Hec1^{57-61Δ80}-GFP, a short-tail mutant with a higher ratio of charge per amino acid, was developed to compare experimentally with the Hec1^{Δ1-70}-GFP construct (Tables 5.2-8&9). Because the C-terminal portion of the 80 amino acid tail domain lacks a significant stretch of positive charge, a ligation technique was used as an alternative approach to an N-terminal truncation method of mutation. For the Hec1^{57-61Δ80}-GFP ligation mutant, a cDNA encoding small, positively charged segment of Hec1's native tail (amino acids 57 to 61) was ligated to a cDNA encoding the N-terminus of a tailless Hec1 construct (Hec1^{Δ1-80}-GFP). The resulting Hec1^{57-61Δ80}-GFP ligation construct yields an 8 amino acid tail domain (5 native amino acids, and 3 engineered amino acids required for cloning) with a charge per amino acid of 0.22 (Table 5.2.9). Cells rescued with the Hec1^{57-61Δ80}-GFP (Figure 5.2.13) exhibited an intermediate binding phenotype, where inter-kinetochore tension and end-associated kinetochore-MT attachments were significantly elevated above cells rescued with either Hec1^{Δ1-70}-GFP or Hec1^{K166D}-GFP, and were similar to cells rescued with FL Hec1-GFP (Figures 5.2-14&15; Tables 5.2-10&11). Interestingly, when comparing the fixed cell scoring parameters, kinetochores in cells expressing Hec1^{57-61Δ80}-GFP bound MTs better than did

cells expressing the longer truncation mutant Hec1^{Δ1-55}-GFP. The Hec1 tail charge per amino acid ratio for Hec1^{57-61Δ80} was considerably higher than that of Hec1^{Δ1-55} (Table 5.2.9), and given the proposed role for electrostatic interactions between Hec1 and MTs, may explain the more robust binding phenotype observed in Hec1^{57-61Δ80} expressing cells. Strikingly, metaphase plate formation was impaired in cells rescued with Hec1^{57-61Δ80}-GFP (Figure 5.2.16; Table 5.2.12), albeit in the presence of robust kinetochore-MT attachments. The impairment of metaphase plate formation may be linked to the removal of Hec1 tail phosphorylation sites implicated in dynamic regulation of kinetochore-MT attachments. The data presented here correlate well with the Hec1^{Δ1-55}-GFP/Hec1^{Δ1-55/2D}-GFP experiments; short, positively charged Hec1 tail mutants established moderate kinetochore-MT attachments, while being impaired in metaphase plate formation. However, these data do not rule out the possibility that a truncated Hec1 tail domain is sufficient to mediate either Ndc80 complex oligomerization, or direct MT lattice binding. It is also worth noting that truncation to the Hec1 80 amino acid tail removes phosphorylation sites previously suggested to play a role in regulation of Ndc80 complex binding to the MT lattice [47, 52, 55, 64] (sections 5.2.1 through 5.2.3). For cells rescued with Hec1 tail truncation mutants, a loss of ABK phosphorylation to the Hec1 tail domain would preclude dynamic regulation of kinetochore-MT interactions, and this may explain the impairment of metaphase plate formation in the presence of kinetochore-MT attachments.

5.2.5 Cells Expressing a Truncated Hec1 Tail Domain Display Defects in Mitotic Progression

The fixed cell analysis indicated that truncation of the Hec1 80 amino acid tail domain did not severely compromise kinetochore-MT attachments, but metaphase plate formation was impaired. This suggests that the dynamics of kinetochore-MT interactions may have been altered in some way. Monitoring a cell's progression through mitosis via live cell microscopy can be used to determine if chromosomes align at a metaphase plate.

Additionally, cellular exit from mitosis after fulfillment of the SAC serves as an indirect assessment that kinetochore-MT attachments have been made. Live cells expressing a Hec1 truncation construct were imaged and movies were made to address if 1) metaphase plates could form and 2) kinetochore-MT attachments could satisfy the SAC. From the fixed cell analysis, cells expressing Hec1^{57-61Δ80} were determined to have the most robust kinetochore-MT attachments, and so this mutant was used in the live cell analysis.

As compared to FL Hec1-GFP rescued cells, where 84.6% were capable of metaphase plate formation, only 37.8% of cells rescued with Hec1^{57-61Δ80}-GFP achieved metaphase plates (Figure 5.2-17&18; Table 5.2.13). For FL Hec1-GFP and Hec1^{57-61Δ80}-GFP rescued cells 100% and 93.3%, respectively, were capable of entering anaphase in under 2 h (Figure 5.2.19; Table 5.2.14). In cells rescued with Hec1^{57-61Δ80}-GFP, the progression through mitosis in the absence of metaphase plate formation is reminiscent of cells rescued with Hec1^{9A}-GFP (Figures 5.2-17,18&19; Tables 5.2-13&14). In cells rescued with Hec1^{9A}-GFP, kinetochore-MT hyper-attachments result from alanine mutations that preclude dynamic ABK phosphorylation of the Hec1 80 amino acid tail domain [47, 52]. The hyper-attachments induced by the 9A Hec1 tail often perpetuate chromosome segregation errors as the SAC's need for kinetochore-MT attachments is satisfied, while a loss in dynamic regulation of kinetochore-MT attachments impairs chromosome alignment. Previous studies have identified that removal of the 80 amino acid tail domain does not disrupt the SAC, as a mitotic arrest is observed [52]. This supports our notion that manipulation of the Hec1 tail domain will not affect SAC function, and any progression through mitosis can be attributed to the SAC being satisfied and not simply abrogated. Ultimately the un-regulated, hyper-attachments generated in Hec1^{9A}-GFP rescued cells permit the SAC to be satisfied, and cells divide albeit with chromosomes in a partially aligned state. Comparatively, cells rescued with Hec1^{9A}-GFP or Hec1^{57-61Δ80}-GFP are similar in that they both made attachments (as determined by fixed cell analysis), and exited from mitosis with unaligned

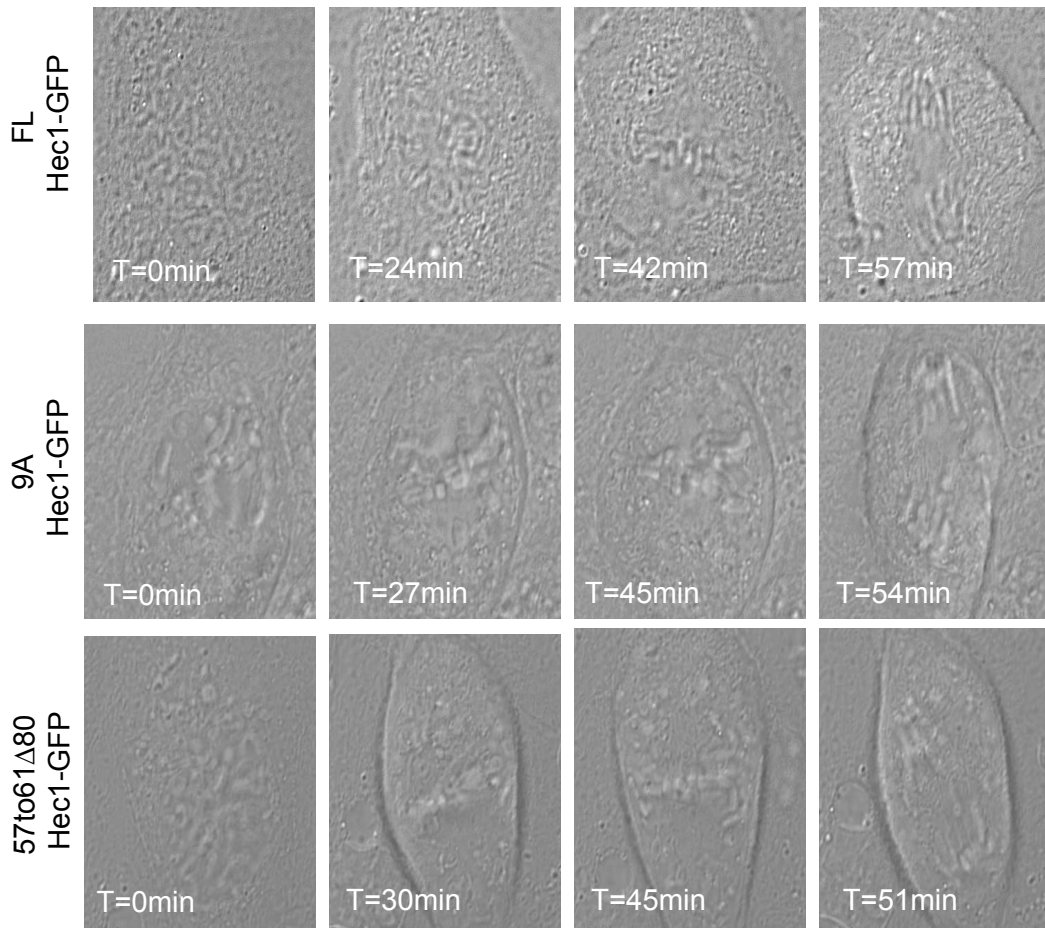


Figure 5.2.17: Cells expressing Hec1 with a short tail domain progress through mitosis in a timely fashion

Using time-lapse DIC microscopy, timing through mitosis was recorded for cells rescued with various Hec1 mutants. Cells were initially identified as being GFP positive for a particular Hec1 construct, and then confirmed to have a Cy5 labeled Hec1 siRNA. Individual images shown for each panel are still images from time lapse-movies, with time stamps indicating the elapsed time in min.

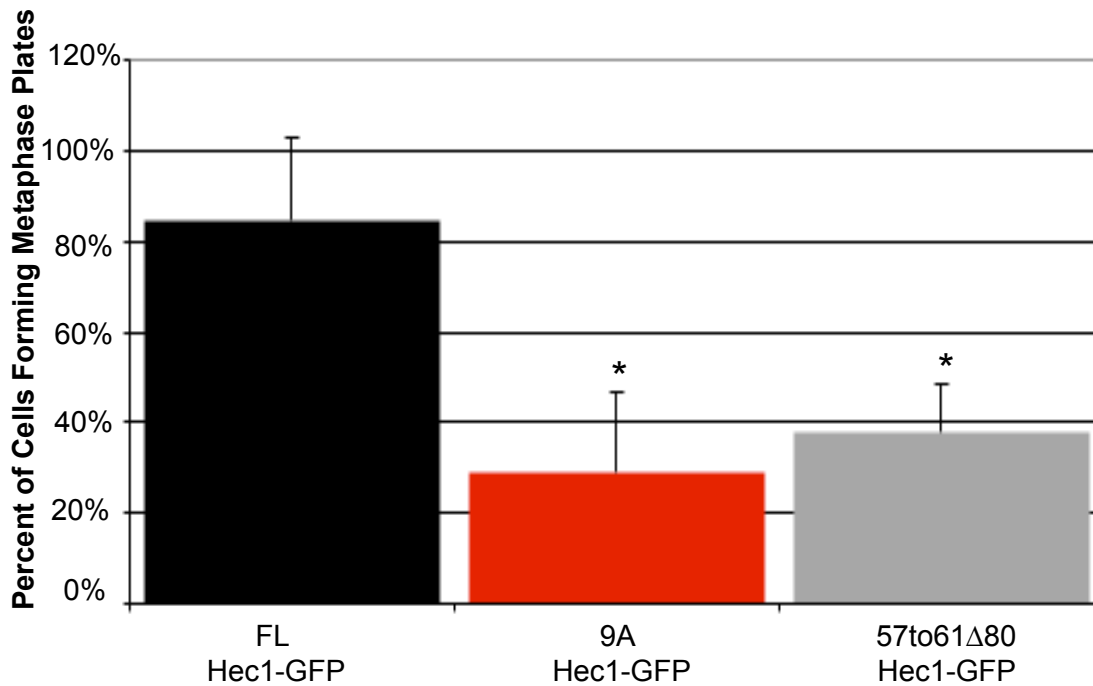
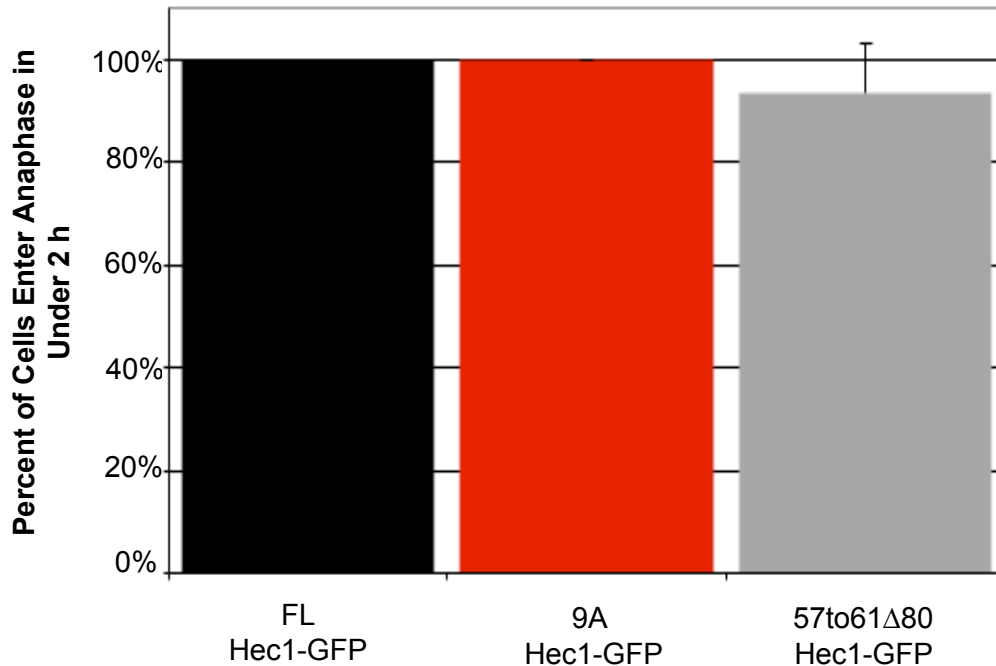


Figure 5.2.18: Cells expressing a short Hec1 tail are impaired in metaphase plate formation

Quantification of metaphase plates formed during live cell imaging. Bar graph represents the percent of cells that form metaphase plates during the time-lapse imaging. FL-Hec1= 84.6%, 9A-Hec1= 29.0%, 57to61Δ80-Hec1= 37.8%. Black asterisk indicates a statistically significant difference with respect to FL Hec1-GFP ($p < 0.001$).

Table 5.2.13: Time lapse movies- percent of cells rescued with a Hec1 truncation mutant achieving metaphase alignment

Hec1 Mutant	% of Cells that form Metaphase Plates	Std. Dev.	Total Number of Cells
FL	84.6	18.2	22
9A	29.0	17.6	38
57to61ΔDel80	37.8	10.9	37



5.2.19: Cells expressing a short Hec1 tail mutant can satisfy the SAC and enter anaphase in under two hours

Quantification of cells that enter anaphase during live cell imaging. Bar graph represents the percent of cells which entered anaphase within 2 h of time-lapse imaging. FL Hec1-GFP=100±0%, 9A Hec1-GFP=100±0%, 57to61Δ80 Hec1-GFP=93.3%

Table 5.2.14: Time lapse movies- percent of cells rescued with a Hec1 truncation mutant entering anaphase in under two hours

Hec1 Construct	Percent of Cells Entering Anaphase in Under 2 h	Std. Dev.	Total # of Cells
FL	100.0	0.0	22
9A	100.0	0.0	16
57to61Δ80	93.3	10.0	15

chromosomes (as determined by live cell analysis). The impairment of tail phosphorylation to either mutant proteins encoded for by the Hec1^{9A} or Hec1^{57-61Δ80} constructs supports previously suggested models for ABK mediated regulation of kinetochore-MT attachments necessary for a faithful mitotic progression. This model was additionally supported in sections 5.2.1 through 5.2.3. The work here only strengthens the notion that a dynamic regulation of kinetochore-MT interactions mediated through Hec1 tail phosphorylation is essential to the maintenance of a flexible kinetochore-MT interaction. Together, the time-lapse movies suggest that a short tail domain is sufficient to establish kinetochore-MT attachments, capable of satisfying the SAC, while phosphorylation-regulation to a more complete portion of the Hec1 tail domain is needed to produce dynamic kinetochore-MT attachments required for correct chromosomal positioning at the metaphase plate.

5.2.6 Cells Expressing a Truncated Hec1 Tail Domain Display Dampened Kinetochore Oscillations

Recent reports have demonstrated that regulation of the Hec1 80 amino acid tail domain may play an essential role in regulation of kinetochore-MT dynamics, either through modulation of Ndc80 complex oligomerization or by directly affecting the Hec1-MT interaction [52, 55]. Kinetochore-MT binding was observed in cells rescued with Hec1^{57-61Δ80}-GFP, suggesting that the entire 80 amino acid tail domain is non-essential for this function. Thus, kinetochore oscillations were imaged to address how chromosome dynamics would be affected in the presence of a kinetochore capable of MT attachments, but lacking the entire length of the native Hec1 80 amino acid tail domain. Rescuing cells with Hec1^{57-61Δ80}-GFP resulted in decreased oscillation velocities ($1.60 \pm 0.28 \mu\text{m}/\text{min}$; Figure 5.2.20; Table 5.2.15). This phenotype is similar to the Hec1^{9A}-GFP rescue, where hyper-stabilized kinetochore-MT attachments resulted in decreased kinetochore oscillation velocity. The similarities of Hec1^{9A}-GFP and Hec1^{57-61Δ80}-GFP phenotypes are further emphasized when

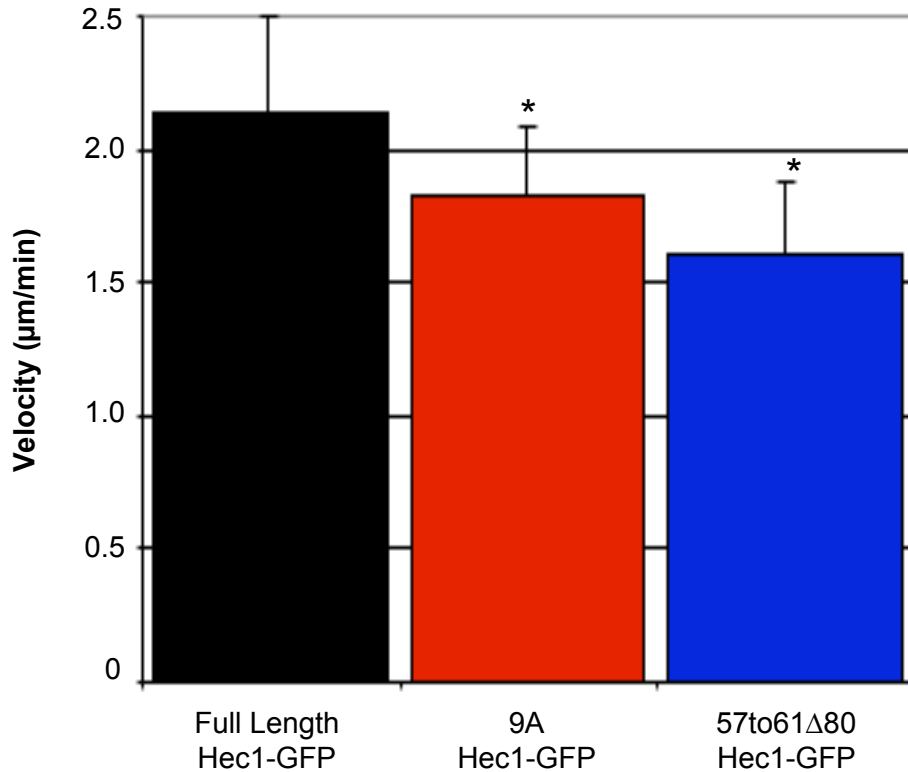


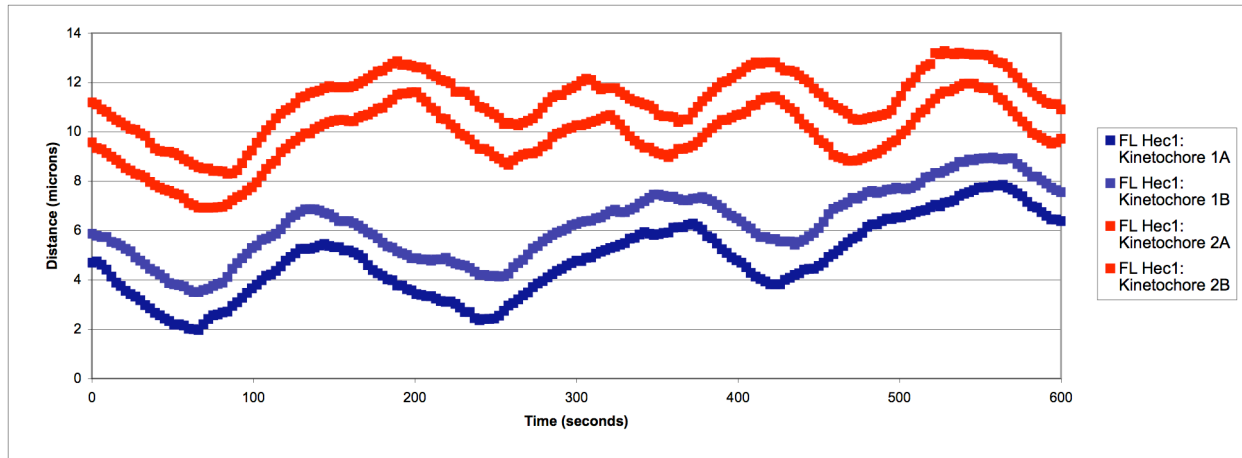
Figure 5.2.20: Truncating the 80 amino acid tail domain decreases chromosome oscillation velocities

Oscillation movies were filmed by imaging the GFP channel in 3x500 nm thick Z-stacks, every 3 s for 10 min. Z-stacks were compressed at each time point, and movies were built. Individual kinetochores pairs at the metaphase plate were tracked using Metamorph software. FL-Hec1 GFP= 2.13 ± 0.37 $\mu\text{m}/\text{min}$; 9A-Hec1 GFP= 1.83 ± 0.26 $\mu\text{m}/\text{min}$; 57to61 Δ 80-Hec1 GFP= 1.60 ± 0.28 $\mu\text{m}/\text{min}$. Black asterisk indicates a statistically significant difference with respect to FL Hec1 ($p < 0.001$).

Table 5.2.15: Oscillation velocity values for cells rescued with a Hec1 truncation mutant

Hec1 Construct	Avg. Oscillation Velocity ($\mu\text{m}/\text{min}$)	Total # of Cells
FL	2.13 ± 0.37	14
9A	1.83 ± 0.26	16
57to61 Δ 80	1.60 ± 0.28	9

FL Hec1-GFP



Hec1^{9A}-GFP

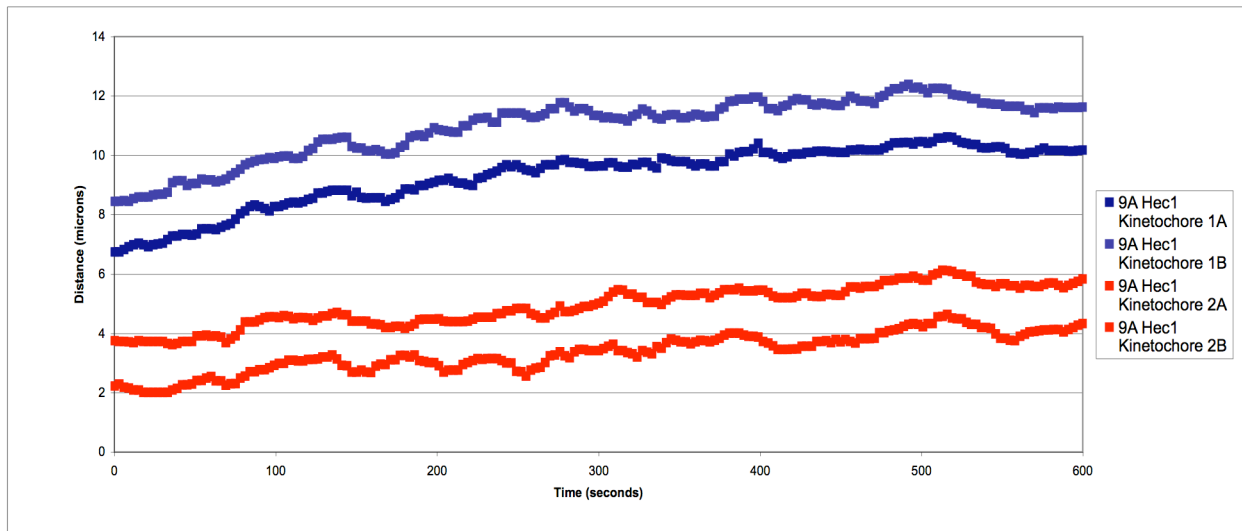
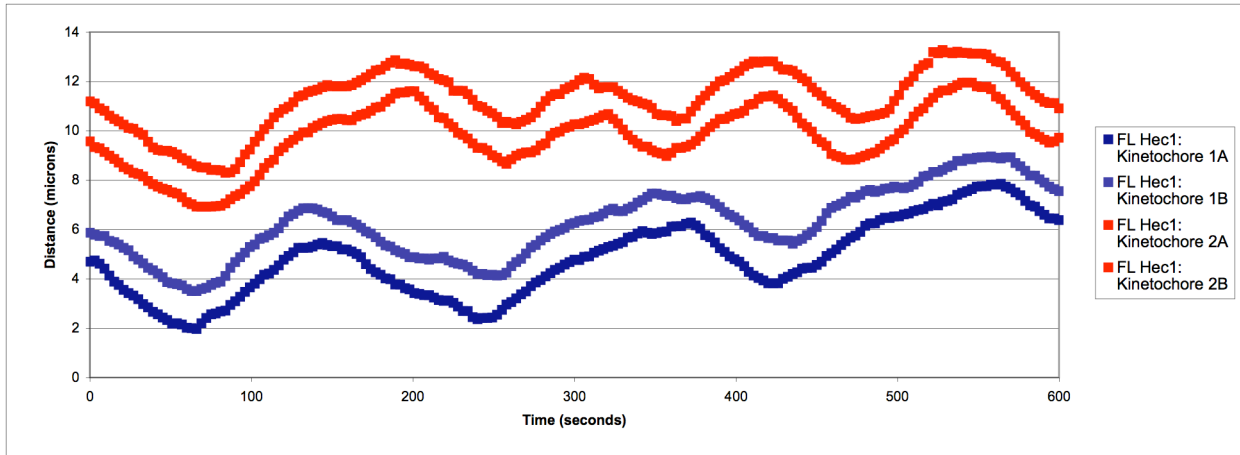


Figure 5.2.21: Precluding phosphorylation to the Hec1 tail domain results in stagnant chromosome movements

Representative graphs for oscillation movies where cells were rescued with either FL Hec1-GFP (top) or Hec1^{9A}-GFP (bottom). The points in the graph represent the track of a given kinetochore as it oscillates through a cell (distance in μm) over time (movie length = 600 s).

FL Hec1-GFP



Hec1^{57-61Δ80}-GFP

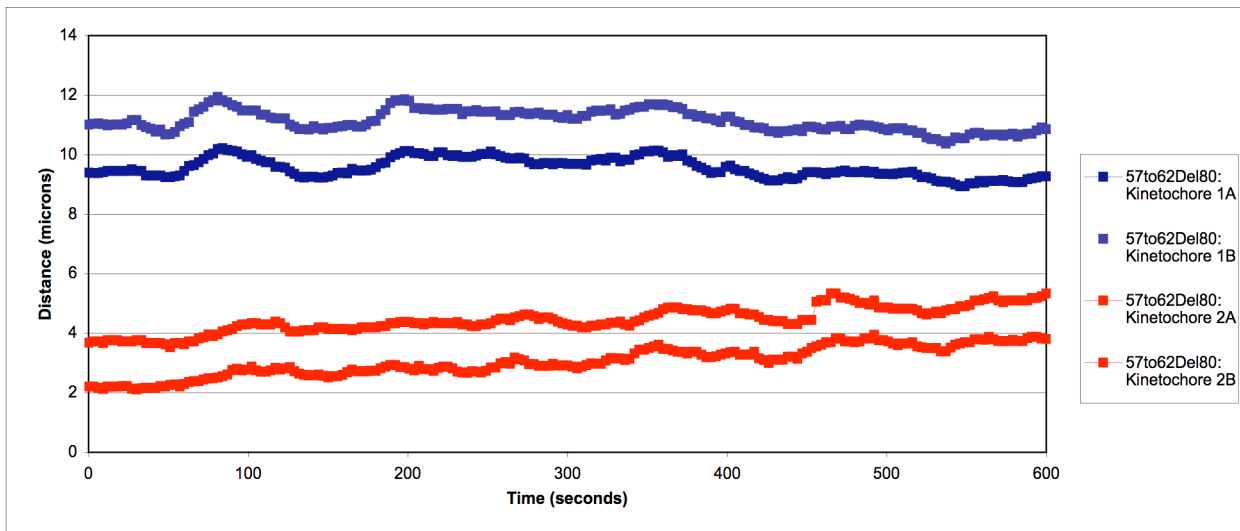
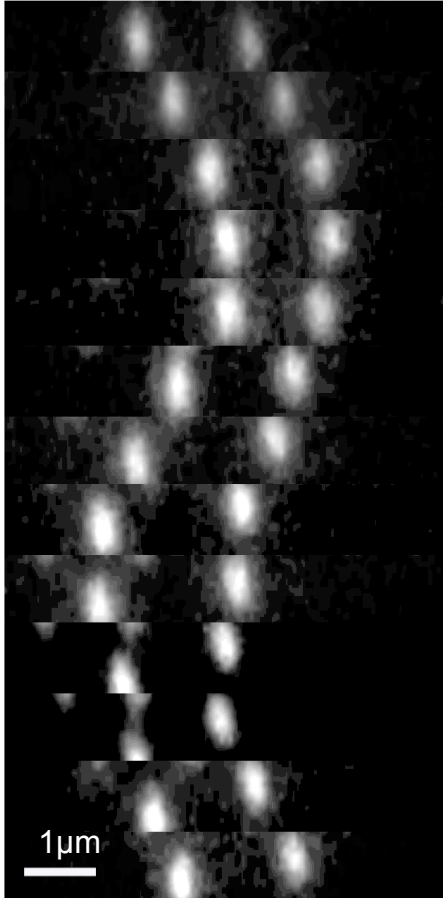


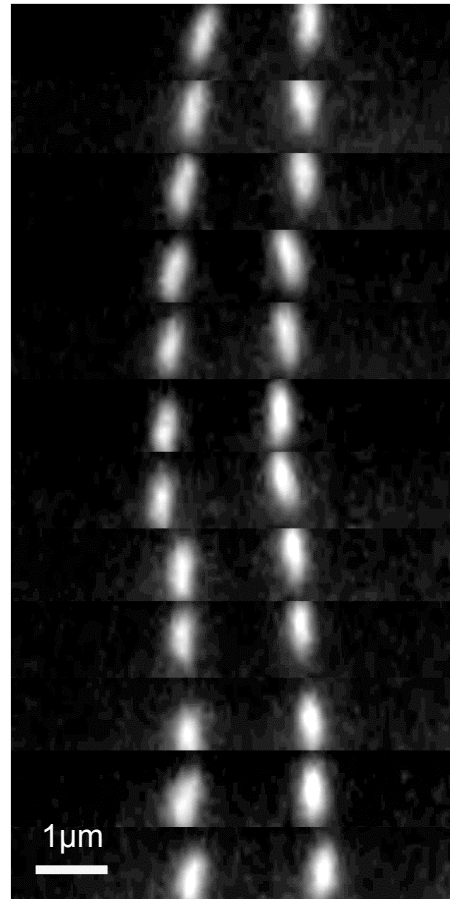
Figure 5.2.22: Truncation to the Hec1 tail domain results in stagnant chromosome movements

Representative graphs for oscillation movies where cells were rescued with either FL Hec1-GFP (top) or Hec1^{57-61Δ80}-GFP (bottom). The points in the graph represent the track of a given kinetochore as it oscillates through a cell (distance in μm) over time (movie length = 600 s).

FL Hec1-GFP

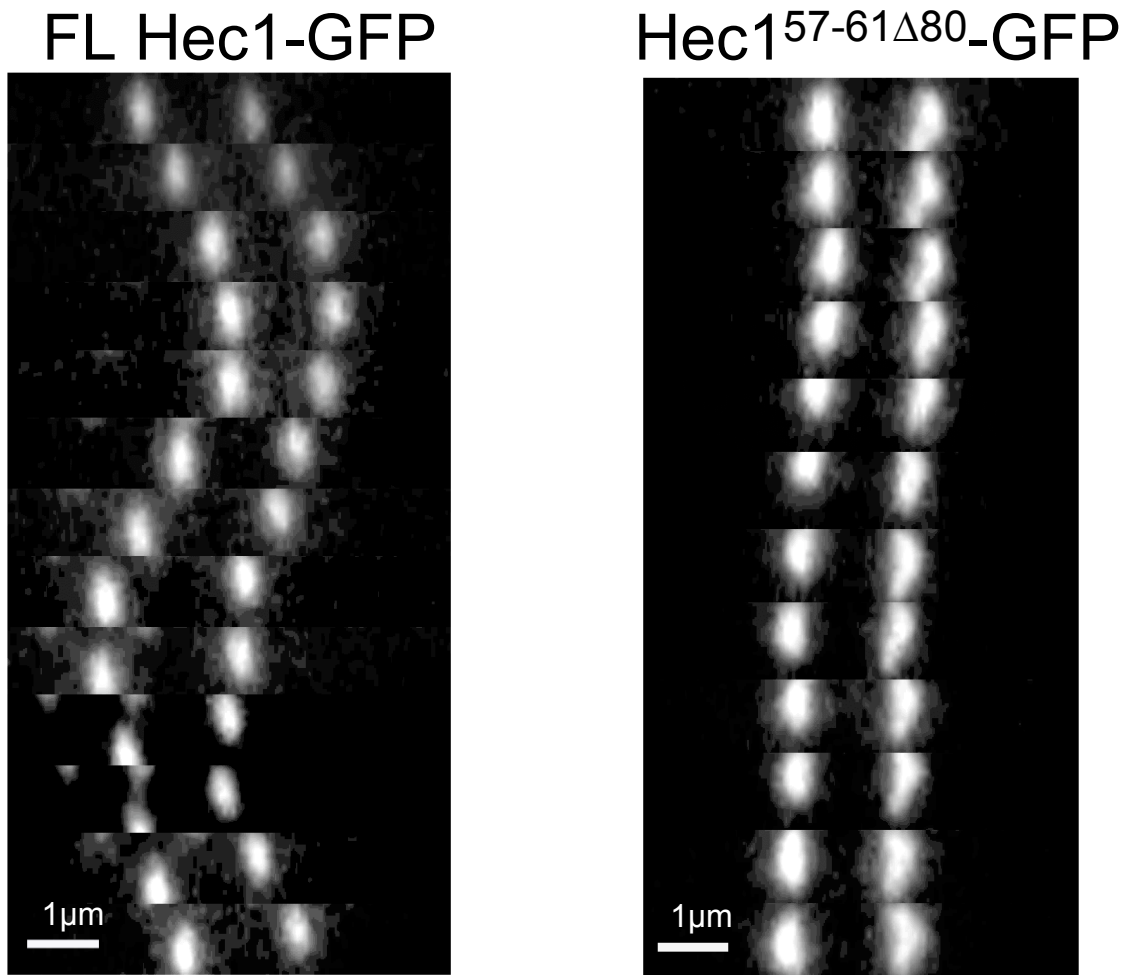


Hec1^{9A}-GFP



5.2.23: Precluding phosphorylation to the Hec1 tail domain yields stagnant chromosome movements

Kinetochores oscillation kymographs for the FL and 9A Hec1-GFP rescued cells. Frames in the kymograph were taken every 9 s.



5.2.24: Truncating the Hec1 tail domain yields stagnant chromosome movements

Kinetochores oscillation kymographs for the FL Hec1-GFP and Hec1^{57-61Δ80}-GFP rescued cells. Frames in the kymograph were taken every 9 s.

looking at the oscillation graphs and kymographs; FL Hec1-GFP rescued cells exhibit oscillatory movements (Figures 5.2-21&23), while the kinetochores from cells rescued with Hec1^{9A}-GFP, and Hec1^{57-61Δ80}-GFP remain nearly motionless (Figures 5.2-21,22,23&24).

Together, the results have demonstrated that kinetochores from cells rescued with Hec1^{57-61Δ80}-GFP are nearly motionless albeit in the presence of kinetochore-MT attachments, reminiscent of the Hec1^{9A}-GFP rescue phenotype. In the Hec1^{9A}-GFP rescue, the resulting phenotype is attributed to loss of dynamic kinetochore-MT regulation as ABK phosphorylation sites have been precluded. In cells rescued with Hec1^{57-61Δ80}-GFP, truncation to the Hec1 tail domain may also result in a loss of ABK phosphorylation-regulation, and suggest a more complete segment of the native tail domain is needed for dynamic kinetochore-MT interactions. Exactly how the native Hec1 tail contributes to dynamic kinetochore-MT regulation, whether through Ndc80 complex oligomerization, direct interactions with the MT lattice, or some combination of these mechanisms, remains unclear.

5.2.7 The Primary Sequence of the Hec1 80 Amino Acid Tail Domain is Not Required for Establishing Kinetochore-MT Interactions

Experimentation to this point has allowed us to address how phosphorylation status and length of the Hec1 80 amino acid tail domain affects kinetochore-MT attachments. On the surface, length and phosphorylation status of the Hec1 80 amino acid tail domain are fundamentally different features. Yet these experiments have revealed a clear relationship between Hec1 tail charge and MT binding capacity. A combination of the Hec1-MT electrostatic model for interaction and work on intrinsically disordered proteins led us to hypothesize that the amino acid composition, and not primary sequence, of the Hec1 tail domain is sufficient to establish kinetochore-MT attachments. To test this, two constructs were made whereby the Hec1 80 amino acid tail primary sequence was scrambled in a

random order (Hec1^{Scr80#1}-GFP and Hec1^{Scr80#2}-GFP; Table 5.2.17), while still maintaining the native amino acid composition. Using a silence and rescue strategy, both scrambled 80 Hec1 tail constructs localized to the kinetochore (Figure 5.2.25), and exhibited levels of tension and a percent of stably bound kinetochore-MT bundles that were not statistically different as compared to cells rescued with FL Hec1-GFP (Figures 5.2-26&27; Tables 5.2-18&19). However, even in the presence of stable, tension-generating attachments, scrambling of the native 80 amino acid tail sequence impeded chromosome congression to the metaphase plate (Figure 5.2.28; Table 5.2.20). Taken together, these results indicate that the physical properties associated with the amino acid composition of Hec1's unstructured tail domain, and not the primary sequence, are capable of promoting kinetochore-MT attachments. The inability of Hec1^{Scr80#1}-GFP and Hec1^{Scr80#2}-GFP rescued cells to align their chromosomes at the spindle equator in the presence of kinetochore-MT attachments argues that Hec1's primary sequence is required for the proper regulation of kinetochore-MT attachment status needed for metaphase plate formation. Notably, upon scrambling the 80 amino acid tail domain, there is disruption to Aurora B kinase recognition sites. It has been proposed that a dynamic phosphorylation of Aurora B kinase phosphorylation to the Hec1 tail domain is required for a faithful mitotic progression [47], and may explain why bi-orientation is impaired in cells rescued with Hec1^{Scr80#1}-GFP or Hec1^{Scr80#2}-GFP. The same phenotype was observed in cells rescued with a Hec1 construct where ABK phosphorylation of the 80 amino acid tail domain is precluded (either Hec1^{9A}-GFP and Hec1^{57-61Δ80}-GFP; sections 5.2.4 through 5.2.6), and resulted in kinetochore-MT attachments impaired in their ability to form of metaphase plates.

5.2.8 Cells Rescued with a Scrambled 80 Amino Acid Hec1 Tail Domain Display Defects in Mitotic Progression

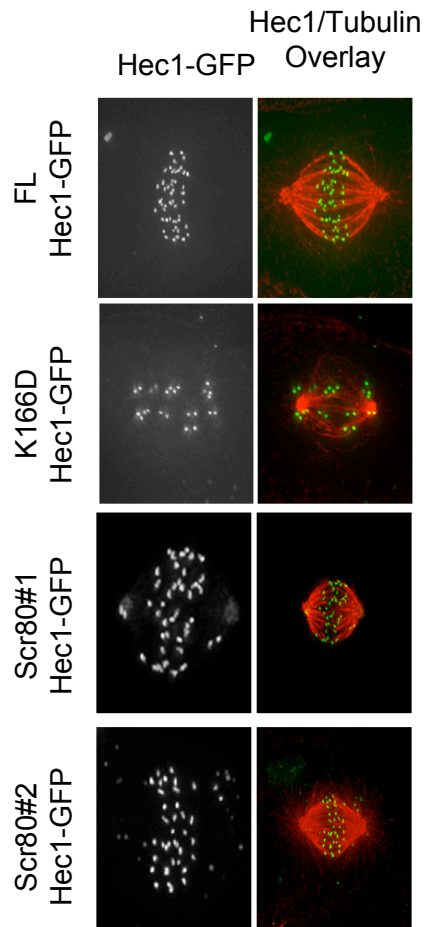


Figure 5.2.25: Primary sequence of the Hec1 tail domain is essential for metaphase plate formation

Projections of deconvolved immunofluorescent images of PtK1 cells depleted of endogenous Hec1 and rescued with the indicated GFP-fusion protein.

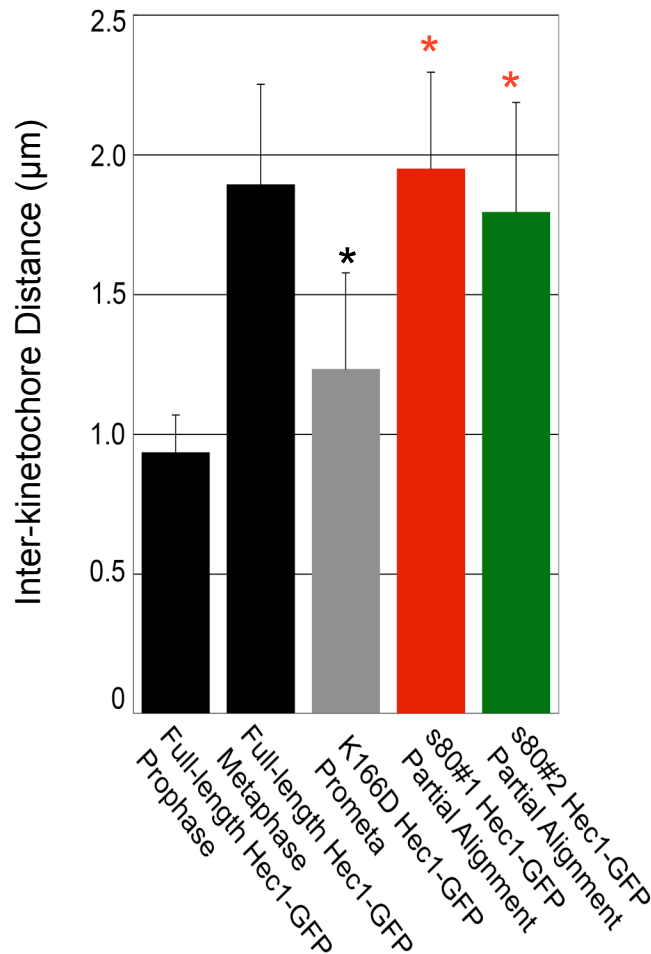


Figure 5.2.26: Cells expressing a scrambled Hec1 80 amino acid tail domain are capable of establishing kinetochore-MT attachments

Quantification of inter-kinetochore distances, which were measured from Hec1-GFP centroid to Hec1-GFP centroid (Prophase FL Hec1-GFP: IKD=0.93±/0.13, n=11 cells, 46 kinetochores; Bioriented FL Hec1-GFP: IKD=1.89±/0.36, n=33 cells, 426 kinetochores; Prometa K166D Hec1-GFP: IKD=1.22±/0.33, n=42 cells, 644 kinetochores; Bioriented scr80#1 Hec1-GFP: IKD=1.95±/0.35, n=21 cells, 262 kinetochores; scr80#2 Hec1-GFP: IKD= 1.81±/0.42, n=10 cells, 106 kinetochores). Measurements were made from the terminal phenotype achieved in cells expressing a given construct. Black asterisk indicates a statistically significant difference with respect to the FL Hec1-GFP rescue, while a red asterisk indicates a statistically significant difference with respect to Hec1^{K166D}-GFP rescue (p<0.001).

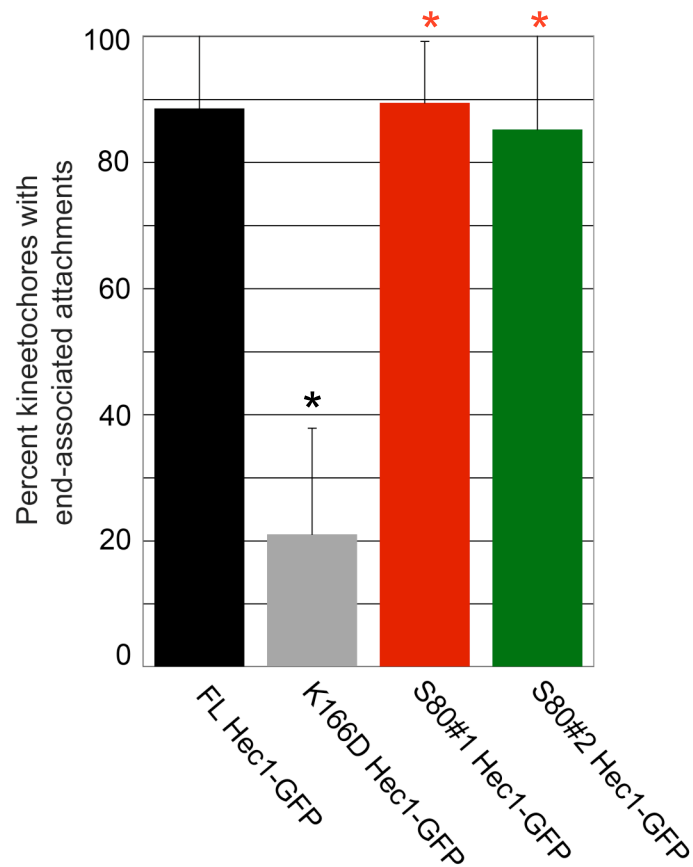


Figure 5.2.27: Cells expressing a scrambled 80 amino acid tail domain establish stable kinetochore-MT attachments

Quantification of end-on microtubule association with kinetochores (FL Hec1-GFP: Attachment=82.5±17.4%, n=63 cells, 1778 kinetochores; Hec1^{K166D}-GFP: Attachment=21.0±16.8%, n=52 cells, 1812 kinetochores; scr80#1 Hec1-GFP: Attachment=89.4±9.8%, n=13 cells, 297 kinetochores; scr80#2 Hec1-GFP: Attachment=85.1±19.4%, n=18, 577 kinetochores). Measurements were made by averaging values of cells rescued with a given construct from all phases of mitosis. Black asterisk indicates a statistically significant difference with respect to the FL Hec1-GFP rescue, while a red asterisk indicates a statistically significant difference with respect to the Hec1^{K166D}-GFP rescue (p<0.001).

Table 5.2.16: Electrostatic potential existing between the Hec1 and tubulin tail domains

<u>Protein</u>	<u># of Acids</u>	<u># of Bases</u>	<u>Sum of Charge</u>	<u>Amino Acid Length</u>	<u>Charge per Amino Acid</u>
Hec1 80 amino acid tail	5	16	11	80	0.14
C-terminal tubulin tail isotype 1	11	0	-11	18	-0.61

Table 5.2.17: Amino acid sequence for the scrambled 80 Hec1 tail domain mutants

<u>Human Hec1 Mutant Name</u>	<u>Amino Acid Sequence: only the 80 amino acid tail domain is shown</u>
FL Hec1	MKRSSVSSGGAGRLSMQELRSQDVNKQGL YTPQTKEKPTFGKLSINKPTSERKVSLFGKRT SGHGSRNSQLGIFSSSEKI
Scr80 #1	MHHSGSQLLLSQGKKTNTQLSFMSKFISSKP GGSEGFTLRRYERNLIESGKKSQSVKDENP QRASTRGSKVKVGGSSIRS
Scr80 #2	MSRLIAQQQSNKRIFSLKQKVTPDKFGEKGS NQSSRNVGKSRTFKLETLGSGLRSKSQKSM PGSGTSGHPYSLESTVERI

Table 5.2.18: Inter kinetochore distances for cells rescued with a scrambled 80 Hec1 tail

Hec1 Construct	IKD Average	Std. Dev.	# of Ks	# of Cells
FL Prophase	0.93	0.13	46	11
FL Partial	1.89	0.36	243	18
FL Metaphase	1.89	0.36	183	15
FL Bioriented	1.89	0.36	426	33
K166D Prometa	1.22	0.33	740	69
Scr80#1 Bioriented	1.95	0.35	262	21
Scr80#2 Bioriented	1.81	0.42	85	10

Table 5.2.19: Percent end on kinetochore-MT attachments for cells rescued with a scrambled 80 Hec1 tail

Hec1 Construct	# of Attach. Ks	# of Unattach. Ks	Total # of Ks	% of Attach. Ks	Std. Dev.	# of Cells
FL	1778	377	2155	82.5	1.74	63
K166D	380	1432	1812	21.0	16.8	52
Scr80#1	1017	121	1138	89.4	9.8	29
Scr80#2	577	101	678	85.1	19.4	18

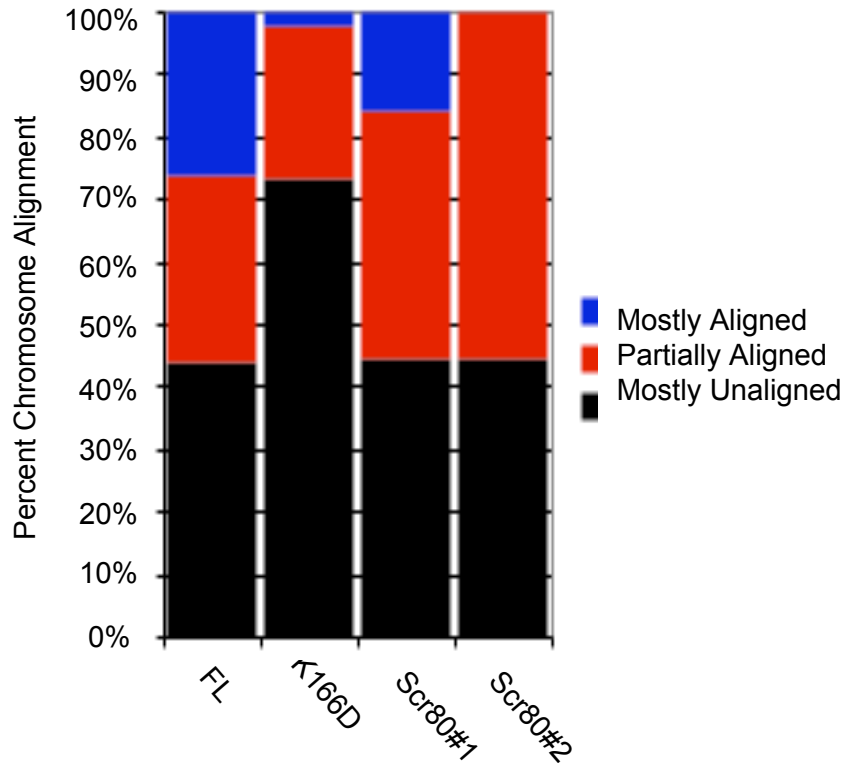


Figure 5.2.28: A scrambled 80 amino acid tail domain impairs metaphase plate formation

Quantification of chromosome alignment phenotypes in cells depleted of Hec1 and rescued with a scrambled 80 amino acid Hec1 tail domain. Cells with Mostly Aligned (MA) chromosomes (blue) had no chromosomes off the metaphase plate, cells with Partially Aligned (PA) chromosomes (red) exhibited 1-4 chromosomes off of a metaphase plates, and cells with Mostly Unaligned (MU) chromosomes (black) had either no chromosome alignment or more than 4 chromosomes off of the metaphase plate.

Table 5.2.20: Percent chromosome alignment values for cells rescued with a scrambled 80 Hec1 tail

Phenotype	FL	K166D	Scr80	Scr80#2
% Mostly Unaligned	43.2	73.4	45	44.5
% Partially Aligned	36.4	24.4	40	55.5
% Mostly Aligned	20.4	2.1	15	0
Total # of Cells	88	94	38	15

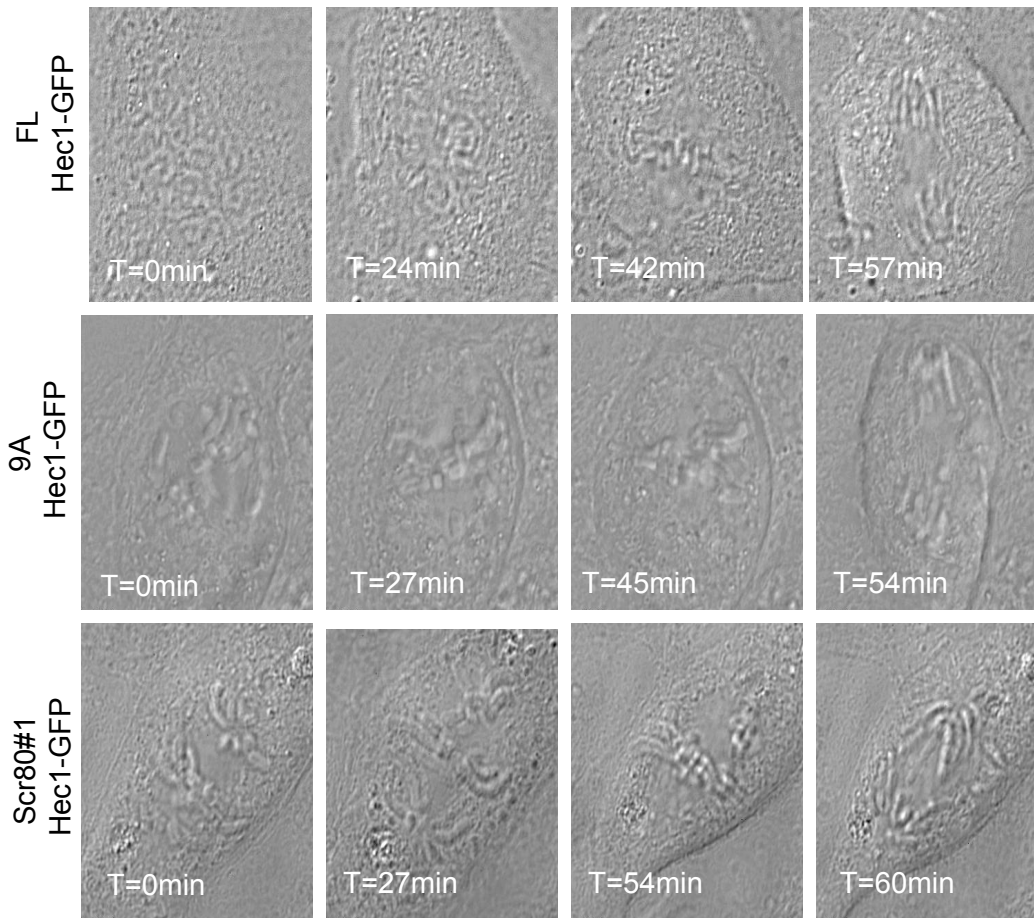


Figure 5.2.29: Cells rescued with a scrambled Hec1 80 amino acid tail domain progress through mitosis in a timely fashion

Using time-lapse DIC microscopy, timing through mitosis was recorded for cells expressing various Hec1 mutants. Cells were initially identified as being GFP positive for a particular Hec1 construct, and then confirmed to have a Cy5 labeled Hec1 siRNA. Individual images shown for each panel are still images from time lapse-movies, with time stamps indicating the elapsed time in min.

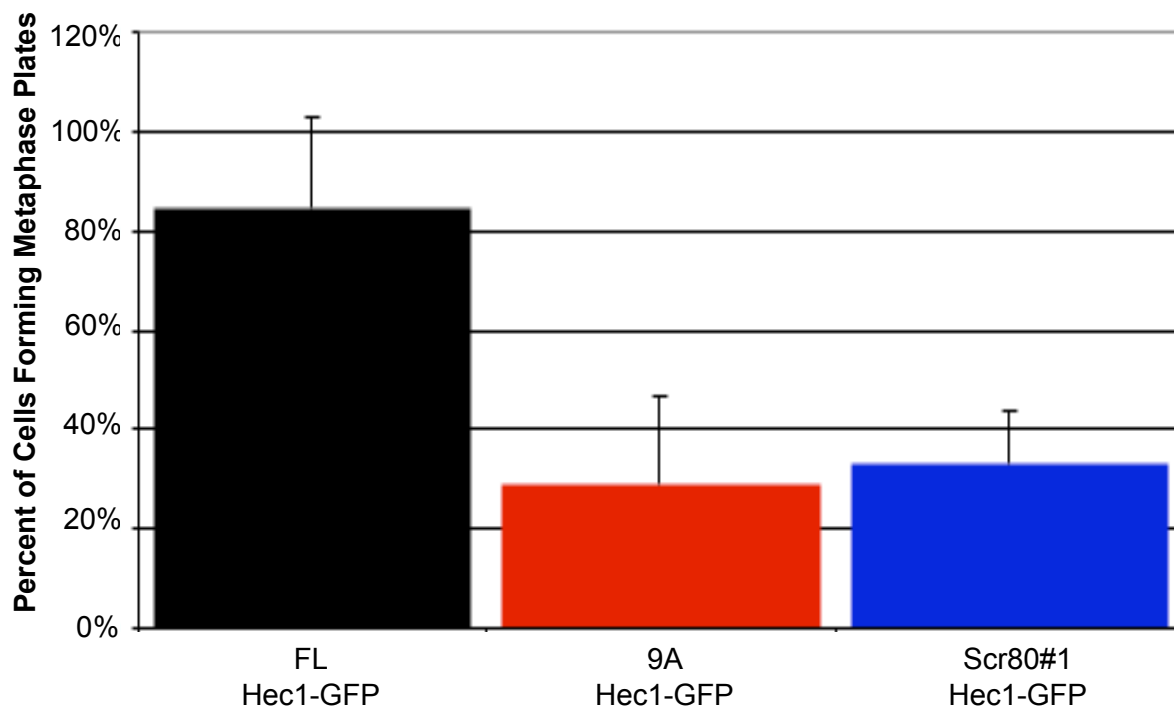
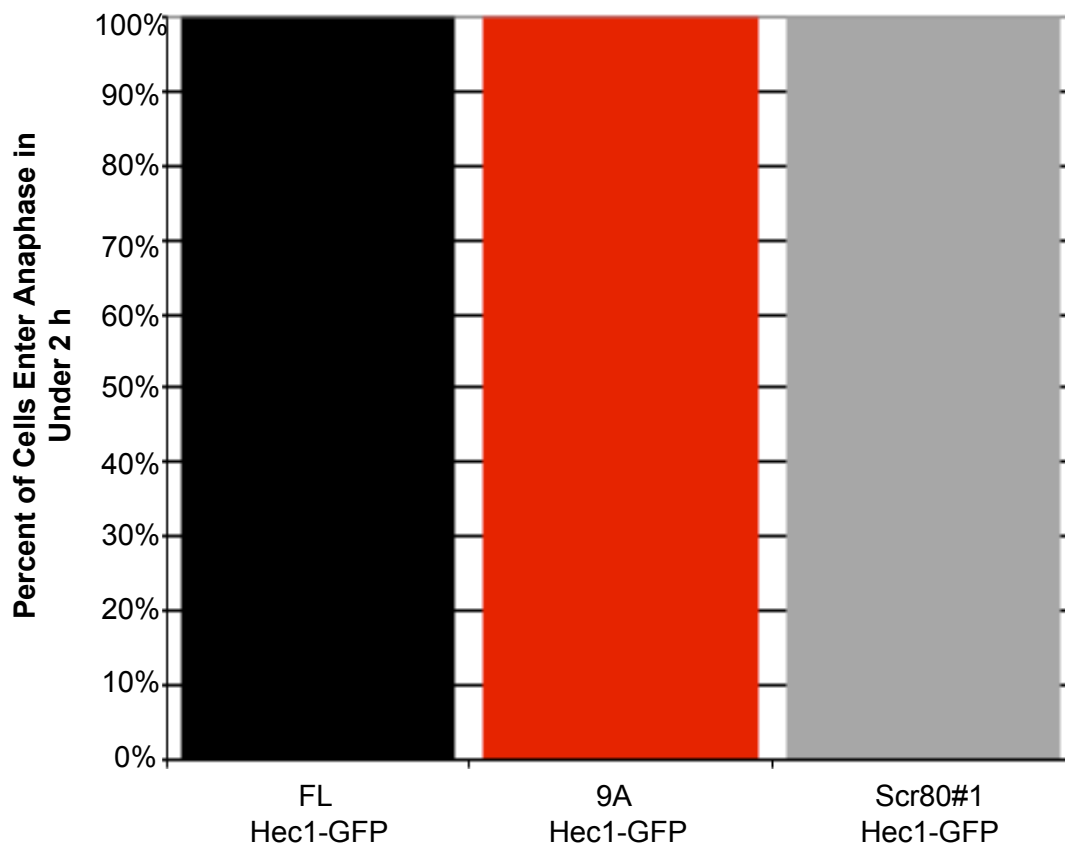


Figure 5.2.30: Scrambling of the Hec1 80 amino acid tail domain impairs metaphase plate formation

Quantification of metaphase plates formed during live cell imaging. Bar graph represents the percent of cells that form metaphase plates during the time-lapse imaging. FL-Hec1= 84.6%, 9A-Hec1= 29.0%, Scr80#1-Hec1= 33.3%. Black asterisk indicates a statistically significant difference with respect to FL Hec1-GFP ($p < 0.001$).

Table 5.2.21: Time lapse movies- percent of cells achieving metaphase alignment for cells rescued with a scrambled 80 Hec1 tail

Hec1 Mutant	% of Cells that Form Metaphase Plates	Std. Dev.	Total # of cells
FL	84.6	18.2	22
9A	29.0	17.6	38
Scr80#1	33.3	10.4	16



5.2.31: Scrambling of the Hec1 80 amino acid tail domain does not impair anaphase entry

Quantification of cells that enter anaphase during live cell imaging. Bar graph represents the percent of cells which entered anaphase within 2 h of time-lapse imaging. FL-Hec1=100.0%, 9A-Hec1=100.0%, Scr80#1-Hec1=100.0%.

Table 5.2.22: Time lapse movies- percent of cells entering anaphase in under two hours when rescued with a scrambled 80 Hec1 tail

Hec1 Construct	% of cells entering anaphase under 120 min	Std. Dev.	Total # of Cells
FL	100.0	0.0	22
9A	100.0	0.0	16
Scr80#1	100.0	0.0	16

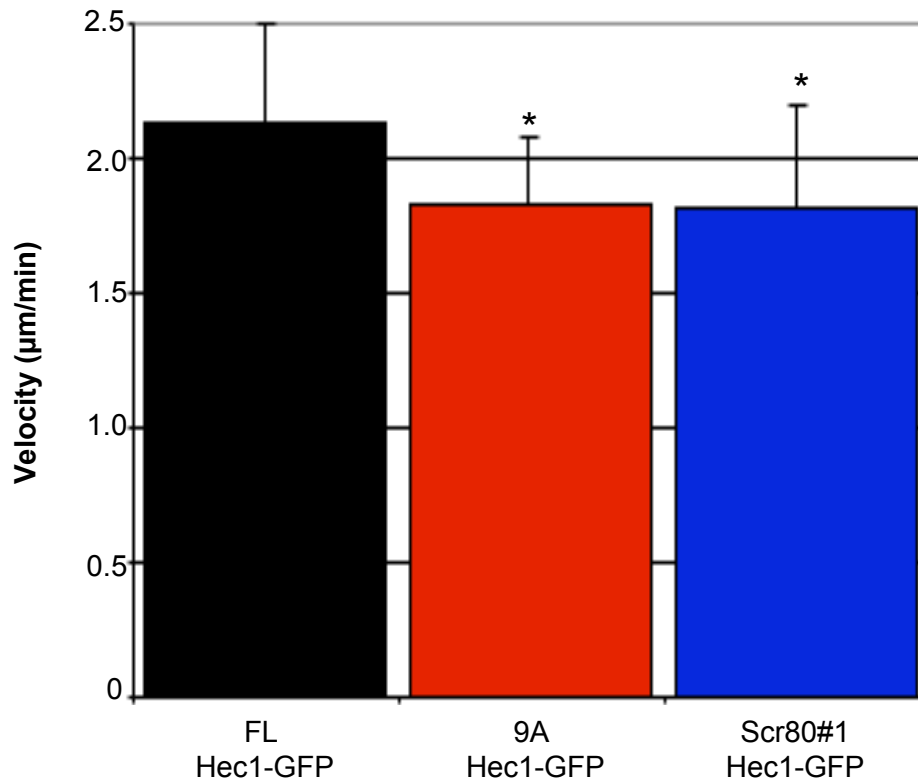


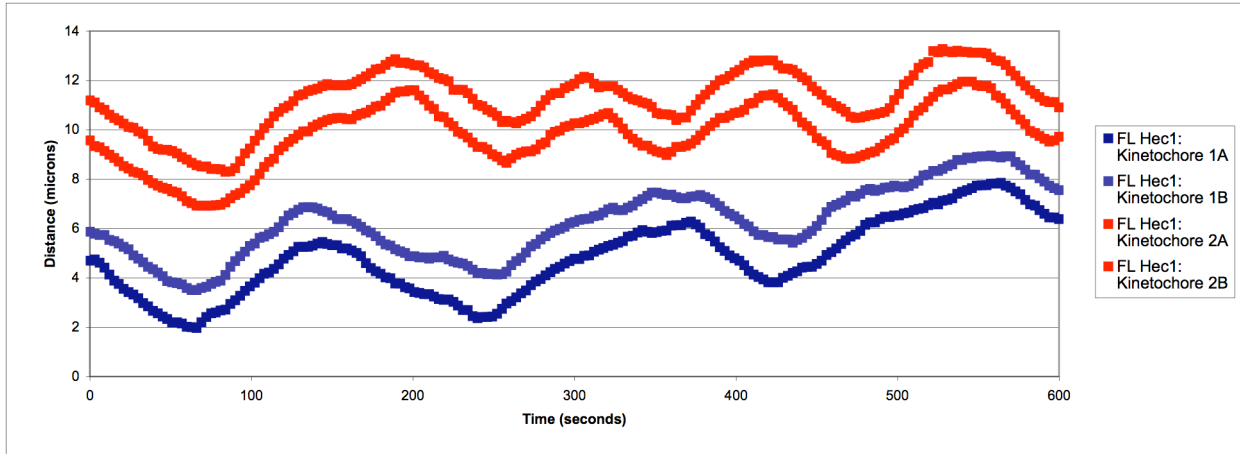
Figure 5.2.32: Scrambling of the 80 amino acid tail domain decreases chromosome oscillation velocities

Oscillation movies were filmed by imaging the GFP channel in 3x500 nm thick Z-stacks, every 3 s for 10 min Z-stacks were compressed at each time point, and movies were built. Individual kinetochore pairs found to exist at the metaphase plate were tracked using Metamorph software. FL-Hec1 GFP= 2.13±0.37 µm/min; 9A-Hec1= 1.83±0.26 µm/min; Scr80#1-Hec1 GFP= 1.81±0.39 µm/min. Black asterisk indicates a statistically significant difference with respect to FL Hec1-GFP (p<0.001).

Table 5.2.23: Oscillation velocity values for cells rescued with a scrambled 80 Hec1 tail

Hec1 Construct	Avg. Oscillation Velocity (µm/min)	Total # of Cells
FL	2.13±0.37	14
9A	1.83±0.26	16
Scr80#1	1.81±0.39	12

FL-Hec1



9A-Hec1

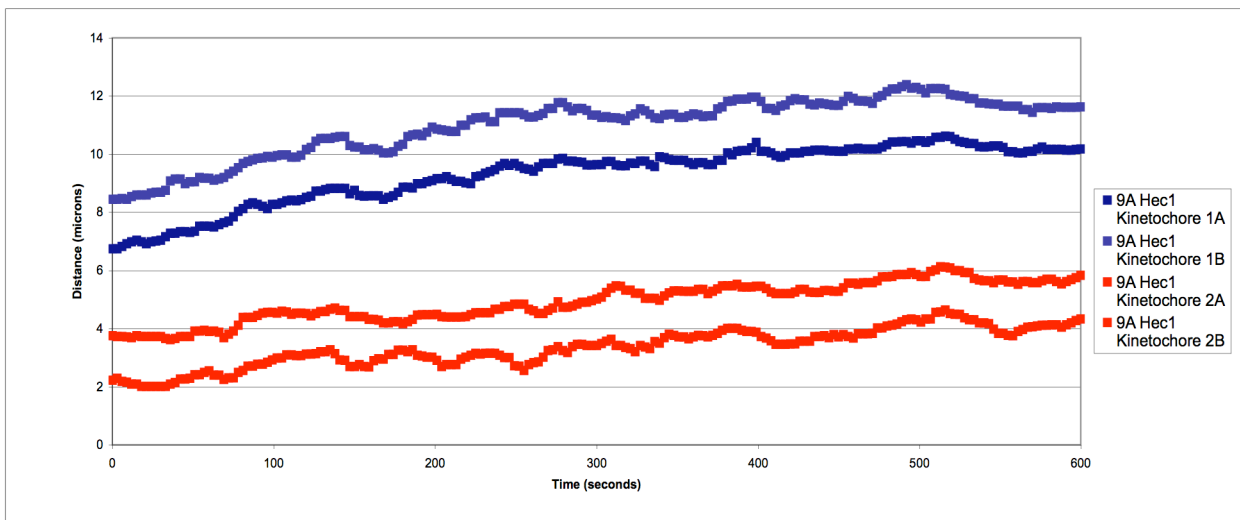
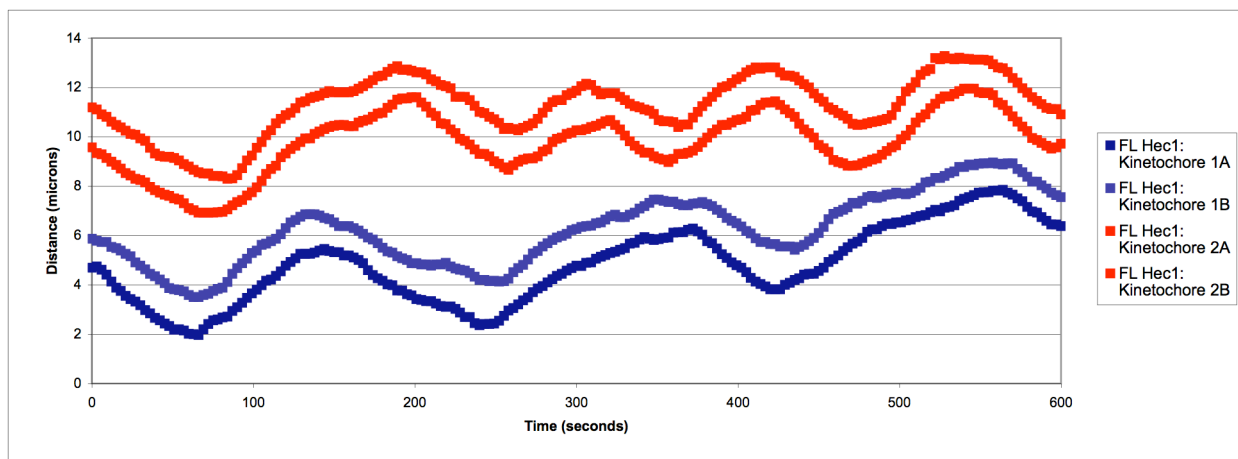


Figure 5.2.33: Precluding phosphorylation to the Hec1 tail domain results in stagnant chromosome movements

Representative graphs for oscillation movies where cells were rescued with either FL Hec1-GFP (top) or 9A Hec1-GFP (bottom). The points in the graph represent the track of a given kinetochore as it oscillates through a cell (distance in μm) over time (movie length = 600 s).

FL-Hec1



Scr80#1 Hec1-GFP

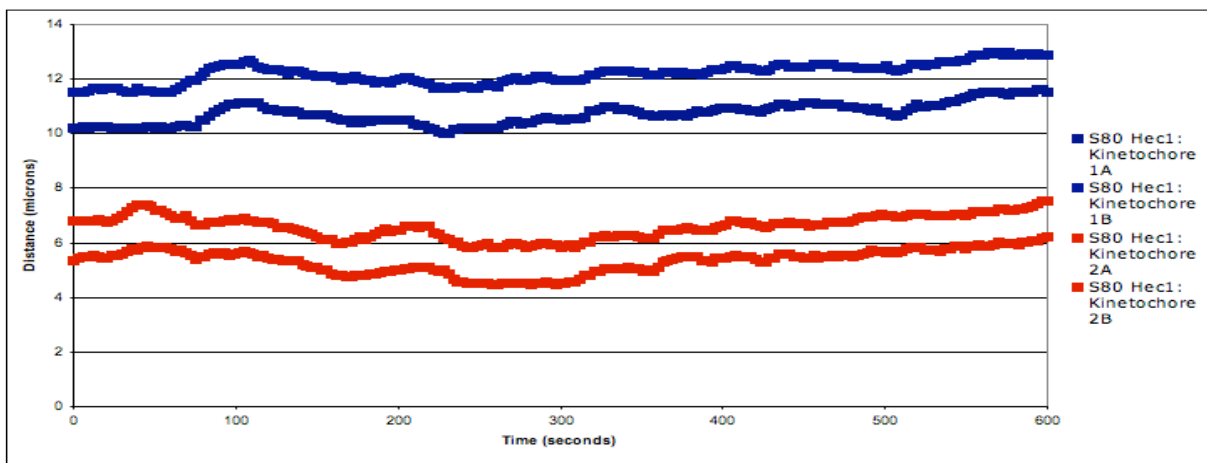
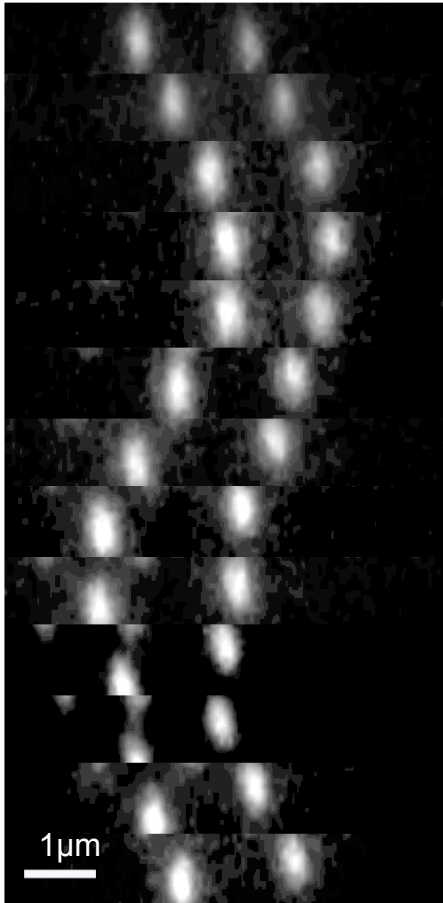


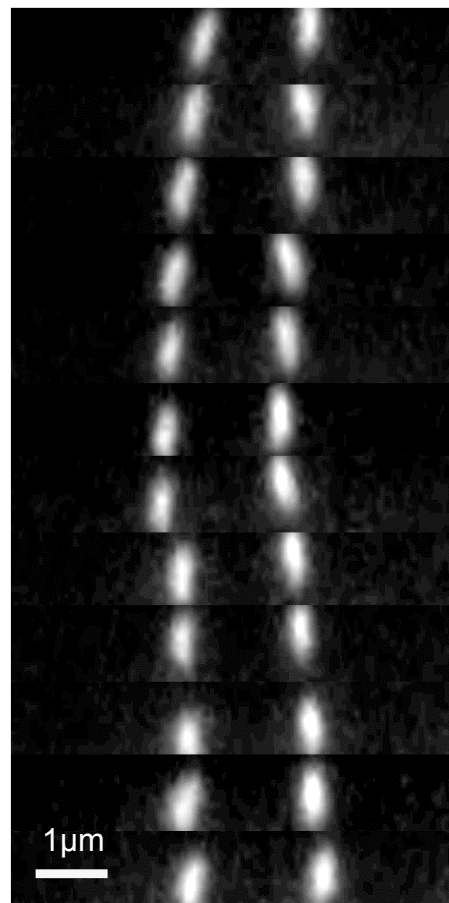
Figure 5.2.34: Scrambling of the Hec1 80 amino acid tail domain results in stagnant chromosome movements

Representative graphs for oscillation movies where cells were rescued with either FL Hec1-GFP (top) or Scr80#1 Hec1-GFP (bottom). The points in the graph represent the track of a given kinetochore as it oscillates through a cell (distance in μm) over time (movie length = 600 s).

FL Hec1-GFP



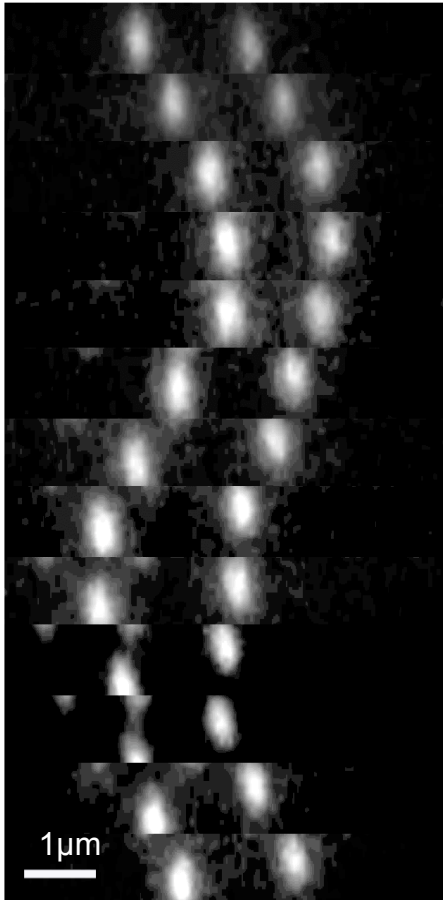
9A Hec1-GFP



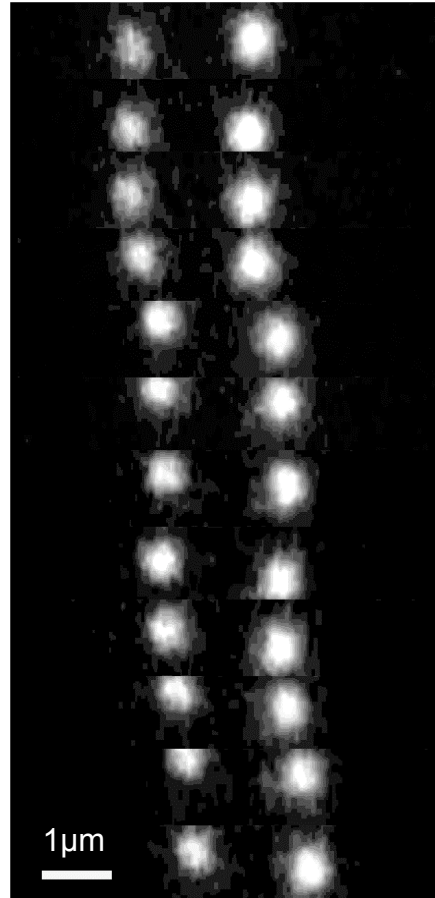
5.2.35: Scrambling of the Hec1 80 amino acid tail domain yields stagnant chromosome movements

Kinetochores oscillation kymographs for the FL Hec1-GFP and 9A Hec1 GFP-GFP rescued cells. Frames in the kymograph were taken every 9 s.

FL Hec1-GFP



Scr80#1 Hec1-GFP



5.2.36: Oscillation kymographs- FL-Hec1 and scrambled 80-Hec1

Kinetochore oscillation kymographs for the FL Hec1-GFP and Scr80#1 Hec1-GFP rescued cells. Frames in the kymograph are taken every 9 s.

For cells rescued with Hec1^{Scr80#1}-GFP and Hec1^{Scr80#2}-GFP constructs, the lack of full metaphase plate formation in the presence of kinetochore-MT attachments is reminiscent of Hec1^{9A}-GFP and Hec1^{57-61Δ80}-GFP rescued cells. In Hec1^{9A}-GFP rescued cells, hyper-stabilized kinetochore-MT attachments generated from an inability to phosphorylate the Hec1 80 amino acid tail domain result in a partial alignment phenotype, whereby numerous chromosomes fail to congress to the metaphase plate. These cells proceed through mitosis in a timely fashion, albeit with unaligned chromosomes, ultimately yielding an unequal segregation of chromosomes. Normally the spindle assembly checkpoint (SAC) functions to ensure that chromosomes are divided into two daughter cells. One of the ways in which the SAC monitors a faithful mitotic progression is by sensing if kinetochores have established a full complement of MT attachments. For cells rescued with Hec1^{9A}-GFP this becomes problematic, as hyper-stabilized attachments serve to satisfy the SAC requirement for kinetochore-MT attachments, but prevention of phosphorylation of the Hec1 tail domain impedes regulation of kinetochore-MT attachments needed for metaphase plate formation. The resulting phenotype is a large percentage of Hec1^{9A}-GFP rescued cells satisfying the SAC and progressing through mitosis in under 2 h, but doing so with unaligned chromosomes (Figures 5.2.29,30,&31; Tables 5.2.21&22). Of note, we believe the logic used to describe the Hec1^{9A}-GFP phenotype can be applied to explain the similar phenotype observed for cells rescued with Hec1^{57-61Δ80}-GFP (sections 5.2.4 through 5.2.6). Previous work has demonstrated that when the Hec1 80 amino acid tail domain is removed and formation of stable kinetochore-MT attachments is impaired, the SAC remains active and cells will arrest in mitosis for >3 h [52]. Thus, with manipulation to the Hec1 80 amino acid tail domain the SAC should also remain functionally active, and mitotic exit can be attributed to the satisfying of the SAC and not simply abrogating it. Cells expressing the Hec1^{Scr80#1}-GFP mutant yielded a very similar phenotype to the Hec1^{9A}-GFP and Hec1^{57-61Δ80}-GFP rescues, in that a large percentage of cells proceeded through mitosis in under 2 h

with unaligned chromosomes (Figures 5.2.29,30,&31; Tables 5.2.21&22). These findings further support the notion that upon scrambling of the 80 amino acid tail domain, kinetochore-MT attachments are still established, thus satisfying the SAC. However, preventing phosphorylation of the scrambled 80 amino acid tail domain, which is needed for regulation of kinetochore-MT attachments, impairs metaphase plate formation. These results compare with the Hec1^{9A}-GFP and Hec1^{57-61Δ80}-GFP rescues, and together suggest that biorientation of chromosomes requires dynamic manipulation to the charge of the Hec1 tail domain through ABK mediated phosphorylation.

5.2.9 Cells Rescued with a Scrambled 80 Amino Acid Hec1 Tail Domain Display Dampened Kinetochore Oscillations

The time-lapse microscopy and fixed cell analysis on Hec1^{Scr80#1}-GFP support a model where electrostatics between the Hec1 tail domain and MTs are capable of forming kinetochore-MT attachments. However, an inability to dynamically phosphorylate the scrambled Hec1 tail domain prevents dynamic regulation of the kinetochore-MT interaction. To further investigate how dynamic kinetochore-MT attachments were affected in response to scrambling of the Hec1 80 amino acid tail domain, live cell kinetochore oscillations were imaged. As compared to FL Hec1-GFP, a decrease in velocity and dampened oscillations were observed for Hec1^{Scr80#1}-GFP rescued cells (Figures 5.2.32,34&36; Table 5.2.23). This phenotype is reminiscent of the Hec1^{9A}-GFP and Hec1^{57-61Δ80}-GFP rescues (Figures 5.2.32,33&35; Table 5.2.23), where the preclusion of phosphorylation resulted in stabilized kinetochore-MT attachments, and ultimately impaired dynamic kinetochore-MT turnover needed for robust oscillations. The reduced oscillation velocities associated with dampened kinetochore-MT dynamics for Hec1^{Scr80#1}-GFP rescued cells further suggest that phosphorylation of ABK sites found within the native Hec1 tail sequence are required to achieve wild-type levels of kinetochore oscillations

5.3.1 Discussion

Mutation targeted to the length, charge, and ABK-mediated phosphorylation potential of the Hec1 80 amino acid tail domain has afforded us a better understanding of how the Hec1 tail contributes to kinetochore-MT attachments and their regulation. A long-standing question in the field has been how the kinetochore association with MTs could harness the energy from MT depolymerizing, while also allowing for tubulin subunit addition during MT polymerization. Recent work has supported the necessity for a flexible kinetochore-MT interaction; when the stability of kinetochore-MT binding was increased errors in chromosome segregation were induced [83], while ablation of the kinetochore-MT interaction through phospho-mimetic mutation of the Hec1 80 amino acid tail domain disrupted kinetochore-MT binding all together [45, 52]. Work from numerous labs suggests that electrostatics promote binding between the Hec1 tail domain and MTs [45, 47, 52, 64, 92]. It has been further suggested that the kinetochore can accommodate for dynamic changes in MT polymerization/depolymerization by appropriately adjusting the kinetochore-MT binding affinity. Specifically, through multiple phosphorylation events to the Hec1 80 amino acid tail, the Hec1-MT electrostatic binding potential can be adjusted [85]. Dynamic ABK phosphorylation of multiple Hec1 sites would allow a fine-tuning of the kinetochore-MT binding interaction necessary for accommodating stochastically growing and shortening MTs [93]. From our fixed cell data, the progressive destabilization of interaction between the kinetochore and MTs correlating with a step-wise increase in phospho-mimetic mutation to conserved Aurora B kinase phosphorylation residues (S8,15,44 and 55) fits into a model of adjustable electrostatic-based kinetochore-MT binding interactions. Furthermore, from our live cell data, correlating a decrease in kinetochore-MT attachments with a loss in wild-type kinetochore oscillations strongly supports the notion that phospho-mimetic mutation to the 80 amino acid tail domain can be used to manipulate the affinity of kinetochores for MTs.

An interesting observation was the ability of cells expressing Hec1-GFP SD^{8,15,44,55} to form partially aligned plates, while a more complete alignment of chromosomes towards metaphase plates was impaired. One possible explanation for this phenotype is that initial chromosome positioning towards the center of the cell is independent of the Hec1 tail domain, while metaphase plate formation is dependent on Hec1 tail regulation. If true, this would argue that metaphase plate formation depends on phospho-regulation of the Hec1 tail domain for proper chromosome positioning along the equatorial axis of the cell.

Previous *in vitro* binding data suggested that the length of the Hec1 80 amino acid tail domain facilitated cooperative binding of Ndc80 complexes on MTs [34, 55], and/or may have also served to directly bind the MT lattice [53]. Here we show that a positively charged truncated Hec1 tail domain is sufficient for establishing kinetochore-MT attachment. Thus it appears that building a kinetochore binding site, functional in MT binding, can occur independent of a complete 80 amino acid tail domain. The dependence of kinetochore-MT attachments on positive charge with respect to a truncated Hec1 tail domain is striking, and strongly supports a previously reported role for charge-mediated interaction at the Hec1/kinetochore-MT interface [90]. The work performed on cells rescued with Hec1 mutant constructs expressing tail truncations additionally corroborates with work done on the Hec1 tail phospho-mimetic mutants (sections 5.2.1 through 5.2.3); Hec1 mutant constructs having a high charge on the tail can establish kinetochore-MT interactions (FL Hec1-GFP, Hec1^{Δ1-55}-GFP, and Hec1^{57-61Δ80}-GFP), while those cells expressing Hec1 constructs with a lower charge associated on the tail domain were significantly impaired in kinetochore-MT binding (Hec1^{Δ1-55/2D}-GFP, Hec1^{Δ1-70}-GFP, and Hec1-GFP SD^{8,15,44,55}).

In cells expressing Hec1^{57-61Δ80}-GFP, a short, positively charged Hec1 tail domain, kinetochore-MT attachments were established while chromosome congression needed for metaphase plate formation was impaired. This suggested that dynamic kinetochore-MT interactions were defective. Indeed, the kinetochore oscillation data demonstrated a loss in

dynamic kinetochore-MT interactions for cells rescued with Hec1^{57-61Δ80}-GFP. These data support a model of Ndc80-MT binding based on electrostatics, which could occur in the absence of the full 80 amino acid tail domain. However, the dampened oscillations observed for cells rescued with Hec1^{57-61Δ80}-GFP strongly suggests that the native tail is essential for regulation of dynamic kinetochore-MT interaction. It has been shown that ABK phosphorylation of the Hec1 tail domain is required for regulation of dynamic kinetochore-MT attachments [45, 55], and in cells rescued with Hec1^{57-61Δ80}-GFP these ABK target sites are removed.

From the Hec1 truncation and phospho-mimetic mutations, a dependence of kinetochore-MT interactions on the Hec1 tail charge has been observed. To address the role of Hec1 tail charge further, a mutant Hec1 construct expressing a scrambled tail domain was developed, where primary sequence had been lost but composition maintained. Interestingly, composition and not primary sequence, of the Hec1 80 amino acid tail domain was sufficient for establishing kinetochore-MT attachments. However, when the primary sequence of Hec1 tail domain was scrambled, ABK recognition sites were lost and defects in chromosome alignment were observed. Such is the case in cells rescued with Hec1^{9A}-GFP and Hec1^{57-61Δ80}-GFP, where prevention of Aurora B kinase phosphorylation disrupts kinetochore-MT dynamics necessary for chromosome orientation at the metaphase plate. Together, these results strengthen a model of electrostatic-mediated Ndc80-MT binding, where a faithful kinetochore-MT association requires phospho-regulation of the Hec1 tail domain.

Together this work demonstrates that charge associated with the Hec1 80 amino acid tail domain is essential to kinetochore-MT binding. However, establishment of kinetochore-MT attachments alone does not ensure a faithful progression through mitosis, as dynamic Ndc80-MT interaction is required for chromosome biorientation. By manipulating Ndc80-MT interactions through Hec1 tail phospho-mimetic mutations, we have

demonstrated that kinetochore-MT attachments can be regulated, and this may play a mechanistic role in promoting dynamic kinetochore-MT associations needed for biorientation and metaphase plate formation.

Chapter 6

Discussion and Future Directions

Through various mutations to the native 80 amino acid tail domain of Hec1, a dependence on some of its physical properties that affect kinetochore-MT attachments and metaphase plate formation have been demonstrated. A common trend throughout these experiments was the dependence of kinetochore-MT attachments on the charge associated with the Hec1 tail domain, supporting the hypothesis that charge mediates an interaction between the kinetochore and MTs. However, kinetochore-MT attachments alone were not sufficient for metaphase plate formation. In cells expressing Hec1 mutants where phosphorylation of the 80 amino acid tail domain is compromised (either through truncation to the tail domain, or scrambling of the native sequence), kinetochore-MT attachments persisted while a chromosome alignment was terminally halted in a partially aligned state. This implies that the 80 amino acid tail domain of Hec1 is not required for initial positioning of chromosomes towards the equatorial axis of the cell, whereas the native 80 amino acid tail domain, or at least an ABK regulatable tail, is required to produce kinetochore-MT dynamics needed for metaphase plate formation. These results serve to further implicate the 80 amino acid tail domain as a regulator of dynamic kinetochore-MT interactions, potentially through ABK modification.

Kinetochore oscillations were used to address how dynamic kinetochore-MT interactions were affected upon rescue with Hec1 mutant tail constructs. In a wild-type scenario, the kinetochore-MT interaction exists in a stable yet flexible state. The fidelity of mitosis is dependent upon the kinetochore having a controlled regulation of these stable yet flexible kinetochore-MT interactions. If the kinetochore-MT attachment is not stable, the interaction will simply be lost resulting in aberrant chromosome movements with increased velocities, as was the case for cells rescued with the kinetochore-null phospho-mimetic Hec1 mutant constructs. Conversely, kinetochore-MT attachments that are too tight will lock

MTs in place, dampening the native chromosome movements and reducing velocity values, as was shown for cells rescued with either Hec1^{9A}-GFP, Hec1^{Scr80#1}-GFP, or Hec1^{57-61Δ80}-GFP. Together, these experiments support a model whereby dynamic phosphorylation of the Hec1 tail domain is essential to the regulation of kinetochore-MT interactions.

Interestingly, for all cells rescued with Hec1 tail mutants, in which native kinetochore-MT dynamics have been impaired, the propensity for chromosomes to align towards the center of the cell existed, although metaphase plate formation was impaired. This finding suggests that initial chromosome congression towards the equatorial center of the cell can occur irrespective of the of the 80 amino acid tail domain, but downstream dynamic regulation of the 80 amino acid tail domain may be required for correct chromosome segregation.

In cells expressing Hec1^{K166D}-GFP kinetochore-MT attachments were abolished, and cells arrested in a prometaphase state, lending support for the idea that this region is an essential MT binding factor at the kinetochore. For the Hec1 tail mutants tested, regardless of attachment status, a terminal phenotype of partial chromosome alignment was achieved. This distinct difference in chromosome alignment phenotypes for cells expressing Hec1^{K166D}-GFP (prometaphase) as compared to various Hec1 tail mutants where phospho-regulation is impaired (partial alignment), suggests that the two regions of Hec1 contribute separate functions to kinetochore-MT interactions. Given the joint contribution that the tail and CH domains of Hec1 make towards kinetochore-MT attachments, it is reasonable to assume that these domains may work together in chromosome positioning and segregation. The mechanism of this cooperative interaction remains elusive. The data discussed provide preliminary support for a model whereby the CH domain of Hec1 is required for an initial positioning of chromosomes towards the center of the cell, after which metaphase plate formation relies on dynamic kinetochore-MT interactions regulated through the 80 amino acid tail domain of Hec1 (Figure 6.1A,B&C). Indeed, structural information supports a similar model whereby the 80 amino acid tail domain of Hec1 serves as a ratchet, used to shift

Model: Ndc80 Complex Binding to the MT Lattice

A) Stable kinetochore-MT interaction and no MT growth or shrinkage

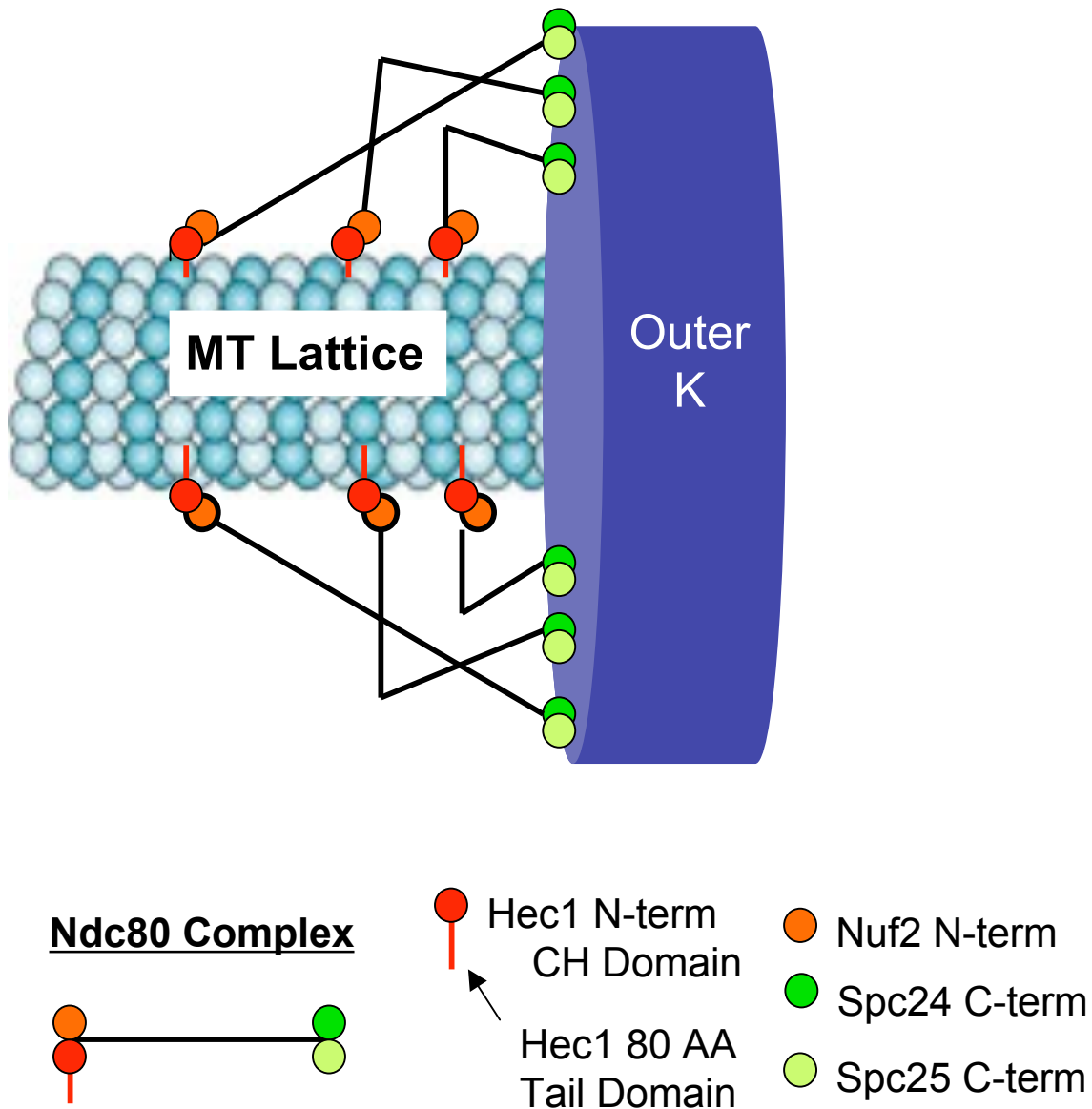


Figure 6.1.A: Model for Ndc80/microtubule binding and tracking along the microtubule lattice

A stable kinetochore-MT interaction, where multiple Ndc80 complexes are bound along the microtubule lattice. For simplicity, only 6 Ndc80 complexes are shown. A kink formed at the loop domain of the Ndc80 complex coiled-coil domain allows for a given Ndc80 complex to stretch variable distances.

Model: Ndc80 Complex Binding to the MT Lattice

B) MT growth and kinetochore tracking

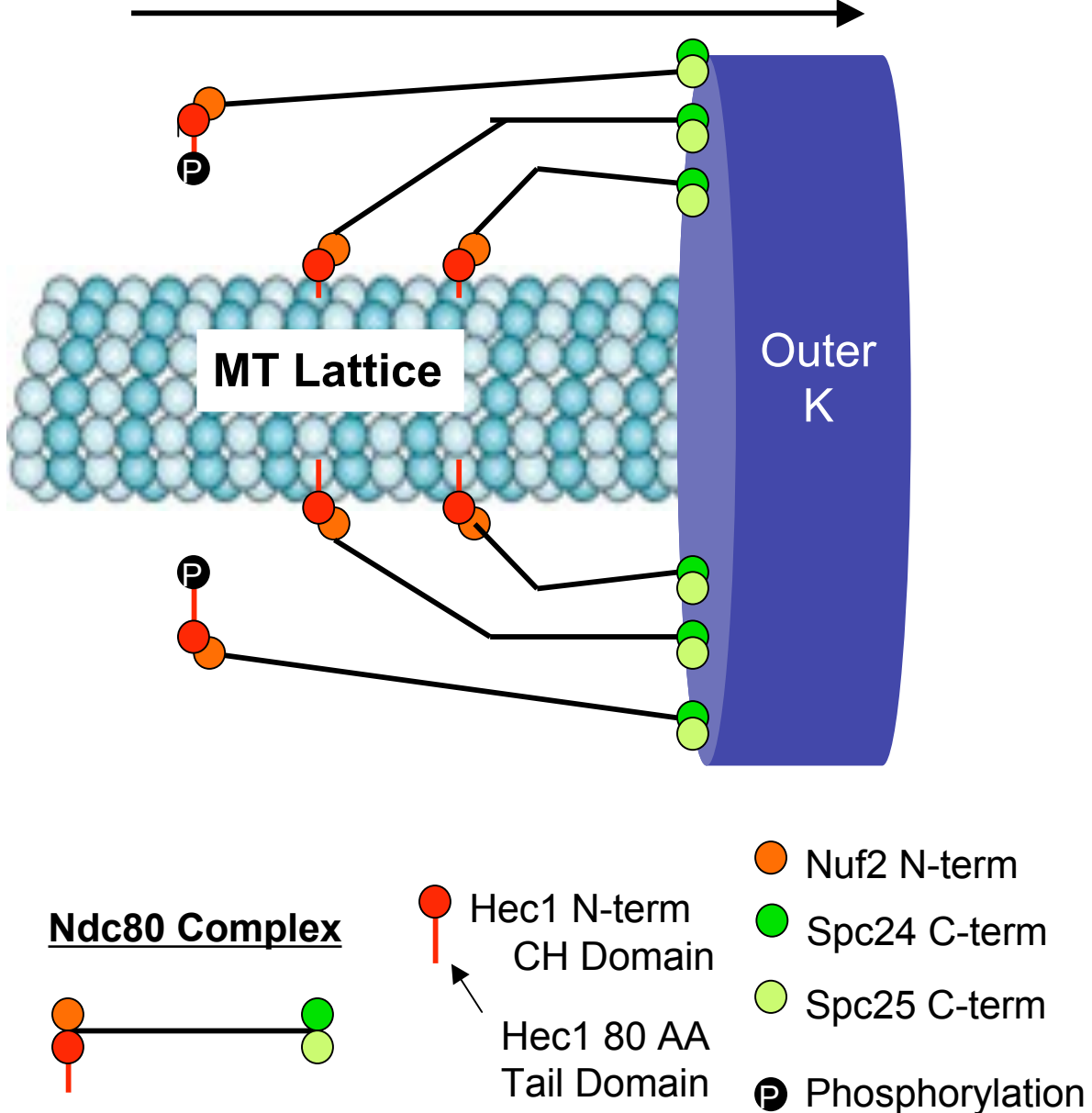


Figure 6.1.B: Model for Ndc80/microtubule binding and tracking along the microtubule lattice

As the microtubules polymerize, a population of Ndc80 complexes detach while other complexes remain associated with the lattice. Multiple phosphorylation events to the 80 amino acid tail domain trigger detachments, which can not be rescued by the Hec1 CH domain alone.

Model: Ndc80 Complex Binding to the MT Lattice

C) Rebinding of the Ndc80 complex to the MT lattice

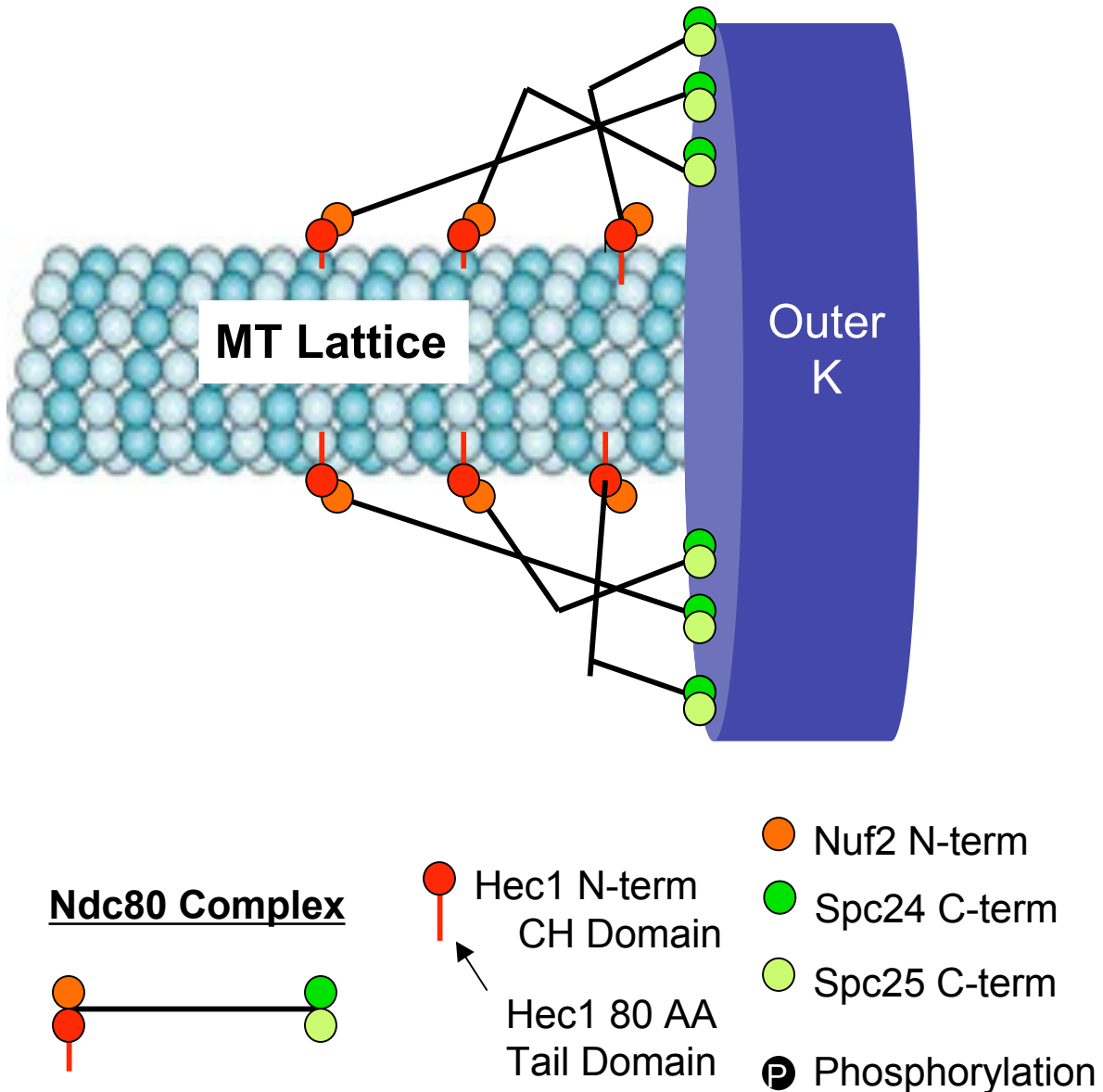


Figure 6.1.C: Model for Ndc80/microtubule binding and tracking along the microtubule lattice.

Phosphate groups are removed from the released Ndc80 complex, and the complex allowed to rebind to the MT lattice in a position closer to the outer-kinetochore.

Ndc80 complex binding along a MT lattice, while the Hec1 CH domain serves as the main point of contact used to lock MT interactions in place [55, 90].

Future Experiments

One of the most striking observations from the data presented here was the requirement for region-specific phosphorylation along the tail domain of Hec1 to induce a kinetochore-MT release. While the Hec1^{S4,49,62,69D}-GFP mutant was designed to mimic a similar drop in charge along the tail domain as is seen in the Hec1^{S8,15,44,55D}-GFP mutant, the charge positioning still differs greatly. Thus, to better address how charge positioning along the tail domain of Hec1 affects kinetochore-MT attachment, the “4D Neighbor Hec1 mutant” has been designed where residues directly adjacent to 8,15,44, and 55 have been mutated to aspartic acid (7,16,45,56D). To further confirm that region-specific phosphorylation of the tail domain is the dominant factor in triggering phosphorylation-induced kinetochore-MT release, a phospho-mimetic/charge neutralization mutant has also been developed. In the Hec1^{4D4K}-GFP mutant, four positively charged lysines (Q17,33K, N46K, and G58K) have been introduced within the tail domain of Hec1^{S8,15,44,55D}-GFP. By balancing the 4 negatively charged aspartic acid residues with 4 positively charged lysine residues, the net charge of Hec1^{4D4K}-GFP will return to that of the native state while still possessing phospho-mimetic mutation at the four evolutionarily conserved phosphorylation residues. Thus, with the Hec1^{4D-Neighbor} mutant it will be possible to assay if site-specific charges in the context of a natively charged tail domain can still trigger kinetochore-MT release. Lastly, the single phospho-mimetic mutation to one of four conserved Aurora B kinase phosphorylation residues demonstrated a modest dampening of kinetochore-MT attachments (Hec1^{S15D}-GFP). It will be interesting to test each of the other three phosphorylation sites individually to assess their contribution towards the kinetochore-MT interaction. Using Hec1^{4D-Neighbor}, Hec1^{4D4K}-GFP, and single phospho-mimetic mutations will be helpful in better understanding

how phosphorylation events to discrete regions within the Hec1 tail domain contribute to regulation of kinetochore-MT interactions.

References

1. Schrader, F., *Mitosis, the Movements of Chromosomes in Cell Division*. Columbia University Press, New York, 1953: p. 170 pp.
2. Maiato, H., et al., *The dynamic kinetochore-microtubule interface*. J Cell Sci, 2004. **117**(Pt 23): p. 5461-77.
3. Kline-Smith, S.L., S. Sandall, and A. Desai, *Kinetochore-spindle microtubule interactions during mitosis*. Curr Opin Cell Biol, 2005. **17**(1): p. 35-46.
4. Hill, T.L., *Theoretical problems related to the attachment of microtubules to kinetochores*. Proc Natl Acad Sci U S A, 1985. **82**(13): p. 4404-8.
5. Inoue, S. and E.D. Salmon, *Force generation by microtubule assembly/disassembly in mitosis and related movements*. Mol Biol Cell, 1995. **6**(12): p. 1619-40.
6. Rogers, G.C., et al., *Two mitotic kinesins cooperate to drive sister chromatid separation during anaphase*. Nature, 2004. **427**(6972): p. 364-70.
7. Kirschner, M. and T. Mitchison, *Beyond self-assembly: From microtubules to morphogenesis*. Cell, 1986. **45**(3): p. 329-342.
8. Holy, T.E. and S. Leibler, *Dynamic instability of microtubules as an efficient way to search in space*. Proc Natl Acad Sci U S A, 1994. **91**(12): p. 5682-5.
9. Echeverri, C.J., et al., *Molecular characterization of the 50-kD subunit of dynactin reveals function for the complex in chromosome alignment and spindle organization during mitosis*. J Cell Biol, 1996. **132**(4): p. 617-33.
10. Pfarr, C.M., et al., *Cytoplasmic dynein is localized to kinetochores during mitosis*. Nature, 1990. **345**(6272): p. 263-5.
11. Vaisberg, E.A., M.P. Koonce, and J.R. McIntosh, *Cytoplasmic dynein plays a role in mammalian mitotic spindle formation*. J Cell Biol, 1993. **123**(4): p. 849-58.
12. Waters, J.C., R.W. Cole, and C.L. Rieder, *The force-producing mechanism for centrosome separation during spindle formation in vertebrates is intrinsic to each aster*. J Cell Biol, 1993. **122**(2): p. 361-72.
13. Sharp, D.J., G.C. Rogers, and J.M. Scholey, *Cytoplasmic dynein is required for poleward chromosome movement during mitosis in Drosophila embryos*. Nat Cell Biol, 2000. **2**(12): p. 922-30.
14. Rieder, C.L. and E.D. Salmon, *The vertebrate cell kinetochore and its roles during mitosis*. Trends Cell Biol, 1998. **8**(8): p. 310-8.
15. Mitchison, M.K.a.T., 1986.
16. Wood, K.W., et al., *CENP-E is a plus end-directed kinetochore motor required for metaphase chromosome alignment*. Cell, 1997. **91**(3): p. 357-66.
17. Kapoor, T.M., et al., *Chromosomes can congress to the metaphase plate before biorientation*. Science, 2006. **311**(5759): p. 388-91.
18. Schaar, B.T., et al., *CENP-E function at kinetochores is essential for chromosome alignment*. J Cell Biol, 1997. **139**(6): p. 1373-82.
19. McEwen, B.F., et al., *CENP-E is essential for reliable bioriented spindle attachment, but chromosome alignment can be achieved via redundant mechanisms in mammalian cells*. Mol Biol Cell, 2001. **12**(9): p. 2776-89.
20. Putkey, F.R., et al., *Unstable kinetochore-microtubule capture and chromosomal instability following deletion of CENP-E*. Dev Cell, 2002. **3**(3): p. 351-65.
21. Koshland, D.E., T.J. Mitchison, and M.W. Kirschner, *Polewards chromosome movement driven by microtubule depolymerization in vitro*. Nature, 1988. **331**(6156): p. 499-504.

22. Musacchio, A. and E.D. Salmon, *The spindle-assembly checkpoint in space and time*. Nat Rev Mol Cell Biol, 2007. **8**(5): p. 379-93.
23. McEwen, B.F., et al., *A new look at kinetochore structure in vertebrate somatic cells using high-pressure freezing and freeze substitution*. Chromosoma, 1998. **107**(6-7): p. 366-75.
24. Dong, Y., et al., *The outer plate in vertebrate kinetochores is a flexible network with multiple microtubule interactions*. Nat Cell Biol, 2007. **9**(5): p. 516-22.
25. Palmer, D.K., et al., *Purification of the centromere-specific protein CENP-A and demonstration that it is a distinctive histone*. Proc Natl Acad Sci U S A, 1991. **88**(9): p. 3734-8.
26. Black, B.E., et al., *Structural determinants for generating centromeric chromatin*. Nature, 2004. **430**(6999): p. 578-82.
27. Oegema, K., et al., *Functional analysis of kinetochore assembly in Caenorhabditis elegans*. J Cell Biol, 2001. **153**(6): p. 1209-26.
28. Howman, E.V., et al., *Early disruption of centromeric chromatin organization in centromere protein A (Cenpa) null mice*. Proc Natl Acad Sci U S A, 2000. **97**(3): p. 1148-53.
29. Van Hooser, A.A., et al., *Specification of kinetochore-forming chromatin by the histone H3 variant CENP-A*. J Cell Sci, 2001. **114**(Pt 19): p. 3529-42.
30. Goshima, G., et al., *Human centromere chromatin protein hMis12, essential for equal segregation, is independent of CENP-A loading pathway*. J Cell Biol, 2003. **160**(1): p. 25-39.
31. McEwen, B.F., Y. Ding, and A.B. Heagle, *Relevance of kinetochore size and microtubule-binding capacity for stable chromosome attachment during mitosis in PtK1 cells*. Chromosome Res, 1998. **6**(2): p. 123-32.
32. Cleveland, D.W., Y. Mao, and K.F. Sullivan, *Centromeres and kinetochores: from epigenetics to mitotic checkpoint signaling*. Cell, 2003. **112**(4): p. 407-21.
33. McEwen, B.F., et al., *Structure of the colcemid-treated PtK1 kinetochore outer plate as determined by high voltage electron microscopic tomography*. J Cell Biol, 1993. **120**(2): p. 301-12.
34. Cheeseman, I.M., et al., *The conserved KMN network constitutes the core microtubule-binding site of the kinetochore*. Cell, 2006. **127**(5): p. 983-97.
35. Desai, A., et al., *KNL-1 directs assembly of the microtubule-binding interface of the kinetochore in C. elegans*. Genes Dev, 2003. **17**(19): p. 2421-35.
36. DeLuca, J.G., et al., *hNuf2 inhibition blocks stable kinetochore-microtubule attachment and induces mitotic cell death in HeLa cells*. J Cell Biol, 2002. **159**(4): p. 549-55.
37. McClelland, M.L., et al., *The highly conserved Ndc80 complex is required for kinetochore assembly, chromosome congression, and spindle checkpoint activity*. Genes Dev, 2003. **17**(1): p. 101-14.
38. Martin-Lluesma, S., V.M. Stucke, and E.A. Nigg, *Role of Hec1 in spindle checkpoint signaling and kinetochore recruitment of Mad1/Mad2*. Science, 2002. **297**(5590): p. 2267-70.
39. Hori, T., et al., *Dynamic behavior of Nuf2-Hec1 complex that localizes to the centrosome and centromere and is essential for mitotic progression in vertebrate cells*. J Cell Sci, 2003. **116**(Pt 16): p. 3347-62.

40. Bharadwaj, R., W. Qi, and H. Yu, *Identification of two novel components of the human NDC80 kinetochore complex*. J Biol Chem, 2004. **279**(13): p. 13076-85.
41. McClelland, M.L., et al., *The vertebrate Ndc80 complex contains Spc24 and Spc25 homologs, which are required to establish and maintain kinetochore-microtubule attachment*. Curr Biol, 2004. **14**(2): p. 131-7.
42. Wigge, P.A. and J.V. Kilmartin, *The Ndc80p complex from Saccharomyces cerevisiae contains conserved centromere components and has a function in chromosome segregation*. J Cell Biol, 2001. **152**(2): p. 349-60.
43. He, X., et al., *Molecular analysis of kinetochore-microtubule attachment in budding yeast*. Cell, 2001. **106**(2): p. 195-206.
44. Wei, R.R., P.K. Sorger, and S.C. Harrison, *Molecular organization of the Ndc80 complex, an essential kinetochore component*. Proc Natl Acad Sci U S A, 2005. **102**(15): p. 5363-7.
45. Ciferri, C., et al., *Implications for kinetochore-microtubule attachment from the structure of an engineered Ndc80 complex*. Cell, 2008. **133**(3): p. 427-39.
46. DeLuca, J.G., et al., *Hec1 and nuf2 are core components of the kinetochore outer plate essential for organizing microtubule attachment sites*. Mol Biol Cell, 2005. **16**(2): p. 519-31.
47. DeLuca, J.G., et al., *Kinetochore microtubule dynamics and attachment stability are regulated by Hec1*. Cell, 2006. **127**(5): p. 969-82.
48. Joglekar, A.P., K. Bloom, and E.D. Salmon, *In vivo protein architecture of the eukaryotic kinetochore with nanometer scale accuracy*. Curr Biol, 2009. **19**(8): p. 694-9.
49. McEwen, B.F., et al., *Kinetochore fiber maturation in PtK1 cells and its implications for the mechanisms of chromosome congression and anaphase onset*. J Cell Biol, 1997. **137**(7): p. 1567-80.
50. Wei, R.R., J. Al-Bassam, and S.C. Harrison, *The Ndc80/HEC1 complex is a contact point for kinetochore-microtubule attachment*. Nat Struct Mol Biol, 2007. **14**(1): p. 54-9.
51. Slep, K.C. and R.D. Vale, *Structural basis of microtubule plus end tracking by XMAP215, CLIP-170, and EBI*. Mol Cell, 2007. **27**(6): p. 976-91.
52. Guimaraes, G.J., et al., *Kinetochore-microtubule attachment relies on the disordered N-terminal tail domain of Hec1*. Curr Biol, 2008. **18**(22): p. 1778-84.
53. Miller, S.A., M.L. Johnson, and P.T. Stukenberg, *Kinetochore attachments require an interaction between unstructured tails on microtubules and Ndc80(Hec1)*. Curr Biol, 2008. **18**(22): p. 1785-91.
54. Powers, A.F., et al., *The Ndc80 kinetochore complex forms load-bearing attachments to dynamic microtubule tips via biased diffusion*. Cell, 2009. **136**(5): p. 865-75.
55. Alushin, G.M., et al., *The Ndc80 kinetochore complex forms oligomeric arrays along microtubules*. Nature, 2010. **467**(7317): p. 805-10.
56. Mitchison, T. and M. Kirschner, *Microtubule assembly nucleated by isolated centrosomes*. Nature, 1984. **312**(5991): p. 232-7.
57. Coue, M., V.A. Lombillo, and J.R. McIntosh, *Microtubule depolymerization promotes particle and chromosome movement in vitro*. J Cell Biol, 1991. **112**(6): p. 1165-75.

58. Alexander, S.P. and C.L. Rieder, *Chromosome motion during attachment to the vertebrate spindle: initial saltatory-like behavior of chromosomes and quantitative analysis of force production by nascent kinetochore fibers*. J Cell Biol, 1991. **113**(4): p. 805-15.
59. Skibbens, R.V., V.P. Skeen, and E.D. Salmon, *Directional instability of kinetochore motility during chromosome congression and segregation in mitotic newt lung cells: a push-pull mechanism*. J Cell Biol, 1993. **122**(4): p. 859-75.
60. Emanuele, M.J., et al., *Measuring the stoichiometry and physical interactions between components elucidates the architecture of the vertebrate kinetochore*. Mol Biol Cell, 2005. **16**(10): p. 4882-92.
61. Joglekar, A.P., et al., *Molecular architecture of the kinetochore-microtubule attachment site is conserved between point and regional centromeres*. J Cell Biol, 2008. **181**(4): p. 587-94.
62. Joglekar, A.P., et al., *Molecular architecture of a kinetochore-microtubule attachment site*. Nat Cell Biol, 2006. **8**(6): p. 581-5.
63. Asbury, C.L., J.F. Tien, and T.N. Davis, *Kinetochores' gripping feat: conformational wave or biased diffusion?* Trends Cell Biol, 2010.
64. DeLuca, K.F., S.M. Lens, and J.G. DeLuca, *Temporal changes in Hecl phosphorylation control kinetochore-microtubule attachment stability during mitosis*. J Cell Sci, 2011. **124**(Pt 4): p. 622-34.
65. Hwang, L.H., et al., *Budding yeast Cdc20: a target of the spindle checkpoint*. Science, 1998. **279**(5353): p. 1041-4.
66. Stout, J.R., et al., *Deciphering protein function during mitosis in PtK cells using RNAi*. BMC Cell Biol, 2006. **7**: p. 26.
67. Hoffman, D.B., et al., *Microtubule-dependent changes in assembly of microtubule motor proteins and mitotic spindle checkpoint proteins at PtK1 kinetochores*. Mol Biol Cell, 2001. **12**(7): p. 1995-2009.
68. Rieder, C.L. and S.P. Alexander, *Kinetochores are transported poleward along a single astral microtubule during chromosome attachment to the spindle in newt lung cells*. J Cell Biol, 1990. **110**(1): p. 81-95.
69. Mitchison, T., et al., *Sites of microtubule assembly and disassembly in the mitotic spindle*. Cell, 1986. **45**(4): p. 515-27.
70. Walczak, C.E. and R. Heald, *Mechanisms of mitotic spindle assembly and function*. Int Rev Cytol, 2008. **265**: p. 111-58.
71. Ciferri, C., et al., *Architecture of the human ndc80-hec1 complex, a critical constituent of the outer kinetochore*. J Biol Chem, 2005. **280**(32): p. 29088-95.
72. Wilson-Kubalek, E.M., et al., *Orientation and structure of the Ndc80 complex on the microtubule lattice*. J Cell Biol, 2008. **182**(6): p. 1055-61.
73. Cheeseman, I.M. and A. Desai, *Molecular architecture of the kinetochore-microtubule interface*. Nat Rev Mol Cell Biol, 2008. **9**(1): p. 33-46.
74. DeLuca, J.G., et al., *Nuf2 and Hecl are required for retention of the checkpoint proteins Mad1 and Mad2 to kinetochores*. Curr Biol, 2003. **13**(23): p. 2103-9.
75. Meraldi, P., V.M. Draviam, and P.K. Sorger, *Timing and checkpoints in the regulation of mitotic progression*. Dev Cell, 2004. **7**(1): p. 45-60.
76. Gimona, M., et al., *Functional plasticity of CH domains*. FEBS Lett, 2002. **513**(1): p. 98-106.

77. Korenbaum, E. and F. Rivero, *Calponin homology domains at a glance*. J Cell Sci, 2002. **115**(Pt 18): p. 3543-5.
78. Prilusky, J., et al., *FoldIndex: a simple tool to predict whether a given protein sequence is intrinsically unfolded*. Bioinformatics, 2005. **21**(16): p. 3435-8.
79. Cassimeris, L., et al., *Stability of microtubule attachment to metaphase kinetochores in PtK1 cells*. J Cell Sci, 1990. **96 (Pt 1)**: p. 9-15.
80. Howell, B.J., et al., *Cytoplasmic dynein/dynactin drives kinetochore protein transport to the spindle poles and has a role in mitotic spindle checkpoint inactivation*. J Cell Biol, 2001. **155**(7): p. 1159-72.
81. Liu, S.T., et al., *Mapping the assembly pathways that specify formation of the trilaminar kinetochore plates in human cells*. J Cell Biol, 2006. **175**(1): p. 41-53.
82. Pinsky, B.A., et al., *The Ipl1-Aurora protein kinase activates the spindle checkpoint by creating unattached kinetochores*. Nat Cell Biol, 2006. **8**(1): p. 78-83.
83. Cimini, D., et al., *Aurora kinase promotes turnover of kinetochore microtubules to reduce chromosome segregation errors*. Curr Biol, 2006. **16**(17): p. 1711-8.
84. Zimniak, T., et al., *Phosphoregulation of the budding yeast EBI homologue Bim1p by Aurora/Ipl1p*. J Cell Biol, 2009. **186**(3): p. 379-91.
85. Welburn, J.P., et al., *Aurora B phosphorylates spatially distinct targets to differentially regulate the kinetochore-microtubule interface*. Mol Cell, 2010. **38**(3): p. 383-92.
86. Ciferri, C., A. Musacchio, and A. Petrovic, *The Ndc80 complex: hub of kinetochore activity*. FEBS Lett, 2007. **581**(15): p. 2862-9.
87. Lampson, M.A., et al., *Correcting improper chromosome-spindle attachments during cell division*. Nat Cell Biol, 2004. **6**(3): p. 232-7.
88. Tanaka, T.U., et al., *Evidence that the Ipl1-Sli15 (Aurora kinase-INCENP) complex promotes chromosome bi-orientation by altering kinetochore-spindle pole connections*. Cell, 2002. **108**(3): p. 317-29.
89. Suzuki, A., et al., *Spindle microtubules generate tension-dependent changes in the distribution of inner kinetochore proteins*. J Cell Biol, 2011. **193**(1): p. 125-40.
90. Tooley, J.G., S.A. Miller, and P.T. Stukenberg, *The Ndc80 complex uses a tripartite attachment point to couple microtubule depolymerization to chromosome movement*. Mol Biol Cell, 2011. **22**(8): p. 1217-26.
91. Ross, E.D., U. Baxa, and R.B. Wickner, *Scrambled prion domains form prions and amyloid*. Mol Cell Biol, 2004. **24**(16): p. 7206-13.
92. Cheeseman, I.M., et al., *Phospho-regulation of kinetochore-microtubule attachments by the Aurora kinase Ipl1p*. Cell, 2002. **111**(2): p. 163-72.
93. Serber, Z. and J.E. Ferrell, Jr., *Tuning bulk electrostatics to regulate protein function*. Cell, 2007. **128**(3): p. 441-4.